

**Contracted and Expanded Porphyrinoids with
Polycyclic Aromatic Units: Syntheses, Receptor
Properties, Reactivity and Coordination Chemistry**

By

ADINARAYANA BELLAMKONDA

CHEM11201104009

**National Institute of Science Education and Research,
Bhubaneswar, Odisha**

*A thesis submitted to the
Board of Studies in Chemical Sciences
In partial fulfillment of requirements
for the Degree of*

DOCTOR OF PHILOSOPHY

Of

HOMI BHABHA NATIONAL INSTITUTE



February, 2017

Homi Bhabha National Institute¹

Recommendations of the Viva Voce Committee

As members of the Viva Voce Committee, we certify that we have read the dissertation prepared by **Adinarayana Bellamkonda** entitled “**Contracted and Expanded Porphyrinoids with Polycyclic Aromatic Units: Syntheses, Receptor Properties, Reactivity and Coordination Chemistry**” and recommend that it may be accepted as fulfilling the thesis requirement for the award of Degree of Doctor of Philosophy.

Chairman - < Dr. Moloy Sarkar >

Date:

Guide / Convener - < Prof. A. Srinivasan >

Date:

Examiner - < Prof. Srinivasan Natarajan >

Date:

Member 1- < Dr. V. Krishnan >

Date:

Member 2- < Dr. Chandra Shekhar Purohit >

Date:

Member 3- < Dr. Debasmita P. Alone >

Date:

Final approval and acceptance of this thesis is contingent upon the candidate's submission of the final copies of the thesis to HBNI.

I/We hereby certify that I/we have read this thesis prepared under my/our direction and recommend that it may be accepted as fulfilling the thesis requirement.

Date:

Place:

<Signature>

Guide

¹ This page is to be included only for final submission after successful completion of viva voce.

STATEMENT BY AUTHOR

This dissertation has been submitted in partial fulfillment of requirements for an advanced degree at Homi Bhabha National Institute (HBNI) and is deposited in the Library to be made available to borrowers under rules of the HBNI.

Brief quotations from this dissertation are allowable without special permission, provided that accurate acknowledgement of source is made. Requests for permission for extended quotation from or reproduction of this manuscript in whole or in part may be granted by the Competent Authority of HBNI when in his or her judgment the proposed use of the material is in the interests of scholarship. In all other instances, however, permission must be obtained from the author.

Adinarayana Bellamkonda

DECLARATION

I, hereby declare that the investigation presented in the thesis has been carried out by me. The work is original and has not been submitted earlier as a whole or in part for a degree / diploma at this or any other Institution / University.

Adinarayana Bellamkonda

LIST OF PUBLICATIONS

Published

- *1. **Adinarayana, B.**; Thomas, A. P.; Pardhasaradhi Satha and Srinivasan, A.
"Syntheses of Bipyricorroles and Their *Meso-Meso* Coupled Dimers", *Org. Lett.* **2017**, *19*, 1986-1989.
- *2. **Adinarayana, B.**; Thomas, A. P.; Yadav, P.; Mukundam, V.; Srinivasan, A.
"Carbatriphyrin(3.1.1) – Displays two distinct coordination modes with B^{III} to generate organoborane and weak C-H...B interactions", *Chem. Eur. J.* **2017**, *23*, 2993-2997.
- *3. **Adinarayana, B.**; Thomas, A. P.; Yadav, P.; Kumar, A., Srinivasan, A.
"Bipyricorrole: A corrole homologue with a monoanionic core as a fluorescence Zn^{II} sensor", *Angew. Chem. Int. Ed.* **2016**, *55*, 969-973.
- *4. **Adinarayana, B.**; Thomas, A. P.; Suresh, C. H.; Srinivasan, A., "A 6,11,16-Triarylbiarylcorrole with an *adj*-CCNN Core: Stabilization of an Organocopper(III) Complex", *Angew. Chem. Int. Ed.* **2015**, *54*, 10478-10482.
5. Holaday, M. G. D.; Tarafdar, G.; **Adinarayana, B.**; Reddy, M. L. P.; Srinivasan, A. "Chemodosimetric cyanide sensing in a 5,15-porphodimethene Pd(II) complex", *Chem. Commun.* **2014**, *50*, 10834-10836.
6. Thomas, A. P.; Sreedevi, K. G.; **Adinarayana, B.**; Ramakrishnan, S.; Srinivasan, A. "*meso*-Tetrakis(3,5-dihydroxyphenyl)N-Confused Porphyrin: Influence of polar protic and aprotic solvents in tautomeric existence, exchange and morphology", *RSC Adv.* **2013**, *3*, 16967-16972.

Manuscript under preparation

- *1. **Adinarayana, B.;** Srinivasan, A. "Carbahomoporphyrins: Allowed and restricted conjugation of homoporphyrinoids by incorporation of terphenyl systems".
- *2. **Adinarayana, B.;** Murugavel, M.; Mainak Das; Narasinga Rao, P.; Srinivasan, A. "Synthesis, spectral and structural characterization of Cu^{II} and Rh^{III} bipyricorrole complexes".

* Pertaining to this thesis

Adinarayana Bellamkonda

Conferences

1. "Carbatriphyrin(3.1.1) – Displays distinct coordination approach of B^{III} to generate organoborane and weak C-H...B Interactions" **B. Adinarayana**, Ch. Sangya and A. Srinivasan* in 5th Symposium on Advanced Biological Inorganic Chemistry (SABIC-2017), January 7-11th, Organized by the Tata Institute of Fundamental Research (TIFR) and Indian Association for the Cultivation of Science (IACS) 2017 at Kolkata. (**Poster Presentation**)
2. "6,11,16-Triarylbiarylcorrole with *adj*-CCNN core stabilizes organocopper(III) complex"- **B. Adinarayana**, Ajesh P. Thomas, Mainak Das and A. Srinivasan* in International Symposium on Modern Trends Inorganic Chemistry-XVI (MTIC-XVI), December 3-5th, 2015 Organized by Department of Chemistry, Jadavpur University, Jadavpur, Kolkata. (**Poster Presentation**)
3. "Bipyricorrole: A Bipyridine Incorporated *meso*-Aryl Corrole"- **B. Adinarayana**, Ajesh P. Thomas and A. Srinivasan* in Indo-French Symposium on Functional Metal-Organics: Applications in Materials and Catalysis, February 24-26th, 2014 organized at School of Chemical Sciences, NISER, Bhubaneswar. (**Poster Presentation**)

Adinarayana Bellamkonda

Dedicated to....

My Family

&

Prof. A. Srinivasan

ACKNOWLEDGEMENTS

*I am extremely grateful to **God** for blessing this life and giving strength.*

*I would like to express my gratitude to **Prof. A. Srinivasan**, my guide, for continuous support, encouragement, patience exhibited and freedom provided for free thinking. Also I express my sincere thanks to **Meena** madam.*

*I am thankful to **Prof. V. Chandrasekhar**, Director, NISER and also **Prof. T. K. Chandrashekar**, Founder-Director, NISER for providing the laboratory facilities, CSIR-New Delhi and DST for financial support.*

*I thank my TMC members, **Dr. C. S. Purohit** and **Dr. V. Krishnan**, Chairman **Dr. M. Sarkar**, all other faculties in SCS NISER for their useful suggestions and also **Dr. S. Peruncheralathan**, **Dr. V. Krishnan** and scientific officer **Dr. Arun Kumar** support on several occasions.*

*I owe my sincere thanks to my collaborator, **Dr. C. H. Suresh** for his valuable contributions.*

*I sincerely thank **Mr. Deepak**, **Mr. Sanjaya**, **Mr. Amit** and **Mr. Raj Kumar**, NISER for performing characterization of my samples.*

*I am greatly indebted to **all my teachers** of school, graduation (**Satish sirs**) and post-graduation who inculcated knowledge, discipline and encouragement.*

*It gives me immense pleasure to thank all those seniors, friends and juniors who made my life at NISER really enjoyable and memorable. Special mention must be made of my labmates, **Gowri**, **Derry**, **M. Das**, **Sangya**, **Gaurav**, **Prerana**, **Garima**, **Kavya**, **Karthik**, **Antara**, **Yogesh**, **Subbu**, **Jitendra**, **Ranjay**, and my best friends **Woormi**, **Sujatha**, **Durga (late)**, **Arindam**, **Srinu**, **Narsing**, **Narsimha**, **Veeru**, **Ravi**, **Ashoke**, **Kishore & Srinu** for their support and special thanks to my seniors **Ajesh P. Thomas**, **Santosh**, **Appalaraju**, **Gopi**, **Pardha**, **Giri** for their help and guidance. Also I thank **Murugavel**, **Mukundam**, **Venkat**, **Dhanu**, **Chandu**, **Surya**, **Arun**, **Prabhat**, **Anoop**, **Manoj**, **pasha**, **Gargi** and **Suvasmita** for their help.*

I am greatly thankful to my relatives for their support, suggestions and care.

*I am deeply grateful to my beloved **Amma**, **Nanna**, **Brothers** and **Sister-in-law** for their unconditional love, support, sacrifices, blessings and inspiration throughout my career.*

Adinarayana Bellamkonda

CONTENTS

	Page No.
Synopsis	xi
List of Tables	xxi
List of Schemes	xxii
List of Figures	xxiv
List of Abbreviations	xxx
Chapter 1	1
Chapter 2	35
Chapter 3	67
Chapter 4	96
Chapter 5	129
Chapter 6	179
Summary	203

SYNOPSIS

Porphyrins are widely studied well-known tetrapyrrolic macrocycles. These are existing in nature in the form of heme and other derivatives and are termed as "pigments of life".¹ The derivatives of porphyrins and related macrocycles are involved numerous biological functions which includes oxygen carrier and storage, electron transport and photosynthesis in green plants.² It has also been proven as photosensitizers for photodynamic therapy.^{3,4} The porphyrin consists of four pyrrole rings linked by four methylene carbons.^{5,6} These are 18π Hückel aromatic systems, highly intense in color and show strong absorption bands in the visible region. The presence of two imine and two amine nitrogens in the coordination core, it can act as a dianionic tetradentate square planar ligand. The macrocycle cavity size is ideal to bind almost all metal ions in the "pocket" of porphyrin ring system. The unique properties of porphyrin remains fundamental interest for the researchers in various fields, which motivates to develop novel porphyrinoids with several distinct types of modifications in the porphyrin core. The most important and well-studied modifications are (Figure 1); i) Peripheral modifications - by changing the substitutions at the β and *meso*- position in the porphyrin rings;⁷ ii) Porphyrin isomers – have the same molecular formula, however, different in their bonding connectivity of pyrrole units;⁸⁻¹⁰ iii) Contracted porphyrins – the smallest macrocycle has at least one less number of either *meso*-carbon or pyrrole or both in the porphyrin system;¹¹⁻¹³ iv) Core-modified porphyrin - porphyrin analogues with one or more pyrrole nitrogens is replaced by other heteroatoms or carbon atoms^{14,15} and v) Expanded porphyrins - by increasing the number of *meso*-carbons or number of pyrrole rings or both in the porphyrin framework.^{16,17}

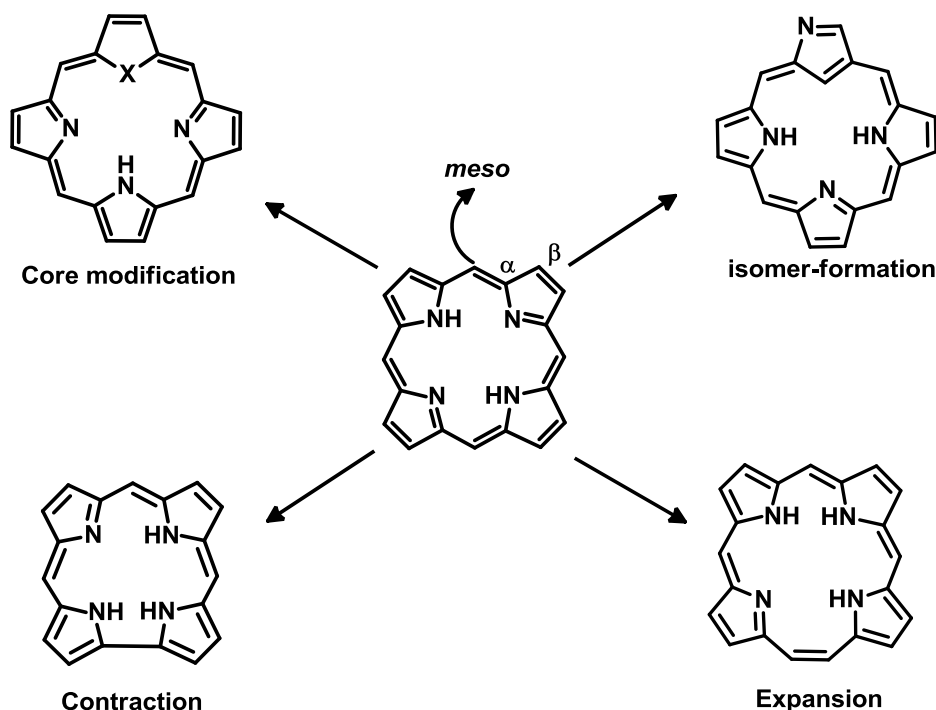


Figure 1: Porphyrin modifications

Scope and Organization of the Present Thesis:

The main objective of this thesis is to develop new synthetic methodologies as well as the synthesis of novel homologues and analogues of contracted and expanded porphyrinoids by introducing the polycyclic aromatic units in the macrocyclic framework. Also highlights the reactivity, receptor property and coordination chemistry of these macrocycles. The thesis has been organized into following six chapters.

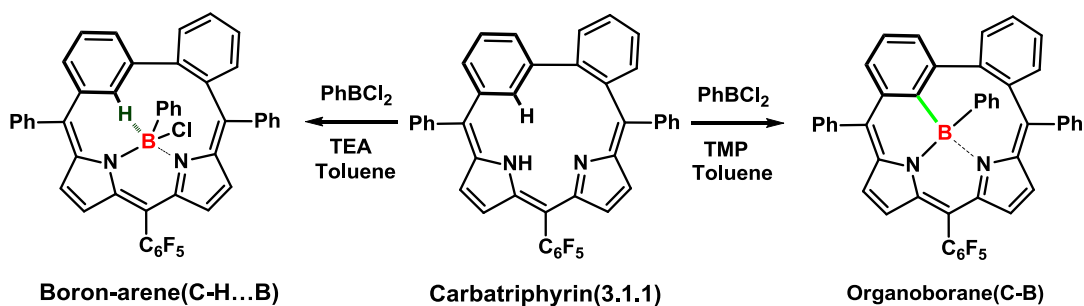
Chapter 1: Introduction

First chapter describes the literature review of various modified porphyrinoids. The porphyrin analogues with carbocyclic and pyridine systems are received much attention in recent years.^{14,15} To date, the synthesis and coordination chemistry of mono-carba and mono-pyridine related porphyrinoids are known and the di-carba and di-pyridine porphyrinoids are scarcely reported in the literature.^{14,15} This chapter mainly highlights the synthesis & important spectral properties of such porphyrinoids. In addition, the

literature review of the respective contracted and expanded porphyrins are also included. Finally, at the end of the chapter, the aim of present thesis is discussed.

Chapter 2: Carbatriphyrin(3.1.1) – Displays two distinct coordination approach of B^{III} to generate organoborane and weak C-H...B interactions

The research on organoboranes have emerged in recent years due to wide range of applications, however, the study of organoborane in porphyrin macrocycle is in infancy stage. In the recently reported borylated porphyrins,¹⁸ porphyrinyl borane¹⁹ and boron embedded π -expanded fused porphyrins,²⁰ the boron ion is inserted on the periphery of the macrocyclic framework. To date, the synthesis of organoborane complex by using porphyrin core is remained unexplored. In this chapter, we have demonstrated the synthesis of carbatriphyrin(3.1.1) with CNN in the core which is achieved by introducing the *o*- and *m*-phenylene units as part of the porphyrin framework and also explored its coordination ability to stabilize the trifluoroacetate ion and B^{III} complexes. The π -electron conjugation in the macrocyclic framework is extended upto *o*-phenylene unit, however restricted in the *m*-phenylene unit and thus adopts non-aromatic character. The similar trend was observed in protonated as well as both B^{III} complexes. The formation of weak boron arene interaction and stabilization of organoborane

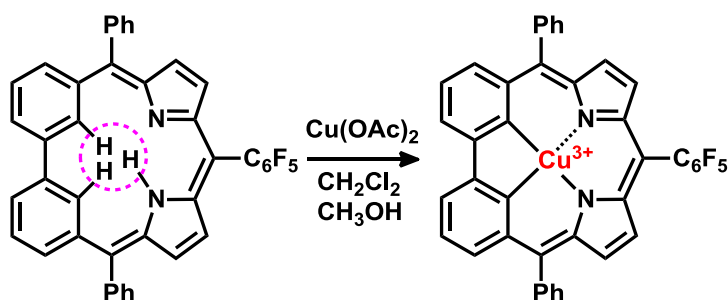


Scheme 1: Synthesis of organoborane(C-B) and boron-arene(C-H...B) complexes from carbatriphyrin(3.1.1).

complex were reflected from the approach of the B^{III} ion to the macrocyclic ligand (Scheme 1). To the best of our knowledge, the weak C-H...B intramolecular interaction and C-B bond formation through C-H activation are exploited for the first time in the porphyrin chemistry.

Chapter 3: A 6,11,16-Triarylbiarylcorrole with an *adj*-CCNN Core: Stabilization of an Organocopper(III) Complex

In the third chapter, we have demonstrated the synthesis of an *adj*-dicarbacorrole with CCNN in the core, where the bipyrrrole unit in the corrole framework is replaced by simple polycyclic aromatic hydrocarbon, such as, biphenyl unit.²¹ Upon macrocyclic aromatization, the aromatic biphenyl unit and the π -delocalized dipyrromethene units are linked together to generate overall non-aromatic character, which is confirmed by spectral studies and structural characterization. The macrocycle is found suitable to stabilize higher oxidation state metal complex, where the trianionic core affords Cu^{III} complex to generate the organocopper complex (Scheme 2). The absence of two inner core biphenyl-CHs and pyrrolic NH signals from the spectral analysis proves the complex formation and further confirmed by single crystal analysis. Upon metal ion insertion, the complex retains the non- aromatic character as such. The possible equilibrium between the diamagnetic Cu^{III} complex and paramagnetic Cu^{II} -radical

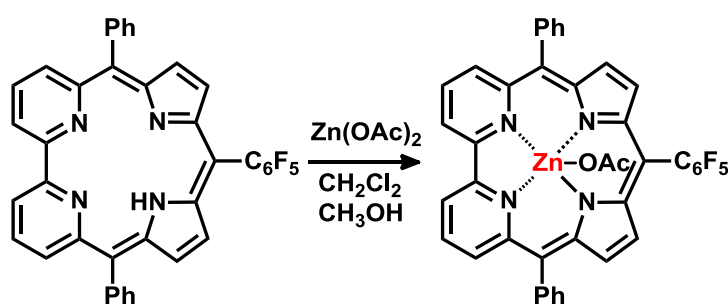


Scheme 2: Synthesis of organocopper(III) complex from *adj*-dicarbacorrole.

cation was investigated by variable temperature NMR experiments, solution and solid state EPR spectral studies and crystal analysis. These results rule out the possible equilibrium and prove the formation of stable organocopper(III) complex.

Chapter 4: Bipyricorrole: A Corrole Homologue with a Monoanionic Core as a Fluorescence Zn^{II} Sensor

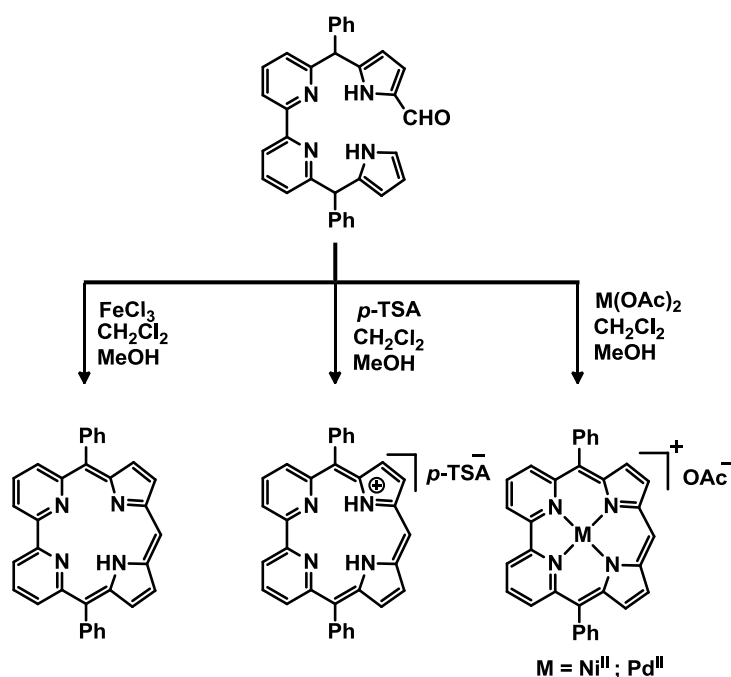
In the fourth chapter, we have described the synthesis of novel corrole homologue such as 6,11,16-triarylbiopyricorrole and its Zn^{II} complex. Introduction of 2,2'-bipyridyl unit in the macrocycle is unprecedented in the corrole chemistry, which provides stable tetra nitrogen (NNNN) core. The modification effectively alters the corrole N4 coordination sphere from the trianionic [(NH)3N] to monoanionic [N3NH] core.²² The spectral and structural characterization reveals that the overall macrocyclic π -conjugation is interrupted by bipyridyl unit and confirms the non-aromatic characteristics. The monoanionic core is effectively utilized to stabilize the Zn^{II} ion with Chelation Induced Emission Enhancement (CIEE). The enhanced emission profile prompted us to explore the sensing properties, where the macrocycle selectively senses Zn^{II} ion over 100 equivalents of other metal ions. The metal ion insertion retains the non-aromatic character as such.



Scheme 3: Synthesis of Zn^{II}-complex from 6,11,16-triarylbiopyricorrole.

Chapter 5: Corrole homologues: Metal-templated monomers and oxidative coupled dimers

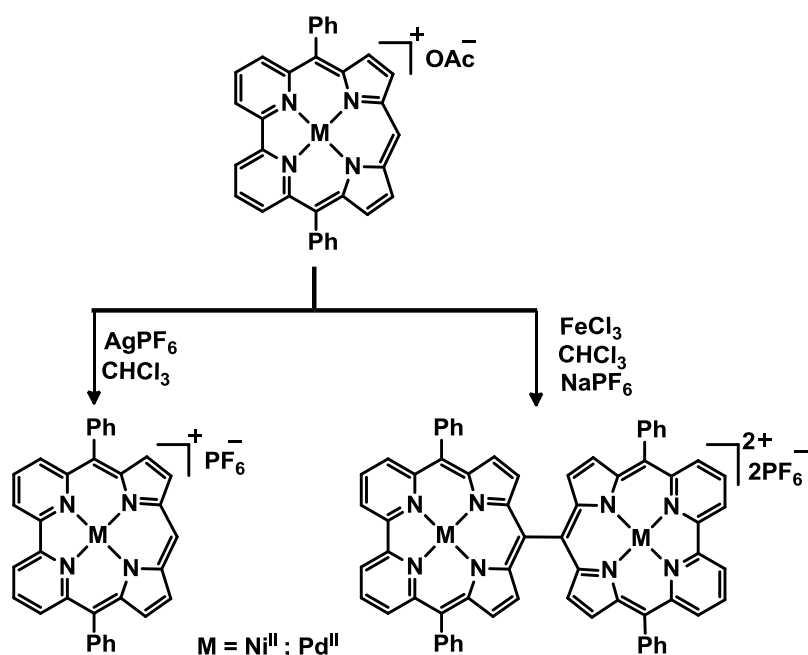
The fifth chapter is divided into two parts. In the first part, we have demonstrated the novel synthetic methodology for the synthesis of *meso*-free monomer bipyricorrole and their complexes. The *meso*-free bipyricorrole is achieved by acid-catalyzed condensation reaction of formylated bipyridyl dipyrromethane followed by open-air oxidation. Here, the FeCl_3 is used as an acid-catalyst as well as oxidizing agent. The traditional acid-catalyzed condensation reactions by using either Lewis acid or protic acid is afforded the respective anion bound complex as the major product. On the other hand, the coordination chemistry of *meso*-free bipyricorrole is achieved through metal-templated condensation strategy, where the Ni^{II} and Pd^{II} salts are used as a templating agent (Scheme 4). The synthetic methodology adopted for monomer complexes is an alternative strategy for; i) the routine step-wise strategy such as *acid*-



Scheme 4: Synthesis of *meso*-free corrole homologue & protonated and coordinated complexes.

catalyzed condensation reaction followed by oxidation and metal ion insertion and ii) the metal-templated *oxidative* macrocyclization.

The second part of this chapter describes the reactive studies. The reactive CH in the *meso*-free bipyricorrole complexes are further utilized for covalently linked dimer reaction by using various oxidative coupling reagents such as AgPF₆, AgOTf and FeCl₃ (Scheme 5). By using Ag^I salts, the anion exchanged products are observed, where as in the presence Fe^{III} salts, the *meso*-CH is actively participated in oxidative coupling reaction to afford the respective *meso-meso* linked corrole homologue dimer complexes. The spectral and structural analyses of the *meso*-free monomer and its complexes and the respective dimeric complexes reveal the non-aromatic characteristics. In addition, to the best of our knowledge, the nonaromatic Pd^{II} monomer as well as dimer corrole homologue complexes are characterized by spectral studies and further confirmed by structural analysis, which are first time addressed in corrole chemistry.



Scheme 5: Reactivity studies of corrole homologue monomer complexes.

Chapter 6: Carbahomoporphyrins: Allowed and restricted conjugation in homoporphyrinoids by incorporation of terphenyl systems

The homoporphyrin is the smallest expanded porphyrin which contains an extra atom between a *meso*- and α -pyrrolic carbon with 17 atoms in the inner framework. It was first reported by Grigg and coworkers in 1971, however, found to be unstable and subsequently reported homoporphyrin derivatives led to species with interrupted conjugation.²³ After four decades, the core-modified homoporphyrins are very recently reported,^{24,25} however, the macrocyclic ring with polycyclic aromatic unit as part of the framework is hitherto unknown in the literature. In this chapter, the *meso*-aryl di-carba and tetra-carba homoporphyrins are synthesized by introducing the *o*-terphenyl unit into the porphyrin core. The newly formed two carbahomoporphyrins are structural isomers to each other. One of the isomer, *o*-terphenyl unit is connected through 4,4'' bonding mode to the dipyrromethene unit and allowed the conjugation throughout the macrocycle framework. The spectral analysis reveals the non-aromatic character. Whereas in another isomer, *o*-terphenyl unit is connected through 3,3'' bonding mode with the dipyrromethene and restrict the overall conjugation at the *m*-position of the phenyl unit, thus, retains the overall non-aromatic character. The coordination chemistry was further performed with $[\text{Rh}(\text{CO})_2\text{Cl}]_2$, where the dipyrromethene unit is involved in the coordination and stabilizes the Rh^{I} complex. Both the Rh^{I} complexes are highly deviated from the mean plane and maintain the non-aromatic character. The crystal structure of tetra-carba homoporphyrin and its Rh^{I} complex is shown in Figure 2, where the intramolecular hydrogen bonding interaction is observed between amine NH and imine N with the bond distance and angle of N1-H1...N2 is: 2.37 Å & 120° (Figure 2a).

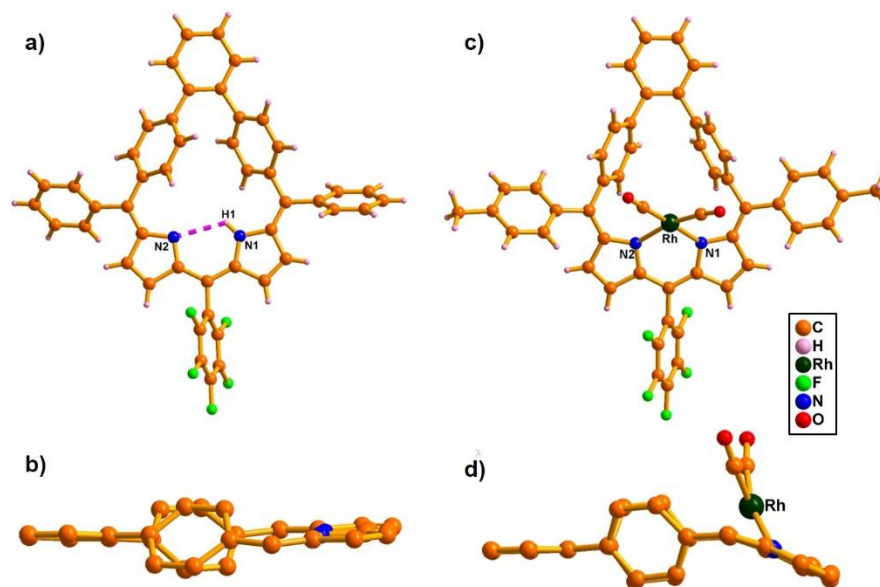


Figure 2: Single crystal X-ray structure of tetra-carba homoporphyrin and its Rh(I) complex. (a & c) Top view and (b & d) side view. The *meso*-aryl groups and hydrogen atoms are omitted for clarity in the side view.

References:

1. Battersby, A. R.; Fookes, C. J.; Matcham, G. W.; McDonald, E., *Nature* **1980**, 285, 17-21.
2. Lippard, S. J.; Berg, J. M., *Principles of bioinorganic chemistry*. University Science Books: **1994**.
3. Dougherty, T. J.; Marcus, S. L., *Eur. J. Cancer* **1992**, 28, 1734-1742.
4. Moan, J.; Berg, K., *Photochem. Photobiol.* **1992**, 55, 931-948.
5. Kadish, K.; Smith, K.; Guillard, R., *The Porphyrin Handbook; Volume 1, Synthesis and Organic Chemistry*. Academic Press–San Diego, CA and London, UK: **2000**.
6. Sessler, J. L.; Weghorn, S. J., *Expanded, contracted & isomeric porphyrins*. Elsevier: **1997**; Vol. 15.
7. Hiroto, S.; Miyake, Y.; Shinokubo, H. *Chem. Rev.* **2016**, DOI: 10.1021/acs.chemrev.6b00427.

-
8. Toganoh, M.; Furuta, H. *Chem. Commun.* **2012**, 48, 937-954.
 9. Sánchez-García, D.; Sessler, J. L. *Chem. Soc. Rev.* **2008**, 37, 215-232.
 10. Srinivasan, A.; Furuta, H. *Acc. Chem. Res.* **2005**, 38, 10-20.
 11. Aviv-Harel, I.; Gross, Z. *Coord. Chem. Rev.* **2011**, 255, 717-736.
 12. Claessens, C. G.; Gonzalez-Rodriguez, D.; Rodríguez-Morgade, M. S.; Medina, A.; Torres, T. *Chem. Rev.* **2013**, 114, 2192-2277.
 13. Flamigni, L.; Gryko, D. T. *Chem. Soc. Rev.* **2009**, 38, 1635-1646.
 14. Brückner, Ch.; Akhigbe, J.; Samankumara, P. L. *Handbook of Porphyrin Science; With Applications to Chemistry, Physics, Materials Science, Engineering, Biology and Medicine; Vol. 31*, World Scientific, **2014**.
 15. Lash, T. D. *Chem. Rev.* **2016**, DOI: 10.1021/acs.chemrev.6b00326.
 16. Saito, S.; Osuka, A. *Angew. Chem. Int. Ed.* **2011**, 50, 4342-4373.
 17. Tanaka, T.; Osuka, A. *Chem. Rev.* **2016**, DOI: 10.1021/acs.chemrev.6b00371.
 18. Hata, H.; Shinokubo, H.; Osuka, A. *J. Am. Chem. Soc.* **2005**, 127, 8264-8265.
 19. Fujimoto, K.; Yorimitsu, H.; Osuka, A. *Chem. Eur. J.* **2015**, 21, 11311-11314.
 20. Fujimoto, K.; Oh, J.; Yorimitsu, H.; Kim, D.; Osuka, A. *Angew. Chem. Int. Ed.* **2016**, 55, 3196-3199.
 21. Adinarayana, B.; Thomas, A. P.; Suresh, C. H.; Srinivasan, A. *Angew. Chem. Int. Ed.* **2015**, 54, 10478-10482.
 22. Adinarayana, B.; Thomas, A. P.; Yadav, P.; Kumar, A.; Srinivasan, A. *Angew. Chem. Int. Ed.* **2016**, 55, 969-973.
 23. Grigg, R. *J. Chem. Soc. C.* **1971**, 3664-3668.
 24. Ganapathi, E.; Lee, W.-Z.; Ravikanth, M. *J. Org. Chem.* **2014**, 79, 9603-9612.
 25. Ganapathi, E.; Kuilya, S.; Chatterjee, T.; Ravikanth, M. *Eur. J. Org. Chem.* **2016**, 282-290.
-

List of Tables

1	Table 2.1	Selected Bond lengths in 23 , 23.H⁺ , 24 and 25 (Å)	54
2	Table 2.2	The dihedral angle (°) of various units deviate from the mean macrocyclic plane containing 14 inner core atoms	55
3	Table 2.3	Crystal data for 23 , 23.H⁺ , 24 and 25	63
4	Table 3.1	Selected bond angles in 4 (A) (Å)	78
5	Table 3.2	Selected bond angles in 4 (B) (Å)	79
6	Table 3.3	Selected bond angles in 5 (Å)	84
7	Table 3.4	Saddling dihedral angle (°) (χ) value in 5	87
8	Table 3.5	Crystal data for 4 and 5	93
9	Table 4.1	Saddling dihedral angle (χ) value in 11 , 12 and 13 (°)	113
10	Table 4.2	Crystal data for 11 , 12 and 12a	124
11	Table 5A.1	Saddling dihedral angle (χ) value in 6 , 7 , 8a and 9 (°)	142
12	Table 5A.2	Bond angles (°) around the metal ion in 8a and 9	142
13	Table 5A.3	Crystal data for 6 , 7 , 8a and 9	152
14	Table 5B.1	Bond length (Å) and Bond angle (°) around the metal ion in 22 , 22a and 24	169
15	Table 5B.2	Saddling dihedral angle (°) in 22 , 22a and 24	170
16	Table 5B.3	Selected bond angles in 24 (°)	170
17	Table 5B.4	Mean plane deviation (containing 25 atoms) of various units in 22 , 22a and 24	170
18	Table 5B.5	Crystal data for 20 , 21a , 22a and 24	176
19	Table 6.1	Crystal data for 14 , 19a and 20	201

List of Schemes

1	Scheme 1.1	One-pot synthesis of porphyrin	5
2	Scheme 1.2	Synthesis of porphycene	6
3	Scheme 1.3	One-pot synthesis of <i>meso</i> -aryl corrole	8
4	Scheme 1.4	Synthesis of subphthalocyanine	9
5	Scheme 1.5	Synthesis of tribenzosubporphine	9
6	Scheme 1.6	Synthesis of isocorrole	10
7	Scheme 1.7	Synthesis of iron norcorrole	10
8	Scheme 1.8	[3+1] MacDonald-type condensation reaction	13
9	Scheme 1.9	One-pot syntheses of carbaporphyrinoids	13
10	Scheme 1.10	Synthesis of benzocarbaporphyrins	14
11	Scheme 1.11	One-pot synthesis of azuliporphyrins	15
12	Scheme 1.12	Synthesis of neo-confused porphyrin	16
13	Scheme 1.13	Synthesis of <i>adj</i> -dicarbaporphyrin	17
14	Scheme 1.14	Synthesis of <i>opp</i> -dicarbaporphyrin	18
15	Scheme 1.15	Synthesis of <i>meta</i> -benziporphyrin	19
16	Scheme 1.16	Synthesis of tetraphenyl- <i>m</i> -benziporphyrin	19
17	Scheme 1.17	Synthesis of tetraaryl- <i>p</i> -benziporphyrin	20
18	Scheme 1.18	Synthesis of Tropiporphyrin	21
19	Scheme 1.19	Synthesis of pyriporphyrin	22
20	Scheme 1.20	Synthesis of <i>para</i> -confused pyriporphyrin	23
21	Scheme 1.21	Synthesis of <i>meta</i> -confused pyriporphyrin	23
22	Scheme 2.1	Synthesis of 23	42
23	Scheme 2.2	Synthesis of 23.H⁺ , 24 and 25	43
24	Scheme 3.1	Synthesis of 4 and 5	72
25	Scheme 4.1	Synthesis of 11 and 12	107
26	Scheme 5A.1	Metal-templated synthetic strategies for contracted Porphyrinoids	132
27	Scheme 5A.2	Synthesis of 6 and 7	134
28	Scheme 5A.3	Synthesis of 8 , 8a and 9	138
29	Scheme 5A.4	Plausible mechanism for the formation of 8 and 9	145
30	Scheme 5B.1	Syntheses of <i>meso-meso</i> linked corrole dimers	161
31	Scheme 5B.2	Synthesis of doubly (17) and triply (18) linked corrole dimers	162

32	Scheme 5B.3	Synthesis of anionic (20) and anionic exchanged (21a and 22a) corrole homologue complexes	164
33	Scheme 5B.4	Synthesis of 23 and 24	166
34	Scheme 6.1	Synthesis of azahomoporphyrin (2) and its ring contraction	182
35	Scheme 6.2	Synthesis of Ni ^{II} homoporphyrins	182
36	Scheme 6.3	Synthesis of free base homoporphyrins	183
37	Scheme 6.4	Metallation of homoporphyrins	183
38	Scheme 6.5	Synthesis of core-modified homoporphyrins	184
39	Scheme 6.6	Synthesis of carba-homoporphyrins 14 , 14a and 18	186
40	Scheme 6.7	Metallation of carba-homoporphyrins	190

List of Figures

1	Figure 1.1	Structures of biologically relevant porphyrinoids	4
2	Figure 1.2	Structures of porphyrin isomers	6
3	Figure 1.3	Contracted porphyrins	7
4	Figure 1.4	Core-modified porphyrinoids	11
5	Figure 1.5	Structures of carbaporphyrinoids	12
6	Figure 1.6	Structures of dicarbaporphyrinoids	16
7	Figure 1.7	Structures of expanded porphyrinoids	25
8	Figure 2.1	Structures of subporphyrin and subpyriporphyrin	37
9	Figure 2.2	Structures of triphyrin(2.1.1) derivatives	38
10	Figure 2.3	Structures of core-modified triphyrin(2.1.1) derivatives	39
11	Figure 2.4	Structures of triphyrin(n.1.1) analogues	39
12	Figure 2.5	Organoboron porphyrinoids	40
13	Figure 2.6	Carbatriphyrin(3.1.1) and their B ^{III} complexes	41
14	Figure 2.7	ESI-MS spectrum of a) 23 , b) 24 and c) 25	44
15	Figure 2.8	¹ H NMR spectrum of 23 (a), 24 (b) and 25 (c) in CDCl ₃	45
16	Figure 2.9	¹ H-NMR spectrum of 23.H ⁺ in CDCl ₃	46
17	Figure 2.10	Low temperature ¹ H-NMR spectrum of 23.H ⁺ in CDCl ₃	46
18	Figure 2.11	¹¹ B-NMR spectra of a) 24 and b) 25 in CDCl ₃	47
19	Figure 2.12	Single crystal X-ray structure of 23 . a) Top view and b) side view. The peripheral hydrogen atoms in a) & b) and <i>meso</i> -aryl groups in b) are omitted for clarity in the side view	48
20	Figure 2.13	Self-assembled dimers of 23	49
21	Figure 2.14	Single crystal X-ray structure of 23.H ⁺ . a) Top view and b) side view. The peripheral hydrogen atoms in a) & b) and <i>meso</i> -aryl groups in b) are omitted for clarity	50

22	Figure 2.15	Single crystal X-ray analysis of 23.H⁺ . a) self- assembled dimer and b) 1-D array	50
23	Figure 2.16	Single crystal X-ray structure of 24 . a) Top view, b) side view and c) geometry around the Boron center with bond length (Å) and angle (°).The peripheral hydrogen atoms in a) & b) and <i>meso</i> - aryl groups in b) are omitted for clarity	52
24	Figure 2.17	1-D arrays of 24	52
25	Figure 2.18	Single crystal X-ray structure of 25 . a) Top view, b) side view and c) geometry around the Boron center with bond length (Å) and angle (°).The peripheral hydrogen atoms in a) & b) and <i>meso</i> - aryl groups in b) are omitted for clarity	53
26	Figure 2.19	The single crystal X-ray analysis of 25 . The distance between the B ^{III} ion and the mean plane. The plane contains C5-C6-C10-C11-C15-C16- C16 (7 atoms)	54
27	Figure 2.20	Self-assembled dimer of 25	54
28	Figure 2.21	The electronic absorption spectrum of 23 , 24 and 25 in CH ₂ Cl ₂	56
29	Figure 2.22	The electronic absorption spectrum of 23 with various equivalents of TFA in CH ₂ Cl ₂	57
30	Figure 3.1	Structures of phenanthriporphyrin and its organophosphorus(V) complex	70
31	Figure 3.2	Structures of monocarbacorrole analogues	70
32	Figure 3.3	Structures of <i>adj</i> -dicarbacorrole and its organocopper(III) complex	71
33	Figure 3.4	ESI-MS spectrum of 4	73
34	Figure 3.5	The electronic absorption spectrum of 4 and 4.H⁺ (a) in CH ₂ Cl ₂ . Titration of 4 with various equivalents of TFA (b)	74
35	Figure 3.6	¹ H-NMR spectrum of 4 in CD ₂ Cl ₂	75
36	Figure 3.7	¹ H - ¹ H COSY spectrum of 4 in CD ₂ Cl ₂	76

37	Figure 3.8	Single crystal X-ray structure of 4 . a) Top view; b) side view and c) molecules present in the unit cell. The <i>meso</i> -aryl groups are omitted for clarity in the side view	77
38	Figure 3.9	Bond distances in 4 (A) and 4 (B) , (°)	78
39	Figure 3.10	Single crystal X-ray analyses of 4 . a) 1-D array in A ; b) 1-D array in B ; c) Self-assembled dimer and 1-D array between A and B	79
40	Figure 3.11	ESI-MS spectrum of 5	80
41	Figure 3.12	The normalized electronic absorption spectrum of 4 and 5 in CH ₂ Cl ₂	81
42	Figure 3.13	¹ H-NMR spectrum of 5 in CD ₂ Cl ₂	82
43	Figure 3.14	¹ H - ¹ H COSY spectrum of 5 in CD ₂ Cl ₂	82
44	Figure 3.15	Single crystal X-ray analysis of 5 . a) Top view; b) side view; c) self-assembled dimer and d) Bond length distances in 5 (Å)	84
45	Figure 3.16	Single crystal X-ray analysis of 5 . a) 1-D array and b) 2-D array	85
46	Figure 3.17	Variable temperature ¹ H-NMR spectrum of 5 in DMSO-d ₆	88
47	Figure 3.18	EPR spectrum of 5 in a) liquid state (toluene) b) solid state at variable temperature	88
48	Figure 3.19	¹ H-NMR spectrum of 5 in Pyridine-d ₅ (*residual solvent peak)	89
49	Figure 4.1	(a) Structures of dipyrins(1-3) and tripyrrinone (4); (b) Fluorescence images upon addition of Zn ^{II} to the probes and (c) Zn ^{II} imaging in living KB cells using probe 4	101
50	Figure 4.2	(a) Proposed sensing mechanism for detecting Zn ^{II} by using probe 5 ; (b) The fluorescence image of 5 upon addition of various metal ions under a portable UV lamp	102

51	Figure 4.3	Structures of phenanthroline (7) and carbazole-pyridine (8) embedded porphyrins	104
52	Figure 4.4	Structures of subpyriporphyrin (9) and pyricorrole (10)	105
53	Figure 4.5	Structures of Bipyricorrole (11) and its Zn ^{II} complexes (12 and 13).	106
54	Figure 4.6	ESI-MS spectrum of 11	107
55	Figure 4.7	ESI-MS spectrum of 12	108
56	Figure 4.8	¹ H-NMR spectrum of 11 in CDCl ₃	109
57	Figure 4.9	¹ H - ¹ H COSY spectrum of 11 in CDCl ₃	109
58	Figure 4.10	¹ H-NMR spectrum of 12 in CDCl ₃	109
59	Figure 4.11	¹ H - ¹ H COSY spectrum of 12 in CDCl ₃	110
60	Figure 4.12	Single crystal X-ray structure of 11 . a) Top view and b) side view and c) bond lengths (Å). The <i>meso</i> -aryl groups are omitted for clarity in (b) and (C)	111
61	Figure 4.13	1-D array of 11	111
62	Figure 4.14	Single crystal X-ray structure of 12 . a) Top view, b) side view and c) bond lengths (Å). The <i>meso</i> -aryl groups are omitted for clarity in (b) and (c)	113
63	Figure 4.15	Hexameric structure of 12	114
64	Figure 4.16	The electronic absorption and emission spectrum of 11 and 12 in CH ₃ OH along with absorption (left) and emission (right) color changes	115
65	Figure 4.17	Sensing properties of 11 . a) The emission spectral changes upon addition of Zn ^{II} in CH ₃ OH solution; b) The Job's plot for the complexation; c) Metal ion selectivity of 11 in the presence of various metal ions and d) Competitive recognition study of 11 with 10 equiv. of Zn ^{II} in presence of 100 equiv. of other metal ions	117

66	Figure 4.18	Single crystal X-ray structure of 7 . a) Top view, b) side view and c) bond lengths in 13 (Å). The <i>meso</i> -aryl groups are omitted for clarity in (b) and (c)	118
67	Figure 5A.1	ESI-MS spectrum of 6	135
68	Figure 5A.2	¹ H-NMR spectrum of 6 and 7 in CDCl ₃	136
69	Figure 5A.3	The single crystal X-ray structures of 6 (a & b) and 7 (c & d). The <i>meso</i> -aryl groups in (b) & (d) and the counter anion in (d) are omitted for clarity	137
70	Figure 5A.4	ESI-MS spectrum of 8	139
71	Figure 5A.5	ESI-MS spectrum of 9	139
72	Figure 5A.6	¹ H-NMR spectrum of 8 and 9 in CDCl ₃	140
73	Figure 5A.7	The single crystal X-ray structures of 8a (a & b) and 9 (c & d). The <i>meso</i> -aryl groups in (d) are omitted for clarity	141
74	Figure 5A.8	Bond lengths (Å) in 6 (a), 7 (b), 8a (c) and 9 (d). The anionic ligands in b), c) and d) and <i>meso</i> -aryl units in (a-d) are omitted for clarity	143
75	Figure 5A.9	The electronic absorption spectrum of 6 and 7 in CH ₂ Cl ₂	144
76	Figure 5A.10	The electronic absorption spectrum of 8a and 9 in CH ₂ Cl ₂	144
77	Figure 5A.11	Emission spectrum of 2 and 5 in CH ₂ Cl ₂	145
78	Figure 5B.1	Structures of porphyrin arrays	158
79	Figure 5B.2	Structures of β-β linked corrole dimer and their fused derivatives	160
80	Figure 5B.3	¹ H NMR spectrum of 20 , 21a and 22a in CDCl ₃	164
81	Figure 5B.4	Single crystal X-ray structure of 20 (a & b), 21a (c & d) and 22a (e & f). The <i>meso</i> -phenyl groups in 20 , 21a & 22a are omitted for clarity in the side view	165
82	Figure 5B.5	¹ H NMR spectrum of 23 and 24 in CDCl ₃	167
83	Figure 5B.6	Single crystal X-ray structure of 24 . a) Top view, b) side view and c) bond lengths (Å). The <i>meso</i> -	168

		aryl groups and counter anions are omitted for clarity in b) and c)	
84	Figure 5B.7	The electronic absorption spectrum of 21a and 23 in CH ₂ Cl ₂	171
85	Figure 5B.8	The electronic absorption and emission spectrum of 22a and 24 in CH ₂ Cl ₂	172
86	Figure 6.1	Structures of homoporphyrins A-D	181
87	Figure 6.2	ESI-MS spectrum of 14	187
88	Figure 6.3	ESI-MS spectrum of 18	187
89	Figure 6.4	¹ H NMR spectrum of 14 and 18 in CDCl ₃	188
90	Figure 6.5	Single crystal X-ray structure of 14 . a) Top view; b) side view and c) self-assembled dimer. The <i>meso</i> -aryl groups are omitted for clarity in the side view	189
91	Figure 6.6	ESI-MS spectrum of 19	191
92	Figure 6.7	ESI-MS spectrum of 20	191
93	Figure 6.8	¹ H NMR spectrum of 19 and 20 in CDCl ₃	192
94	Figure 6.9	Single crystal X-ray structure of 19a and 20 . a), c) Top view; b), d) side view. The <i>meso</i> -aryl groups are omitted for clarity in the side view	193
95	Figure 6.10	Bond length distances in 14 , 19a and 20 (Å)	193
96	Figure 6.11	Electronic absorption spectrum of 14 and 18 in CH ₂ Cl ₂	194
97	Figure 6.12	Electronic absorption spectrum of 19 and 20 in CH ₂ Cl ₂	195

List of Abbreviations

^1H NMR	Proton Nuclear Magnetic Resonance
^{13}C NMR	Carbon-13 Nuclear Magnetic Resonance
^{11}B NMR	Boron-11 Nuclear Magnetic Resonance
^{19}F NMR	Fluorine-19 Nuclear Magnetic Resonance
^{31}P NMR	Phosphorus-31 Nuclear Magnetic Resonance
EPR	Electron Paramagnetic Resonance
UV-Vis	Ultraviolet–Visible
ESI	Electrospray Ionization
GOF	Goodness of Fit
CCDC	Cambridge Crystallographic Data Centre
DFT	Density Functional Theory
DDQ	2,3-Dichloro-5,6-dicyano-1,4-benzoquinone
CH_2Cl_2	Dichloromethane
CHCl_3	Chloroform
EtOAc	Ethyl acetate
CH_3CN	Acetonitrile
CH_3OH	Methanol
THF	Tetrahydrofuran
$\text{ClCH}_2\text{CH}_2\text{Cl}$	1,2-Dichloroethane
DMF	Dimethylformamide
$\text{C}_6\text{F}_5\text{COCl}$	Benzoyl chloride
$\text{CH}_3\text{SO}_2\text{Cl}$	Methanesulfonyl chloride
NaBH_4	Sodium borohydride
$\text{C}_6\text{F}_5\text{CHO}$	Pentafluorobenzaldehyde
POCl_3	Phosphorus oxychloride
PhMgBr	Phenylmagnesium bromide
PhBCl_2	Dichlorophenyl borane
TEA	Triethylamine
DMAP	4-Dimethylaminopyridine
TMP	Tetramethylpiperidine
NCP	N-confused porphyrin

CO	Carbon monoxide
HCl	Hydrogen chloride
TFA	Trifluoroacetic acid
BF ₃ .Et ₂ O	Boron trifluoride diethyl etherate
<i>p</i> -TSA	<i>para</i> -toluenesulphonic acid
TMS	Tetramethylsilane
CDCl ₃	Deuterated chloroform
CD ₂ Cl ₂	Dideuteromethylenechloride
CD ₃ CN	Deuterated acetonitrile
CD ₃ OD	Deuterated methanol
Toluene-d ₈	Deuterated toluene
DMSO- <i>d</i> ₆	Hexadeuterodimethyl sulfoxide
FB	Free-Base
TLC	Thin Layer Chromatography
Na ₂ SO ₄	Sodium sulphate
Zn(OAc) ₂	Zinc acetate
Cu(OAc) ₂	Copper acetate
Pd(OAc) ₂	Palladium acetate
Zn(ClO ₄) ₂	zinc perchlorate
Ag(PF ₆)	silver hexafluorophosphate
Ag(OTf)	silver triflate
[Rh(CO) ₂ Cl] ₂	Di- μ -chloro-tetracarbonyldirhodium(I)
NaBF ₄	sodium tetrafluoroborate
FeCl ₃	Iron(III) chloride
PIFA	[Bis(trifluoroacetoxy)iodo]benzene
BAHA	Tris(4-bromophenyl)ammoniumyl hexachloroantimonate

CHAPTER 1

Derivatives of porphyrins designed by Nature and synthetic Chemist

1.1	Porphyrin	3
1.2	Synthesis	4
1.3	Modifications of porphyrins	5
1.3.1	Porphyrin Isomers	5
1.3.2	Contracted porphyrins	7
1.3.2.1	Corroles	7
1.3.2.2	Subphthalocyanines	9
1.3.2.3	Subporphyrins	9
1.3.2.4	Isocorroles	10
1.3.2.5	Norcorrole	10
1.3.3	Core-modified porphyrins	11
1.3.3.1	Carbaporphyrinoids	11
1.3.3.1.1	Five-membered ring embedded carba derivatives	13
1.3.3.1.2	Six-membered ring embedded carba derivatives	18
1.3.3.1.3	Seven-membered ring embedded carba derivatives	20
1.3.3.2	Pyridine embedded porphyrinoids	21
1.3.3.2.1	Pyriporphyrins	21
1.3.3.2.2	Confused pyriporphyrins	22
1.3.4	Expanded porphyrins	24
1.4	Conclusion and objectives of the present thesis	26
1.5	References	29

1.1 Porphyrins

Porphyrins are tetrapyrrolic macrocycles, exist in nature in the form of heme and other derivatives and are termed as "pigments of life" (Figure 1.1).¹ The derivatives of porphyrins and related macrocycles are involved in numerous biological functions such as; i) oxygen transport and storage by hemoglobin and myoglobin (**1**); ii) several electron transport processes mediated by cytochromes and iii) the harvesting of light energy for photosynthesis, a) in green plants by chlorins (**2**) in the chlorophylls, b) in bacteria by bacteriochlorophyll (**3**).² They have also been proved as photosensitizers for photodynamic therapy^{3,4} and found applications in many research fields ranging from biology, material sciences, electronics, catalysis to medicine.⁵

In porphyrins, four pyrrole rings are linked by four methylene carbons and are highly conjugated systems.⁵ The term porphyrin is derived from the Greek word "porphura" means purple. Porphyrins and their derivatives are intense in color and show strong absorption bands in the visible region. The Soret band at around 400 nm and weak Q-bands in the range of 450-700 nm. Though they are 22π electron systems, the smallest conjugation pathway contains 18π electrons and hence considered as Hückel aromatic molecules. The aromatic nature of the porphyrin reflects in ^1H NMR studies, where the inner NH protons appear in the shielded region and *meso*-protons as well as β -pyrrolic protons resonate at deshielded region. The coordination sphere contains two imine and two amine nitrogens thus it can act as a dianionic tetradentate square planar ligand. The macrocycle cavity size is ideal to bind almost all metal ions in the "pocket" of porphyrin ring system. The richness of porphyrin chemistry has inspired researchers to synthesis and study the novel porphyrin analogues in past three decades.⁵⁻⁷

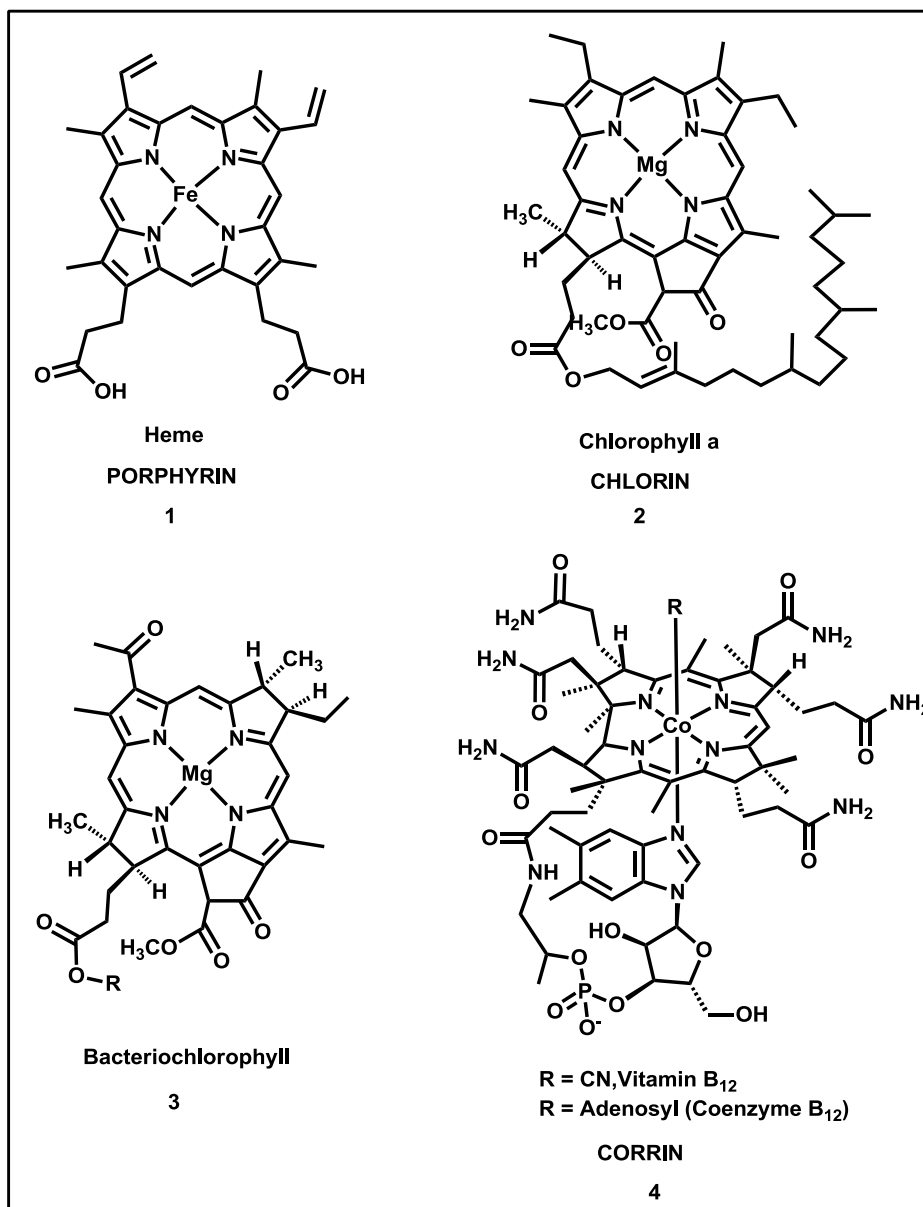
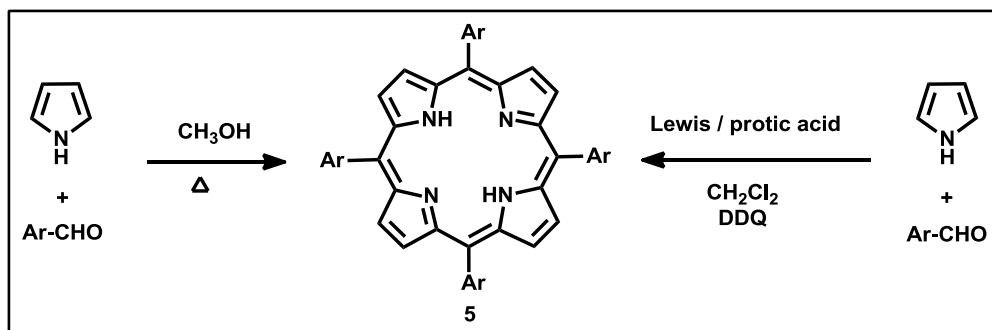


Figure 1.1: Structures of biologically relevant porphyrinoids.

1.2 Synthesis

The synthesis of porphyrin **5** started in 1935 by Rothmund,⁸ which describe the condensation of pyrrole and aldehydes in methanol at various temperatures. Since then, several improved synthetic methodologies have been developed which includes i) the condensation of pyrrole and benzaldehyde in propionic acid under open air condition by Adler and Longo;⁹ ii) the protic or Lewis acid catalyzed condensation of pyrrole and

aryl aldehydes followed by oxidation with Chloranil or 2,3-Dichloro-5,6-dicyano-1,4-benzoquinone (DDQ) (Scheme 1.1) resulted in the synthesis of porphyrin in good yields reported by Lindsey and co-workers, and iii) MacDonald [2+2] condensation of a dipyrromethane and aldehyde for the synthesis of the less symmetrical porphyrins.¹¹



Scheme 1.1: One-pot synthesis of porphyrin.

1.3 Modifications of porphyrins

The unique properties of porphyrin remain fundamental interest for the researchers in various fields. This motivates to develop the novel porphyrinoids with several distinct types of modifications in the porphyrin core for various applications. However, the most important modifications are presented in the following sections.

1.3.1 Porphyrin Isomers

Isomeric porphyrins are porphyrin analogues having the same molecular formula and can be obtained by rearranging pyrrole and *meso*-carbons in porphyrin structure. These are further classified on the basis of "nitrogen in" and "nitrogen out" isomers. The "nitrogen in" porphyrin isomers are porphycene (2.0.2.0) **6**,¹² corpphycene (2.1.0.1) **7**,¹³ hemiporphycene **8** (2.1.1.0),¹⁴ isoporphycene **9** (3.0.1.0)¹⁵ and the "nitrogen out" isomer is N confused porphyrin **10** (NCP)^{16,17} (Figure 1.2). Among these isomers porphycene **6** and N-confused porphyrin **10** have emerged as attractive synthetic targets

for versatile coordination chemistry. The first synthetic porphyrin isomer, porphycene was reported in 1986 by Vogel and co-workers.¹² The synthetic methodology involves reductive McMurray coupling reaction between 5,5'-diformyl-2,2'-bipyrrole subunits followed by DDQ oxidation (Scheme 1.2). Porphycene is the most stable isomer and shows porphyrin like 18π aromaticity. The trivial name porphycene was proposed by Vogel because of their structural features reminiscent to those of porphyrin and acenes.

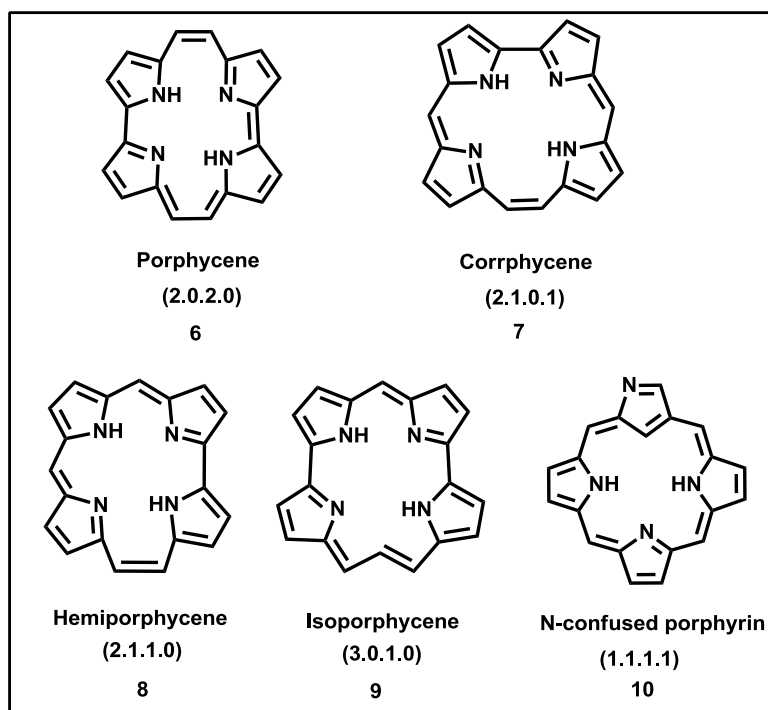
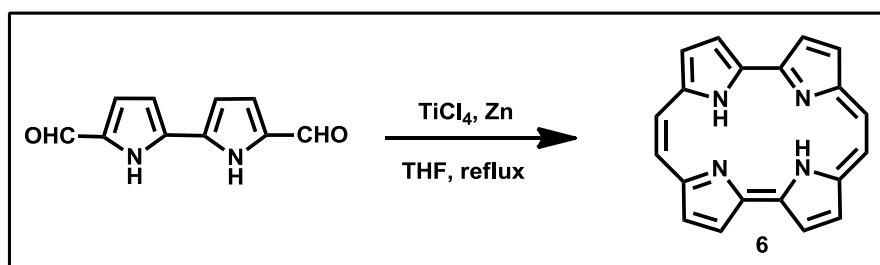


Figure 1.2: Structures of porphyrin isomers.



Scheme 1.2: Synthesis of porphycene.

1.3.2 Contracted porphyrins

The contracted porphyrin contains smaller internal cavity with at least one or more *meso*-carbons or one pyrrole ring less as compared to porphyrin frame work. Several contracted porphyrins have been synthesized and explored their chemistry, which include notable examples such as corroles **11**, subphthalocyanines **12**, subporphyrins **13**, isocorroles **14** and norcorroles **15** (Figure 1.3)

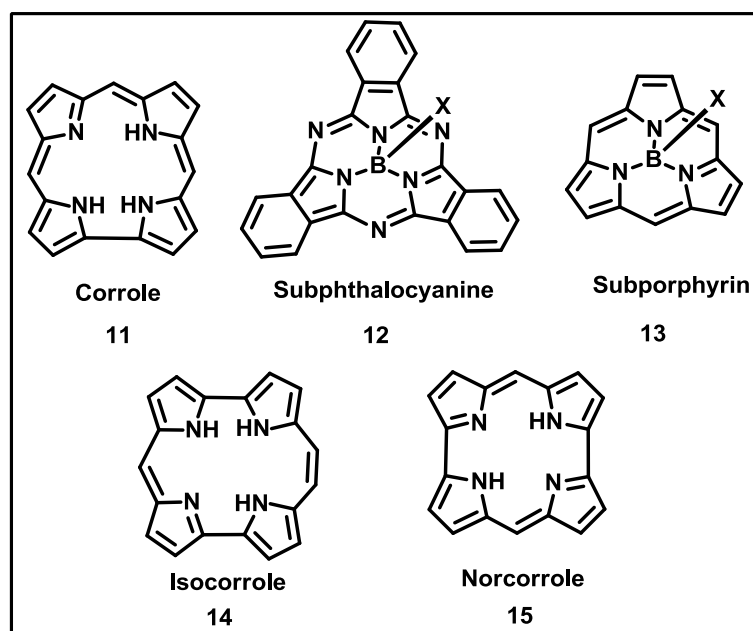
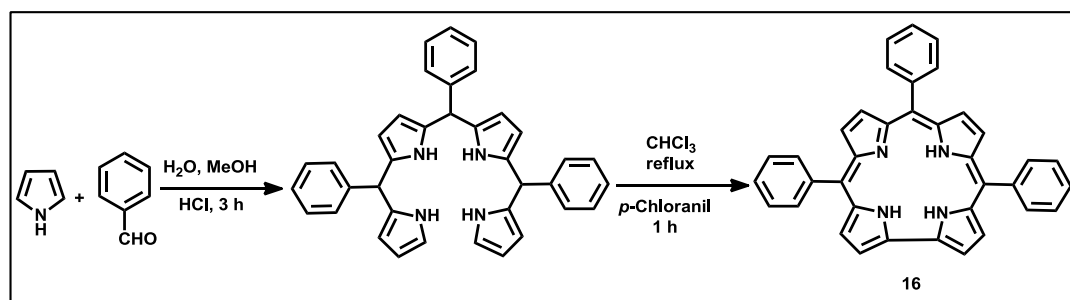


Figure 1.3: Contracted porphyrins.

1.3.2.1 Corroles

The chemistry of contracted porphyrins begins with corrole **11** system. During the structural elucidation of vitamin B₁₂ **4**, it was revealed that the structure was similar to naturally occurring tetrapyrrolic porphyrin macrocycle, with one *meso* carbon unit less. Later the vitamin B₁₂ was found to have a corrin ring.^{18,19} Soon after the synthesis of corrole by Jonson and Kay in 1965, it was clarified that corrole was an oxidized form of corrin system and can act as an intermediate between porphyrins and corrins.^{20,21} The most distinct structural difference between porphyrin and corrole is that one *meso*-

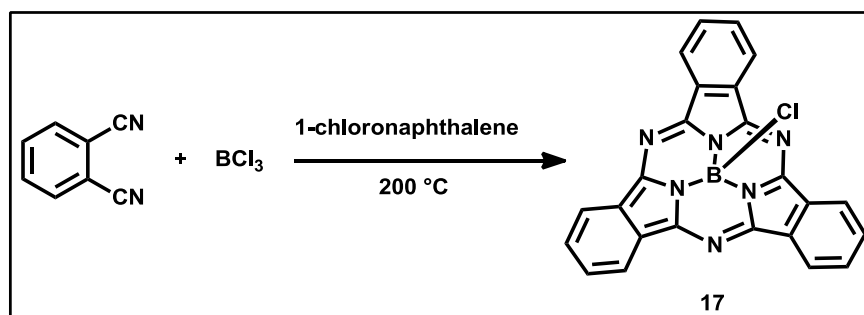
carbon less resulting in two pyrroles are connected through direct pyrrole-pyrrole linkage. These are stable 18π aromatic systems. The presence of three protons in the inner core, it can act as a trianionic ligand and stabilizes the metal ions in their higher oxidation states. The UV-visible spectra of corroles display a close relationship to that of porphyrin and show strong Soret-type band at around 400 nm and weaker Q-bands in the region of 500-600 nm. ^1H NMR spectra of corrole exhibit strong diatropic ring current akin to porphyrin clearly indicate the aromaticity in corroles. The *meso*-protons and β -pyrrolic protons are in the deshielded region and resonated at 7.5 to 9.5 ppm, while the inner NH protons are in the shielded region and appeared at -2.00 to -3.00 ppm. Even though the first synthesis of corrole was reported in the year 1965 by Jonson and co-workers, the chemistry of corroles remains in its infancy and far behind from porphyrins due to their synthetic limitations.²¹ The corrole (**16**) research received much attention after introducing the efficient synthetic methods by different groups Gross *et al.*, Paolesse *et al.*, and Gryko *et al.*²²⁻²⁴ The most important and widely followed synthetic report include one-pot condensation of pyrrole and aldehyde by Gryko and co-workers in 2006 which is shown in Scheme 1.3.²⁵ The corrole ligand and its high-valent metal complexes have been explored as molecular catalysts, sensors, dye-sensitized solar cells and in medicinal research.



Scheme 1.3: One-pot synthesis of *meso*-aryl corrole.

1.3.2.2 Subphthalocyanines

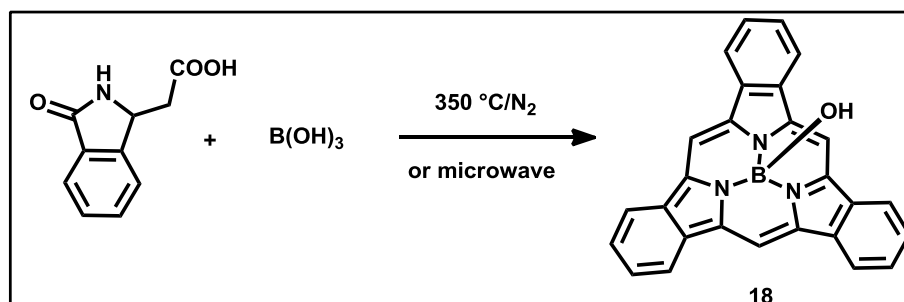
Subphthalocyanine (**12**) is one of the widely studied 14π aromatic contracted phthalocyanine. These are known to be a tetra coordinated boron derivatives. The first synthesis was reported by Meller and Ossko in 1972 as shown in Scheme 1.4.²⁶ The unexpected product (**17**) was formed during the attempt to prepare boron complex of phthalocyanine derivative.



Scheme 1.4: Synthesis of subphthalocyanine.

1.3.2.3 Subporphyrins

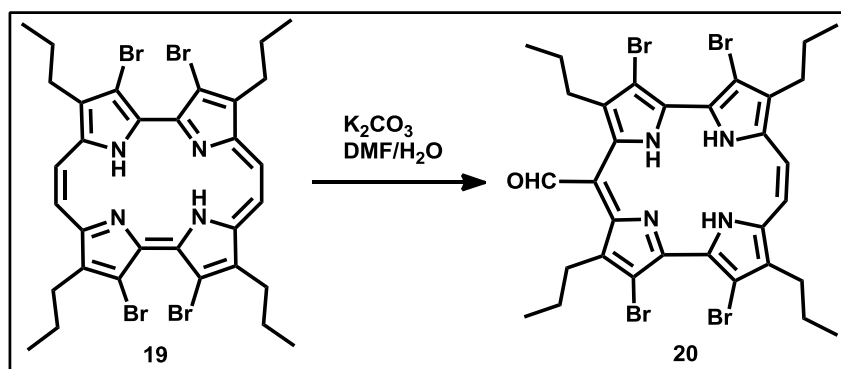
Subporphyrins **13** are the genuine ring contracted porphyrins. The first subporphyrin, tribenzosubporphine **18**, which is the porphyrinic counterpart of subphthalocyanine. It was first synthesized by the group of Osuka in 2006 as the B^{III} complex (Scheme 1.5) under harsh reaction conditions.²⁷ Since then, a series of subporphyrin derivatives were synthesized and studied their peculiar properties in various fields.²⁸



Scheme 1.5: Synthesis of tribenzosubporphine.

1.3.2.4 Isocorroles

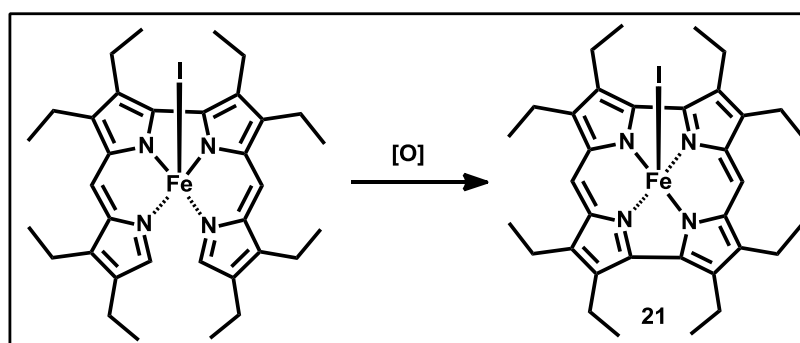
Isocorrole **14** is a stable corrole isomer and has structural similarities with porphycene by removal of one of its *meso*-carbon atoms. It was first isolated by Vogel and co-workers in 1990.²⁹ The isocorrole **20** was synthesized from porphycene **19** through ring contraction process (Scheme 1.6).³⁰



Scheme 1.6: Synthesis of isocorrole.

1.3.2.5 Norcorrole

Norcorrole **15** is a contracted porphyrinoid and lacks two *meso*-carbon atoms from a regular porphyrin. On the basis of the Hückel rule, the norcorrole is a 16π -electronic system and exhibits antiaromatic character. The first norcorrole-iron(III) **21** complex was reported by Bröring *et al.* in 2008 (Scheme 1.7).³¹ The compound is found to be unstable and tends to dimerize spontaneously.



Scheme 1.7: Synthesis of iron norcorrole.

1.3.3 Core-modified porphyrins

These porphyrin analogues are achieved by replacing one of the pyrrole rings by other heterocyclic rings such as furan, thiophene, selenophene, tellurophene, N-CH₃ pyrrole, five membered ring with 'Si' or 'P' atom (**22**) and pyridine or carbocyclic rings (e.g. **23-24**) from the regular porphyrin (Figure 1.4). These modifications provide great opportunity to study the wide range of chemistry and generate potential applications in various fields.⁵ In this section, the synthesis of carbaporphyrin and its derivatives are mainly highlighted.

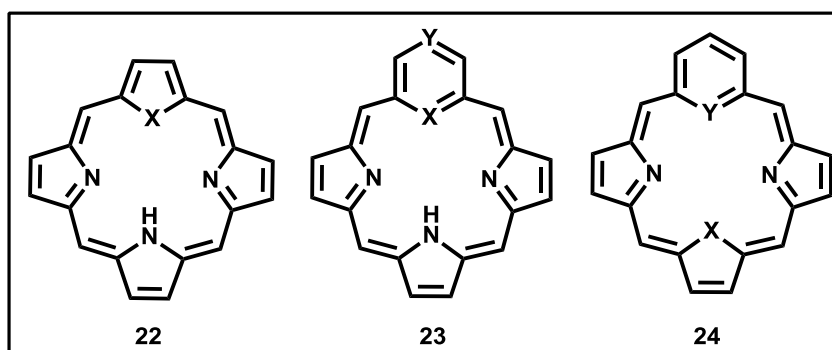


Figure 1.4: Core-modified porphyrinoids.

1.3.3.1 Carbaporphyrinoids

Carbaporphyrinoids (**25-32**) are porphyrin analogues in which one or more pyrrole nitrogens in the coordination sphere is replaced by one or more carbon atom. The inner C-H can be part of either carbocyclic or heterocyclic rings. The incorporation of carbocyclic or heterocyclic rings in porphyrins leads to produce distinct physical and chemical properties. The carbaporphyrinoid (Figure 1.5) systems provide a unique platform to study aromaticity, unusual reactivity and act as versatile ligands, which offers to study the organometallic chemistry and weak metal C-H bond interactions in the macrocyclic environment. These carbaporphyrinoids can be classified according to; i) the size of the carbocyclic or heterocyclic rings and ii) the number of carbon atoms

present in the macrocycle. Therefore, by using efficient synthetic methodologies many carbaporphyrinoids have been developed and studied their peculiar properties.

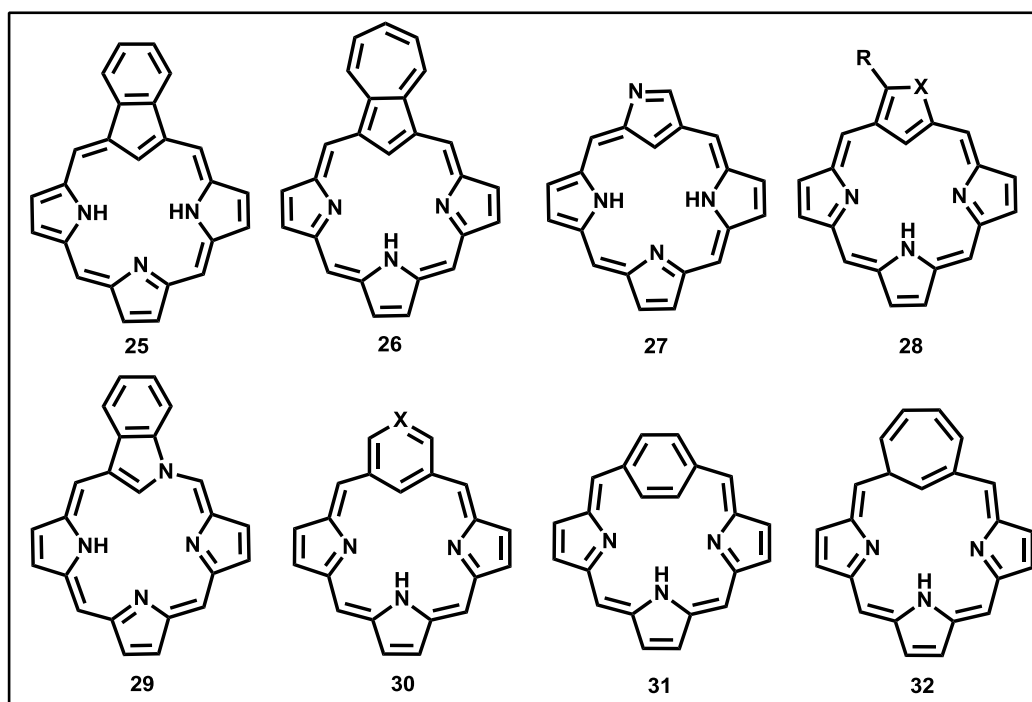
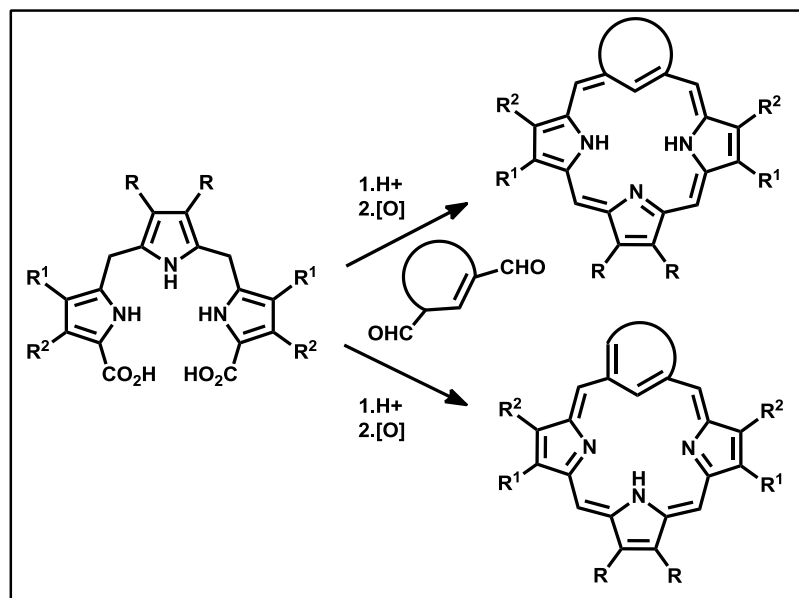


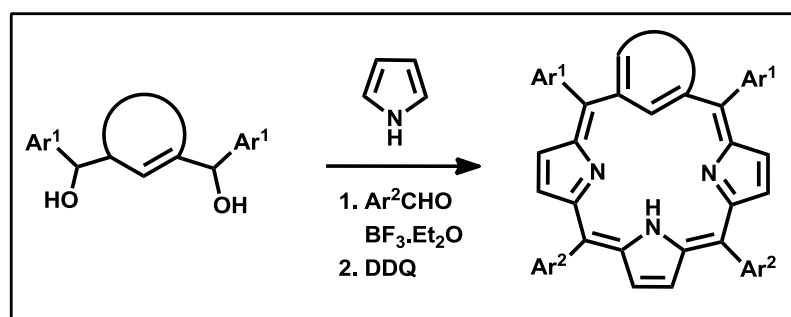
Figure 1.5: Structures of carbaporphyrinoids.

Synthetic methodologies

Synthesis of carbaporphyrinoids is adopted in few principle synthetic pathways. Initially the synthesis of carbaporphyrinoids relied on stepwise MacDonald [3+1] condensation.³² In this method, acid-catalyzed condensation of tripyrrane derivatives with aromatic dialdehydes followed by oxidation (Scheme 1.8) produces the corresponding carbaporphyrinoid. This method has been proven to be effective for the synthesis of novel porphyrin analogues. The second synthetic approach is one-pot synthesis where the pyrrole and aromatic dicarbinol reacts in the presence of acid followed by oxidation (Scheme 1.9).^{33,34}



Scheme 1.8: [3+1] MacDonald-type condensation reaction.



Scheme 1.9: One-pot syntheses of carbaporphyrinoids.

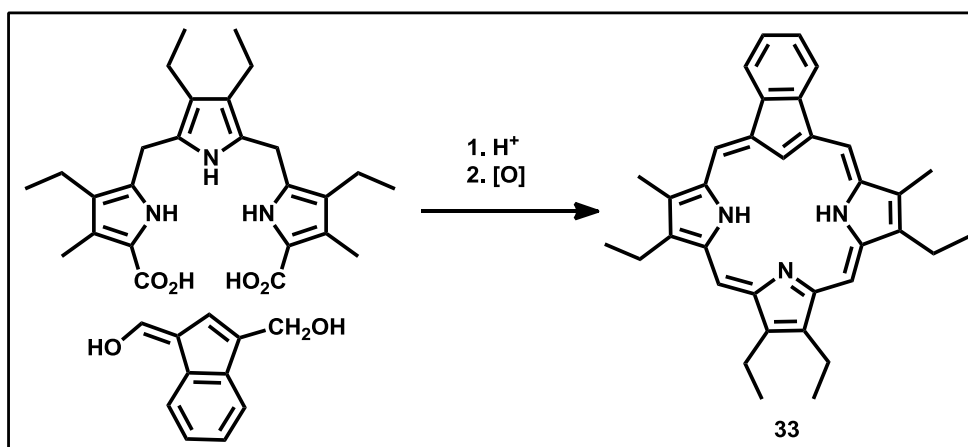
1.3.3.1.1 Five-membered ring embedded carba derivatives

The replacement of pyrrole by cyclopentadienyl moiety in regular porphyrins generates carbaporphyrin analogues. These carbaporphyrins can represent a link between annulenes and porphyrins. The synthesis and coordination properties of series of carbaporphyrins are mentioned below.

a) Benzocarbaporphyrins

The first benzocarbaporphyrin **33** was synthesized by Berlin *et al.* using MacDonald [3+1] condensation method. The reaction of tripyrrane with

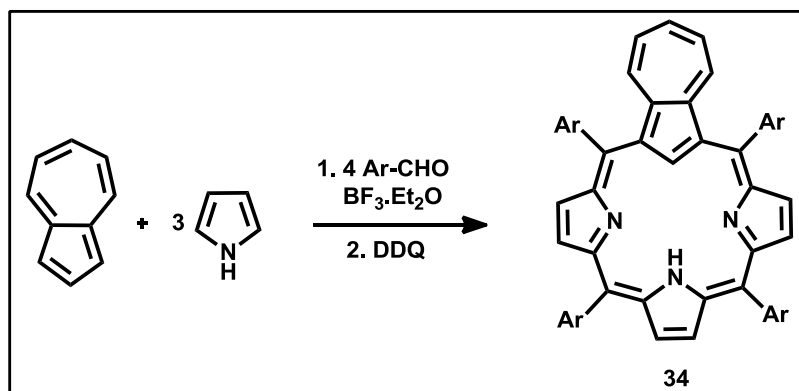
indenedicarbaldehyde (Scheme 1.10).³⁵ Because of synthetic feasibility benzocarbaporphyrin has become the most studied system in the carbaporphyrin series. The absorption and NMR spectral analysis, this analogue closely resembles to the porphyrin and is considered to be a benzo[18]annulene. It acts as a trianionic ligand and it stabilizes Ag^{III} and Au^{III} organometallic complexes. In addition, *N*-, *C*-alkylated Pd^{II} complexes and core-modified benzoporphyrins were reported.³⁴



Scheme 1.10: Synthesis of benzocarbaporphyrins.

b) Azuliporphyrins

Azuliporphyrins **34** are carbaporphyrins with reduced aromatic character as compared to benzocarbaporphyrins. These are first carbaporphyrins and synthesized by [3+1] MacDonald condensation. Lash *et al.* reported the synthesis of azuliporphyrin by reaction of tripyrrane with azulene dialdehyde.³³ The improved synthesis was reported by same group, where they adopted the Lindsey type condensation reaction by using azulene, pyrrole and benzaldehyde for the synthesis of *meso*-tetraphenylazuliporphyrin.³⁶ The diatropicity of the azuliporphyrin was significantly increased upon protonation with TFA. The dianionic coordination sphere was shown to act as organometallic ligand to generate a stable Ni^{II}, Pd^{II} and Pt^{II} complexes.

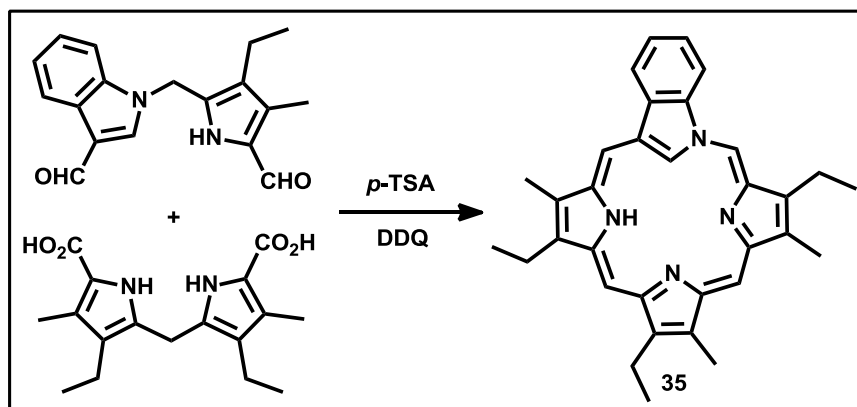


Scheme 1.11: One-pot synthesis of azuliporphyrins.

c) Confused porphyrins

Confused porphyrins can be achieved by changing the bonding mode of heterocyclic rings in the normal porphyrins. For example, in normal porphyrins, the pyrrole rings are connected through α , α' -linkage whereas in confused porphyrins one or more pyrrole rings are linked by α , β' -linkage. Confused porphyrins are further classified according to their heterocyclic counterparts, such as N-confused, O-confused, S-confused, Se-confused and their hetero-analogues.^{34,37} Among the confused porphyrins, N-confused porphyrins are of particular research interest in many fields. The first N-confused porphyrin was independently synthesized in 1994 by Furuta and Latos-Grażyński research groups.^{16,17} Since then, series of other confused derivatives have been developed and exploited their coordination properties. Recently neo-confused porphyrins **35** were synthesized by Lash and co-workers by reacting the 2,2-linked dipyrane and an intriguing 1,2-linked indol dipyrromethane derivative through modified [2+2] pathway (Scheme 1.12).³⁸ The pyrrole nitrogen atom is connected to a *meso*-carbon atom (N-C). These are considered as the youngest member of constitutional porphyrin isomers and it shows 18π electron delocalisation as porphyrins. The presence of C-H in coordination core can act as organometallic ligand and

forms complexes with Ni^{II} and Pd^{II}.³⁴



Scheme 1.12: Synthesis of neo-confused porphyrin.

d) Dicarbaporphyrins and related systems

Dicarbaporphyrins (**36-41**) are porphyrin analogues with two carbons present in the coordination core. These can be further classified according to the position of carbon in internal core, where it can be adjacent or opposite to each other. Here, the doubly-N-confused porphyrins (**36, 37**), benzocarpa- and azuliporphyrins (**38-41**)

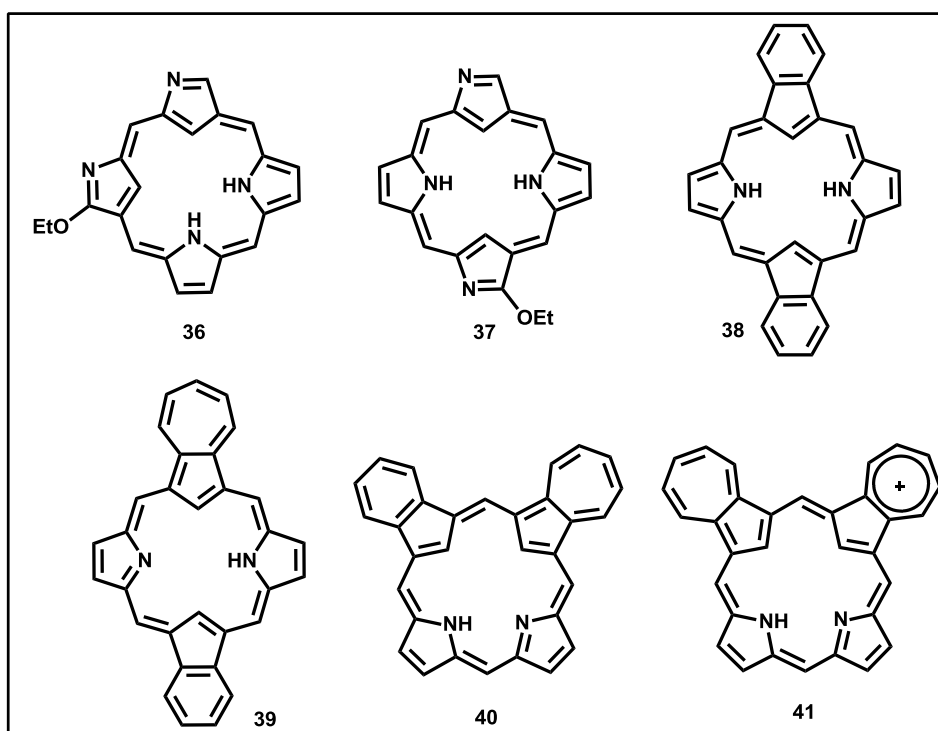
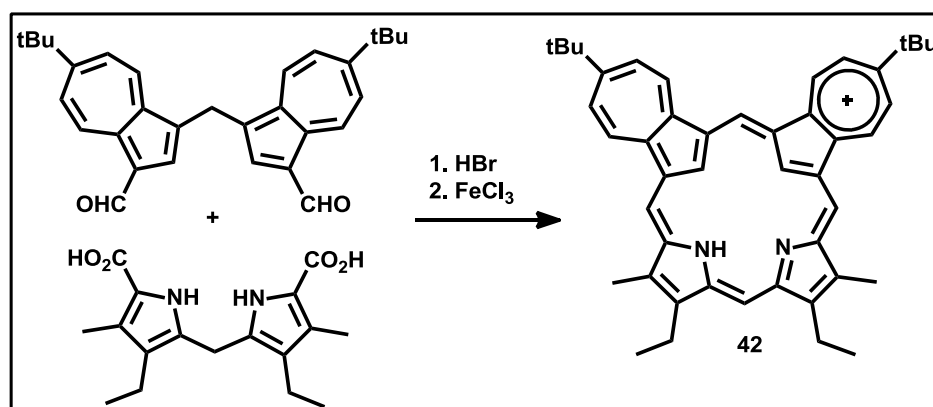


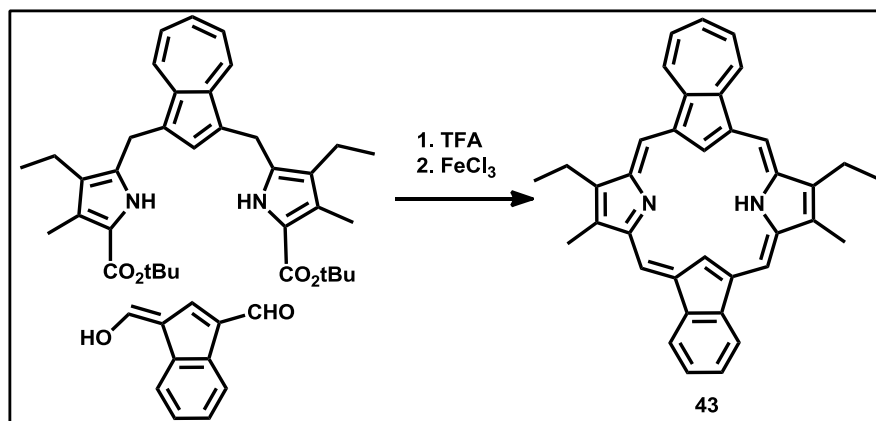
Figure 1.6: Structures of dicarbaporphyrinoids.

(Figure 1.6) and their hetero-analogues are part of these systems. The chemistry of dicarbaporphyrins are started with doubly N-confused porphyrins such as *cis*- (**36**) and *trans*- (**37**) Doubly N-confused porphyrins.^{39,40} Both isomers can act as a trianionic ligands and forms organo-copper(III), organo-silver(III) complexes.³⁴

The true dicarbaporphyrins are achieved by introducing the two indene or two azulene or both in porphyrin framework by Lash group.⁴¹⁻⁴⁴ Which are either *opp*-dicarbaporphyrins (**38, 39**) or *adj*-dicarbaporphyrins (**40, 41**). For the synthesis of *adj*-dicarbaporphyrin **42** modified [2+2] MacDonald-type condensation of dipyrromethane with dialdehyde indene derivative (Scheme 1.13) is mainly adopted. Whereas *opp*-dicarbaporphyrin **43** is obtained by modified [3+1] MacDonald condensation approach using fulvene dialdehyde and azulitripyrrane (Scheme 1.14). The Pd(II) complexation of dicarba derivatives is recently known however, the coordination chemistry of these ligands are yet to be explored. The hetero analogues of dicarbaporphyrins are also synthesized and studied.⁴⁵



Scheme 1.13: Synthesis of *adj*-dicarbaporphyrin.



Scheme 1.14: Synthesis of *opp*-dicarbaporphyrin.

1.3.3.1.2 Six-membered ring embedded carba derivatives

Introduction of six-membered rings into the porphyrins brings the arene chemistry in a macrocyclic environment which leads to the distinguishable physical and chemical properties. Series of six-membered rings embedded porphyrins are reported such as benziporphyrins, naphthiporphyrins, anthriporphyrins, pyridine related porphyrins and their hetero-analogues. Among these, benziporphyrin is widely studied carbaporphyrinoid.

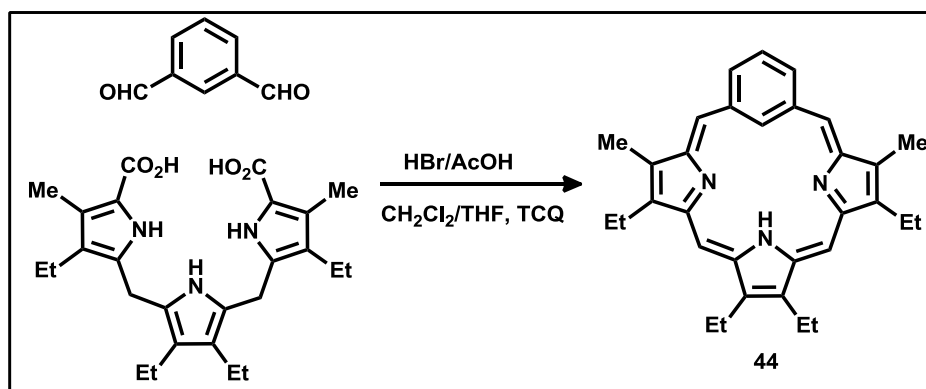
i) Benziporphyrin

Benziporphyrins are porphyrin analogues in which one of the pyrrole rings is replaced by benzene unit. These analogues are further classified according to the bonding motif of benzene in macrocycle where it can be 1,3- or 1,4- linkage and referred as a *meta*- or *para*-benziporphyrins, respectively. The properties of the macrocycle vary depending on the nature of bonding motif (*m*-/*p*-).⁴⁶

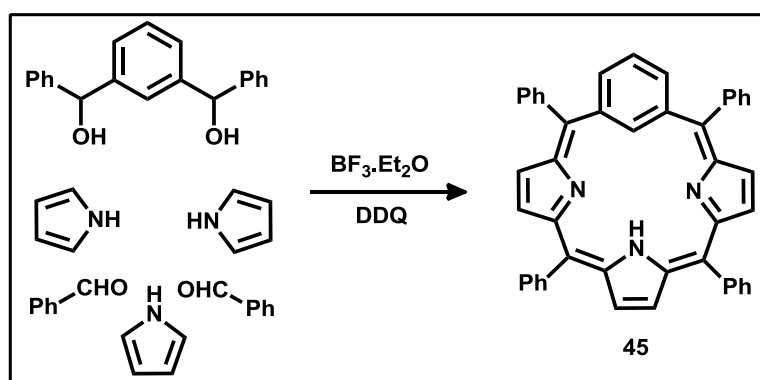
a) *meta*-Benziporphyrin:

The *meta*-benziporphyrin **44** was reported by Berlin and Breitmaier in 1994 (Scheme 1.15).⁴⁷ The acid-catalyzed [3+2] MacDonald type condensation using

isophthalaldehyde with a tripyrrane followed by oxidation afforded the *meta*-benziporphyrin (**44**). Later Stępień and co-workers reported an improved synthesis of *meso*-substituted *m*-benziporphyrin **45** by the condensation of pyrrole, benzaldehyde, and 1,3-bis(phenylhydroxymethyl)benzene (Scheme 1.16).⁴⁸ The *m*-phenylene moiety in **45** remains isolated from the π -electron system of the tripyrrolic fragment which lacks overall conjugation in the system, thus shows non-aromatic behaviour. The absence of macrocyclic conjugation is reflected from spectral studies. The presence of C-H in the core offers to study the organometallic chemistry and weak metal C-H bond interactions in the macrocyclic environment. The nonaromatic *m*-benziporphyrin forms organometallic complexes with Pd^{II}, Pt^{II}, Ni^{II} and Rh^{III} and weak metal-arene interaction with Zn^{II}, Cd^{II}, Hg^{II}, Ni^{II} and Fe^{III}.³⁴



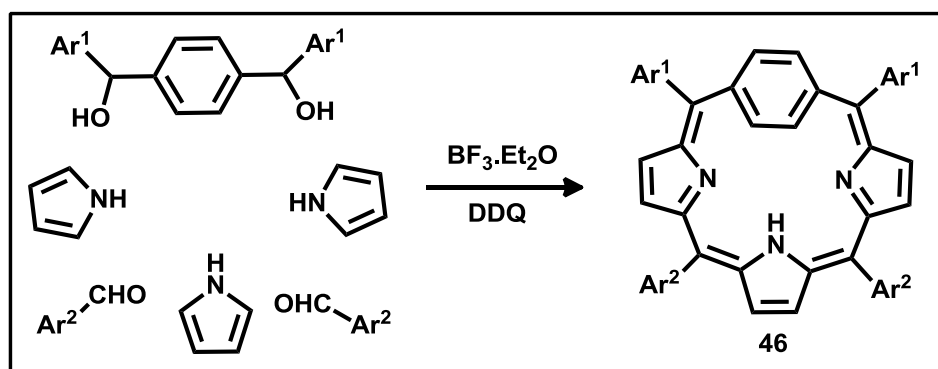
Scheme 1.15: Synthesis of *meta*-benziporphyrin.



Scheme 1.16: Synthesis of tetraphenyl-*m*-benziporphyrin.

b) *para*-Benziporphyrin:

The *para*-benziporphyrin **46** is the aromatic isomer of nonaromatic *meta*-benziporphyrin where *p*-phenylene unit is incorporated in porphyrin ring. *Meso*-substituted *para*-benziporphyrin is obtained by simple modification of the synthesis described for the *meta*-benziporphyrin. In these compounds precursor 1,3-disubstituted carbinol is replaced by 1,4-disubstituted carbinol (Scheme 1.17).⁴⁹ The structural and spectral features shows the porphyrin like aromaticity thus confirm 18π electrons in the framework. The *para*-benziporphyrins is further utilized to study the weak metal arene interaction as well as coordination.⁵⁰ Along with benziporphyrins extended π -systems of benzene moieties, such as naphthiporphyrin⁵¹ and anthriporphyrins⁵² also synthesized and studied their properties.

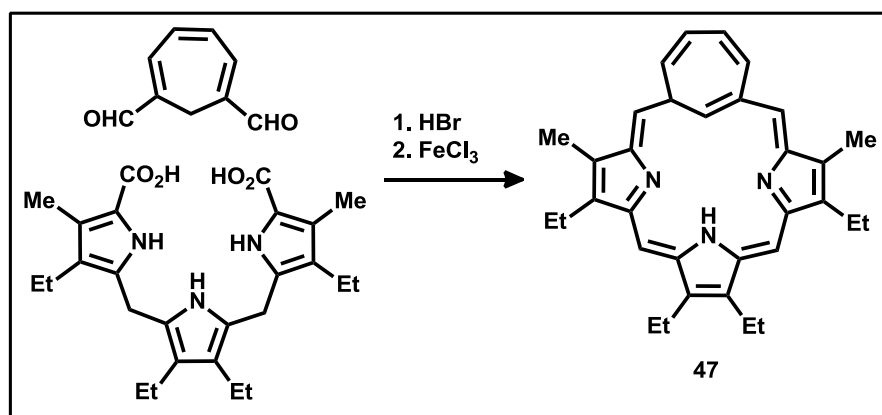


Scheme 1.17: Synthesis of tetraaryl-*p*-benziporphyrin.

1.3.3.1.3 Seven-membered ring embedded carba derivatives

Tropiporphyrin **47** is a cycloheptatriene containing porphyrin analogue. It was synthesized by Lash *et al.* by a modified [3+1] MacDonald acid-catalyzed condensation using 1,6-cycloheptatriene-dicarboxaldehyde with tripyrrane followed by oxidation. Tropiporphyrin is an aromatic porphyrinoid, however optical properties of tropiporphyrins are considerably different compared to those of carbaporphyrins. In

particular, addition of TFA shows different aromatic properties where the monoprotonated specie is aromatic in nature however, the excess of TFA leads to diminish the aromaticity and shows non-aromatic character. It can also act as trianionic ligand similar to that of benzocarporphyrins, and generate organo-Ag^{III} complex.³⁴



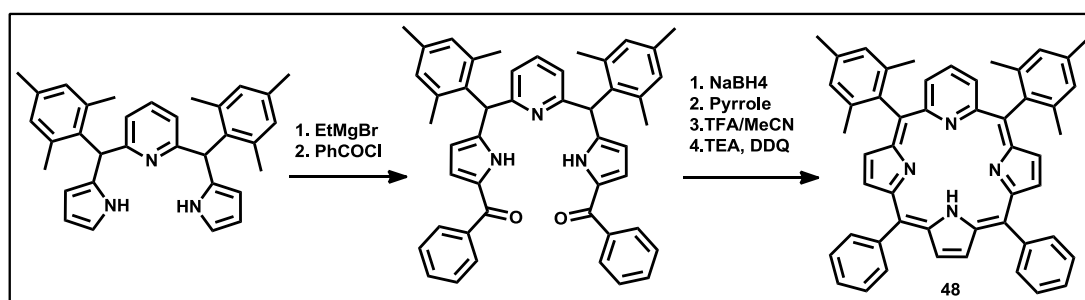
Scheme 1.18: Synthesis of Tropiporphyrin.

1.3.3.2 Pyridine embedded porphyrinoids

1.3.3.2.1 Pyriporphyrins

Pyriporphyrin is a porphyrin homologue in which one of the pyrrole units is replaced by pyridine ring. It can also be considered as pyridine analogue of *meta*-benziporphyrin. The aromaticity of pyriporphyrin is similar to that of *m*-benziporphyrin where the overall aromaticity is restricted by pyridine and remains isolated from the π -electron system of the tripyrrolic fragment, thus shows nonaromatic character. It was first reported by Berlin and Breitmaier in 1994 through [3+1] MacDonald type condensation between pyridine-2,6-dicarbaldehyde with tripyrran.⁵⁴ Instead of pyriporphyrin the reaction is ended up with pyrioxophlorin. The tetraarylpyriporphyrin **48** was achieved through an inverse strategy and reported by Latos-Grażyński. In this method the pyridine incorporated tripyrrane analogue reacts with pyrrole followed by

oxidation produces *meso*-tetraarylpyriporphyrin **48** (Scheme 1.19).⁵⁵ The electronic absorption spectrum of pyriporphyrin resembles to the non-aromatic benziporphyrin **45**. The presence of an NH in the core, it can act as a monoanionic ligand. In addition, the porphyrin like N₄ core in coordination sphere, it forms complexes with Zn^{II} and Fe^{III}.⁵⁵ The oxypyriporphyrin is an aromatic analogue of pyriporphyrin, was also synthesized and studied its coordination with Ni^{II} and Fe^{III}.^{56,57}

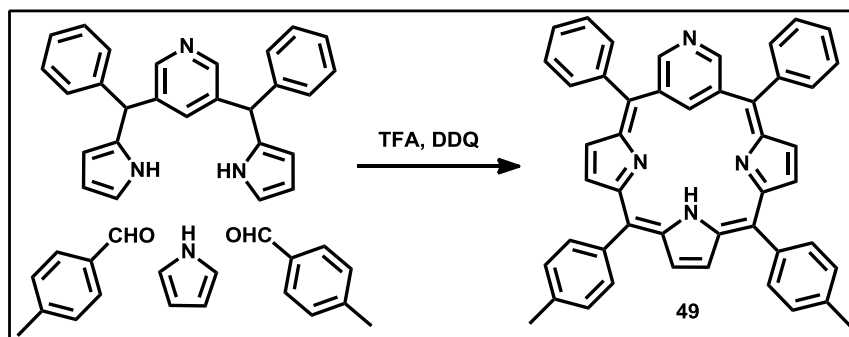


Scheme 1.19: Synthesis of pyriporphyrin.

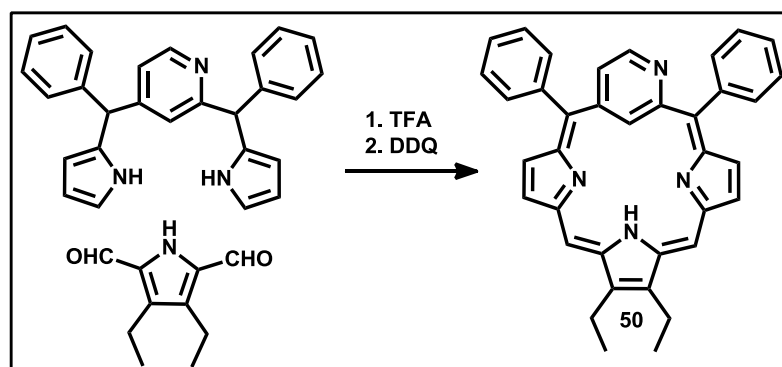
1.3.3.2.2 Confused pyriporphyrins

Confused pyriporphyrin is an isomer of pyriporphyrin where the pyridine nitrogen points outwards. Because of the inner core carbon atom, it can also be considered as a class of carbaporphyrins. Two types of confused pyriporphyrins were achieved depending on the position of the nitrogen atom from pyridine ring *para* or *meta* to inner core carbon atom. The *para*- isomer **49** was synthesized from 3,5-bis[aryl(hydroxy)methyl]pyridine, which is the key precursor and achieved by two steps. The first step involves lithiation of 3,5-dibromopyridine followed by reaction with aryl aldehyde affords the 1,3-disubstituted carbinol derivative, which was further reacted with methanesulphonyl chloride, TEA, followed by condensation with pyrrole, yielded main precursor. The final macrocycle **49** was achieved by acid-catalyzed condensation of pyrrole and *p*-tolualdehyde followed by oxidation (Scheme 1.20).⁵⁸

Whereas the *meta*- isomer **50** was achieved by the acid-catalyzed condensation reaction of 2,4-bis-pyrrolyl-substituted pyridine with 2,5 diformyl pyrrole followed by oxidation (Scheme 1.21).⁵⁹ The confused isomers are further utilized for metal ion insertion reaction and obtained Fe^{II}, Fe^{III} and Pd^{II} complexes.⁵⁹⁻⁶¹



Scheme 1.20: Synthesis of *para*-confused pyriporphyrin.



Scheme 1.21: Synthesis of *meta*-confused pyriporphyrin.

Since the development of pyriporphyrins, several pyridine-based similar derivatives have been described and characterized which includes (i) expanded porphyrins, such as 12-hydroxypyrisapphyrin,⁶² dipyrrihexaphyrin,⁶³ tetrapyrriooctaphyrin,⁶⁴ bipyriooctaphyrin,⁶⁵ and cyclo[m]pyridine-[n]pyrroles;⁶⁶ (ii) phthalocyanine derivatives such as hemiporphyrazines;⁶⁷ (iii) calixpyrrole derivatives such as *meso*-octaethyl calix[4]pyridine;⁶⁸ and (iv) cryptand-like pyriporphyrinoid macrocycles and explored their unusual properties.⁶⁹

1.3.4 Expanded porphyrins

Expanded porphyrins are higher analogues of porphyrins and possess larger internal cavities. These are obtained by increasing either the number of heterocyclic rings or by increasing the *meso*-positions or both in a manner that the internal ring pathway contains a minimum of 17 atoms.⁷⁰ Expanded porphyrins exhibit electronic properties, coordination chemistry, structures and reactivities that are entirely different from those of porphyrins. The study of expanded porphyrins has been inspired by many factors. Among them; i) the large core size can often accommodate more than one metal ions to produce multi-metallic complexes; ii) bind with anionic and neutral substrates and iii) to study the nature of aromaticity. It has also been demonstrated to serve as an effective platform to realize stable Möbius aromatic and even antiaromatic systems, which is very difficult with any other classes of macrocycles. In addition, the generation of stable radical species from expanded porphyrins has been reported.⁷⁰

The chemistry of expanded porphyrin was initiated through serendipitous discovery of sapphyrin in 1966 by Woodward and co-workers.⁷¹ Sapphyrin contains five pyrrole rings linked to each other with four *meso*-carbons and one direct pyrrole-pyrrole linkage. In the early stages (1966–1990), the main contributions were made by Johnson and co-workers on sapphyrins. Later apart from porphyrin isomers a series of octaphyrin derivatives were reported by Vogel and co-workers.⁷² On the other hand core-modified expanded porphyrins were synthesized by various groups.⁷³⁻⁷⁵ However, from last two decades, most of the efforts towards efficient synthetic methods in expanded porphyrins and demonstrated them as a potential candidates in many fields including anion recognition, functional dyes, aromaticity, magnetic resonance imaging (MRI), and photodynamic therapy (PDT) by Sessler & co-workers and Osuka & co-

workers.^{70,75} The series of expanded porphyrins are reported in the literature which includes sapphyrins **52**,⁷¹ smaragdyrins,⁷⁸ pentaphyrins,⁷⁹ hexaphyrins,⁸⁰ amethyrins⁵³,⁸¹ heptaphyrins,⁸² octaphyrins,⁷² rosarins,⁸³ rubyrins **54**,⁸⁴ turcasarins,⁷⁷ dodecaphyrins,⁸⁵ hexadecaphyrins,⁸⁵ icosapphyrins, tetracosapphyrin and the expanded derivative with 96π e- in the macrocyclic framework.⁸⁶ The selective examples of expanded porphyrinoids are shown in (Figure 1.7).

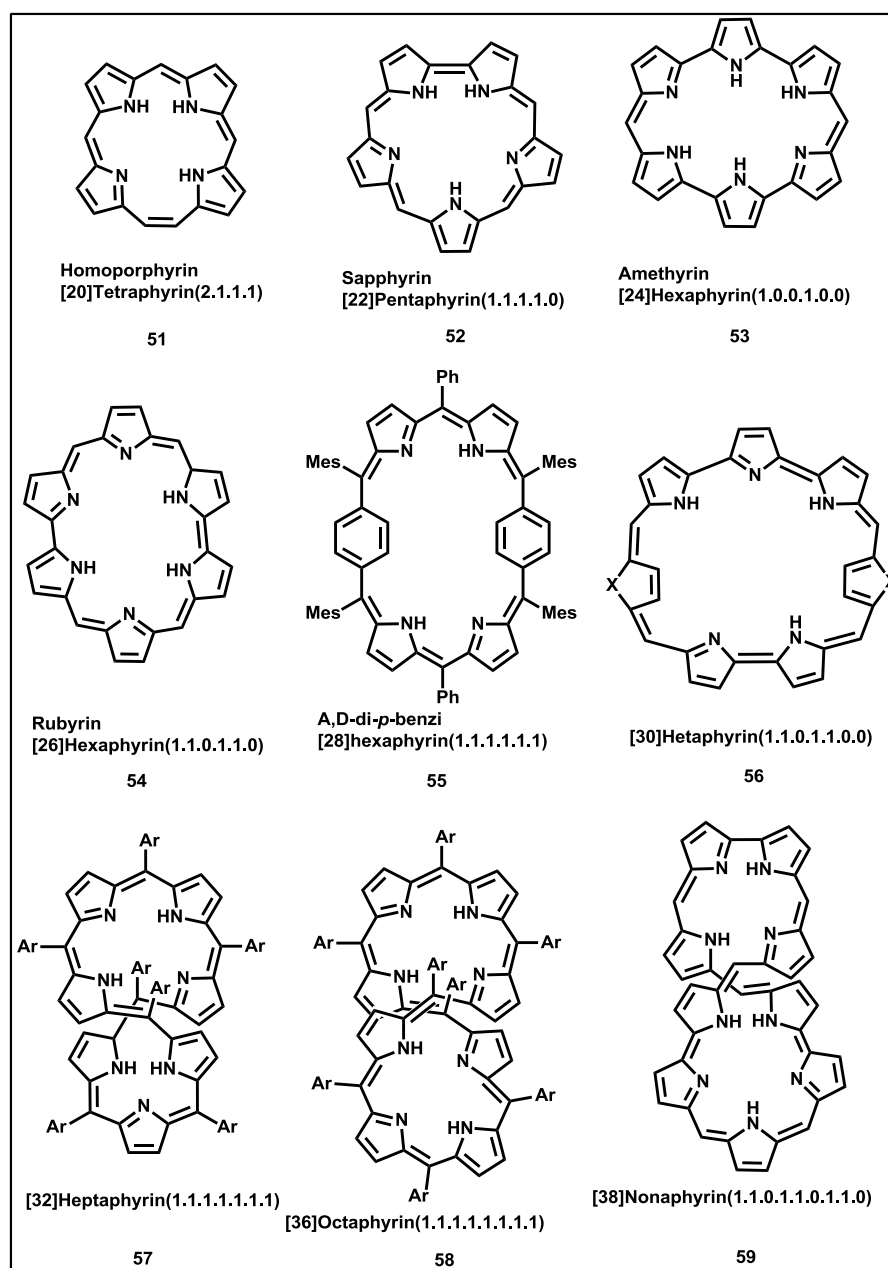


Figure 1.7: Structures of expanded porphyrinoids.

1.4 Conclusion and objectives of the present thesis

From the brief introduction about the modified porphyrinoids, the chemistry of carbocyclic and pyridine embedded macrocycles are emerged as an interesting area of research in recent years. So far, the research is mainly focused on mono-carba and mono-pyridine related porphyrinoids. However, the dicarba and dipyridine porphyrinoids are scarcely reported in the literature. In particular the chemistry of contracted and expanded porphyrins of respective derivatives are relatively rare. Hence, the development of such derivatives provides an ideal platform to explore diverse applications. It is also pertinent to point out that the synthetic methodologies involved to generate a novel contracted and expanded derivatives with polycyclic aromatic as a part of the macrocyclic framework relatively less explored. The main objective of this thesis is to develop new synthetic methodologies as well as synthesis of novel homologues and analogues of contracted and expanded porphyrinoids by introducing the polycyclic aromatic units in the macrocyclic framework. This also highlights the reactivity, receptor property and coordination chemistry of these macrocycles.

In this chapter, we have described the synthesis of carbatrityrin(3.1.1) with CNN in the core which is the structural isomer of biphenylcorrole. The presence of *m*-phenylene unit in the macrocyclic framework restricts the π -electron conjugation, thus adopts non-aromatic character. The similar trends were observed even in the protonation state. The core is effectively utilized to stabilize the B^{III} ion. The formation of weak boron arene interaction and stabilization of organoborane complex were reflected from the approach of the B^{III} ion to the macrocyclic core. To the best of our knowledge, the weak C-H...B intramolecular interaction and C-B bond formation through C-H activation are exploited for the first time in the porphyrin chemistry.

In the third chapter, the synthesis of an *adj*-dicarbacorrole derivative and its organometallic complex is described. A bipyrrole unit in the corrole macrocycle is replaced by a biphenyl unit to form *adj*-dicarbaporphyrinoid with CCNN in the core. The spectral studies and structural analyses prove that the aromatic biphenyl unit and the π -delocalized dipyrromethene units are linked together to generate overall nonaromatic macrocycle. The trianionic core is found suitable to stabilize higher oxidation state organometallic complexes. Herein, the core is effectively utilized to stabilize organo-copper(III) complex. The results were proved by various spectral techniques and further confirmed by crystal analysis. The complex retains the nonaromatic character as such upon metal ion insertion.

In the fourth chapter, the corrole homologue such as *meso*-triarylbiopyricorrole with tetra nitrogen (NNNN) synthesized by incorporating a 2,2'-bipyridyl unit in the corrole framework. The modification alters the corrole N4 coordination sphere from the trianionic [(NH)3N] to the monoanionic [N3NH]. The nonaromatic monoanionic core is further utilized to stabilize the Zn^{II} ion with chelation induced emission enhancement (CIEE). The enhanced emission profile prompted us to explore the sensing properties, where the macrocycle selectively senses Zn^{II} ion over 100 equivalents of other metal ions. As reflected from the spectral studies, the Zn^{II} complex maintain the nonaromatic character & the results are further conformed by structural analysis.

The chapter 5 addresses two important issues; a) novel synthetic methodology for the synthesis of *meso*-free corrole homologues monomer and their complexes and b) the reactivity studies of *meso*-free biopyricorrole. In the first part, the free base *meso*-free biopyricorrole is achieved by *condensation* reaction of formylated bipyridyl dipyrromethane in the presence of FeCl₃ followed by open-air oxidation. Whereas the

protonated complex was synthesized as a major product by using traditional acid-catalyzed (*p*-TSA) condensation reaction. The newly introduced metal-templated *condensation* strategy is widely used for the metal ion insertion upon macrocyclic framework. The metal salts such as Ni^{II}, Pd^{II} and Cu^{II} salts were used as a templating agent. In the second part, the reactive *meso*-CH in the monomer complex is further explored for covalently linked dimer reaction by using various oxidative coupling reagents such as AgPF₆, AgOTf and FeCl₃. In the case of Ag^I salts, anion exchanged products were observed whereas in the presence of FeCl₃, the *meso*-CH is actively participated in oxidative coupling reaction and afforded the *meso-meso* linked corrole homologue dimers. It is also pertinent to point out that the Pd^{II}-corrole monomer and dimer complexes are not known so far. To the best of our knowledge, the nonaromatic Pd^{II} monomer as well as dimer corrole homologue complexes are first time addressed in corrole chemistry.

In the final chapter, the smallest expanded porphyrin such as homoporphyrin with carba derivative is reported & its coordination chemistry is further addressed. The *meso*-aryl di-carba and tetra-carba homoporphyrins are achieved by introduction of the terphenyl unit into the porphyrin core. The newly formed both carbahomoporphyrins are structural isomers to each other. Though there is an overall π -conjugation in the tetracarba derivative, however lose in planarity leads to non-aromatic character. On the other hand, the *meta*-phenylene unit in the dicarba derivative restrict the π -conjugation thus, adopts non-aromaticity. The coordination chemistry revealed that insertion of Rh(I) ion in the macrocyclic framework. The spectral and structural analyses of Rh(I) complexes proves that the complexes maintain the non-aromatic character.

1.5 References

1. Battersby, A. R.; Fookes, C. J.; Matcham, G. W.; McDonald, E. *Nature* **1980**, 285, 17-21.
2. Lippard, S. J.; Berg, J. M. *Principles of bioinorganic chemistry*. University Science Books: **1994**.
3. Dougherty, T. J.; Marcus, S. L. *Eur. J. Cancer* **1992**, 28, 1734-1742.
4. Moan, J.; Berg, K. *Photochem. Photobiol.* **1992**, 55, 931-948.
5. Kadish, K.; Smith, K.; Guillard, R. *The Porphyrin Handbook, Volume 1: Synthesis and Organic Chemistry*. Academic Press—San Diego, CA and London, UK: **2000**.
6. Sessler, J. L.; Weghorn, S. J. *Expanded, contracted & isomeric porphyrins*. Elsevier: **1997**; Vol. 15.
7. Jasat, A.; Dolphin, D. *Chem. Rev.* **1997**, 97, 2267-2340.
8. Rothmund, P. *J. Am. Chem. Soc.* **1935**, 57, 2010-2011.
9. Adler, A. D.; Longo, F. R.; Finarelli, J. D.; Goldmacher, J.; Assour, J.; Korsakoff, L. *J. Org. Chem.* **1967**, 32, 476.
10. Lindsey, J. S.; Schreiman, I. C.; Hsu, H. C.; Kearney, P. C.; Marguerettaz, A. *M. J. Org. Chem.* **1987**, 52, 827-836.
11. Ravikanth, M.; Strachan, J.-P.; Li, F.; Lindsey, J. S. *Tetrahedron* **1998**, 54, 7721-7734.
12. Vogel, E.; Köcher, M.; Schmickler, H.; Lex, J. *Angew. Chem., Int. Ed. Engl.* **1986**, 25, 257-259.
13. Sessler, J. L.; Brucker, E. A.; Weghorn, S. J.; Kisters, M.; Schäfer, M.; Lex, J.; Vogel, E. *Angew. Chem., Int. Ed. Engl.* **1994**, 33, 2308-2312.

-
14. Callot, H.; Rohrer, A.; Tschamber, T.; Metz, B., *New J. chem.* **1995**, *19*, 155-159.
 15. Vogel, E. *J. Heterocycl. Chem.* **1996**, *33*, 1461-1487.
 16. Furuta, H.; Asano, T.; Ogawa, T. *J. Am. Chem. Soc.* **1994**, *116*, 767-768.
 17. Chmielewski, P. J.; Latos-Grażyński, L.; Rachlewicz, K.; Glowiak, T. *Angew. Chem., Int. Ed. Engl.* **1994**, *33*, 779-781.
 18. Hodgkin, D. C.; Kamper, J.; Lindsey, J.; MacKay, M.; Pickworth, J.; Robertson, J.; Shoemaker, C. B.; White, J.; Prosen, R.; Trueblood, K. In *The Structure of Vitamin B12. An Outline of the Crystallographic Investigation of Vitamin B12*, Proceedings of the Royal Society of London A: Mathematical, Physical and Engineering Sciences, The Royal Society: **1957**; pp 228-263.
 19. Johnson, A.; Todd, A. *Vitamins & Hormones* **1957**, *15*, 1-30.
 20. Johnson, A.; Price, R. *J. Chem. Soc.* **1960**, 1649-1653.
 21. Johnson, A.; Kay, I. *J. Chem. Soc.* **1965**, 1620-1629.
 22. Gross, Z.; Galili, N.; Saltsman, I. *Angew. Chem. Int. Ed.* **1999**, *38*, 1427-1429.
 23. Paolesse, R.; Mini, S.; Sagone, F.; Boschi, T.; Jaquinod, L.; J. Nurco, D.; M. Smith, K. *Chem. Commun.* **1999**, 1307-1308.
 24. Gryko, D. T.; Jadach, K. *J. Org. chem.* **2001**, *66*, 4267-4275.
 25. Koszarna, B.; Gryko, D. T. *J. Org. Chem.* **2006**, *71*, 3707-3717.
 26. Meller, A.; Ossko, A. *Monatshefte für Chemie / Chemical Monthly* **1972**, *103*, 150-155.
 27. Inokuma, Y.; Kwon, J. H.; Ahn, T. K.; Yoo, M. C.; Kim, D.; Osuka, A. *Angew. Chem. Int. Ed.* **2006**, *45*, 961-964.
 28. Inokuma, Y.; Osuka, A. *Dalton Trans.* **2008**, 2517-2526.
-

-
29. Will, S.; Rahbar, A.; Schmickler, H.; Lex, J.; Vogel, E., *Angew. Chem., Int. Ed. Engl.* **1990**, *29*, 1390-1393.
 30. Vogel, E.; Binsack, B.; Hellwig, Y.; Erben, C.; Heger, A.; Lex, J.; Wu, Y. D., *Angew. Chem., Int. Ed. Engl.* **1997**, *36*, 2612-2615.
 31. Bröring, M.; Köhler, S.; Kleeberg, C. *Angew. Chem. Int. Ed.* **2008**, *47*, 5658-5660.
 32. Lash, T. D. *Chem. Eur. J.* **1996**, *2*, 1197-1200.
 33. Lash, T. D. *Eur. J. Org. Chem.* **2007**, 5461-5481.
 34. Lash, T. D. *Chem. Asian J.* **2014**, *9*, 682-705.
 35. Berlin, K.; Steinbeck, C.; Breitmaier, E. *Synthesis* **1996**, *1996*, 336-340
 36. Colby, D. A.; Lash, T. D. *Chem. Eur. J.* **2002**, *8*, 5397-5402.
 37. Pawlicki, M.; Latos-Grażyński, L. *Chem. Rec.* **2006**, *6*, 64-78.
 38. Lash, T. D.; Lammer, A. D.; Ferrence, G. M. *Angew. Chem. Int. Ed.* **2011**, *50*, 9718-9721.
 39. Furuta, H.; Maeda, H.; Osuka, A. *J. Am. Chem. Soc.* **2000**, *122*, 803-807.
 40. Maeda, H.; Osuka, A.; Furuta, H. *J. Am. Chem. Soc.* **2003**, *125*, 15690-15691.
 41. D. Lash, T.; L. Romanic, J.; J. Hayes, M.; D. Spence, J. *Chem. Commun.* **1999**, 819-820.
 42. Graham, S. R.; Colby, D. A.; Lash, T. D. *Angew. Chem. Int. Ed.* **2002**, *41*, 1371-1374.
 43. Lash, T. D.; Colby, D. A.; Idate, A. S.; Davis, R. N. *J. Am. Chem. Soc.* **2007**, *129*, 13800-13801.
 44. Zhang, Z.; Ferrence, G. M.; Lash, T. D. *Org. Lett.* **2009**, *11*, 101-104.
 45. Kadish, K. M.; Smith, K. M.; Guillard, R. *World Scientific: Singapore* **2014**, 1-35.
-

-
46. Stępień, M.; Latos-Grażyński, L. *Acc. Chem. Res.* **2005**, *38*, 88-98.
47. Berlin, K.; Breitmaier, E. *Angew. Chem., Int. Ed. Engl.* **1994**, *33*, 1246-1247.
48. Stępień, M.; Latos-Grażyński, L. *Chem. Eur. J.* **2001**, *7*, 5113-5117.
49. Stępień, M.; Latos-Grażyński, L. *J. Am. Chem. Soc.* **2002**, *124*, 3838-3839.
50. Stępień, M.; Latos-Grażyński, L.; Szterenber, L.; Panek, J.; Latajka, Z. *J. Am. Chem. Soc.* **2004**, *126*, 4566-4580.
51. Lash, T. D.; Young, A. M.; Rasmussen, J. M.; Ferrence, G. M. *J. Org. Chem.* **2011**, *76*, 5636-5651.
52. Szyszko, B.; Latos-Grażyński, L.; Szterenber, L. *Chem. Commun.* **2012**, *48*, 5004-5006.
53. Lash, T. D.; Chaney, S. T. *Tetrahedron Lett.* **1996**, *37*, 8825-8828.
54. Berlin, K.; Breitmaier, E. *Angew. Chem., Int. Ed. Engl.* **1994**, *33*, 219-220.
55. Myśliborski, R.; Latos-Grażyński, L.; Szterenber, L. *Eur. J. Org. Chem.* **2006**, 3064-3068.
56. Lash, T. D.; Chaney, S. T. *Chem. Eur. J.* **1996**, *2*, 944-948.
57. Neya, S.; Suzuki, M.; Ode, H.; Hoshino, T.; Furutani, Y.; Kandori, H.; Hori, H.; Imai, K.; Komatsu, T. *Inorg. Chem.* **2008**, *47*, 10771-10778.
58. Myśliborski, R.; Latos-Grażyński, L. *Eur. J. Org. Chem.* **2005**, 5039-5048.
59. Lash, T. D.; Pokharel, K.; Serling, J. M.; Yant, V. R.; Ferrence, G. M. *Org. Lett.* **2007**, *9*, 2863-2866.
60. Myśliborski, R.; Rachlewicz, K.; Latos-Grażyński, L. *Inorg. Chem.* **2006**, *45*, 7828-7834.
61. Myśliborski, R.; Rachlewicz, K.; Latos-Grażyński, L. *J. Porphyrins Phthalocyanines* **2007**, *11*, 172-180.
62. Richter, D. T.; Lash, T. D. *J. Org. Chem.* **2004**, *69*, 8842-8850.
-

-
63. Setsune, J.-i.; Yamato, K. *Chem. Commun.* **2012**, *48*, 4447-4449.
64. Bell, T. W.; Cragg, P.; Drew, M. G.; Firestone, A.; Kwok, A.-I.; Liu, J.; Ludwig, R.; Papoulis, A. *Pure Appl. Chem.* **1993**, *65*, 361-366.
65. Setsune, J.-i.; Kawama, M.; Nishinaka, T. *Tetrahedron Lett.* **2011**, *52*, 1773-1777.
66. Zhang, Z.; Lim, J. M.; Ishida, M.; Roznyatovskiy, V. V.; Lynch, V. M.; Gong, H.-Y.; Yang, X.; Kim, D.; Sessler, J. L. *J. Am. Chem. Soc.* **2012**, *134*, 4076-4079.
67. Fernández-Lázaro, F.; Torres, T.; Hauschel, B.; Hanack, M. *Chem. Rev.* **1998**, *98*, 563-576.
68. Kral, V.; A. Gale, P.; Anzenbacher Jr, P.; Jursikova, K.; Lynch, V.; L. Sessler, J.; Kral, V.; Anzenbacher Jr, P. *Chem. Commun.* **1998**, 9-10.
69. Setsune, J.-i.; Watanabe, K. *J. Am. Chem. Soc.* **2008**, *130*, 2404-2405.
70. Saito, S.; Osuka, A. *Angew. Chem. Int. Ed.* **2011**, *50*, 4342-4373.
71. Bauer, V. J.; Clive, D. L. J.; Dolphin, D.; Paine, J. B.; Harris, F. L.; King, M. M.; Loder, J.; Wang, S. W. C.; Woodward, R. B. *J. Am. Chem. Soc.* **1983**, *105*, 6429-6436.
72. Vogel, E.; Bröring, M.; Fink, J.; Rosen, D.; Schmickler, H.; Lex, J.; Chan, K. W. K.; Wu, Y.-D.; Plattner, D. A.; Nendel, M.; Houk, K. N. *Angew. Chem., Int. Ed. Engl.* **1995**, *34*, 2511-2514.
73. Misra, R.; Chandrashekar, T. K. *Acc. Chem. Res.* **2008**, *41*, 265-279.
74. Sprutta, N.; Latos-Grażyński, L. *Chem. Eur. J.* **2001**, *7*, 5099-5112.
75. Jeong, S.-D.; Sessler, J. L.; Lynch, V.; Lee, C.-H. *J. Am. Chem. Soc.* **2008**, *130*, 390-391.
76. Callot, H. J.; Schaeffer, E. *J. Org. Chem.* **1977**, *42*, 1567-1570.
-

-
77. Sessler, J. L.; Weghorn, S. J.; Lynch, V.; Johnson, M. R. *Angew. Chem., Int. Ed. Engl.* **1994**, *33*, 1509-1512.
78. Broadhurst, M. J.; Grigg, R.; Johnson, A. W. *J. Chem. Soc., Perkin Trans. 1* **1972**, 1124-1135.
79. Rexhausen, H.; Gossauer, A. *J. Chem. Soc., Chem. Commun.* **1983**, 275.
80. Gossauer, A. *Bull. Soc. Chim. Belg.* **1983**, *92*, 793-795.
81. Sessler, J. L.; Weghorn, S. J.; Hiseada, Y.; Lynch, V. *Chem. Eur. J.* **1995**, *1*, 56-67.
82. Sessler, J. L.; Seidel, D.; Lynch, V. *J. Am. Chem. Soc.* **1999**, *121*, 11257-11258.
83. Sessler, J. L.; Weghorn, S. J.; Morishima, T.; Rosingana, M.; Lynch, V.; Lee, C.-H. *J. Am. Chem. Soc.* **1992**, *114*, 8306-8307.
84. Sessler, J. L.; Morishima, T.; Lynch, V., *Angew. Chem., Int. Ed. Engl.* **1991**, *30*, 977-980.
85. Setsune, J.-i.; Katakami, Y.; Iizuna, N. *J. Am. Chem. Soc.* **1999**, *121*, 8957-8958.
86. Setsune, J.-i.; Maeda, S. *J. Am. Chem. Soc.* **2000**, *122*, 12405-12406.

CHAPTER 2

Carbatriphyrin(3.1.1) – Displays two distinct coordination approach of B^{III} to generate organoborane and weak C-H...B interactions

2.1	Introduction	37
2.2	Objective of our work	41
2.3	Results and Discussion	42
2.3.1	Synthesis	42
2.3.2	Complexation	42
2.3.3	Spectral characterisation	43
2.3.3.1	Mass spectrometric analysis	43
2.3.3.2	NMR Analysis	44
2.3.3.3	Single crystal X-ray analysis	47
2.3.3.4	Electronic spectral analysis	56
2.4	Conclusions	57
2.5	General Information	57
2.6	Synthetic procedure and spectral characterization of 20-25	58
2.7	References	64

2.1 Introduction

Contracted porphyrins are one of the important major modifications in the porphyrins. Triphyrins (**1**) are class of contracted porphyrin in which three pyrrole rings are linked by *meso*-sp² carbon atoms. Among these triphyrins, subporphyrins are the genuine ring contracted porphyrins. These are synthesized as B^{III} complex (**1**) (Figure 2.1) by rational approach, where boron plays as a templating agent. The first subporphyrin, tribenzosubporphine was prepared by the group of Osuka in 2006 as the B^{III} complex under harsh reaction conditions.¹ The complex shows attractive characteristic features such as; 14 π electron aromatic circuit, bright-green emission and nonlinear optical properties.^[2-4] Because of their promising applications in the field of chemistry, physical and material sciences, series of modifications have been carried out and studied their peculiar properties.²⁻⁴ However, the chemistry of freebase subporphyrins are not much explored as compared to porphyrinoids. Subpyriporphyrin⁵ (**2**) (Figure 2.1) is the only freebase subporphyrin known so far which was reported by Latos-Grażyński and co-workers. The ligand is further exploited for coordination with B^{III} ion. The spectral studies reveal that aromatization arising upon coordination and allows delocalization of 14 π electrons in **2**.

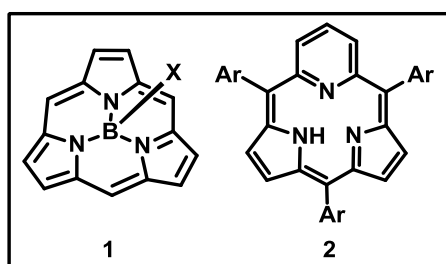


Figure 2.1: Structures of subporphyrin and subpyriporphyrin.

On the other hand, triphyrin(*n*.1.1) are the subporphyrin analogues where *n* varies from 2 to 6 which are relatively new comers in the contracted series and gained

momentum in recent years. In this series, the first [14]triphyrin(2.1.1) (**3**, **4**) (Figure 2.2) was serendipitously discovered by Kobayashi *et al.* during the reaction of $\text{BF}_3 \cdot \text{Et}_2\text{O}$ catalyzed Rothemund condensation of 4,7-dihydro-4,7-ethano-2H-isoindole with aryl aldehyde. Later the improved synthetic protocols for the synthesis of [14]benzotriphyrin(2.1.1) was reported by same group by simple condensation of pyrrole derivative and aryl aldehyde in the presence of high concentration of $\text{BF}_3 \cdot \text{Et}_2\text{O}$.⁶ Recently, Yamada and co-workers synthesized *meso*-unsubstituted [14]triphyrin(2.1.1) (**5**) by using McMurray coupling reaction.⁷ Very recently, from our group reported *meso*-aryl [14]triphyrin(2.1.1) (**6**) (Figure 2.2) through condensation reaction of 5,6-diphenyldipyrroethane with pentafluorobenzaldehyde.⁸ These triphyrins act as monoanionic tridentate ligand and exhibit electronic properties of 14π aromatic systems.

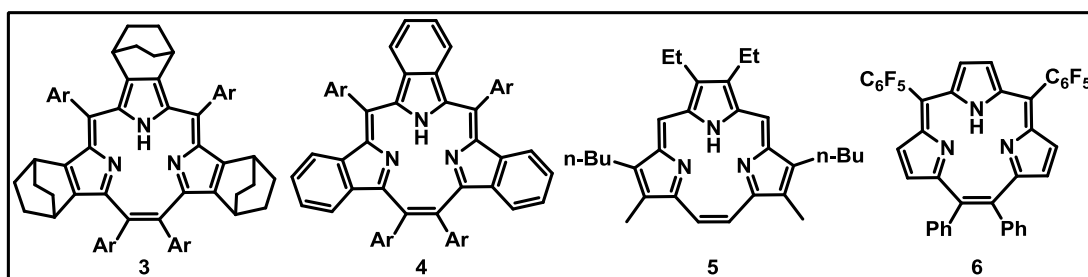


Figure 2.2: Structures of triphyrin(2.1.1) derivatives.

Further the chemistry of triphyrin(2.1.1) extended to core-modified analogues (**7-10**) (Figure 2.3).⁹⁻¹¹ Yamada and co-workers synthesized thiatriphyrin(2.1.1) (**7**). Whereas thiophene fused oxatriphyrin(2.1.1) (**8**, **9**) and phenylene ring fused oxatriphyrin(2.1.1) (**10**) was achieved by Latos-Grażyński and co-workers. The triphyrin(2.1.1) shows moderate aromaticity upon protonation. The compounds **8**, **9** and **10** act as switch between aromatic and anti-aromatic.

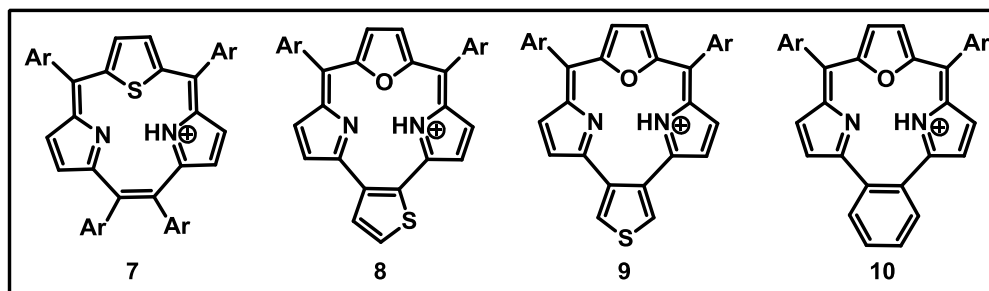


Figure 2.3: Structures of core-modified triphyrin(2.1.1) derivatives.

In addition to these triphyrins(2.1.1), a series of other triphyrin analogues (**11-16**) (Figure 2.4) were synthesized and studied, and mainly reported by Latos-Grażyński and co-workers which includes oxatriphyrin(4.1.1),¹² thia-¹³ and dithia-^{14,15} triphyrin(4.1.1), triphyrin(1.1.3),¹⁶ oxatriphyrin(3.1.1),^{17,18} carbatriphyrin(4.1.1) (**15**)¹⁹ and triphyrin(6.1.1) (**16**).^{20,21}

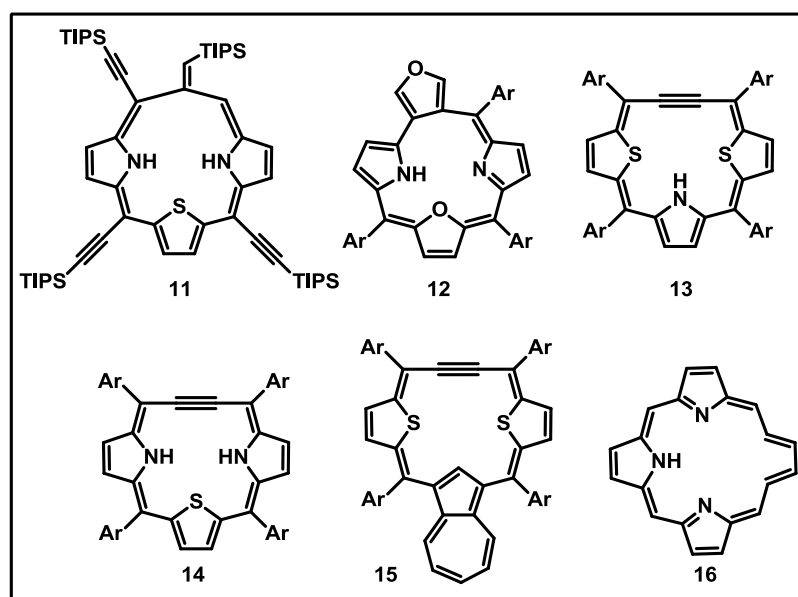


Figure 2.4: Structures of triphyrin(n.1.1) analogues.

On the other hand, chemistry of organoborane (**C-B**) has emerged as an important class of synthetic materials due to its intriguing features such as high luminescence properties, large nonlinear optical responses, anionic sensors and as

potential precursors and intermediates for many organic reaction transformations.²²⁻²⁵ Numerous synthetic methodologies have been introduced for the formation **C-B** bonds on aromatic frameworks, however, such bond formation in porphyrin macrocycle is in infancy stage and recently received considerable attention.²⁶⁻²⁸ The initial reports on borylated porphyrins (**17**) (Figure 2.5) is utilized mainly for peripheral modification of the macrocycle.²⁶ The recent reports on porphyrinyl boranes such as diaryl boranes (**18**)²⁷ and boron embedded π -expanded fused porphyrins (**19**)²⁸ (Figure 2.5) exhibit high chemical stability, photophysical properties, red-shifted absorption and enhanced electron-accepting ability due to effective interaction between the porphyrin and empty *p*-orbital of the boron atom. Despite these promising applications, the synthesis of organoborane complex by using porphyrin core is remained unexplored so far.

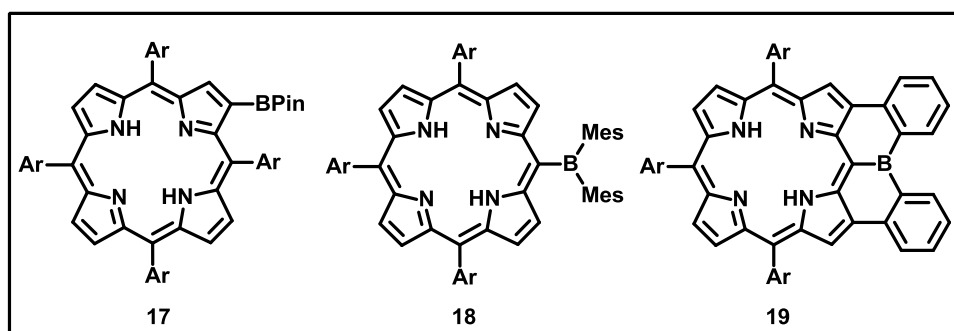


Figure 2.5: Organoboron porphyrinoids.

Furthermore, redesign the porphyrin framework by incorporating the arene rings generates novel carbaporphyrinoids.²⁹⁻³² These porphyrin analogues are well known promising candidates for; i) study the nature of aromaticity, ii) weak metal-arene interaction and iii) stabilize higher oxidation state organometallic complexes. However, as compared to porphyrinoids, the arene chemistry in contracted porphyrinoids are scarcely reported. This includes oxatriphyrin (**10**) with *o*-phenylene motif¹¹ and biphenylcorrole.³³ In addition, the only known example, the carbatriphyrin (**15**) with

azulene unit as part of the framework was synthesized and stabilized by organo-Ru^{II} complex and confirmed by spectral techniques.¹⁹

2.2 Objective of our work

From the brief review of carbaporphyrinoids, it reveals that the properties of these carbaporphyrins will vary depending on the nature of carbocyclic rings and bonding motif (*o-/m-/p-*).^{11,29,34} Though the individual arene unit play major role, the combination of any two bonding motif (*o,m-/m,p-/o,p-*) in the porphyrin skeleton in general and triphyrin in particular are not known in the literature. Moreover, to date, the insertion of B^{III} ion by using inner core of the macrocyclic framework to form the organoborane complex is hitherto unknown in the porphyrin chemistry.

In this chapter, we wish to report the synthesis of carbatriphyrin(3.1.1) (**23**) with CNN in the core. The macrocycle is structural isomer of biphenylcorrole and achieved by switching the bonding mode of biphenyl unit from 3,3' to 2,3' which turns the corrole into triphyrin analogue. It shows two different coordination modes with boron such as NNC-H...B (**24**) and NNC-B (**25**) and stabilizes the B^{III} ion (Figure 2.6) and also forms complex with trifluoroacetate ion during protonation experiment. These results are unambiguously confirmed by single crystal X-ray analysis.

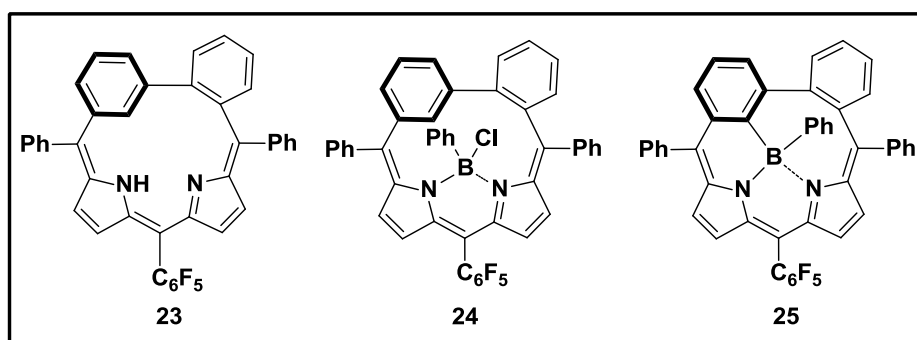
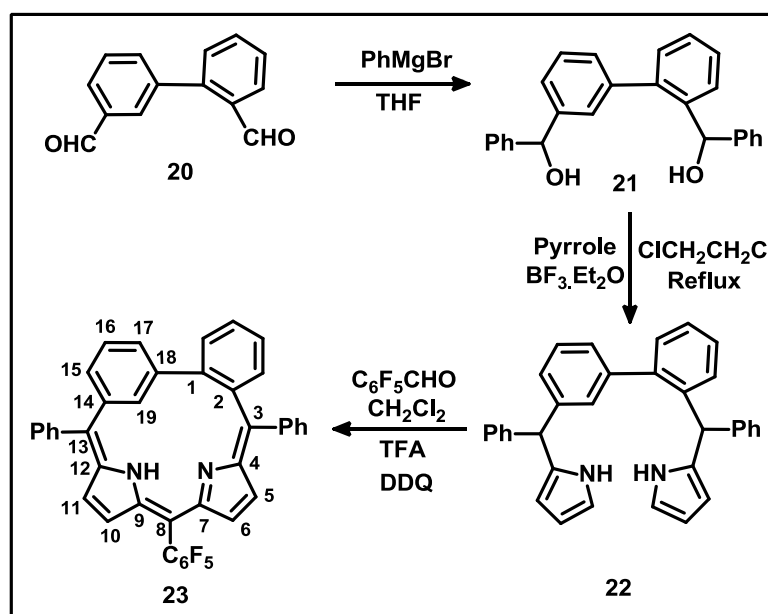


Figure 2.6: Carbatriphyrin(3.1.1) and their B^{III} complexes.

2.3 Results and discussion

2.3.1 Synthesis

The synthesis is outlined in Scheme 2.1. We adopted similar synthetic methodology of biphenylcorrole,³³ and initiated with biphenyl-2,3'-dicarbaldehyde (**20**). The Grignard reaction followed by Lewis acid-catalyzed condensation reaction with pyrrole under reflux condition to form the required precursor **22** in 40% yield. The final step is the trifluoroacetic (TFA) acid-catalyzed condensation reaction with pentafluorobenzaldehyde followed by oxidation with 2,3-dichloro-5,6-dicyano-*p*-benzoquinone (DDQ) afforded **23** as blue color solid in 35% yield.

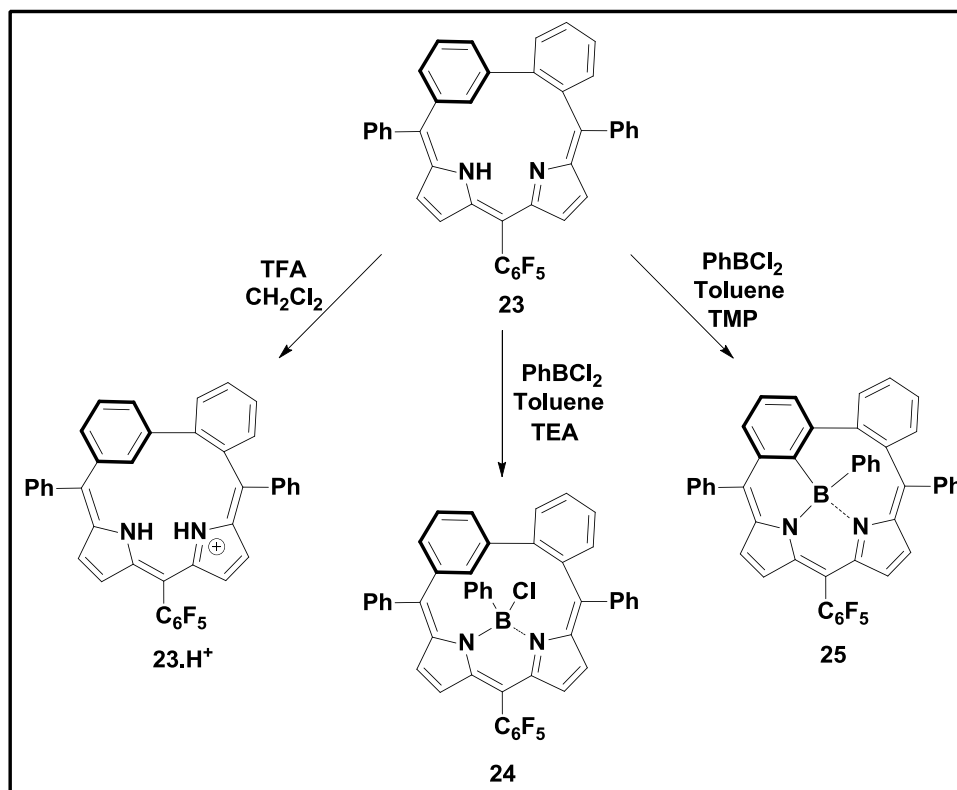


Scheme 2.1: Synthesis of **23**.

2.3.2 Complexation:

The protonated complex (**23.H⁺**) was achieved by NMR titration experiments of **23** with TFA. Further, the small macrocyclic cavity and the presence of CNN in the core prompted us to do the coordination chemistry with boron. The boron(III) complexes of **24** and **25** were synthesized by refluxing **23** with dichlorophenylborane in toluene under basic conditions (Scheme 2.2). Initially, the reaction was performed with weak base

such as triethylamine (TEA) afforded **24** in 70% yield and trace amount (<1%) of **25**. However, **25** was successfully synthesized in the presence of strong base 2,2,6,6-tetramethylpiperidine (TMP) in 60% yield and **24** in 20% yield.



Scheme 2.2: Synthesis of **23.H⁺**, **24** and **25**.

2.3.3 Spectral characterisation

2.3.3.1 Mass spectrometric analysis

The electron spray ionization (ESI) mass spectrometric analysis of **23** shows the molecular ion signal at 639.1843 [M+1] and confirms the exact composition (Figure 2.7a). Whereas the complex **24** and **25** shows the molecular ion signals at 760.1882 [M] and 747.2010 [M+Na] and confirms the formation of the complexes (Figure 2.7b, c).

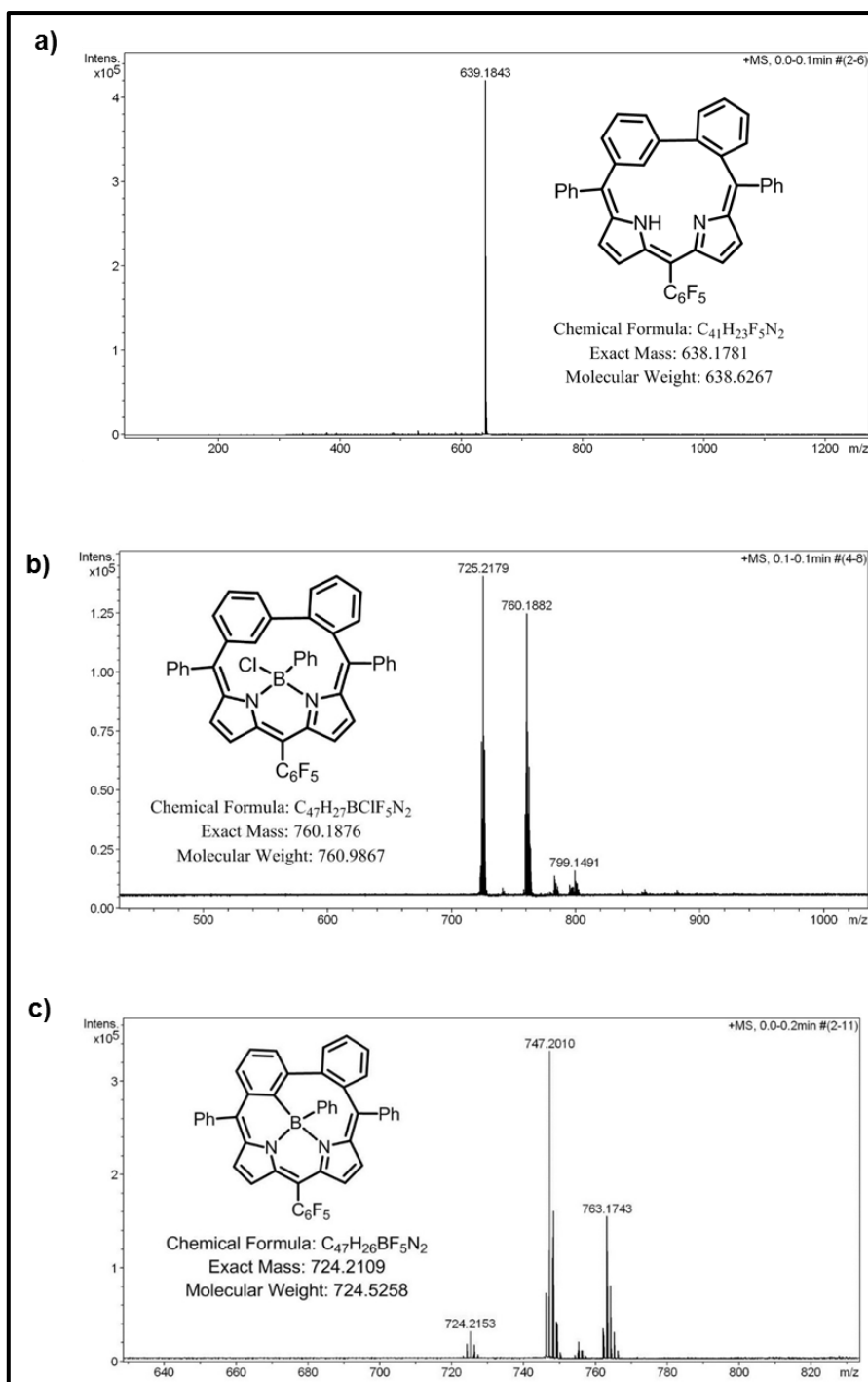


Figure 2.7: ESI-MS spectrum of **a) 23**, **b) 24** and **c) 25**.

2.3.3.2 NMR Analysis

The 1H NMR spectrum of **23** is shown in Figure 2.8a. The inner CH [H19] signal from the *m*-phenylene unit is resonated at 7.51 ppm, while the remaining peripheral CH [H15-H17] protons are appeared at 7.02 to 7.27 ppm. The *o*-phenylene proton signals

[H1',H1'',H2',H2''] are observed between 7.43 and 7.58 ppm. The pyrrolic protons are resonated at 7.06, 6.26 ppm [H5,6] and 6.55, 7.27 ppm [H10,11], respectively. All the proton signals are assigned by ^1H - ^1H COSY spectral analysis. The NH proton [H20] is observed as a broad singlet at 10.71 ppm and further confirmed by D_2O exchange experiment. The observed deshielded signal suggests the intramolecular hydrogen bonding interaction. Overall, the spectral feature resembles the nonaromatic pattern.^{29,32}

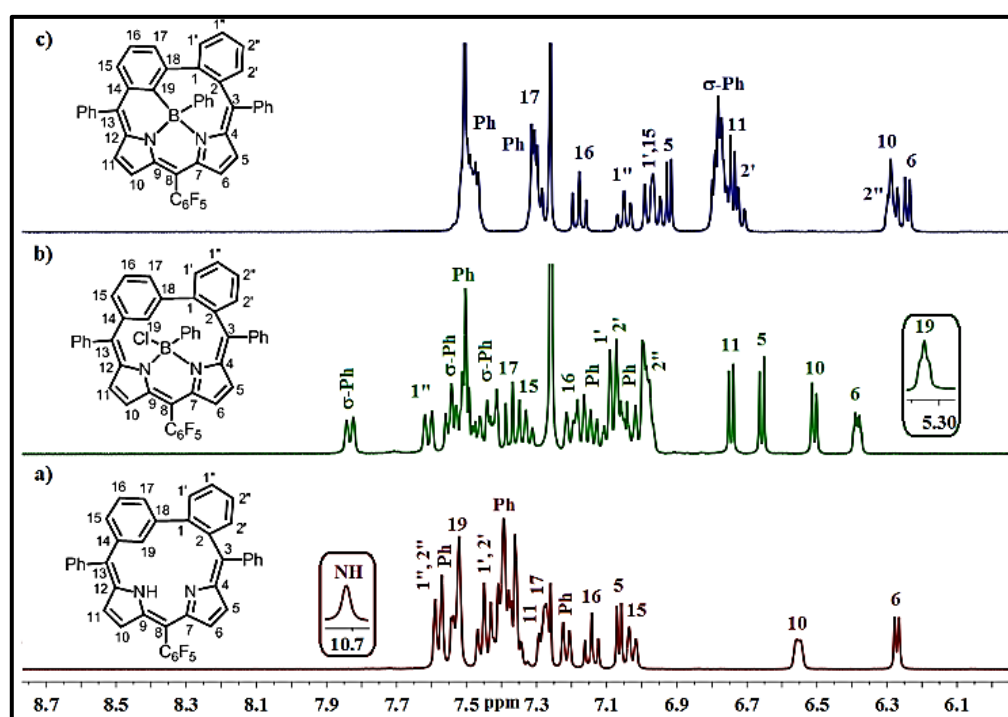


Figure 2.8: ^1H NMR spectrum of **23** (a), **24** (b) and **25** (c) in CDCl_3 .

The ^1H NMR spectrum of **23.H⁺** is shown in Figure 2.9. The protonation experiment was performed by CDCl_3 solution of **23** with excess equiv. of TFA. Upon protonation the following changes were observed; (i) the regular amine NH [H20] signal is slightly upfield shifted and resonated at 10.39 ppm; (ii) the newly formed protonated NH [H21] signal is resonated at 7.27 ppm and, (iii) the inner CH [H19] in *m*-phenyl unit is marginally upfield shifted, while the remaining *m*-phenyl, *o*-phenyl, pyrrolic β -CH and *meso*-phenyl proton signals are slightly deshielded as compared to **23**. Up field pyrrolic NH [H20] suggests the intramolecular hydrogen bonding

interaction, as observed in **23**. The low temperature $^1\text{H-NMR}$ experiment (Figure 2.10) does not show any major change from the spectral analysis, thus maintain the nonaromatic character.

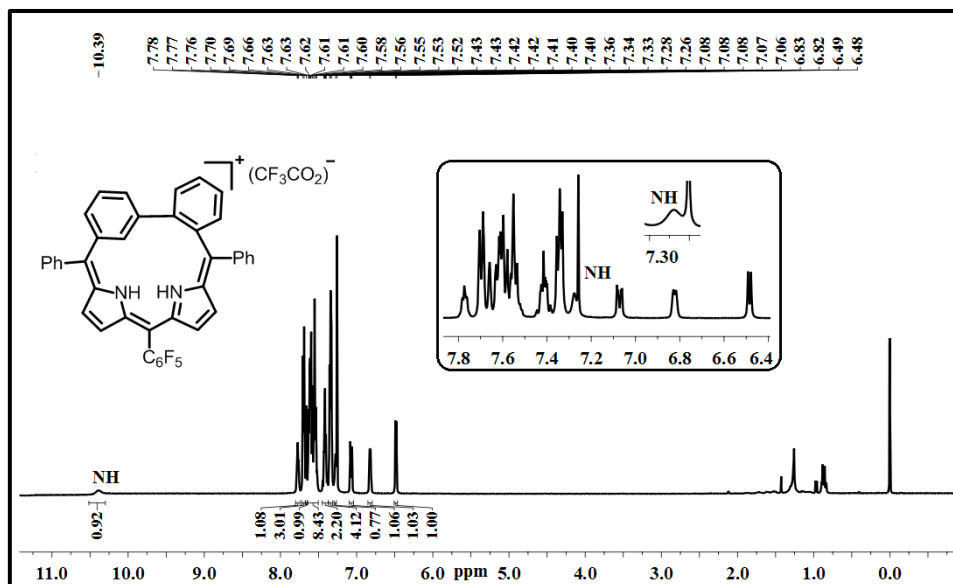


Figure 2.9: $^1\text{H-NMR}$ spectrum of **23.H⁺** in CDCl_3 .

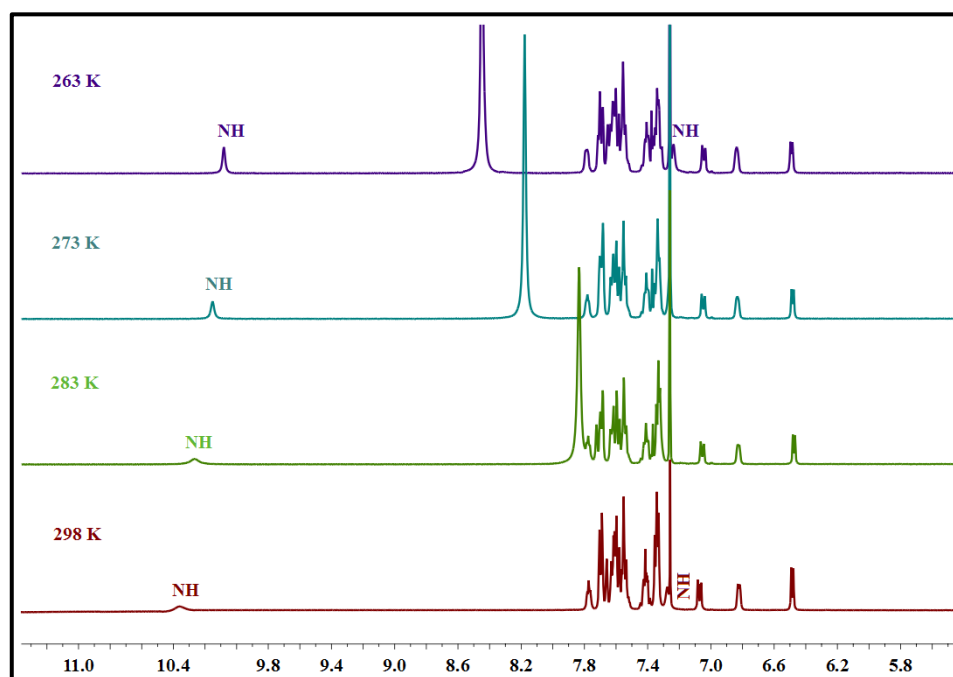


Figure 2.10: Low temperature $^1\text{H-NMR}$ spectrum of **23.H⁺** in CDCl_3 .

The formation of complex **24** and **25** is reflected from the ^1H NMR spectral analyses. The disappearance of inner NH signal confirms the formation of **24** (Figure

2.8b). The spectral analysis reveals that the inner CH [H19] is 2.20 ppm upfield shifted and resonated at 5.31 ppm suggests the weak non-bonding interaction with the boron ion.³⁵ The σ -phenyl protons are merged with biphenyl as well as *meso*-phenyl units, however, one of the σ -phenyl protons is distinctly resonated at 7.90 ppm. On the other hand, in case of **25**, in addition to the absence of inner NH, the disappearance of inner CH[19] signal reveals the formation organoborane complex (Figure 2.8c). Upon C-H activation, the axially coordinated σ -phenyl protons are marginally upfield shifted and resonated between 6.30 ppm and 7.20 ppm. Finally, the ^{11}B NMR analysis of **24** and **25** shows the signal at -1.94 ppm and -1.66 ppm (Figure 2.11) further confirms the boron ion insertion in the macrocyclic framework. Overall, the NMR signals of σ -phenyl protons in **24** and **25** are exactly appeared in between the aromatic¹⁻⁵ and antiaromatic^{10,11} triphyrin B^{III} complexes, thus confirms the non-aromatic character.

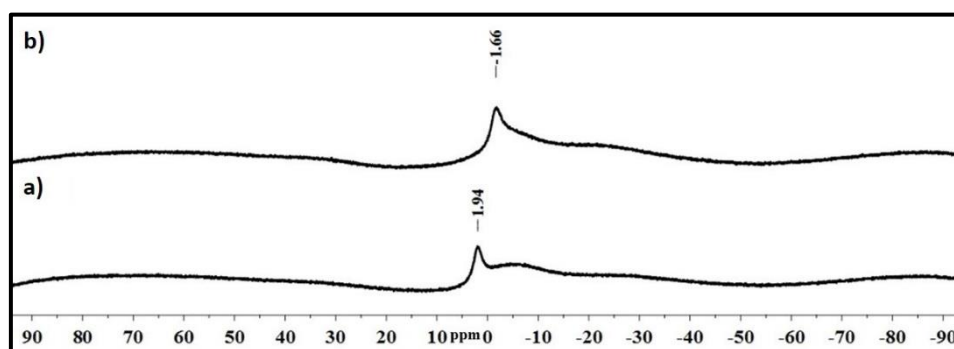


Figure 2.11: ^{11}B -NMR spectrum of a) **24** and b) **25** in CDCl_3 .

2.3.3.3 Single crystal X-ray analysis:

The single crystal X-ray structure of **23** is shown in Figure 2.12 (Table 2.3). The macrocycle crystallizes in monoclinic system with space group $P 2_1/c$. As predicted from the NMR analysis, the pyrrolic NH is in intramolecular hydrogen bonding interaction with imine N with distance and angle of $\text{N2-H2}\dots\text{N1}$ is 2.05(2) Å and $129.59(12)^\circ$ respectively (Figure 2.12a). The crystal analysis reveals that the π -conjugation in the dipyrromethene unit is further extended upto *o*-phenyl unit (C18-C1:

1.493(3) Å; C1-C2: 1.402(3) Å; C2-C3: 1.503(3) Å) with alternate sp^2 - sp^2 single and double bond character (Table 2.1). Whereas, the *m*-phenyl unit restricts the overall π -conjugation, however, maintains the individual aromatic character (1.382(3) to 1.401(3) Å), as observed in the derivatives of *m*-benzporphyrin,^{29,30,35} thus confirms the overall non-aromatic character. The macrocyclic units are deviated from the mean plane which contains 14 inner core atoms (Figure. 2.12b), where the *o*- (56.84(4)°) and *m*-phenyl (77.25(5)°) units are highly tilted from the plane as compared to dipyrromethene pyrrole units (14.23(6) and 38.59(5)°) (Table 2.2). The *meso*-aryl units in **23** are tilted between 21.24(5)° and 34.10(4)°, which are less tilted as compared to **1** (>38°)¹⁻⁵ and **10** (>44°).¹¹

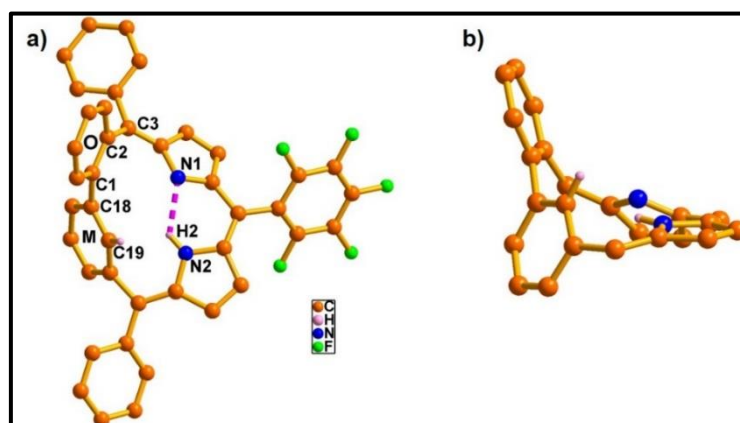


Figure 2.12: Single crystal X-ray structure of **23**. **a)** Top view and **b)** side view. The peripheral hydrogen atoms in **a** & **b** and *meso*-aryl groups in **b** are omitted for clarity in the side view.

Further, the presence of fluorine atoms in the pentafluoro unit as well as the arene units generates three type of self-assembled dimer (Figure 2.13). Out of three dimers two dimers are due to the C-H... π , while the other is due to C-H...F, and C-H... π intermolecular hydrogen bonding interactions. The C-H... π , interactions between; (a) pyrrolic β -CH (C10-H10) and biphenyl π -cloud [Ph(π)]; (b) biphenyl C-H (C16-H16) and pyrrole π -cloud [Py(π)] and (c) phenyl CH (C34-H34) with another unit phenylic π -cloud [Ph(π)]. The bond distance and angles are C10-H10...Ph(π): 2.86(7) Å &

159.48(13)°; C16-H16...Py(π): 2.86(11) Å & 153.33(14)°; C34-H34...Ph(π): 2.80(10) Å & 130.45(14)° (Figure 2.13). The C-H...F interaction is between biphenyl C-H (C16-H16) unit with one of the fluorine atom (F5) in the pentafluorophenyl unit with the distance and angles are C16-H16...F5: 2.82(16) Å & 130.18(14)° (Figure 2.13).

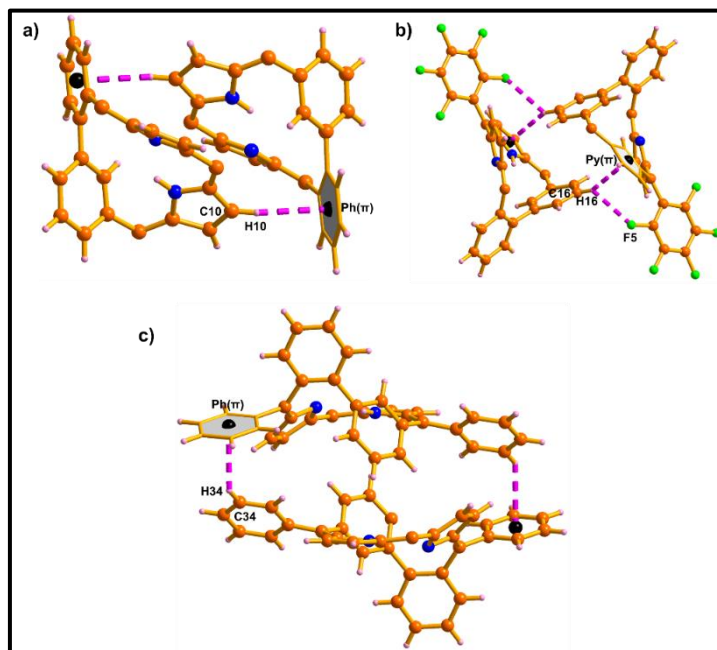


Figure 2.13: Self-assembled dimers of **23**.

The crystal structure of **23.H⁺** is shown in Figure 2.14 (Table 2.3). The **23.H⁺** is in intermolecular hydrogen bonding interaction with the anion with distance and angle of C10-H10...O1 is 2.44(5) Å and 153.78(3)°, respectively. The interaction is further extended by the presence of fluorine and oxygen atoms in the anion with the *m*-phenyl unit and generate 1-D array with the distance and angle of C16-H16...O2 & C17-H17...F8 are 2.99(9) Å and 163.75(3)° & 2.69(4) Å and 129.53(3)° (Figure 2.15). As compared to **23**, the normal (N2) and protonated pyrrole (N1) units and *o*-aryl unit are slightly deviated from the plane, whereas the *m*-phenyl unit is marginally less tilted to the mean macrocyclic plane (Figure 2.15b, Table 2.2). Further, the intramolecular hydrogen bonding observed in **23** (Figure 2.15a), is disappeared in **23.H⁺**, however, the amine NH [N2-H2] generates similar interaction with the *m*-phenyl unit π -cloud [*m*-

$\text{Ph}(\pi)$] with the distance and angle of $\text{N2-H2}\dots m\text{-Ph}(\pi)$ is $2.74(10)$ Å and $130.86(2)^\circ$ (Figure 2.15a), thus the observed deshield signal of amine NH from the NMR spectral studies is further reflected from the single crystal analysis. In addition, the *m*-phenyl CH unit (C15-H15) interacts with pyrrolic π -cloud [$\text{Py}(\pi)$] with distance and angles of $\text{C15-H15}\dots \text{Py}(\pi)$ is $\text{C15-H15}\dots \text{Py}(\pi)$: 2.84 Å & 133° to generate the self-assembled dimer.

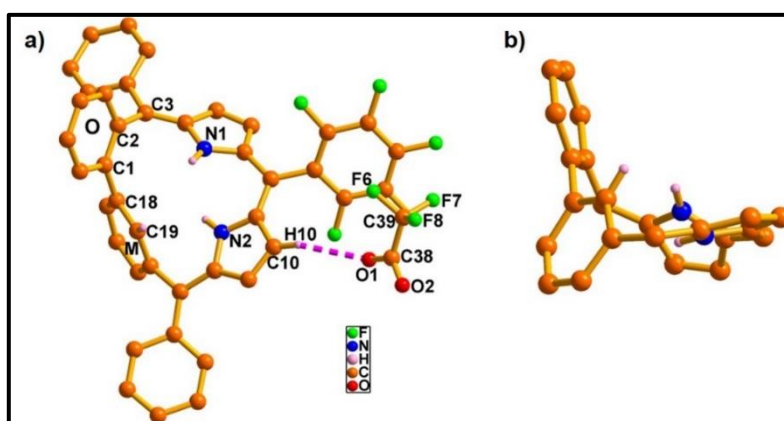


Figure 2.14: Single crystal X-ray structure of $23.\text{H}^+$. **a)** Top view and **b)** side view. The peripheral hydrogen atoms in **a** & **b** and *meso*-aryl groups in **b** are omitted for clarity.

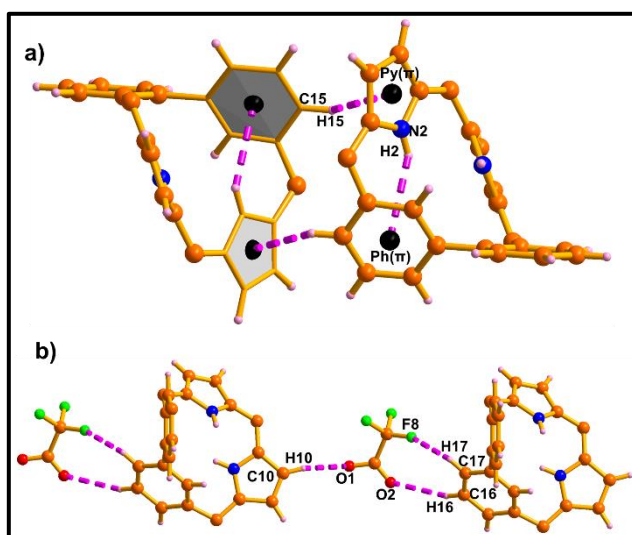


Figure 2.15: Single crystal X-ray analysis of $23.\text{H}^+$. **a)** Self-assembled dimer and **b)** 1-D array.

The final confirmation of **24** has come from the single crystal X-ray analyses (Figure 2.16, Table 2.3). As reflected from the spectral analysis, the B^{III} in **24** is

coordinated with the dipyrromethene unit and the remaining two positions are occupied by σ -phenyl and the chloride ion to generate the B^{III} complex. The B-N bond lengths [B-N1 and B-N2] are 1.604(8) Å and 1.571(8) Å, which are longer than the B-N bond lengths reported earlier.^{1-5,36} The geometry around the boron center is tetrahedral (Figure 2.16c) and the boron(III) ion is 1.45(6) Å above the mean macrocyclic plane. The pyrrole units in **24** are tilted by 52.34(15)° and 37.80(14)°, whereas the *o*- and *m*-phenyl units are tilted by 34.54(16)° (*m*-) and 41.98(15)° (*o*-) (Figure 2.16b, Table 2.2), respectively. As compared to **23**, the deviation in the dihedral angle values of **24** reveals that the coordinated B^{III} ion; (i) approaches on the opposite side of the *o*-phenylene unit, (ii) shifts the pyrrole units away from the plane and (iii) promotes the *m*-phenyl unit towards the plane to generate the weak boron-arene (C19-H19...B) intramolecular interaction with the distance of 3.11(7) Å (Figure 2.16a). The distance is smaller than the corresponding Van der Waals radii (3.28 Å). Similar trend was observed in boron-anthracene linked complex³⁷ and weak metal-arene interaction in *m*-benzi-porphyrin. Thus, the observed *m*-phenyl CH[19] signal at 5.31 ppm in the NMR spectral analysis is further reflected from the crystal analysis. As observed in **23**, the intermolecular hydrogen bonding interaction in the form of one-dimensional array is formed between (a) *o*-phenylene (C1''-H1'') unit with F1 and (b) *o*-phenylene (C2'-H2') with phenyl π -cloud [Ph(π)] with distance and angles of C1''-H1''...F1: 2.72 Å & 144° and C2'-H2'...Ph(π): 2.70 Å & 144°, respectively (Figure 2.17).

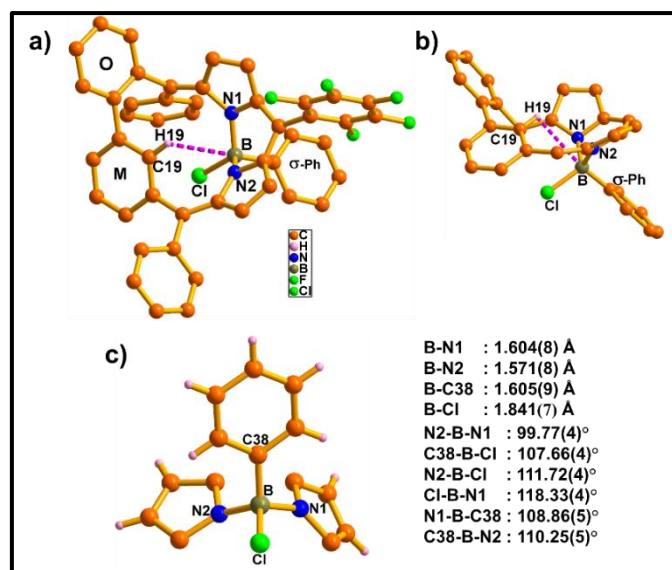


Figure 2.16: Single crystal X-ray structure of **24**. **a)** Top view, **b)** side view and **c)** geometry around the Boron center with bond length (Å) and angle (°). The peripheral hydrogen atoms in **a** & **b** and *meso*-aryl groups in **b** are omitted for clarity.

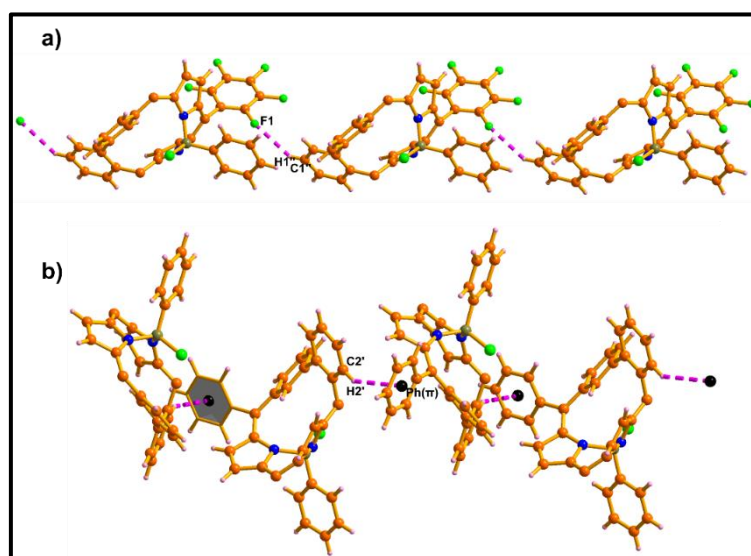


Figure 2.17: 1-D arrays of **24**.

On the other hand, the pyrrole units in **25** are 32.91(10)° (N1), 6.95(9)° (N2), *o*- and *m*-phenyl units are 62.42(9)° (*o*-) and 31.43(8)° (*m*-) deviated from the mean plane (Figure 2.18). The deviation in the dihedral angle values in **25**, as compared to **23** and **24** reveals that the coordinated B^{III} ion; (i) approaches on the same side of the *o*-phenylene unit; (ii) shifts the N1, N2 and *m*-phenylene unit towards the plane to stabilize the organoborane complex **25**. The complex adopts cone conformation where

the B^{III} is 0.63(4) Å above the mean plane. The bowl depth is 1.37(4) Å, as calculated from the peripheral *m*-phenyl CHs and pyrrolic β-CH containing 7 atoms and the value is comparable with **1** (Figure 2.19).⁵ The geometry around the boron center is tetrahedral. The B-N bond lengths [B-N1 and B-N2] are 1.616(6) Å and 1.556(5) Å, which are comparable with the respective bond distances in **24** (Figure 2.18c). The C19-B bond distance in **25** is 1.626(4) Å, which is marginally larger than the respective values observed in **17-19**.²⁶⁻²⁸ The σ-phenyl unit is almost perpendicular (82.80(9)°) to the plane as compared to other *meso*-aryl units (Table 2.2), where the σ-phenyl π-cloud generate the self-assembled dimer with pyrrolic β-CH with the bond distance and angle of 2.69(1) Å & 159(25)°, respectively (Figure 2.20). In addition, as observed in **23**, the complex (**24** and **25**) formation maintains the non-aromatic character as such (Table 2.1)

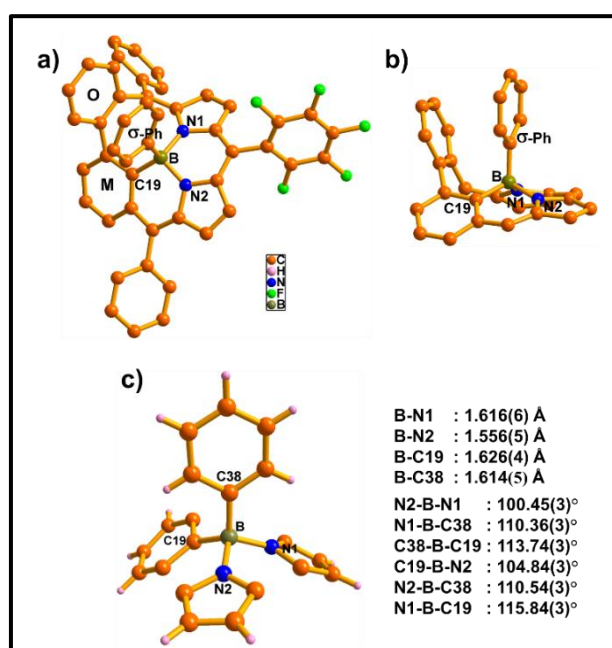


Figure 2.18: Single crystal X-ray structure of **25**. **a)** Top view, **b)** side view and **c)** geometry around the Boron center with bond length (Å) and angle (°). The peripheral hydrogen atoms in **a** & **b** and *meso*-aryl groups in **b** are omitted for clarity.

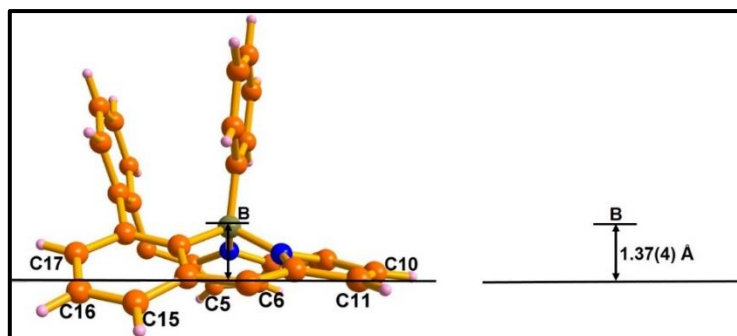


Figure 2.19: The single crystal X-ray analysis of **25**. The distance between the B^{III} ion and the mean plane. The plane contains C5-C6-C10-C11-C15-C16-C17 (7 atoms).

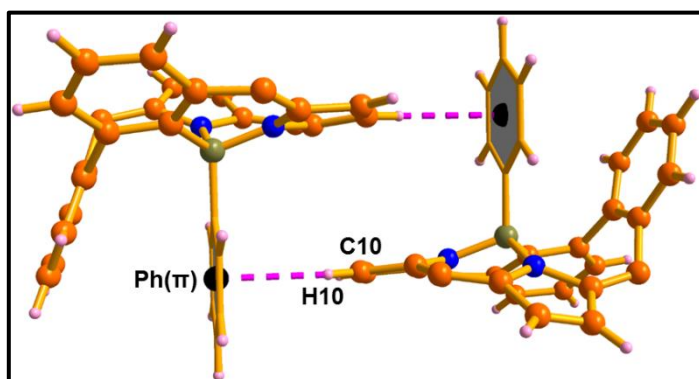
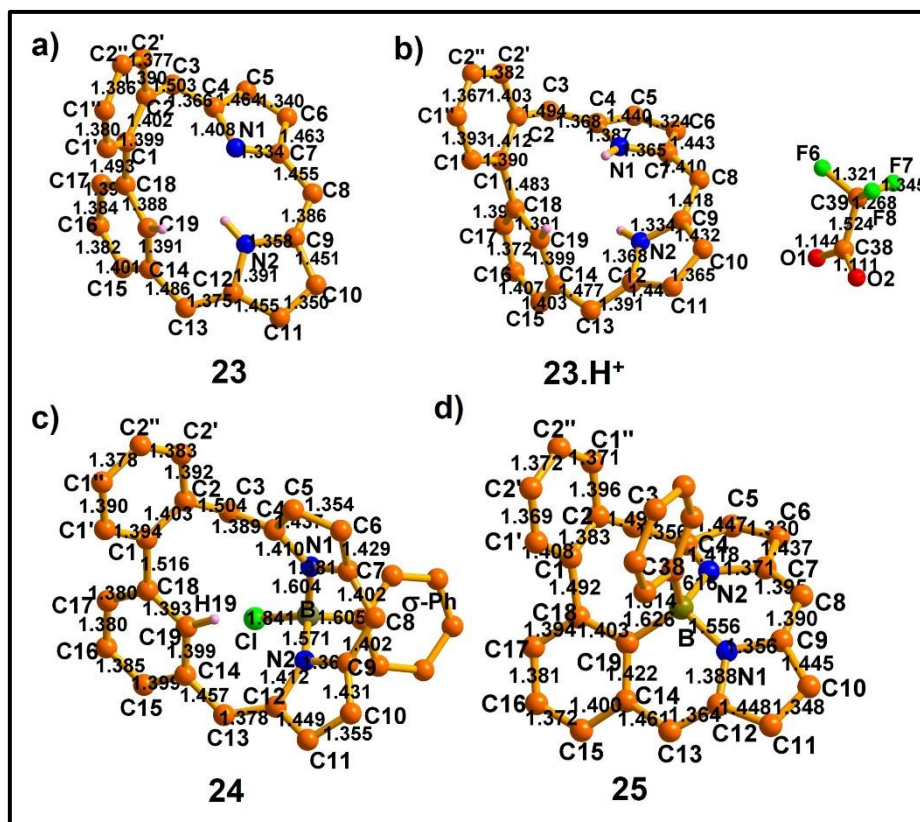


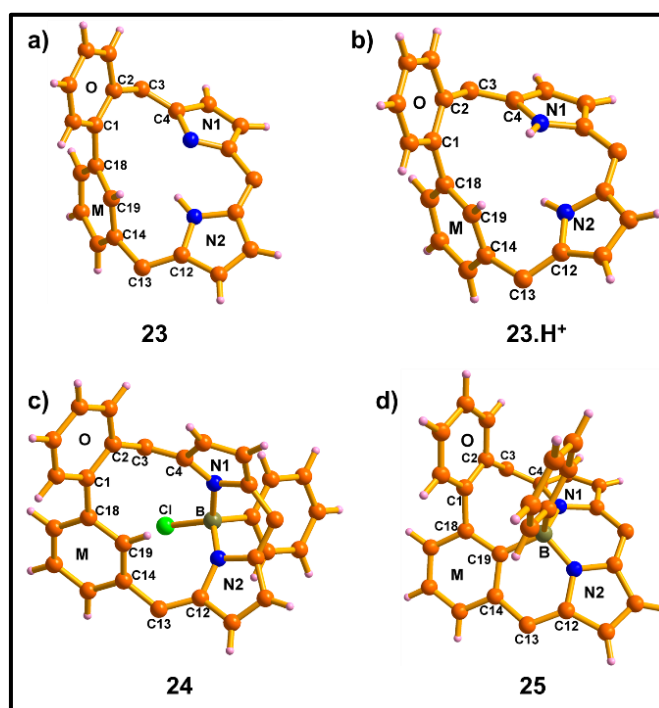
Figure 2.20: Self-assembled dimer of **25**.

Table 2.1: Selected Bond lengths in **23**, **23.H⁺**, **24** and **25** (Å)



Bond Lengths	23 (Å)	23.H ⁺ (Å)	24 (Å)	25 (Å)
C12-C13	1.375(3)	1.391(5)	1.378(7)	1.364(5)
C13-C14	1.486(3)	1.477(4)	1.457(8)	1.461(6)
C14-C19	1.391(3)	1.399(4)	1.399(7)	1.422(5)
C19-C18	1.388(3)	1.391(4)	1.393(8)	1.403(5)
C18-C1	1.493(3)	1.483(4)	1.516(7)	1.492(5)
C1-C2	1.402(3)	1.412(5)	1.403(8)	1.383(6)
C2-C3	1.503(3)	1.494(5)	1.504(8)	1.499(6)
C3-C4	1.366(3)	1.368(3)	1.389(8)	1.356(5)

Table 2.2: The dihedral angle (°) of various units deviate from the mean macrocyclic plane containing 14 inner core atoms



Mean plane contains: C1-C2-C3-C4-N1-C7-C8-C9-N2-C12-C13-C14-C19-C18 (14 atoms)

Units	23 (°)	23.H ⁺ (°)	24 (°)	25 (°)
O (ortho-)	56.84(4)	58.85(9)	41.98(15)	62.42(9)
M (meta-)	77.25(5)	75.59(7)	34.54(16)	31.43(8)
N1 (Pyrrole-1)	38.59(5)	44.93(11)	52.34(15)	32.91(10)
N2 (Pyrrole-2)	14.23(6)	31.04(10)	37.80(14)	6.95(9)
Ar1 (<i>meso</i> -Phenyl)	34.10(4)	34.41(11)	86.48(11)	75.84(8)
Ar2 (<i>meso</i> -C ₆ F ₅)	32.85(5)	27.25(9)	88.60(12)	54.35(12)
Ar3 (<i>meso</i> -Phenyl)	21.24(5)	4.00(9)	37.84(15)	44.38(9)
Ar4 (σ -Phenyl)	--	--	37.94(15)	82.80(9)

2.3.3.4 Electronic spectral analysis

The electronic absorption spectrum of **23**, **23.H⁺**, **24** and **25** are recorded in CH₂Cl₂ and the spectral analysis of **23**, **24** and **25** are shown in Figure 2.21. The freebase **23** shows an intense band at 372 nm and Q-like band at 616 nm with the molar absorption coefficient for the intense band in the order of 10⁴ M⁻¹cm⁻¹. Upon protonation and B^{III} insertion, the color of the solution changes from blue to green, in addition, the intense band is red shifted by 17, 24 and 7 nm and observed at 389 nm (**23.H⁺**), 396 nm (**24**) and 379 nm (**25**) respectively. Similarly, the Q-like bands are also red shifted and appeared at 738 nm (**23.H⁺**), 686 nm (**24**) and 709 nm (**25**) with higher molar absorption coefficient of **23.H⁺** as compared to **23**, **24** and **25**. Further, the titration experiment was performed by using CH₂Cl₂ solution of **23** with gradual addition of TFA and showed the isosbestic points at 376, 445 and 653 nm (Figure 2.22), which suggested the formation of monocation (**23.H⁺**). Overall, the spectral pattern in **23**, **23.H⁺**, **24** and **25** reflects the typical non-aromatic triphyrin derivatives.¹⁷⁻¹⁸

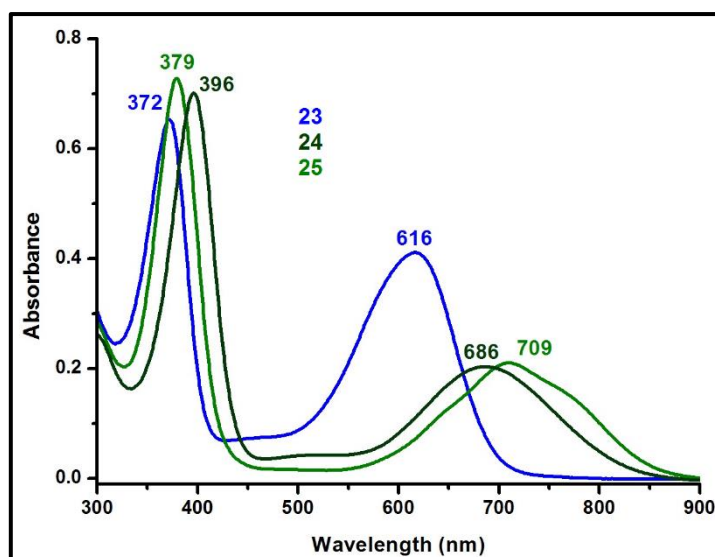


Figure 2.21: The electronic absorption spectrum of **23**, **24** and **25**.

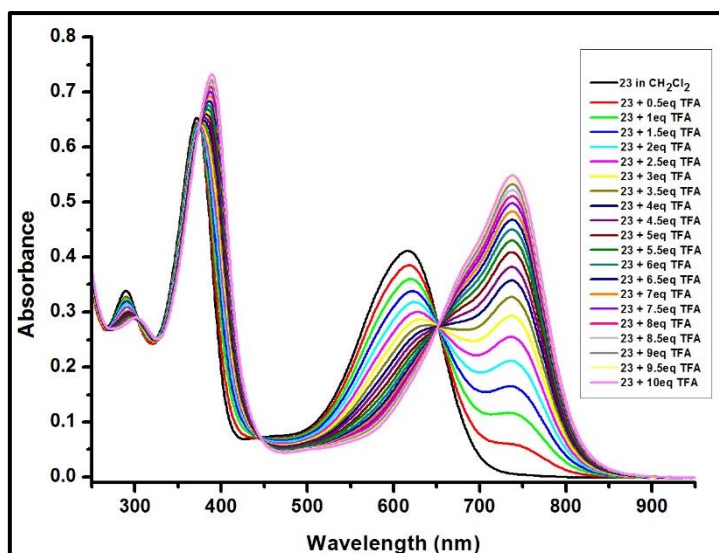


Figure 2.22: The electronic absorption spectrum of **23** with various equivalents of TFA in CH_2Cl_2 .

2.4 Conclusions

In conclusion, we have demonstrated the synthesis of carbatriphyrin(3.1.1) with CNN in the core and explored their coordination ability to stabilize the trifluoroacetate ion and B^{III} complexes. The π -electron conjugation in the macrocyclic framework is extended upto *o*-phenylene unit, however restricted in the *m*-phenylene unit and thus adopts non-aromatic character. The similar trend was observed in protonated as well as both B^{III} complexes. The formation of weak boron arene interaction and stabilization of organoborane complex were reflected from the approach of the B^{III} ion to the macrocyclic ligand. To the best of our knowledge, weak C-H...B intramolecular interaction and C-B bond formation through C-H activation are exploited for the first time in the porphyrin chemistry.

2.5 General Information

The reagents and materials for the synthesis were used as obtained from Sigma Aldrich chemical suppliers. All solvents were purified and dried by standard methods prior to use. The NMR solvents were used as received and the spectra were recorded in

Bruker 400 MHz spectrometer with TMS as internal standard. The ESI mass spectra were recorded in Bruker, micro-TOF-QII mass spectrometer. The Electronic absorption spectra were recorded in Perkin Elmer–Lambda 750 UV-Visible spectrophotometer. The X-ray quality crystals for the compounds were grown by slow diffusion of *n*-hexane over CH₂Cl₂ solution. Single-crystal X-ray diffraction data of **23**, **23.H⁺**, **24** and **25** were collected in a Bruker KAPPA APEX-II, four angle rotation system and Mo-K α radiation (0.71073Å).

The crystals have been deposited in the Cambridge Crystallographic Data Centre for **23**, **23.H⁺**, **24** and **25** with reference no. CCDC 1448161, 1470641, 1448163 and 1497268 respectively. These data can be obtained free of charge from the Cambridge Crystallographic Data Centre via www.ccdc.cam.ac.uk/data_request/cif.

2.6 Synthetic procedure and spectral characterization of 20-25

2.6.1 Synthesis of 20: A mixture of 2-bromobenzaldehyde (1 g, 5.45 mmol), 3-formylphenylboronic acid (1.2 g, 8.10 mmol), and K₂CO₃ (2.24 g, 16.25 mmol) was dissolved in *i*-PrOH/H₂O (1:1, v/v, 60 mL) in an inert atmosphere. After 10 min Pd(OAc)₂ (0.065 g, 0.27 mmol) and pinch of urea was added in to the reaction mixture and allowed to reflux for 6 h. The completion of the reaction was monitored by TLC. The reaction mixture was extracted with CH₂Cl₂ and dried over Na₂SO₄, and concentrated by rotary evaporator. The compound was purified by column chromatography using silica gel (100-200 mesh) in 5% EtOAc/*n*-hexane to afford **20** in 75% yield.

¹H NMR (400 MHz, CDCl₃, 298K): δ = 10.09 (s, 1H), 9.96 (s, 1H), 8.05 (dd, *J* = 7.8, 1.1 Hz, 1H), 8.04 – 7.95 (m, 1H), 7.91 (s, 1H), 7.70 – 7.63 (m, 3H), 7.55 (t, *J* = 7.6 Hz, 1H), 7.45 (d, *J* = 7.6 Hz, 1H).

¹³C NMR (100 MHz, CDCl₃): δ = 191.99, 191.78, 144.36, 139.16, 136.70, 135.99, 134.02, 133.83, 131.02, 130.87, 129.60, 129.35, 128.69, 128.45.

m.p: 46-48°C.

ESI-MS: m/z calculated for C₁₄H₁₀O₂ = 210.0681; found = 211.5084 (M+1).

2.6.2 Synthesis of 21: Freshly prepared phenylmagnesiumbromide (15.86 g, 87.60 mmol) solution in THF (30 ml) was added under N₂ atmosphere at 0 °C into the solution of **20** (1.80 g, 8.760 mmol) in 100 ml THF. The reaction mixture was kept at same temperature for 10 min and then allowed to attain RT. After 6 h the reaction was quenched with saturated NH₄Cl solution and extracted with EtOAc, dried over Na₂SO₄, and concentrated by rotary evaporator. Compound was purified by column chromatography using silica gel (100-200 mesh) in 15% EtOAc/*n*-hexane to afford **21** in 60% yield.

¹H NMR (400 MHz, CDCl₃, 298K): δ = 7.55 (d, *J* = 7.0 Hz, 1H), 7.38 – 7.26 (m, 9H), 7.23 – 7.18 (m, 6H), 7.11 – 7.09 (m, 2H), 5.85 (d, *J* = 3.7 Hz, 1H), 5.79 (d, *J* = 2.9 Hz, 1H), 2.20 (brs, 2H).

¹³C NMR (100 MHz, CDCl₃): δ = 139.12, 139.07, 139.00, 138.97, 138.93, 136.26, 136.22, 136.08, 136.03, 136.01, 135.90, 124.67, 123.22, 123.18, 122.91, 122.62, 122.23, 122.20, 121.77, 121.51, 121.47, 121.45, 114.53, 110.13, 70.63, 66.63.

m.p: 132-136°C.

ESI-MS: m/z calculated for C₂₆H₂₂O₂ = 366.1620; found = 389.1494 (M+Na).

2.6.3 Synthesis of 22: 2,3'-Bis(phenylhydroxymethyl)biphenyl (**21**) (1.2 g, 3.28 mmol) and pyrrole (10 mL) in 1,2-dichloroethane (40 mL) was kept in an inert atmosphere for 10 min. Then 1.4 mL of BF₃·Et₂O solution was added in to the reaction mixture and allowed to stir for 8 h in reflux condition. The solution was cooled to room temperature and quenched by addition of triethylamine (2 mL). The compound was extracted with

CH₂Cl₂, dried over Na₂SO₄ and concentrated by rotary evaporator. The crude mixture was purified by column chromatography using silica gel (100-200 mesh) in 10% EtOAc/*n*-hexane to afford **22** in 40% yield.

¹H NMR (400 MHz, CDCl₃, 298K): δ = 7.61 (brs, 1H), 7.45 (brs, 1H), 7.30 – 7.08 (m, 15H), 6.96 – 6.95 (m, 1H), 6.92 – 6.89 (m, 2H), 6.60 (s, 1H), 6.53 (dd, *J* = 4.4, 2.5 Hz, 1H), 6.09 (dd, *J* = 5.4, 2.7 Hz, 2H), 5.76 (d, *J* = 2.3 Hz, 1H), 5.69 (d, *J* = 2.3 Hz, 1H), 5.41 (s, 1H), 5.32 (d, *J* = 2.9 Hz, 1H).

¹³C NMR (100 MHz, CDCl₃): δ = 143.17, 143.15, 142.90, 141.94, 141.63, 140.67, 134.00, 133.84, 133.66, 130.19, 130.08, 129.93, 129.65, 129.04, 129.00, 128.95, 128.93, 128.66, 128.63, 128.43, 127.77, 127.73, 127.70, 126.86, 126.83, 126.54, 126.47, 117.45, 117.43, 117.18, 117.12, 108.40, 108.36, 108.29, 108.09, 50.91, 46.81.

m.p: 46-48 °C.

ESI-MS: *m/z* calculated for C₃₄H₂₈N₂ = 464.2252; found = 487.2142 (M+Na).

2.6.4 Synthesis of 23: To a 150 ml CH₂Cl₂ solution, **22** (150 mg, 0.32 mmol) and pentafluorobenzaldehyde (75 mg, 0.38 mmol) was added under inert atmosphere covered with aluminium foil and stirred for 10 min. TFA (0.074 ml, 0.96 mmol) was added and allowed to stir under same condition for 3 h. Then 2,3-dichloro-5,6-dicyano-1,4-benzoquinone (0.217 mg, 0.96 mmol) was added to the reaction mixture and opened to air. The mixture was further allowed to stir for 2h. The crude product was passed through basic alumina column followed by neutral alumina column. The blue band was eluted with 15% CH₂Cl₂/*n*-hexane and identified as **23**. The compound was further recrystallized from CH₂Cl₂/*n*-hexane to afford blue crystalline **23** in 35% yield.

¹H NMR (400 MHz, CDCl₃, 298K): δ = 10.71 (brs, 1H), 7.57 (d, *J* = 7.4 Hz, 2H), 7.54 – 7.51 (m, 3H), 7.46 – 7.34 (m, 9H), 7.27 (s, 2H), 7.21 (d, *J* = 7.3 Hz, 1H), 7.14 (t, *J* =

7.6 Hz, 1H), 7.06 (d, $J = 4.7$ Hz, 1H), 7.02 (d, $J = 7.7$ Hz, 1H), 6.55 (s, 1H), 6.26 (d, $J = 4.7$ Hz, 1H).

^{13}C NMR (100 MHz, CDCl_3): $\delta = 169.94, 154.63, 151.40, 143.57, 143.05, 142.95, 141.89, 141.43, 140.03, 139.38, 138.16, 136.55, 135.94, 132.00, 131.60, 131.01, 130.97, 129.87, 128.79, 128.63, 128.35, 128.12, 127.82, 127.54, 127.27, 127.07, 126.99, 125.91, 125.68.$

m.p: 300 °C (decomposition).

ESI-MS: m/z calculated for $\text{C}_{41}\text{H}_{23}\text{F}_5\text{N}_2 = 638.1781$; found = 639.1843 ($\text{M}+1$).

UV-Vis (CH_2Cl_2): $\lambda_{\text{max}}(\text{nm})$ ($\epsilon \times 10^4$ [$\text{M}^{-1}\text{cm}^{-1}$]) = 372 (5.94), 616 (3.74).

$^{23}\text{H}^+$: ^1H NMR (400 MHz, CDCl_3 , 298K): $\delta = 10.39$ (brs, 1H), 7.77 (t, $J = 3.6$ Hz, 1H), 7.70 (d, $J = 6.0$ Hz, 3H), 7.66 (s, 1H), 7.63 – 7.52 (m, 8H), 7.43 – 7.40 (m, 2H), 7.36 – 7.33 (m, 4H), 7.28 (brs, 1H), 7.08 – 7.06 (m, 1H), 6.82 (d, $J = 4.7$ Hz, 1H), 6.48 (d, $J = 5.3$ Hz, 1H).

UV-Vis(CH_2Cl_2): $\lambda_{\text{max}}(\text{nm})$ ($\epsilon \times 10^4$ [$\text{M}^{-1}\text{cm}^{-1}$]) = 389 (6.10), 738 (4.56).

2.6.5 Synthesis of **24:** The dichlorophenylborane (57 mg, 0.31 mmol) was added into the solution of **23** (20 mg, 0.031 mmol) in toluene (20 ml) under inert atmosphere at reflux condition for 30 min. Freshly distilled TEA (0.0218 ml, 0.155 mmol) was added into the reaction mixture at same temperature and kept for 12 h. Completion of the reaction was monitored through TLC and solvent was evaporated by rotary evaporator. The crude complex was purified by neutral alumina column. The green band was eluted with 10% $\text{CH}_2\text{Cl}_2/n$ -hexane and identified as **24**. The compound was further recrystallized from $\text{CH}_2\text{Cl}_2/n$ -hexane to afford green crystalline **24** in 70% yield and <1% yield of **25**.

^1H NMR (400 MHz, CDCl_3 , 298K): $\delta = 7.83$ (d, $J = 7.6$ Hz, 1H), 7.61 (d, $J = 7.9$ Hz, 1H), 7.55 (t, $J = 5.4$ Hz, 1H), 7.53 – 7.46 (m, 4H), 7.44 – 7.33 (m, 4H), 7.21 – 6.98 (m,

11H), 6.74 (d, $J = 5.1$ Hz, 1H), 6.66 (d, $J = 5.2$ Hz, 1H), 6.51 (d, $J = 5.2$ Hz, 1H), 6.39 – 6.38 (m, 1H), 5.31 (s, 1H).

^{13}C NMR (100 MHz, CD_2Cl_2): $\delta = 150.77, 149.67, 147.79, 144.76, 142.94, 142.50, 141.38, 139.81, 138.78, 137.85, 135.36, 133.93, 133.06, 132.47, 132.39, 132.20, 132.08, 131.42, 130.19, 129.61, 129.31, 128.82, 128.76, 128.28, 128.04, 127.90, 127.78, 127.27, 127.23, 126.66, 126.48, 125.91, 125.49, 121.36.$

m.p: 250 °C (decomposition).

ESI-MS: m/z calculated for $\text{C}_{47}\text{H}_{27}\text{BClF}_5\text{N}_2 = 760.1876$; found = 760.1882 (M).

UV-Vis (CH_2Cl_2): $\lambda_{\text{max}}(\text{nm})$ ($\epsilon \times 10^4$ [$\text{M}^{-1}\text{cm}^{-1}$]) = 396 (5.85), 686 (1.69).

2.6.6 Synthesis of 25: The dichlorophenylborane (57 mg, 0.31 mmol) was added into the solution of **23** (20 mg, 0.031 mmol) in toluene (20 ml) under inert atmosphere at reflux condition for 30 min. Freshly distilled TMP (0.026 ml, 0.155 mmol) was added into the reaction mixture at same temperature and kept for 12 h. Completion of the reaction was monitored through TLC and solvent was evaporated by rotary evaporator. The crude complex was purified by neutral alumina column. The green band was eluted with 5% $\text{CH}_2\text{Cl}_2/n$ -hexane and identified as **25**. The compound was further recrystallized from $\text{CH}_2\text{Cl}_2/n$ -hexane to afford green crystalline **25** in 60% yield and 20% yield of **24**.

^1H NMR (400 MHz, CDCl_3 , 298K): $\delta = 7.51 - 7.47$ (m, 7H), 7.31 – 7.29 (m, 4H), 7.18 (t, $J = 7.6$ Hz, 1H), 7.05 (t, $J = 7.1$ Hz, 1H), 6.99 – 6.93 (m, 2H), 6.92 (d, $J = 5.4$ Hz, 1H), 6.80 – 6.71 (m, 7H), 6.29 – 6.27 (m, 2H), 6.24 (d, $J = 5.3$ Hz, 1H).

^{13}C NMR (100 MHz, CDCl_3): $\delta = 157.01, 155.98, 150.54, 147.66, 142.92, 140.41, 139.99, 137.16, 137.11, 136.02, 134.57, 132.72, 132.23, 131.63, 131.37, 131.11, 130.69, 129.76, 129.21, 128.84, 128.46, 128.36, 128.31, 128.20, 127.94, 126.74, 126.27, 125.70, 124.63, 124.49, 123.05.$

^{11}B NMR (128 MHz, CDCl_3): $\delta = -1.66$;

m.p: 250 °C (decomposition).

ESI-MS: m/z calculated for $\text{C}_{47}\text{H}_{26}\text{BClF}_5\text{N}_2 = 724.2109$; found = 747.2010 (M+Na).

UV-Vis (CH_2Cl_2): $\lambda_{\text{max}}(\text{nm})$ ($\epsilon \times 10^4$ [$\text{M}^{-1}\text{cm}^{-1}$]) = 379 (6.07), 709 (1.75).

Table 2.3: Crystal data for **23**, **23.H⁺**, **24** and **25**

Crystal parameters	23	23.H⁺	24	25
Formula	$\text{C}_{41}\text{H}_{23}\text{F}_5\text{N}_2$	$\text{C}_{43}\text{H}_{24}\text{F}_8\text{N}_2\text{O}_2$	$\text{C}_{47}\text{H}_{27}\text{BClF}_5\text{N}_2$	$\text{C}_{47}\text{H}_{26}\text{BF}_5\text{N}_2$
$M/\text{g mol}^{-1}$	638.61	752.64	760.96	724.52
T/K	100	100	100	298
Crystal dimensions/ mm^3	0.10 x 0.08 x 0.05	0.08 x 0.07 x 0.05	0.10 x 0.08 x 0.06	0.1 x 0.08 x 0.06
Crystal system	Monoclinic	Triclinic	Orthorhombic	Triclinic
Space group	$P 2_1/c$	$P-1$	$P 2_1 2_1 2_1$	$P-1$
$a/\text{\AA}$	10.676(5)	11.225(5)	13.3277(7)	11.622(4)
$b/\text{\AA}$	20.696(5)	13.534(5)	15.9727(7)	13.304(5)
$c/\text{\AA}$	13.774(5)	15.488(5)	16.4409(7)	14.734(6)
$\alpha/^\circ$	90.000(5)	102.454(5)	90.000	67.215(17)
$\beta/^\circ$	103.633(5)	97.331(5)	90.000	86.07(2)
$\gamma/^\circ$	90.000(5)	109.009(5)	90.000	83.019(19)
$V/\text{\AA}^3$	2957.6(19)	2121.8(14)	3499.9(3)	2084.4(14)
Z	4	2	4	2
$\rho_{\text{calcd}}/\text{mg m}^{-3}$	1.434	1.178	1.444	1.154
μ/mm^{-1}	0.106	0.097	0.176	0.083
F(000)	1312	768	1560	744
Reflns. collected	36307	27928	20809	19829
Indep.reflns.[$R(\text{int})$]	5629 [0.0757]	9703 [0.0833]	6117 [0.0951]	7715 [0.0675]
Max/min transmission	0.7453 and 0.6092	0.7456 and 0.6301	0.7454 and 0.6623	0.7452 and 0.6133
Data/restraints/parameters	5629 / 0 / 434	9703 / 0 / 496	6117 / 0 / 505	7715 / 0 / 497
GOF on F^2	1.028	0.986	0.992	0.902
Final R indices [$I > 2\sigma(I)$]	R1 = 0.0437, wR2 = 0.1011	R1 = 0.0875, wR2 = 0.2319	R1 = 0.0542, wR2 = 0.0973	R1 = 0.0616, wR2 = 0.1288
R indices (all data)	R1 = 0.0741, wR2 = 0.1160	R1 = 0.1380, wR2 = 0.2559	R1 = 0.1006, wR2 = 0.1158	R1 = 0.1687, wR2 = 0.1530
Largest diff peak and hole [$e \text{\AA}^{-3}$]	0.278 and -0.232	1.317 and -1.240	0.425 and -0.249	0.183 and -0.200

2.7 References

1. Inokuma, Y.; Kwon, J. H.; Ahn, T. K.; Yoo, M.-C.; Kim, D.; Osuka, A. *Angew. Chem. Int. Ed.* **2006**, *45*, 961-964.
2. Claessens, C. G.; González-Rodríguez, D.; Rodríguez-Morgade, M. S.; Medina, A.; Torres, T. *Chem. Rev.* **2014**, *114*, 2192-2277.
3. Osuka, A.; Tsurumaki, E.; Tanaka, T. *Bull. Chem. Soc. Jpn.* **2011**, *84*, 679-697.
4. Inokuma, Y.; Osuka, A. *Dalton Trans.* **2008**, 2517-2526.
5. Myśliborski, R.; Latos-Grażyński, L.; Szterenber, L.; Lis, T. *Angew. Chem. Int. Ed.* **2006**, *45*, 3670-3674.
6. Xue, Z.-L.; Shen, Z.; Mack, J.; Kuzuhara, D.; Yamada, H.; Okujima, T.; Ono, N.; You, X.-Z.; Kobayashi, N. *J. Am. Chem. Soc.* **2008**, *130*, 16478-16479.
7. Kuzuhara, D.; Yamada, H.; Xue, Z.; Okujima, T.; Mori, S.; Shen, Z.; Uno, H. *Chem. Commun.* **2011**, *47*, 722-724.
8. Anju, K. S.; Ramakrishnan, S.; Srinivasan, A. *Org. Lett.* **2011**, *13*, 2498-2501.
9. Kuzuhara, D.; Sakakibara, Y.; Mori, S.; Okujima, T.; Uno, H.; Yamada, H. *Angew. Chem. Int. Ed.* **2013**, *52*, 3360-3363.
10. Pawlicki, M.; Hurej, K.; Szterenber, L.; Latos-Grażyński, L. *Angew. Chem. Int. Ed.* **2014**, *53*, 2992-2996.
11. Pawlicki, M.; Garbicz, M.; Szterenber, L.; Latos-Grażyński, L. *Angew. Chem. Int. Ed.* **2015**, *54*, 1906-1909.
12. Pawlicki, M.; Kędzia, A.; Szterenber, L.; Latos-Grażyński, L. *Eur. J. Org. Chem.* **2013**, *2013*, 2770-2774.
13. Nojman, E.; Berlicka, A.; Szterenber, L.; Latos-Grażyński, L. *Inorg. Chem.* **2012**, *51*, 3247-3260.

-
14. Berlicka, A.; Latos-Grażyński, L.; Lis, T. *Angew. Chem. Int. Ed.* **2005**, *44*, 5288-5291.
 15. Berlicka, A.; Latos-Grażyński, L. *Inorg. Chem.* **2009**, *48*, 7922-7930.
 16. Krivokapic, A.; Cowley, A. R.; Anderson, H. L. *J. Org. Chem.* **2003**, *68*, 1089-1096.
 17. Pawlicki, M.; Latos-Grażyński, L.; Szterenber, L. *J. Org. Chem.* **2002**, *67*, 5644-5653.
 18. Pawlicki, M.; Kędzia, A.; Bykowski, D.; Latos-Grażyński, L. *Chem. Eur. J.* **2014**, *20*, 17500-17506.
 19. Berlicka, A.; Sprutta, N.; Latos-Grażyński, L. *Chem. Commun.* **2006**, 3346-3348.
 20. Pacholska, E.; Latos-Grażyński, L.; Ciunik, Z. *Chem. Eur. J.* **2002**, *8*, 5403-5405.
 21. Pacholska-Dudziak, E.; Gaworek, A.; Latos-Grażyński, L. *Inorg. Chem.* **2011**, *50*, 10956-10965.
 22. Stępień, M.; Gońka, E.; Żyła, M.; Sprutta, N. *Chem. Rev.* **2016**.
 23. Agnoli, S.; Favaro, M. *J. Mater. Chem. A* **2016**, *4*, 5002-5025.
 24. Campbell, P. G.; Marwitz, A. J. V.; Liu, S.-Y. *Angew. Chem. Int. Ed.* **2012**, *51*, 6074-6092.
 25. Jäkle, F. *Chem. Rev.* **2010**, *110*, 3985-4022.
 26. Hata, H.; Shinokubo, H.; Osuka, A. *J. Am. Chem. Soc.* **2005**, *127*, 8264-8265.
 27. Fujimoto, K.; Yorimitsu, H.; Osuka, A. *Chem. Eur. J.* **2015**, *21*, 11311-11314.
 28. Fujimoto, K.; Oh, J.; Yorimitsu, H.; Kim, D.; Osuka, A. *Angew. Chem. Int. Ed.* **2016**, *55*, 3196-3199.
 29. Berlin, K.; Breitmaier, E. *Angew. Chem., Int. Ed. Engl.* **1994**, *33*, 1246-1247.
-

30. Stępień, M.; Latos-Grażyński, L. *Acc. Chem. Res.* **2005**, *38*, 88-98.
31. Lash, T. D. *Chem. Asian J.* **2014**, *9*, 682-705.
32. Lash, T. D. *Acc. Chem. Res.* **2016**, *49*, 471-482.
33. Adinarayana, B.; Thomas, A. P.; Suresh, C. H.; Srinivasan, A. *Angew. Chem. Int. Ed.* **2015**, *54*, 10478-10482.
34. Stępień, M.; Latos-Grażyński, L. *J. Am. Chem. Soc.* **2002**, *124*, 3838-3839.
35. Stępień, M.; Latos-Grażyński, L.; Szterenber, L.; Panek, J.; Latajka, Z. *J. Am. Chem. Soc.* **2004**, *126*, 4566-4580.
36. Młodzianowska, A.; Latos-Grażyński, L.; Szterenber, L.; Stępień, M. *Inorg. Chem.* **2007**, *46*, 6950-6957.
37. Alemany, P.; D'Aléo, A.; Giorgi, M.; Canadell, E.; Fages, F. *Cryst. Growth Des.* **2014**, *14*, 3700-3703.

CHAPTER 3

A 6,11,16-Triarylbiarylcorrole with an adj-CCNN Core: Stabilization of an Organocopper(III) Complex

3.1	Introduction	69
3.2	Objective of our work	71
3.3	Results and Discussion	72
3.3.1	Synthesis	72
3.3.2	Spectral characterisation	73
3.3.2.1	Mass spectrometric analysis	73
3.3.2.2	Electronic spectral analysis of 4	73
3.3.2.3	NMR Analysis	74
3.3.2.4	Single crystal X-ray analysis of 4	76
3.3.3	Coordination Studies	80
3.3.3.1	Spectral characterisation	80
3.3.3.1.1	Mass spectrometric analysis	80
3.3.3.1.2	Electronic spectral analysis	80
3.3.3.1.3	NMR Analysis	81
3.3.3.1.4	Single crystal X-ray analysis of 5	82
3.2.3.2	Confirmation studies for Cu ^{III} ion	86
3.4	Conclusions	89
3.5	Experimental Section	90
3.5.1	General Information	90
3.5.2	Synthetic procedure and spectral characterization of 2-5	90
3.6	References	94

3.1 Introduction

Carbaporphyrinoid is a porphyrin analogue in which one or more nitrogen atoms in the porphyrin core is replaced by carbon atoms and receiving much attention in recent years.^{1,2} The research is mainly focused on monocarbaporphyrinoids with CNNN in the core, which includes N-confused porphyrins,^{3,4} benziporphyrins,⁵⁻⁷ oxybenzporphyrins,⁸ tropiporphyrins,^{9,10} benzocarbaporphyrins,¹¹ azuliporphyrins,^{12,13} N-confused pyriporphyrins,^{14,15} O- and S-confused heteroporphyrins,¹⁶ pyrazoloporphyrins,¹⁷ naphthiporphyrins,¹⁸ and neo-confused porphyrins.¹⁹ These carbaporphyrinoid systems provided unique platform to study, (i) unusual reactivity and spectral properties; (ii) provide information about the aromatic nature of porphyrinoids and (iii) generate organometallic complexes with unusual oxidation states.³⁻¹⁹ Depending on the nature of the aromatic subunits in the framework, the degree of aromaticity varies. For example, benzocarbaporphyrins¹¹ are highly aromatic; azuli derivatives^{12,13} are weakly aromatic, whereas the *m*-benzporphyrin⁵⁻⁷ is nonaromatic. Synthesis and coordination chemistry of mono-carbaporphyrinoids are briefly described in the Chapter 1.

As compared to mono-carbaporphyrinoids, only limited number of dicarbaporphyrinoids with *cis*- or *adj*-CCNN and *trans*- or *opp*-CNCN in the core is known. This includes aromatic *cis*- and *trans*-doubly N-confused porphyrins which forms organo-Cu^{III} and Ag^{III} complexes.^{20,21} Among the dicarbaporphyrins with *opp*-two indene units,²² *opp*-²³/*adj*^{24,25}-azulene & indene units and *adj*-diazuli derivatives,²⁶ only the last two macrocycles are stable. Recently reported stable, aromatic *adj*-dicarbaporphyrin with two indene units forms a tripalladium sandwich complex which is described in the Chapter 1.²⁷

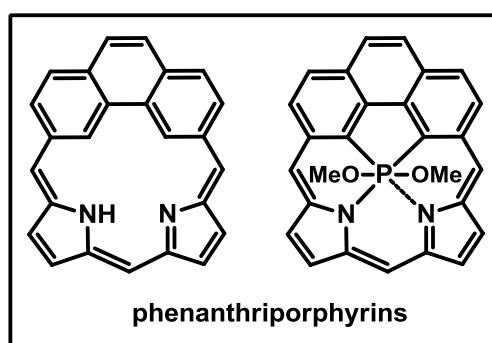


Figure 3.1: Structures of phenanthriporphyrin and its organophosphorus(V) complex.

Very recently Latos-Grażyński and co-workers reported the synthesis of *adj*-CCNN phenanthriporphyrin by acid-catalyzed condensation of phenanthrene diol and dipyrromethane (Figure 3.1). The newly formed antiaromatic aceneporphyrinoid trianionic (CCNN) core, affords a hypervalent organophosphorus(V) complex.²⁸

On the other hand, by removing one of the *meso*-carbon in the porphyrin framework leads to contracted porphyrinoids such as corrole (NNNN), which stabilize the unusually high oxidation state transition metal complexes.²⁹⁻³² As compared to monocarbaporphyrinoids, the monocarbacorroles with CNNN in the inner core are less known which includes isocarbacorrole,³³ series of N-confused corroles,³⁴ norrole

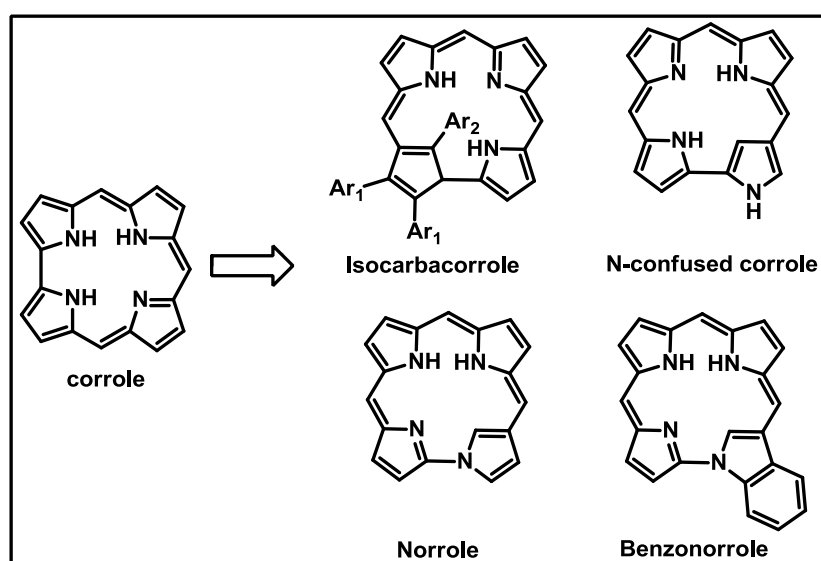


Figure 3.2: Structures of monocarbacorrole analogues.

and benzocorrole (Figure 3.2).³⁵ The non-aromatic isocarbacorrole stabilizes organo- Cu^{III} and Ag^{III} complexes,³³ while the aromatic N-confused corroles bind effectively with anions.³⁴ However, the next level in the carbacorrole chemistry, dicarbacorrole with the core containing *adj*-CCNN or *opp*-CNCN framework is not known in the literature. Such macrocycle can have an ideal platform to stabilize higher oxidation state organometallic complexes, as observed in the porphyrin analogues.

3.2 Objective of our work

In light of the extensive literature reports, it is clear that carbaporphyrinoids are most useful candidates for exploration of various fields in the chemistry. However, such a kind of chemistry is not much known in the corroles. In particular dicarbacorroles are hitherto unknown in the literature.

In this chapter, we have described synthesis of novel corrole analogue with *adj*-dicarba unit in the corrole core for the first time (Figure 3.3). The synthesis of an *adj*-dicarbacorrole with CCNN in the core, is achieved by introducing a biphenyl unit in place of bipyrrrole unit in normal corrole. Based on the spectral studies and structural characterization, the macrocycle is found to be nonaromatic nature and the trianionic core best suits for the Cu^{III} metal ion to form the organocopper complex.

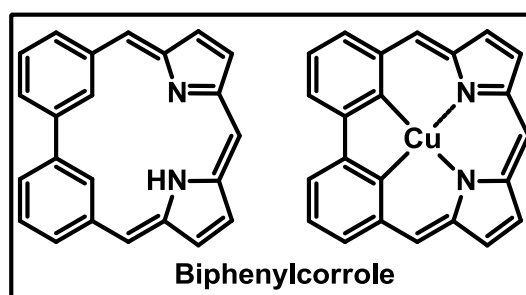
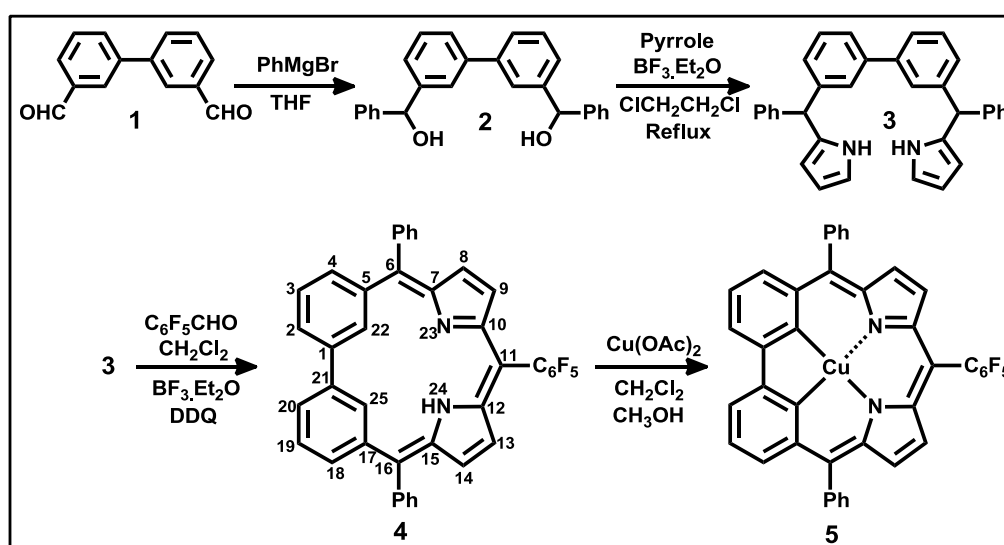


Figure 3.3: Structures of *adj*-dicarbacorrole and its organocopper(III) complex.

3.3 Results and discussions

3.3.1 Synthesis

The synthesis of the target macrocycle and its metal complex is outlined in Scheme 1, where the synthesis involved three steps. The first step is the conversion of biphenyl-3,3'-dicarbaldehyde (**1**)³⁶ to 3,3'-bis(phenylhydroxymethyl)biphenyl (**2**) by using freshly prepared Grignard reagent such as phenylmagnesium bromide in THF to afford **2** in 65% yield. The key precursor, 3,3'-biphenyl-bis(dipyrromethane) (**3**) was synthesized in the second step by condensing **2** with an excess of pyrrole in presence of $\text{BF}_3 \cdot \text{Et}_2\text{O}$, where the direct conversion was not successful, hence, we followed a similar strategy as reported by Latos-Grażyński, *et al.*,³⁷ where the mixture was refluxed for 8 h by using 1,2-dichloroethane as solvent to afford **3** in 42% yield. In the final step, we followed the Lindsey macrocyclization procedure,³⁸ where the $\text{BF}_3 \cdot \text{Et}_2\text{O}$ acid-catalyzed condensation reaction of **3** with pentafluorobenzaldehyde followed by oxidation with 2,3-dichloro-5,6-dicyano-*p*-benzoquinone (DDQ) afforded **4** in 10% yield.



Scheme 3.1: Synthesis of **4** and **5**.

3.3.2 Spectral Characterization

3.3.2.1 Mass spectrometric analysis

The electron spray ionization (ESI) mass spectrometric analysis of **4** exhibits the molecular ion peak at m/z 639.1821 [M+1] (Figure 3.4) and is consistent with the exact composition of the macrocycle.

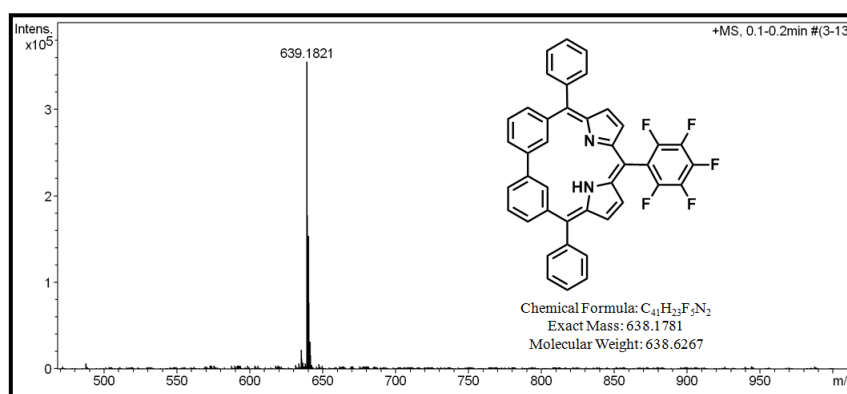


Figure 3.4: ESI-MS spectrum of **4**.

3.3.2.2 Electronic spectral analysis

The electronic absorption spectral analysis of **4** in freebase and its protonated form is shown in Figure 3.5. The freebase form exhibits an intense band at 367 nm and broad absorption bands at 612 nm and 644 nm with the molar absorption coefficient (ϵ) of the intense band is in the order of 10^5 . Comparisons of these data with *m*-benzporphyrin and corrole reveal the following; (i) the similar intense absorption band and the ϵ value is in the order of 10^5 , as observed in *m*-benzporphyrin,⁶ suggests the nonaromatic character in **4**; however reduction in the π -electron delocalization is observed in **4**, where the intense band is blue shifted by 44 nm (tripyrromethene in *m*-benzporphyrin vs dipyrromethene in **4**) and (ii) the absence of intense Soret band and well-defined Q-bands and one order of reduction in the ϵ value, as observed in corrole,³⁰

suggests the macrocycle reported here is not aromatic. Overall, the electronic absorption spectrum of **4** reflects the absence of effective π -delocalization and the spectral profile is similar to *m*-benziporphyrin. Upon protonation of **4** with dilute solution of TFA in CH_2Cl_2 , the color of the solution changed from blue to green. The intense band and weak absorption bands are further red-shifted by 4 nm and 86, 121 nm and observed at 371 and 698, 765 nm, respectively, where the intensity of the higher energy band is reduced as compared to **4** (Figure 3.5a). The titration of **4** (1.99×10^{-5} M) with various equivalents of TFA in CH_2Cl_2 is shown in Figure 3.5b and suggest that the spectral profile does not alter the effective π -electron delocalization.

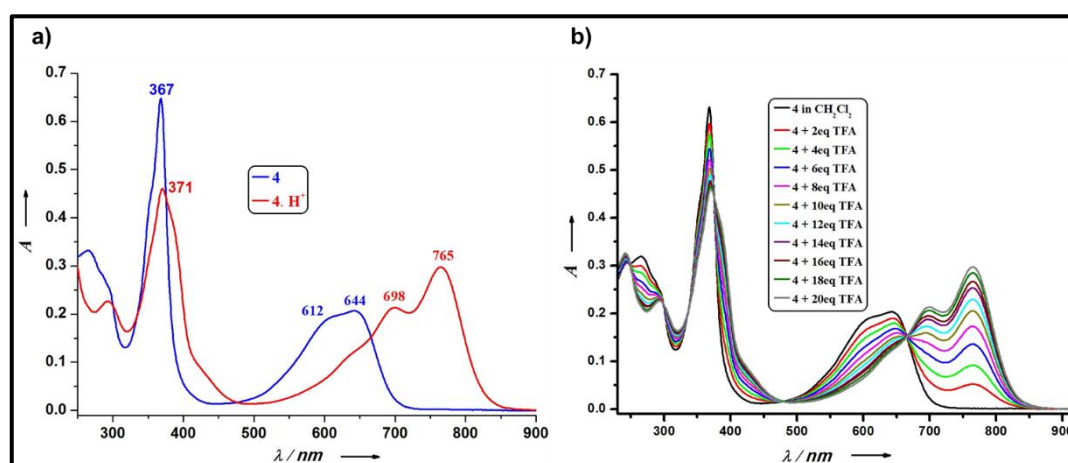


Figure 3.5: The electronic absorption spectrum of **4** and **4.H⁺** (a). Titration of **4** with various equivalents of TFA (b).

3.3.2.3 NMR Analysis

The ^1H NMR spectrum of **4** was recorded in CD_2Cl_2 and shown in Figure 3.6. There are four doublets in the deshielded region between 6.23 to 7.77 ppm, where the initial two doublets at 6.23 [H(9,13)] and 6.79 [H(8,14)] ppm are assigned to the two pyrrolic β -CH protons. The other two doublets resonated at 6.94 [H(4,18)] and 7.77 [H(2,20)] ppm corresponds to the biphenyl-CH protons which are on the periphery,

where the remaining outer biphenyl-CH[H(3,19)] protons appear as a triplet at 7.36 ppm. The inner core biphenyl-CH [H(22,25)] resonated as a singlet at 9.09 ppm, while the pyrrolic NH [H(24)] signal appeared as a broad singlet at 11.15 ppm. This was further confirmed by 2D homonuclear correlation spectroscopy (^1H - ^1H COSY) (Figure 3.7). The presence of NH is further confirmed by CD_2Cl_2 / D_2O exchange experiment. The *meso*-phenyl protons resonated as a multiplet between 7.38 and 7.48 ppm. The chemical shift difference between the pyrrolic inner NH and outer β -CH protons ($\Delta\delta$) and the biphenyl inner-CH and outer-CH ($\Delta\delta'$) in **4** is: 4.64 and 2.15 ppm. Overall, the spectral features and the chemical shift difference clearly reflect the nonaromatic features of **4**. The results are further compared with *m*-benzporphyrin,⁶ corrole³⁰ and phenanthriporphyrin,²⁸ where the $\Delta\delta$ values are: 3.55, 11.84, and 11.86 ppm, on the other hand, the $\Delta\delta'$ values in *m*-benzporphyrin⁶ and phenanthriporphyrin²⁸ are: 0.4 and 10.76 ppm respectively. The shift difference ($\Delta\delta$ and $\Delta\delta'$) is comparable with *m*-benzporphyrin further confirms the nonaromatic character in **4**. Upon protonation of **4** with TFA in CD_2Cl_2 , the biphenyl inner-CH [H(22,25)] and pyrrolic-NH [H(23,24)] with integration of two protons are shielded by 0.69 and 1.53 ppm and observed at 8.40 and 9.62 ppm, respectively, however, the outer core biphenyl-CH and pyrrolic β -CH signals are slightly deshielded. The $\Delta\delta$ and $\Delta\delta'$ values are: 2.67 and 1.17 ppm, predicts no macrocyclic aromatic ring current in the protonated state.³⁹

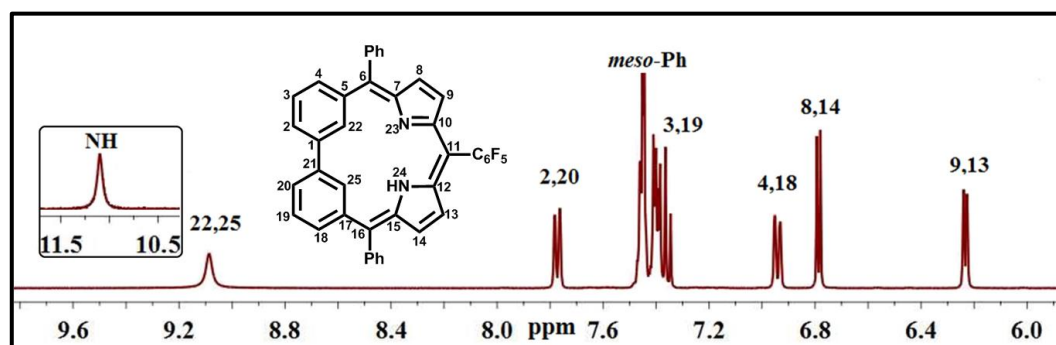


Figure 3.6: ^1H -NMR spectrum of **4** in CD_2Cl_2 .

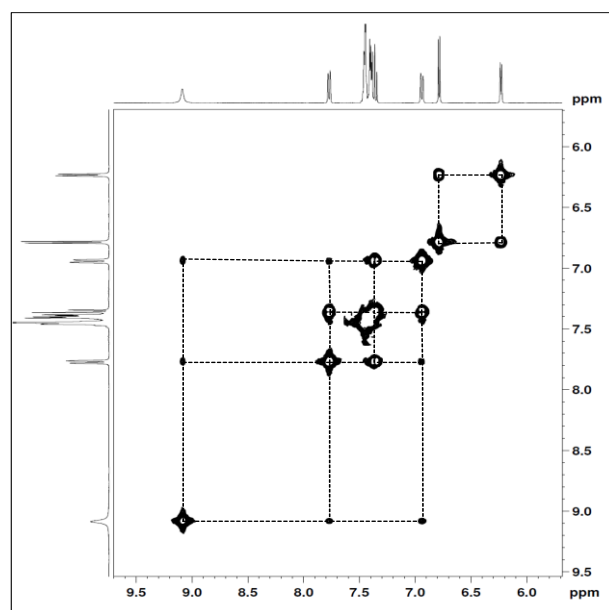


Figure 3.7: ^1H - ^1H COSY spectrum of **4** in CD_2Cl_2 .

3.3.2.4 Single crystal X-ray structure and analysis of **4**

The final confirmation has come from the single crystal X-ray structure of **4** (Figure 3.8, Table 3.5). The unit cell contains two molecules of **4** (A & B) (Figure 3.8c) and one (A) of the two crystallographically independent molecules is shown in Figure 3.8a. As predicted from the spectral analysis, the macrocycle contains a biphenyl, *meso*-pentafluorodipyrromethene units and are connected by two *meso*-phenyl units. Both the molecules (A & B) are connected by intramolecular hydrogen bonding interactions with the bond distance and angles of C43-H43...F1 is 2.65 Å and 155° (Figure 3.8c). The crystal analysis reveals that the biphenyl-CHs (C6-H6), pyrrolic NH (N1-H1) exhibit weak intramolecular hydrogen bonding interactions with pyrrolic imine nitrogen (N2) with the bond distance and angle of 2.26 Å, 123° (N1-H1...N2) and 2.33 Å, 124° (C6-H6...N2), reflects the observed deshielding signals of inner NH and biphenyl-CH protons from the ^1H NMR spectral analysis. The bond lengths of C5-C7, C1-C35 and C11-13 are 1.478 Å, 1.468 Å and 1.473 Å (Figure 3.9), reflects that the dipyrromethene and biphenyl units are connected by $\text{sp}^2\text{-sp}^2$ single bond character.^{6,28} The carbon-

carbon bond lengths within the biphenyl unit are between 1.366 and 1.408 Å, which are sp^2 - sp^2 double bond character and the average bond angle of 119.963° (Figure 3.9; Table 3.1, 3.2), proves that the biphenyl unit maintains the individual aromatic character as such.⁴⁰ The alternative sp^2 - sp^2 single and double bond character between 1.469 and 1.325 Å in the dipyrromethene moiety predicts the effective π -delocalization within the unit (Figure 3.9).²⁸ Overall, the π -electrons present in the biphenyl unit did not participate in the macrocyclic aromatization, thus, remain isolated from the π -electron delocalization of the dipyrromethene unit. Thus, the absence of diatropic ring current as observed from the ^1H NMR spectral studies, further confirms the overall nonaromatic character from the crystal analysis. The pyrrole units in **4** are hardly deviated from the mean plane (contains the core atoms C6-C12-N1-N2) with the maximum deviation of 2.93° , whereas the *m*-benzene rings in the biphenyl unit are deviated by 19.52° and 20.06° which are located above and below the plane (Figure 3.8b). Both the molecules in the unit cell (A & B) are connected individually and combined together to generate series of 1-D arrays and self-assembled dimers (Figure

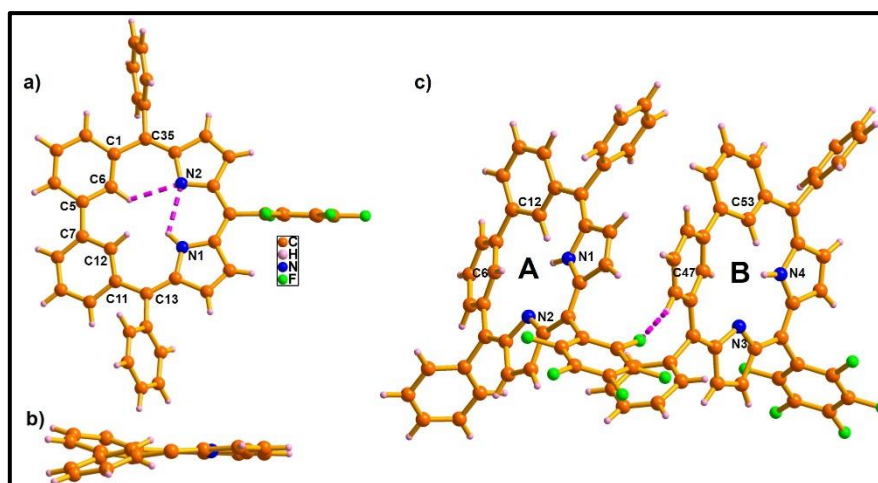


Figure 3.8: Single crystal X-ray structure of **4**. a) Top view; b) side view and c) molecules present in the unit cell. The *meso*-aryl groups are omitted for clarity in the side view.

3.10). The bond distances and angles are: C62-H62...Ph(π): 2.80 Å & 135°, C15 H15...Ph(π): 2.68 Å & 131° (Figure 3.10a), C21-H21...Ph(π): 2.74 Å & 138° (Figure 3.10b) and C60-H60...Ph(π): 2.66 Å & 132°, C37-H37...F4: 2.81 Å & 147° (Figure 3.10c).

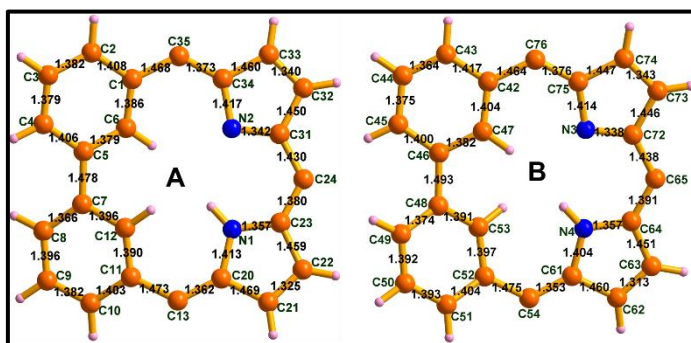


Figure 3.9: Bond distances in **4 (A)** and **4(B)**, (°).

Table 3.1: Selected bond angles in **4 (A)** (Å):

Biphenyl Unit	Bond angle (Å)	Biphenyl Unit	Bond angle (Å)
C6-C1-C2	117.507	C8-C7-C12	118.340
C1-C2-C3	119.926	C7-C8-C9	120.289
C2-C3-C4	121.594	C8-C9-C10	120.632
C3-C4-C5	119.289	C9-C10-C11	120.516
C4-C5-C6	118.442	C10-C11-C12	116.882
C5-C6-C1	123.019	C7-C12-C11	123.120
Average	119.962	Average	119.963

Table 3.2: Selected bond angles in **4 (B)** (\AA):

Biphenyl Unit	Bond angle (\AA)	Biphenyl Unit	Bond angle (\AA)
C47-C42-C43	117.019	C53-C48-C49	118.661
C42-C43-C44	120.677	C48-C49-C50	120.021
C43-C44-C45	121.521	C49-C50-C51	120.983
C44-C45-C46	119.624	C50-C51-C52	119.945
C45-C46-C47	119.074	C51-C52-C53	117.237
C46-C47-C42	121.884	C52-C53-C48	122.905
Average	119.966	Average	119.959

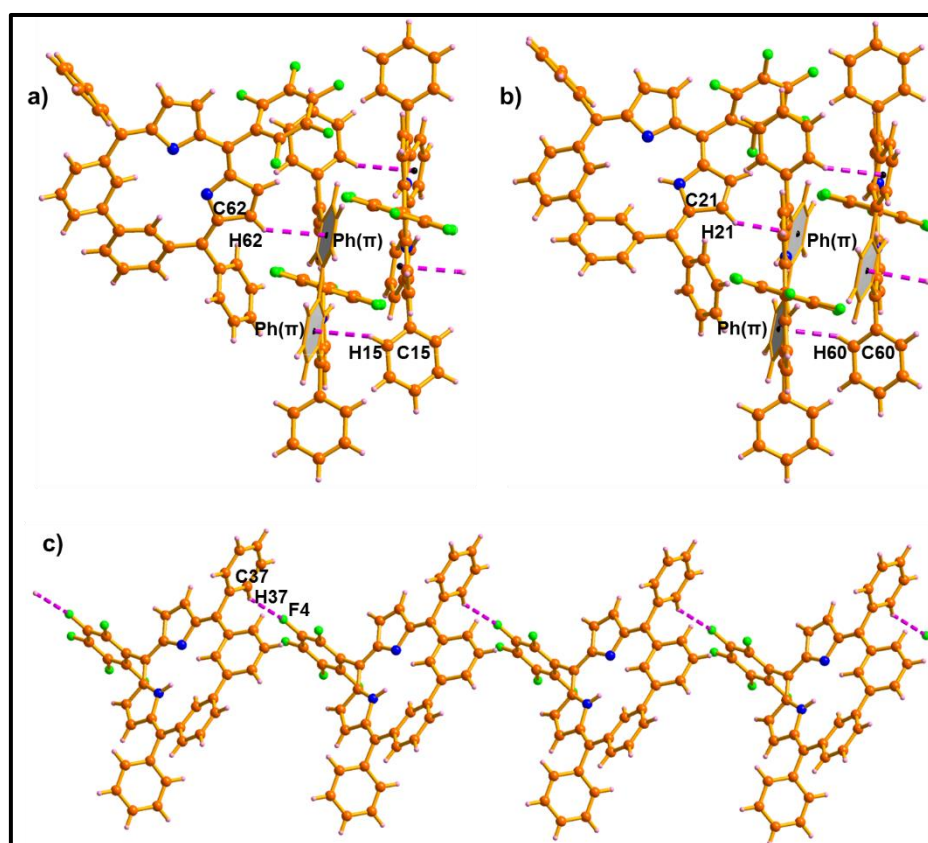


Figure 3.10: Single crystal X-ray analyses of **4**. a) 1-D array in **A**; b) 1-D array in **B**; c) Self assembled dimer and 1-D array between **A** and **B**.

3.3.3 Coordination Studies

The presence of two inner core biphenyl CHs and pyrrolic NH in coordination core prompted us to do the metal ion insertion. The coordination chemistry of **4** was performed by using Cu^{II} salts. When **4** was treated with Cu(OAc)₂ in CH₂Cl₂/CH₃OH mixture, the blue fraction was eluted by neutral alumina column afforded **5** in 90% yield (Scheme 1).

3.3.3.1 Spectral characterization

3.3.3.1.1 Mass spectrometric analysis

The ESI-MS spectrometric analysis of **5** in the solid state showed a molecular ion peak at 699.0691 [M+1] and confirms the exact composition of the metal complex (Figure 3.11).

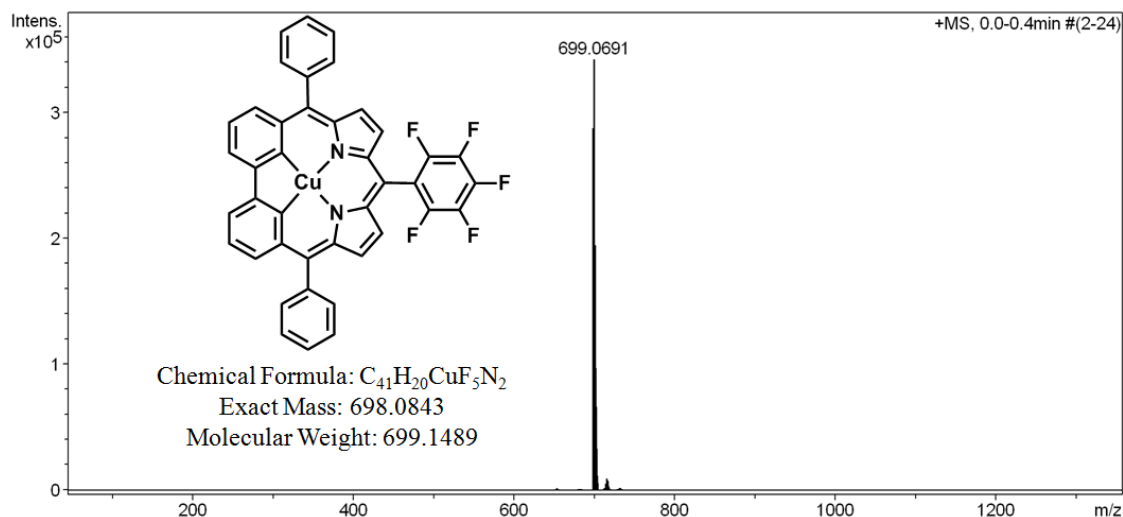


Figure 3.11: ESI-MS spectrum of **5**.

3.3.3.1.2 Electronic spectral analysis of **5**

The electronic absorption spectrum of **5** in CH₂Cl₂ is shown in Figure 3.12. The complex **5** showed an intense band at 380 nm, which was 13 nm red-shifted as

compared to **4**, while the weak bands were 27 and 9 nm blue-shifted and observed at 585 and 635 nm, respectively.

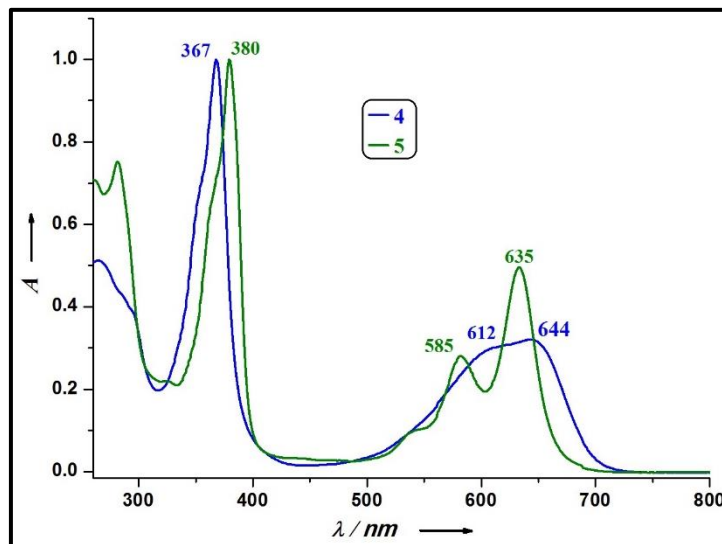


Figure 3.12: The normalized electronic absorption spectrum of **4** and **5**.

3.3.3.1.3 NMR Analysis

The ^1H NMR spectrum was recorded in CD_2Cl_2 and shown in Figure 3.13. The pyrrolic β -CHs resonated as two doublets at 6.96 [H(9,13)] and 7.23 [H(8,14)], on the other hand, the outer core biphenyl CHs are observed at 7.41 [H(4,18)], 7.58 [H(3,19)] and 7.94 [H(2,20)] ppm, respectively. This was further confirmed by ^1H - ^1H COSY spectral analysis (Figure 3.14). The slightly deshielded pyrrolic β -CH and outer core biphenyl-CHs and the disappearance of inner core biphenyl-CHs and pyrrolic NH signals as compared to **4** confirms the formation diamagnetic organometallic Cu^{III} complex **5** and also maintains the nonaromatic character as such upon metal ion insertion. It is pertinent to point out that the reaction of *m*-benzporphyrin with CuCl_2 forms internal carbon chlorinated mixed valence [Cu^{I} & Cu^{II}] tetranuclear copper complex.⁴¹ On the other hand, corrole reacts with $\text{Cu}(\text{OAc})_2$ to form higher oxidation state Cu^{III} complex.²⁹

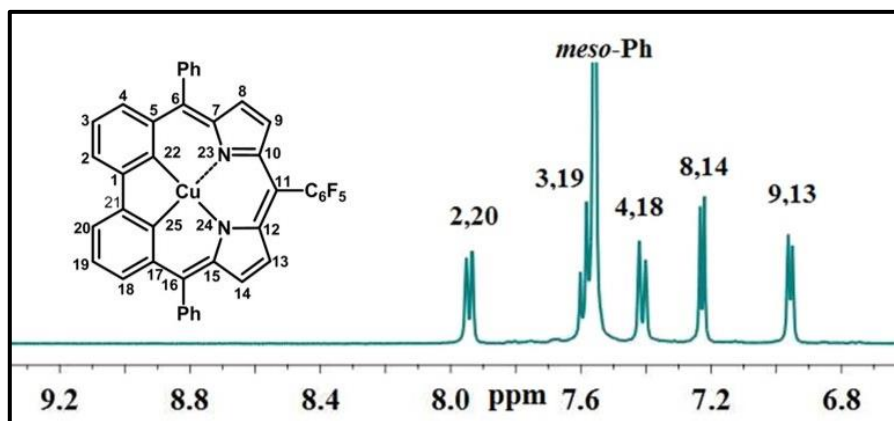


Figure 3.13: ^1H -NMR spectrum of **5** in CD_2Cl_2 .

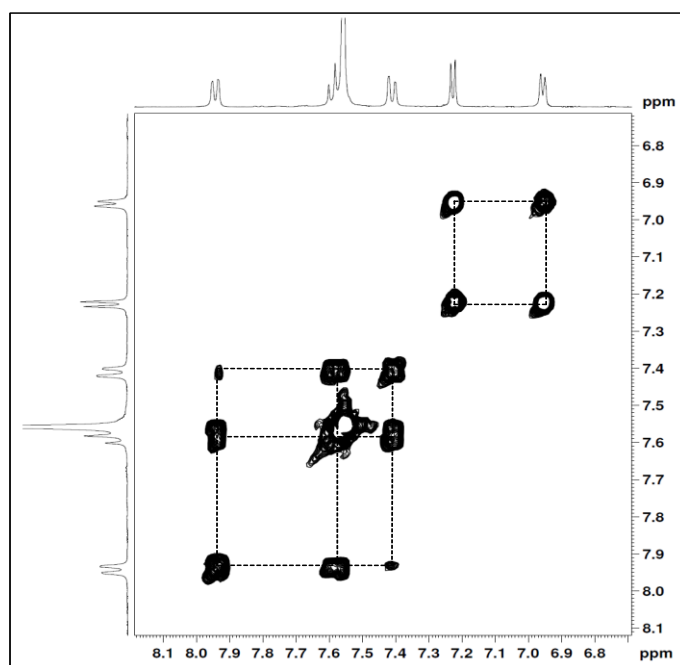


Figure 3.14: ^1H - ^1H COSY spectrum of **5** in CD_2Cl_2 .

3.3.3.1.4 Single crystal X-ray analysis of **5**

The explicit structure of organo-Cu(III) complex of **5** was unambiguously confirmed by single crystal X-ray diffraction analysis (Table 3.5). The structure is shown in Figure 3.15. As predicted from the spectral analysis, the Cu^{III} ion is inserted inside the macrocyclic framework and the geometry around the metal center is square planar with N1-Cu-N2, N2-Cu-C6, C6-Cu-C12 and C12-Cu-N1 angles of 93.175° ,

91.170°, 82.706° and 92.208°, and the Cu-C6; Cu-C12; Cu-N2 and Cu-N1 bond lengths are 1.946 Å; 1.953 Å; 1.918 Å and 1.907 Å, respectively (Figure 3.15d, Table 3.3). As compared to Cu-C and Cu-N bond lengths of organo-Cu(III) complexes of *cis*-²⁰ and *trans*-doubly²¹ N-confused porphyrins, the Cu-C bond lengths of **5** are larger and Cu-N bond lengths are shorter,²⁰ however later bond lengths (Cu-N) are longer as compared to Cu^{III} complexes of corrole.²⁹ The biphenyl and the pyrrole units are deviated from the mean plane containing the core atoms (C6-C12-N1-N2-Cu) with the tilt angle between 6.49° and 8.97°, respectively (Figure 3.15b). As observed in **4**, the complex **5** retains the nonaromatic character, the results are reflected from the crystal analysis, where (i) the biphenyl and dipyrromethene moieties [bond lengths in C5-C7, C1-C35 and C11-C13 are 1.457 Å, 1.441 Å and 1.463 Å] are connected by sp²-sp² single bond character; (ii) individual aromatic character within the biphenyl unit [bond distances are between 1.364 & 1.418 Å and the average bond angle of 119.982°] and (iii) an effective π -delocalization within the dipyrromethene unit [bond distances are between 1.328 and 1.450 Å] (Figure 3.15d). The presence of fluorine atoms in the pentafluoro units generates series of intermolecular hydrogen bonding interaction to form a self-assembled dimer (Figure 3.15b) and 1-D arrays (Figure 3.16a) with the bond distance and angles are C4-H4...F5: 2.59 Å & 165° and C40-H40...F5: 2.39 Å & 145°, respectively. The self-assembled dimer and -D arrays are combined together to generate a 2-D supramolecular assembly in the solid state with the bond distance and angles are C39-H39...Py(π): 2.80 Å & 153°, C40-H40...F1: 2.65 Å & 117°, C19-H19...F3: 2.72 Å & 119°, C21-H21...F3: 2.66 Å & 113°, C18-H18...F4: 2.83 Å & 140° (Figure 3.16b). Overall Crystal data for compound **4** and **5** given in Table 3.5.

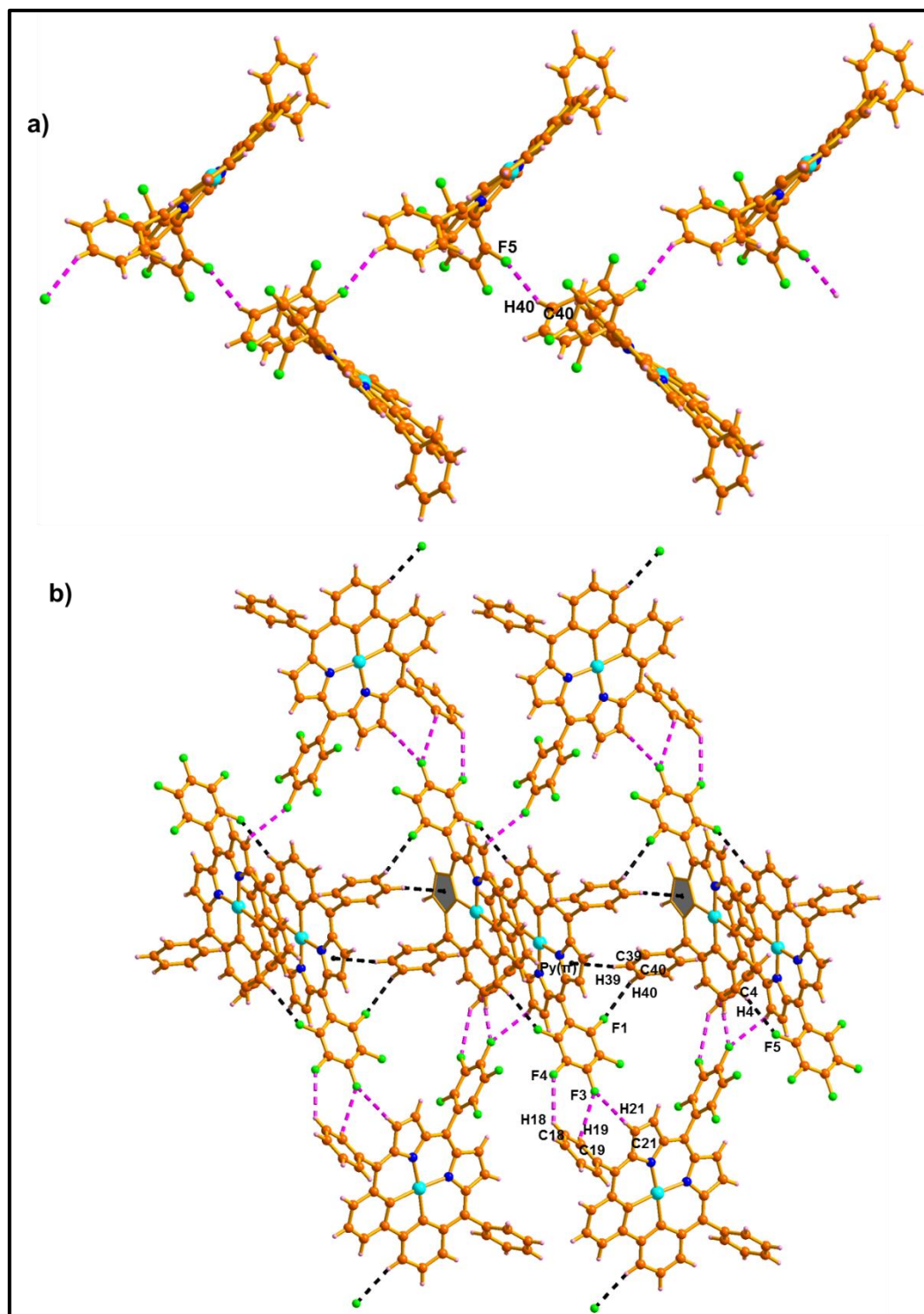


Figure 3.16: Single crystal X-ray analysis of **5**. a) 1-D array and b) 2-D array.

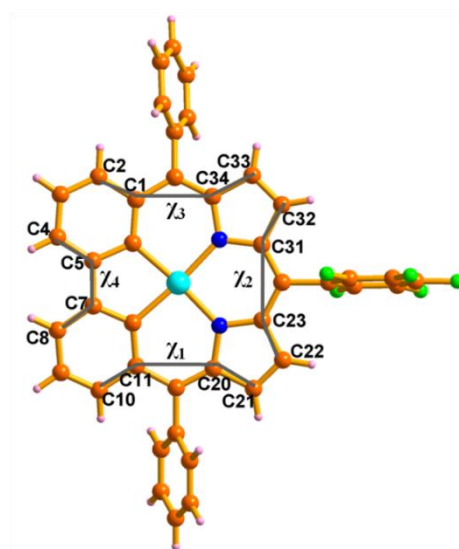
3.3.3.2 Confirmation studies for Cu^{III} ion

The chemistry of copper corroles are of particularly research interest from past decade due to their intriguing feature such as non-innocent character and sterically unhindered nonplanarity.⁴²⁻⁴⁵ The unusual nature of these structures are due to the inherent saddle conformation. The degree of saddling can be explained by the type of substitutions at the β -substituents. In general the copper corroles at room temperature exhibit diamagnetic character and stabilize the Cu^{III} oxidation state. However, at high temperature the saddling conformation induces the orbital interactions thus, shifts the equilibrium state from diamagnetic to paramagnetic Cu^{II} radical cation state which is thermally accessible state. The DFT calculations for the various substituted copper corroles confirmed that the driving force for the saddling is due to the effective orbital interaction between the Cu and the ligand. These results are confirmed by experimentally by various research groups and theoretically mainly by Ghosh *et al.* From these existing reports we have performed several experiments to find out the possible equilibrium between the diamagnetic Cu^{III} complex (**5**) and paramagnetic Cu^{II}-radical cation and the results are summarized below;

(i) The structurally confirmed organo-Cu^{III} complex (**5**) is compared with significantly saddled, extremely saddled Cu^{III} complexes of corrole and planar organo-Cu^{III} complexes of *cis*- and *trans*-N₂CP derivatives (Table 3.4). The respective values (χ_1 - χ_4) in **5** is between 0.674° and 7.603°. These values are almost negligible as compared to Cu^{III} complexes of corrole systems and are comparable with planar organo-Cu^{III} complexes of *cis*- and *trans*-N₂CP derivatives. In summary, the crystal analysis proves that the complex **5** exist in organo-Cu^{III} form.^{20,21}

Table 3.4: Saddling dihedral angle (χ) value in **5** ($^{\circ}$)

Cu(III) Complexes	M-N1/N2	M-N3/N4	χ_1	χ_2	χ_3	χ_4
Significantly Saddled						
Cu(TPTBZC)	1.920	1.931	13.578	15.382	17.683	19.823
Cu(Et ₄ Me ₄ C)	1.884	1.874	24.409	14.400	24.718	10.834
Extremely Saddled						
Cu(TPC)	1.892	1.894	41.487	46.042	52.515	25.03
Cu(Br ₈ (pOmeP) ₂ TC)	1.913	1.916	58.288	67.828	76.155	45.395
Cu((CF ₃) ₈ T(pCF ₃ -P)C)	1.923	1.926	91.611	83.736	83.623	57.319
Organo-Cu(III) complexes						
	M-C1/C2	M-N1/N2	χ_1	χ_2	χ_3	χ_4
Cis-N ₂ CP	1.937	1.962	5.676	1.784	1.061	8.025
Trans-N ₂ CP	1.942	1.966	5.396	3.215	5.347	6.362
5	1.950	1.913	2.251	0.895	7.603	0.674



ii) The variable temperature NMR experiments of **5** in DMSO-*d*₆ is shown in Figure 3.17. The sharp signal at higher temperature reveals that the thermally accessible paramagnetic states are absent, thus maintain Cu(III) form as such.

iii) The resolved diamagnetic spectrum of **5** in pyridine- d_5 (Figure 3.18) further confirms the absence of axial ligation and thus maintains d^8 low-spin configuration.⁴⁶

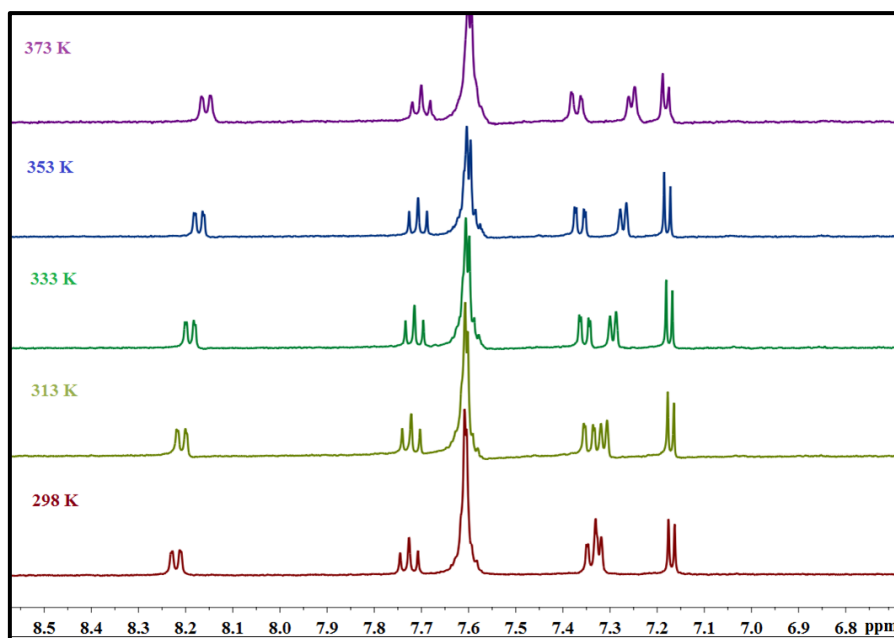


Figure 3.17: Variable temperature $^1\text{H-NMR}$ spectrum of **5** in $\text{DMSO-}d_6$.

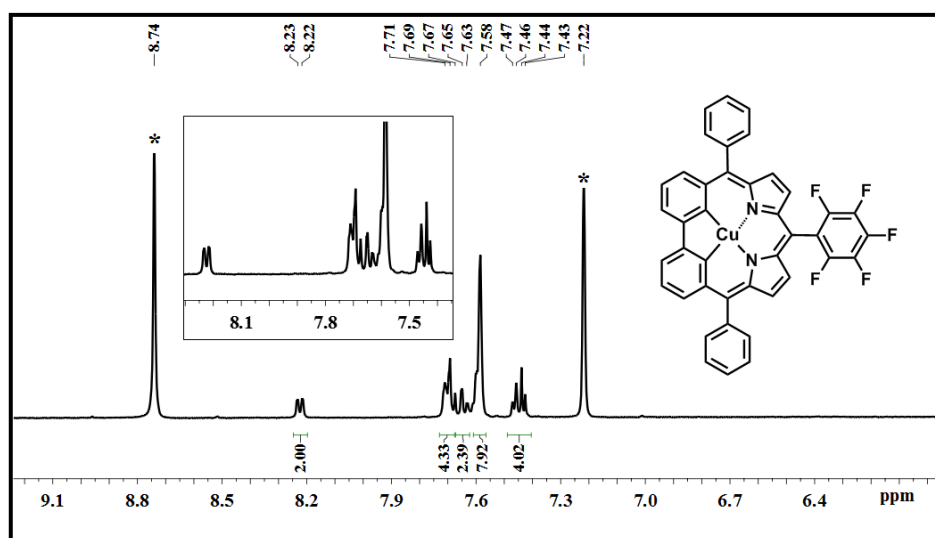


Figure 3.18: $^1\text{H-NMR}$ spectrum of **5** in Pyridine- d_5 (*residual solvent peak).

(iv) The EPR experiments of **5** in solution and solid state at variable temperature are silent, thus ruled out the possibility of Cu(II) radical cation (Figure 3.19). Overall, the

results confirmed the ability of **4** to stabilize the higher oxidation state Cu^{III} ion to form organo- Cu^{III} complex. Soon after these results published, Sanjib kar and co-workers reported the oxidized forms of corrole, the first Cu^{IV} corrolato complexes and confirmed by spectroscopic and also theoretical studies.⁴⁷

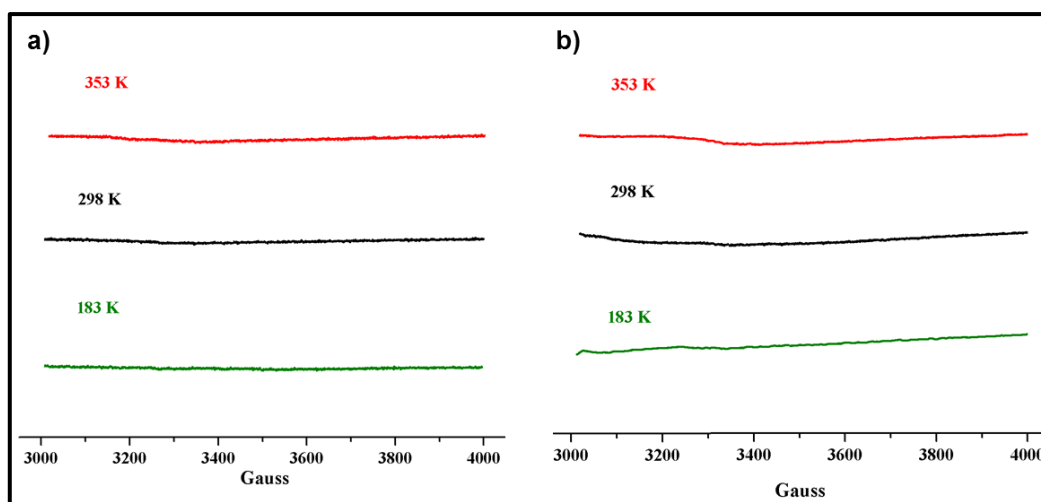


Figure 3.19: EPR spectrum of **5** in a) liquid state (toluene) and b) solid state at variable temperature.

3.4 Conclusion

In conclusion, we have demonstrated the synthesis, spectral and structural characterization of 6,11,16-triarylbiophenylcorrole and its metal complex. The aromatic biophenyl unit and the π -delocalized dipyrromethene moiety were linked together to generate the overall nonaromatic character. The free ligand with contracted size and trianionic nature with *adj*-CCNN core was crucial for the formation of the organocopper complex with two M-C bond, which is diamagnetic and affords square-planar geometry around the metal center. The formation of organocopper complex was confirmed by various spectral studies and crystal analyses.

3.5 Experimental Section

3.5.1 General Information

The reagents and materials for the synthesis were used as obtained from Sigma Aldrich chemical suppliers. All solvents were purified and dried by standard methods prior to use. The NMR solvents were used as received and the spectra were recorded in Bruker 400 MHz spectrometer with TMS as internal standard. The ESI mass spectra were recorded in Bruker, micro-TOF-QII mass spectrometer. The Electronic absorption spectra were recorded in Perkin Elmer–Lambda 750 UV-Visible spectrophotometer. The EPR spectra were recorded in Bruker EMX Micro X instrument with conditions of instrument frequency: 9.451552 GHz, Modulation frequency: 100 KHz, Modulation amplitude: 10 G, Receiver gain: 1.26×10^{10} power 3, time constant: 10.02, Center field: 3500 G and Sweep width: 1000 G. The X-ray quality crystals for the compounds were grown by slow diffusion of *n*-hexane over CH₂Cl₂ solution. Single-crystal X-ray diffraction data of **4** and **5** were collected in a Bruker KAPPA APEX-II, four angle rotation system, Mo-K α radiation (0.71073 Å). The crystals have been deposited in the Cambridge Crystallographic Data Centre with reference no. **CCDC 1052113**, **CCDC 1051683**.

3.5.2 Synthetic procedure and spectral characterization of 2-5

3.5.2.1 Synthesis of 2: Freshly prepared phenylmagnesiumbromide (5.6 g, 35.75 mmol) solution in THF (20 ml) was added under N₂ atmosphere at 0 °C into the solution of **1** (1.5 g, 7.15 mmol) in 100 ml toluene. The reaction mixture was kept at same temperature for 10 min and then allowed to attain RT. After 4 h the reaction was quenched with 1N HCl extracted with EtOAc, dried over Na₂SO₄, and concentrated by rotary evaporator. Compound was purified by recrystallization in CH₂Cl₂/

n-hexane afforded white crystalline compound **2** in 65% Yield. (1.7g).

¹H NMR (400 MHz, CDCl₃, 298K): δ = 7.62 (s, 2H), 7.48 (d, *J* = 7.5 Hz, 2H), 7.38 (m, 12H), 7.28 (d, *J* = 7.1 Hz, 2H), 5.91 (d, *J* = 2.9 Hz, 2H), 2.29 (d, *J* = 2.9 Hz, 2H).

¹³C NMR (100 MHz, CD₃OD): δ = 146.71, 145.99, 142.63, 129.92, 129.47, 128.42, 127.90, 126.99, 126.48, 77.08.

m.p: 118-120 °C.

ESI-MS: *m/z* calculated for C₂₆H₂₂O₂ = 366.1620; found = 389.1526 (M+Na).

3.5.2.2 Synthesis of 3: 3,3'-Bis(phenylhydroxymethyl)biphenyl (**2**) (1.2 g, 3.28 mmol) and pyrrole (10 mL) in 1,2-dichloroethane (40 mL) was kept in an inert atmosphere for 10 min after which 1.4 mL of BF₃·Et₂O solution was added and the resulting mixture was stirred under reflux for 8 h. The solution was cooled to room temperature and quenched by addition of triethylamine (2 mL). The compound was extracted with CH₂Cl₂, dried over Na₂SO₄ and concentrated by rotary evaporator. The crude mixture was purified by column chromatography using silica gel (100-200 mesh) in 10% EtOAc/*n*-hexane to afford **3** in 42% yield (650 mg).

¹H NMR (400 MHz, CDCl₃, 298K): δ = 7.79 (s, 2H), 7.40 – 7.35 (m, 4H), 7.34 – 7.25 (m, 6H), 7.21 (ddd, 6H), 7.12 (d, *J* = 7.6 Hz, 2H), 6.67 (dd, 2H), 6.14 (dd, 2H), 5.81 (s, 2H), 5.48 (s, 2H).

¹³C NMR (100 MHz, CDCl₃): δ = 143.76, 143.12, 141.44, 133.65, 129.08, 128.74, 127.98, 126.93, 125.79, 117.42, 108.47, 108.23, 50.85.

m.p: 59-62 °C.

ESI-MS: *m/z* calculated for C₃₄H₂₈N₂ = 464.5995; found = 487.2130 (M+Na).

3.5.2.3 Synthesis of 4: To a 200 ml CH₂Cl₂ solution, **3** (150 mg, 0.32 mmol) and pentafluorobenzaldehyde (75 mg, 0.38 mmol) was added under inert atmosphere covered with aluminium foil and stirred for 10 min. BF₃·Et₂O (0.04 ml, 0.32 mmol)

was added and allowed to stir under same condition for 3 h. Then 2,3-Dichloro-5,6-dicyano-1,4-benzoquinone (0.217 mg, 0.96 mmol) was added to the reaction mixture and opened to air. The mixture was further allowed to stir for 2 h. The crude product was passed through basic alumina column followed by neutral alumina column. The blue band was eluted with 20% CH₂Cl₂/*n*-hexane and identified as **4**. The compound was further recrystallized from CH₂Cl₂/*n*-hexane to afford blue crystalline **4** in 9% yield.

¹H NMR (400 MHz, CD₂Cl₂, 298K): δ = 11.15 (brs, 1H), 9.09 (s, 2H), 7.77 (d, J = 7.6 Hz, 2H), 7.48 – 7.43 (m, 6H), 7.42 – 7.35 (m, 6H), 6.94 (d, J = 8.2 Hz, 2H), 6.79 (d, J = 5.2 Hz, 2H), 6.23 (d, J = 5.2 Hz, 2H).

¹³C NMR (100 MHz, CD₂Cl₂): δ = 141.15, 140.23, 139.18, 136.23, 131.84, 131.23, 130.42, 128.85, 128.08, 127.98, 126.35, 124.46.

m.p: 300 °C (decomposition).

ESI-MS: m/z calculated for C₄₁H₂₃F₅N₂ = 638.1781; found = 639.1821 (M+1).

UV-Vis (CH₂Cl₂): λ_{\max} (nm) (ϵ [M⁻¹cm⁻¹]) = 367 (32,453), 612 (9,965), 644 (10,276).

4.H⁺: **¹H NMR (400 MHz, CD₂Cl₂, 298K):** δ = 9.62 (s, 2H), 8.40 (s, 2H), 8.03 (d, J = 7.5 Hz, 2H), 7.63 (ddd, 8H), 7.48 (d, J = 7.2 Hz, 4H), 7.31 (d, J = 4.5 Hz, 2H), 7.23 (d, J = 7.3 Hz, 2H), 6.59 (d, J = 4.6 Hz, 2H).

UV-Vis(CH₂Cl₂): λ_{\max} (nm) (ϵ [M⁻¹cm⁻¹]) = 371 (23,113), 698 (10,865), 765(15,326).

3.5.2.4 Synthesis of 5: A solution of Cu(OAc)₂ (57 mg, 0.31 mmol) in 5 ml CH₃OH was added to a solution of **4** (20 mg, 0.031 mmol) in CH₂Cl₂ (20 ml) under inert atmosphere and allowed to stir for 4 h. The solvent was evaporated by rotary evaporator. The crude metal complex was purified by neutral alumina column. The blue band was eluted with 10% CH₂Cl₂/*n*-hexane and identified as **5**. The compound was further recrystallized from CH₂Cl₂/*n*-hexane to afford blue crystalline **5** in 90% yield.

¹H NMR (400 MHz, CD₂Cl₂, 298K): δ = 7.94 (d, J = 6.7 Hz, 2H), 7.61 – 7.53 (m, 12H), 7.41 (d, J = 7.3 Hz, 2H), 7.23 (d, J = 5.2 Hz, 2H), 6.96 (d, J = 5.1 Hz, 2H).

¹³C NMR (100 MHz, CD₂Cl₂): δ = 156.31, 154.74, 145.84, 139.72, 136.14, 135.14, 134.86, 131.73, 129.94, 128.28, 127.95, 127.84, 127.77, 122.43.

m.p: 300 °C (decomposition).

ESI-MS: m/z calculated for C₄₁H₂₀F₅N₂Cu = 698.0843; found = 699.0691 (M+1).

UV-Vis (CH₂Cl₂): $\lambda_{\max}(\text{nm})$ ($\epsilon[\text{M}^{-1}\text{cm}^{-1}]$) = 380 (22,453), 585 (6,175), 635 (10,826).

Table 3.5: Crystal data for **4** and **5**

Crystal parameters	4	5
Formula	C ₈₂ H ₄₆ F ₁₀ N ₄	C ₄₁ H ₂₀ F ₅ N ₂ Cu
$M/\text{g mol}^{-1}$	1277.23	699.13
T/K	100 K	100 K
Crystal dimensions/ mm^3	0.16 x 0.09 x 0.05	0.13 x 0.07 x 0.06
Crystal system	Triclinic	Monoclinic
Space group	$P-1$	$P2(1)/c$
$a/\text{\AA}$	11.231 (11)	16.185 (17)
$b/\text{\AA}$	15.681 (14)	13.375 (14)
$c/\text{\AA}$	17.367 (17)	14.456 (14)
$\alpha/^\circ$	93.353 (6)	90.000
$\beta/^\circ$	99.520 (6)	106.752 (6)
$\gamma/^\circ$	90.071 (5)	90.000
$V/\text{\AA}^3$	3011.1 (19)	2996.5 (18)
Z	2	4
$\rho_{\text{calcd}}/\text{mg m}^{-3}$	1.409	1.550
μ/mm^{-1}	0.104	0.796
F(000)	1312	1416
Reflns. collected	33347	33710
Indep.reflns.[$R(\text{int})$]	10578 [0.0571]	5751 [0.1133]
Max/min transmission	0.7457 and 0.5103	0.7453 and 0.6284
Data/restraints/parameters	10578 / 0 / 865	5751 / 0 / 442
GOF on F^2	1.062	1.068
Final R indices [$I > 2\sigma(I)$]	R1 = 0.0982, wR2 = 0.2552	R1 = 0.0687, wR2 = 0.1750
R indices (all data)	R1 = 0.1226, wR2 = 0.2671	R1 = 0.1176, wR2 = 0.2025
Largest diff peak and hole [$e \text{\AA}^{-3}$]	1.002 and -0.360	1.245 and -0.563

3.6 References

1. Lash, T. D. *Chem. Rev.* **2016**, DOI: 10.1021/acs.chemrev.6b00326.
2. Furuta, H.; Maeda, H.; Osuka, A. *Chem. Commun.* **2002**, 1795-1804.
3. Chmielewski, P. J.; Latos-Grażyński, L.; Rachlewicz, K.; Glowiak, T. *Angew. Chem., Int. Ed. Engl.* **1994**, *33*, 779-781.
4. Furuta, H.; Asano, T.; Ogawa, T. *J. Am. Chem. Soc.* **1994**, *116*, 767-768.
5. Berlin, K.; Breitmaier, E. *Angew. Chem., Int. Ed. Engl.* **1994**, *33*, 1246-1247.
6. Stępień, M.; Latos-Grażyński, L. *Chem. Eur. J.* **2001**, *7*, 5113-5117.
7. Stępień, M.; Latos-Grażyński, L. *Acc. Chem. Res.* **2005**, *38*, 88-98.
8. Lash, T. D. *Angew. Chem., Int. Ed. Engl.* **1995**, *34*, 2533-2535.
9. Lash, T. D.; Chaney, S. T. *Tetrahedron Lett* **1996**, *37*, 8825-8828.
10. Bergman, K. M.; Ferrence, G. M.; Lash, T. D. *J. Org. Chem.* **2004**, *69*, 7888-7897.
11. Lash, T. D.; Hayes, M. J. *Angew. Chem., Int. Ed. Engl.* **1997**, *36*, 840-842.
12. Lash, T. D.; Chaney, S. T. *Angew. Chem., Int. Ed. Engl.* **1997**, *36*, 839-840.
13. Lash, T. D. *Acc. Chem. Res.* **2016**, *49*, 471-482.
14. Myśluborski, R.; Latos-Grażyński, L. *Eur. J. Org. Chem.* **2005**, 5039-5048.
15. Lash, T. D.; Pokharel, K.; Serling, J. M.; Yant, V. R.; Ferrence, G. M. *Org. Lett.* **2007**, *9*, 2863-2866.
16. Pawlicki, M.; Latos-Grażyński, L. *Chem. Rec.* **2006**, *6*, 64-78.
17. Lash, T. D.; Young, A. M.; Von Ruden, A. L.; Ferrence, G. M. *Chem. Commun.* **2008**, 6309-6311.
18. Lash, T. D.; Young, A. M.; Rasmussen, J. M.; Ferrence, G. M. *J. Org. Chem.* **2011**, *76*, 5636-5651.
19. Lash, T. D.; Lammer, A. D.; Ferrence, G. M. *Angew. Chem. Int. Ed.* **2011**, *50*, 9718-9721.

-
20. Furuta, H.; Maeda, H.; Osuka, A. *J. Am. Chem. Soc.* **2000**, *122*, 803-807.
21. Maeda, H.; Osuka, A.; Furuta, H. *J. Am. Chem. Soc.* **2003**, *125*, 15690-15691.
22. Lash, T. D.; Romanic, J.; Hayes, M.; Spence, J. *Chem. Commun.* **1999**, 819-820.
23. Graham, S. R.; Colby, D. A.; Lash, T. D. *Angew. Chem. Int. Ed.* **2002**, *41*, 1371-1374.
24. Lash, T. D.; Colby, D. A.; Idate, A. S.; Davis, R. N. *J. Am. Chem. Soc.* **2007**, *129*, 13800-13801.
25. Lash, T. D.; Lammer, A. D.; Idate, A. S.; Colby, D. A.; White, K. *J. Org. Chem.* **2012**, *77*, 2368-2381.
26. Zhang, Z.; Ferrence, G. M.; Lash, T. D. *Org. Lett.* **2008**, *11*, 101-104.
27. AbuSalim, D. I.; Ferrence, G. M.; Lash, T. D. *J. Am. Chem. Soc.* **2014**, *136*, 6763-6772.
28. Szyszko, B.; Białońska, A.; Szterenber, L.; Latos-Grażyński, L. *Angew. Chem. Int. Ed.* **2015**, *54*, 4932-4936.
29. Will, S.; Lex, J.; Vogel, E.; Schmickler, H.; Gisselbrecht, J. P.; Hauptmann, C.; Bernard, M.; Gorss, M. *Angew. Chem., Int. Ed. Engl.* **1997**, *36*, 357-361.
30. Gross, Z.; Galili, N.; Saltsman, I. *Angew. Chem. Int. Ed.* **1999**, *38*, 1427-1429.
31. Flamigni, L.; Gryko, D. T. *Chem. Soc. Rev.* **2009**, *38*, 1635-1646.
32. Orłowski, R.; Gryko, D.; Gryko, D. T. *Chem. Rev.* **2016**, DOI:10.1021/acs.chemrev.6b00434.
33. Skonieczny, J.; Latos-Grażyński, L.; Szterenber, L. *Chem. Eur. J.* **2008**, *14*, 4861-4874.
34. Fujino, K.; Hirata, Y.; Kawabe, Y.; Morimoto, T.; Srinivasan, A.; Toganoh, M.; Miseki, Y.; Kudo, A.; Furuta, H. *Angew. Chem. Int. Ed.* **2011**, *50*, 6855-6859.
-

-
35. Toganoh, M.; Kawabe, Y.; Uno, H.; Furuta, H. *Angew. Chem. Int. Ed.* **2012**, *51*, 8753-8756.
36. Escobar, C. A.; Fernandez, W. A.; Trujillo, A.; Santos, J. C.; Roisnel, T.; Fuentealba, M. *Tetrahedron Lett* **2014**, *55*, 5271-5274.
37. Stępień, M.; Szyszko, B.; Latos-Grażyński, L. *Org. Lett.* **2009**, *11*, 3930-3933.
38. Lindsey, J. S.; Schreiman, I. C.; Hsu, H. C.; Kearney, P. C.; Marguerettaz, A. M. *J. Org. Chem.* **1987**, *52*, 827-836.
39. Lash, T. D.; Toney, A. M.; Castans, K. M.; Ferrence, G. M. *J. Org. Chem.* **2013**, *78*, 9143-9152.
40. Trotter, J. *Acta Cryst.* **1961**, *14*, 1135-1140.
41. Hung, C.-H.; Chang, F.-C.; Lin, C.-Y.; Rachlewicz, K.; Stępień, M.; Latos-Grażyński, L.; Lee, G.-H.; Peng, S.-M. *Inorg. Chem.* **2004**, *43*, 4118-4120.
42. Brückner, C.; Brinas, R. P.; Bauer, J. A. K. *Inorg. Chem.* **2003**, *42*, 4495-4497.
43. Bröring, M.; Bregier, F.; Cónsul Tejero, E.; Hell, C.; Holthausen, M. C. *Angew. Chem. Int. Ed.* **2007**, *46*, 445-448.
44. Pierloot, K.; Zhao, H.; Vancoillie, S. *Inorg. Chem.* **2010**, *49*, 10316-10329.
45. Thomas, K. E.; Alemayehu, A. B.; Conradie, J.; Beavers, C. M.; Ghosh, A. *Acc. Chem. Res.* **2012**, *45*, 1203-1214.
46. Fox, J. P.; Ramdhanie, B.; Zareba, A. A.; Czernuszewicz, R. S.; Goldberg, D. P. *Inorg. Chem.* **2004**, *43*, 6600-6608.
47. Sinha, W.; Sommer, M. G.; Deibel, N.; Ehret, F.; Bauer, M.; Sarkar, B.; Kar, S. *Angew. Chem. Int. Ed.* **2015**, *54*, 13769-13774.
-

CHAPTER 4

Bipyricorrole: A Corrole Homologue with a Monoanionic Core as a Fluorescence Zn^{II} Sensor

4.1	Introduction	99
4.1.1	Sensing of Zn^{II} ion	99
4.1.2	Conjugated pyrrole based Zn^{II} ion sensors	100
4.1.2.1	Linear conjugated oligopyrroles for Zn ^{II} ion sensing	100
4.1.2.2	Macrocyclic conjugated oligopyrroles for Zn ^{II} ion sensing	101
4.2	Corrole analogues	103
4.3	Pyridine based porphyrinoids	103
4.4	Objective of our work	105
4.5	Results and discussions	106
4.5.1	Synthesis	106
4.5.2	Spectral characterisation	107
4.5.2.1	Mass spectrometric analysis	107
4.5.2.2	NMR Analysis	108
4.5.2.3	Single crystal X-ray analysis of 11 and 12	110
4.5.2.4	Electronic absorption and emission spectral analysis	114
4.5.3	Sensing studies	116
4.6	Conclusion	118
4.7	Experimental Section	119
4.7.1	General Information	119
4.7.2	Synthetic procedure and spectral characterization	119
4.8	References	125

4.1 Introduction

4.1.1 Sensing of Zn^{II} ion

Metal ions play an important role in many neurobiological processes relevant to human health and diseases. The detection of such environmental pollutants or biologically important species continue to be an important and active area of many researchers in various domains including chemistry, biology and material science.^{1,2} The development of small organic molecule based sensors has been demonstrated to be promising candidates due to their advantages of low cost, high sensitivity and wide range of applicability, thus could be employed in various biological functions of targeted metal cations in living systems. Among the cations, transition metal ions such as cadmium, lead, mercury, iron, zinc, cobalt and copper attained great interest. They present in uncontrolled amounts and are considered as essential elements in biological systems.³ Among these, zinc is the second-most-abundant transition-metal ion in the human body, where it plays multiple roles in both intra- and extracellular functions. A large number of proteins and enzymes have been identified with Zn^{II} and also reported to be responsible for neurological disorders such as Alzheimer's disease, amyotrophic lateral sclerosis (ALS), Parkinson's disease, and epilepsy.^{4,5}

Zinc (Zn^{II}) ion is called spectroscopically silent metal ion and invisible to most analytical techniques. Therefore, fluorescent technique can be used to visualize the selective recognition of target Zn^{II} ion using molecular chemosensors. Organic molecule based chemosensors are classified into two types. Type1 consists of mainly two units which are reporter unit and recognition unit, in some cases with or without a linker between the reporter and recognition unit is needed. In this type, the recognition unit selectively interacts with the target analyte and produces changes in their photophysical properties. Based on that various approaches have been developed which

includes, photoinduced electron transfer (PET), intramolecular charge transfer (ICT), fluorescence resonance energy transfer (FRET), aggregation-induced emission (AIE), and excimer/exciple formation. In case of type2 systems, fluorescent molecular probe consists only one component which acts as both recognition and reporting unit simultaneously. The most commonly developed chemosensors of this type are chelation enhanced fluorescence (CHEF).^{6,7}

4.1.2 Conjugated pyrrole based Zn^{II} ion sensors

A wide range of Zn^{II} ion chemosensors has been reported to date such as derivatives of di-2-picolyamine (DPA), Quinoline based receptors like 8-hydroxyquinoline, bipyridine derived receptors, acyclic and cyclic polyamines, iminodiacetic acid and its derivatives, Schiff bases, conjugated linear pyrrole, and conjugated macrocyclic pyrrole derivatives. Among these chemosensors, pyrrole based linear and macrocyclic conjugated structures such as dipyrins, tripyrins, porphyrins and their analogues are receiving much attention due to their inherent features and found to be suitable for the design of ion chemosensors.^{6,7,8}

4.1.2.1 Linear conjugated oligopyrroles for Zn^{II} ion sensing

Dipyrins and tripyrin derivatives are part of the linear conjugated oligopyrrole category. The luminescent properties of these derivatives are influenced by substitutions, coordination modes and the metal ions. In addition to this, the fluorescence wavelength of these materials are highly dependent on the effective π -conjugation in the linear chain. The multiple imino N and amino NH moieties of these oligopyrrolic compounds can act as chelating ligands. By utilizing the chelation enhanced fluorescence (CHEF) property, Xie *et al* developed dipyrins (**1-3**) and

tripyrin (4) derivatives as fluorescent probes for Zn^{II} with advantages of tunable emission wavelengths, high selectivity & sensitivity, and good cell-permeability (Figure 4.1).⁹

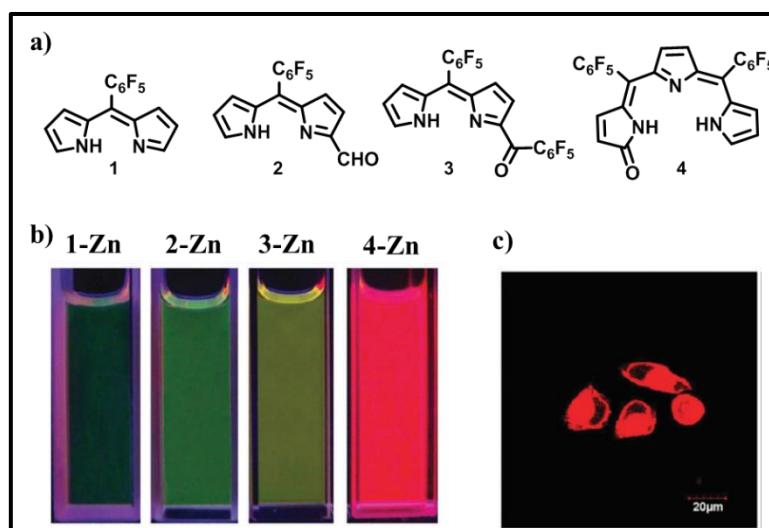


Figure 4.1: (a) Structures of dipyrins(1-3) and tripyrinone (4); (b) Fluorescence images upon addition of Zn^{II} to the probes and (c) Zn^{II} imaging in living KB cells using probe 4.

4.1.2.2 Macrocyclic conjugated oligopyrroles for Zn^{II} ion sensing

Porphyrins are widely studied 18π Hückel aromatic tetrapyrrolic macrocycle. The synthetic porphyrinoids have been applied to various fields depending on their versatile properties such as strong light absorption, high emission, and rich coordination chemistry.¹⁰⁻¹⁴ The large family of porphyrin systems such as the derivatives of porphyrins by functionalization at the *meso*-position, β -position, porphyrin analogues, expanded porphyrins, contracted porphyrins, porphyrin isomers, heteroporphyrins and calixpyrrole and calixpyrin derivatives have been employed for the selective metal ion detection. In this section, the Zn^{II} ion sensor is mainly described. The porphyrin based Zn^{II} probe was synthesized by Lippard et al where, the dipicolylamine (DPA) was introduced at the *meso*-position of the porphyrin system.¹⁵ Here, DPA acts as a selective

binding site for the Zn^{II} and produce 10-fold fluorescence enhancement. The ratiometric fluorescent Zn^{II} probe was synthesised by Wang, Lv and co-workers by combining a triamino chelating unit with a porphyrin system.¹⁶ Hung *et al.* reported a porphyrin analogue by replacing one of the pyrrole units with a 1,3-phenylene moiety. The ligand (**5**) is effectively used as detection of NIR fluorescent probe for the selective Zn^{II} ion.¹⁷ Upon addition of Zn^{II} , the enhanced fluorescent emission was observed at 672 nm, and the binding ratio was found to be 1:1 (Figure 4.2). In the expanded porphyrin area, N-confused hexaphyrin was synthesised and utilized as NIR fluorescent Zn^{II} probe by Furuta and co-workers.¹⁸ However, despite these promising examples, research on Zn^{II} ion probes based on porphyrin analogues are still in its infancy stage. Moreover in case of corrole and its analogues based cation sensors are scarcely reported in particular Zn^{II} ion probes are not known in the literature. Hence, development of selective detection of ion probes based on corrole analogues are desired for real life applications. In this section, synthesis of suitable corroles and their homologues can provide an ideal platform to explore such kind of properties.

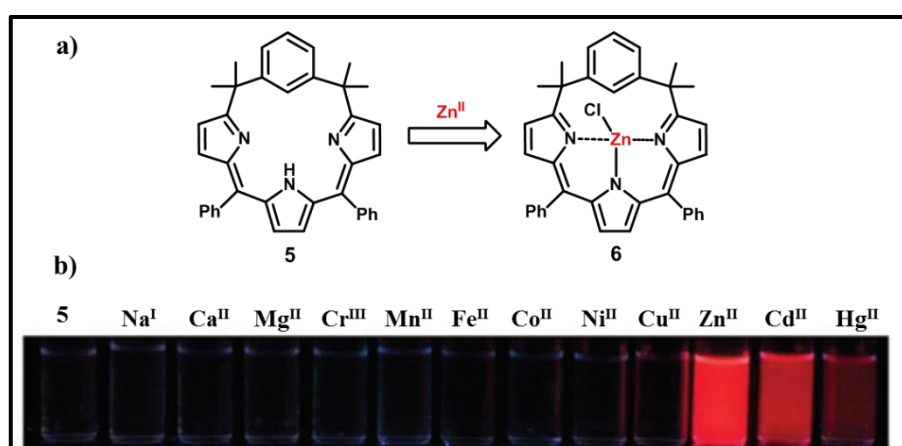


Figure 4.2: (a) Proposed sensing mechanism for detecting Zn^{II} by using probe **5**; (b) The fluorescence image of **5** upon addition of various metal ions under a portable UV lamp.

4.2 Corrole analogues

Corroles are contracted porphyrinoid with 2,2'-bipyrrole unit in the macrocyclic framework and thus, constitute a bridge between corrin and porphyrin units.^{19,20} The *trianionic* core is well-known to stabilize higher oxidation state metal complexes and are widely applied in catalysis, sensors and dye-sensitized solar cells.^{21,22} Structural modification in the framework alters the electronic structure, thus leads to unusual optical, photophysical and coordination properties.^{23,24} A series of core-modified corroles such as, *iso*-carbacorrole,²⁵ N-confused derivative,²⁶ norrole,²⁷ benzonorrole,²⁸ oxacorrole,²⁹ diaoxacorrole,³⁰ and thiacorrole³¹ were introduced. Recently, we have reported a *meso*-aryl biphenylcorrole, where the bipyrrole moiety is replaced by biphenyl unit and the *trianionic* core stabilizes Cu^{III} ion.³² In continuation, introduction of a pyridyl / bipyridyl unit in the molecular framework could be an ideal candidate for metal ion detection.

4.3 Pyridine based porphyrinoids

The first pyridine based porphyrinoid, pyriporphyrinone was synthesized by Berlin and Breitmaier. Since then, series of pyridyl derivatives are reported which includes, true pyriporphyrin, confused pyriporphyrin, oxypyriporphyrin, dipyridinoid substituted porphyrin and its coordination complexes.³³⁻⁴⁰ Some of these porphyrin derivatives and its properties described in the previous chapter. In addition, series of porphyrin related macrocycles with N₄ coordination sphere are reported & described in this section.

Naruta and co-workers reported the 1,10-phenanthroline-embedded porphyrin (**7**) which was synthesized by [2+2] acid catalyzed condensation of 1,10-phenanthroline vinyl derivative with *meso*-phenyldipyrromethane.⁴¹ The spectral and structural

characterisation reveals that the overall macrocyclic π conjugation is interrupted due to the stable exocyclic double bonds and shows non-aromaticity. The titration experiment of **7** with various metal salts showed significant emission enhancement with Mg^{II} salts and further revealed as selective recognition of Mg^{II} ions.

Klaus Müllen and co-workers reported the porphyrin-related macrocycle from carbazole and pyridine (**8**) building blocks by facile palladium-catalyzed cross-coupling reaction.⁴² From the spectral analysis, the macrocycle does not exhibit diamagnetic ring current, and showed nonaromatic character. Further, the dianionic ligand is found suitable to stabilize Co^{II} complex. In addition, the same group also reported a new class of ligands with phenanthroline and indole moieties in macrocycle frame work. The respective Co^{II} complex was further demonstrated as electro catalysts for oxygen reduction.⁴³

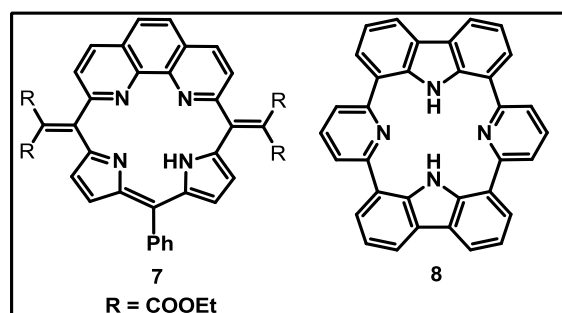


Figure 4.3: Structures of phenanthroline (**7**) and carbazole-pyridine (**8**) embedded porphyrins.

The first pyridine based contracted porphyrin, subpyriporphyrin which was reported by Latos-Grażyński (**9**) and coworkers.⁴⁴ They adopted similar synthetic methodology as reported for the synthesis of pyriporphyrins. The reduction of monobenzoylated pyridine based tripyrrane gave the alcohol derivative which undergoes intramolecular condensation to produce subpyriporphyrin. Upon coordination with boron, the complex showed $[14]\pi$ aromatic behaviour.

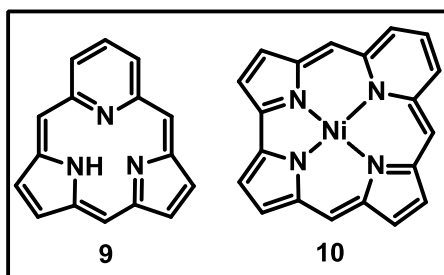


Figure 4.4: Structures of subpyriporphyrin (**9**) and pyricorrole (**10**).

Very recently, Neya and coworkers reported the first pyridine based corrole homologues such as pyricorrole (**10**) (Figure 4.4) in the form of Ni^{II} complex.⁴⁵ The nickel assisted template strategy was used for the synthesis of **10** where the pyridine incorporated bilane derivative was cyclized in the presence of nickel salt. The spectral analyses of **10** revealed the aromatic character and further demonstrated the hybrid properties of porphyrin and corrole.

4.4 Objective of our work

Overall, the corrole and its modified derivatives are in the *trianionic* or *dianionic* form in the neutral state, however, the *monoanionic* form³⁰ is rarely known in the literature. In addition, it is significant to note that the basic framework of biologically important Cob(I)alamin is constituted by ‘corrin’ unit which is in *monoanionic* state and stabilize Co^{III} ion.⁴⁶ Though the corrole and its metal derivatives are well known in various fields, like catalysis, dye sensitized solar cells, medicinal chemistry, and as a sensors for the detection of deadly gases. However, direct metal ion sensors are not known in the literature.

Herein, we wish to report the synthesis of *monoanionic* corrole, 6,11,16-triarylbiopyricorrole (**11**) and its Zn^{II} complex (**12** and **13**) (Figure 4.5). Introduction of 2,2'-bipyridyl unit in the macrocycle is unprecedented in the corrole chemistry and provides stable tetra nitrogen (NNNN) core with *monoanionic* charge. The Zn-complex

is stabilized by the *monoanionic* core with axial coordination, exhibits Chelation Induced Emission Enhancement (CIEE)^{47,48} upon metal ion insertion.

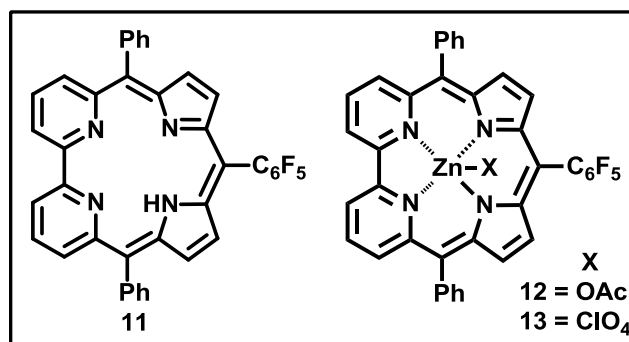


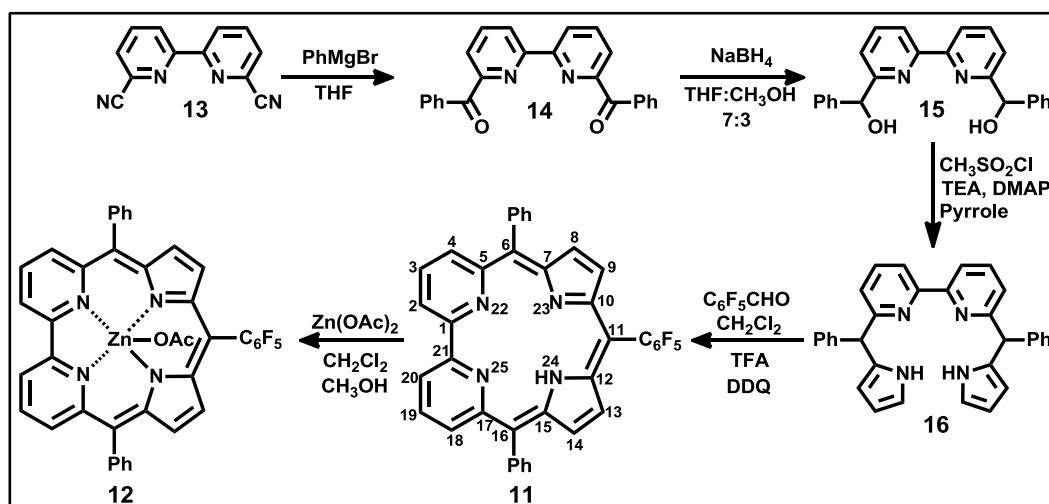
Figure 4.5: Structures of Bipyricorrole (**11**) and its Zn^{II} complexes (**12** and **13**).

4.5 Results and discussions

4.5.1 Synthesis

The synthesis of title compound and its coordination chemistry is described in Scheme 1. The target macrocycle was achieved in four steps. The first step is the synthesis of 2,2'-bipyridine-6,6'-diylbis(phenylmethanone) (**14**) from 2,2'-bipyridine-6,6'-dicyanitrile (**13**)⁴⁹ by using freshly prepared phenylmagnesium bromide in THF in 75% yield. The sodiumborohydride reduction of **14** in THF:CH₃OH (7:3) forms 6,6'-bis(phenylhydroxymethyl)-2,2'-bipyridine (**15**) in quantitative yield in the second step. The key precursor (**16**) was synthesized in the third step, where the direct conversion of **15** in the presence of excess pyrrole and BF₃.Et₂O as an acid-catalyst was not successful. Hence, we adopted a similar strategy as reported by Latos-Grażyński,^{50,51} where the compound **15** was reacted with methanesulphonyl chloride, TEA and DMAP followed by condensation with 100 equiv. of pyrrole afforded **16** in 40% yield. The target macrocycle was achieved in the final step by acid-catalyzed condensation reaction of **12** with pentafluorobenzaldehyde in the presence of trifluoroacetic acid (TFA) in CH₂Cl₂, followed by oxidation with 2,3-dichloro-5,6-dicyano-*p*-

benzoquinone (DDQ). The crude mixture was purified by column chromatographic separation, where a blue color fraction eluted with CH_2Cl_2 and CH_3OH (99:1) was identified as **11** in 12% yield. The coordination chemistry of **11** was further performed by using $\text{Zn}(\text{OAc})_2$ in $\text{CH}_2\text{Cl}_2/\text{CH}_3\text{OH}$ mixture, where green fraction was eluted by silica gel column, afforded **12** in quantitative yield.



Scheme 4.1: Synthesis of **11** and **12**.

4.5.2 Spectral Characterization

4.5.2.1 Mass spectrometric analysis

The electron spray ionization (ESI) mass spectrometric analysis shows the molecular ion signal of **11** at m/z 641.1664 [$\text{M}+1$] (Figure 4.6) and Zn^{II} complex (**12**) at 703.0741 [$\text{M}-\text{OAc}$] and confirms the exact composition (Figure 4.7).

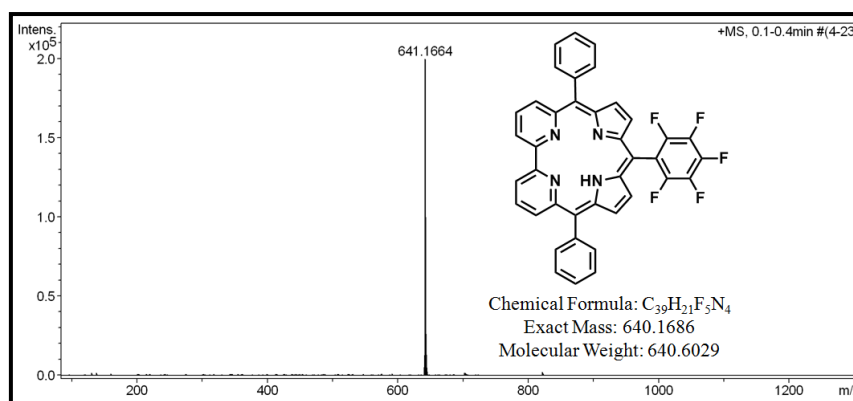


Figure 4.6: ESI-MS spectrum of **11**.

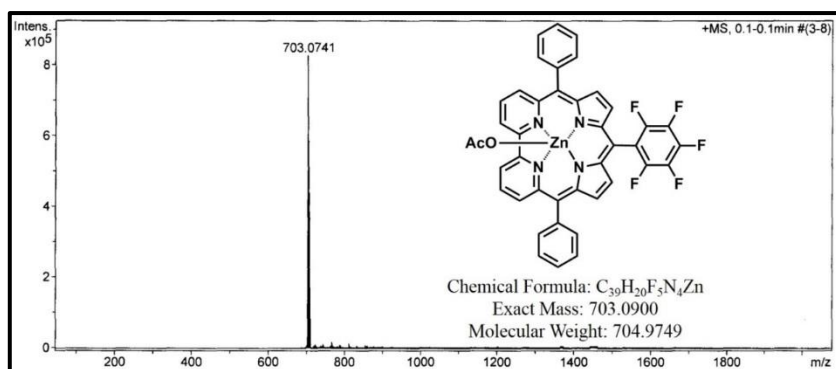


Figure 4.7: ESI-MS spectrum of **12**.

4.5.2.2 NMR Characterization

The ^1H NMR spectrum of **11** and **12** was recorded in CDCl_3 at 298 K. The bipyridyl protons in **11** are resonated as two doublets at 8.16 [H(4,18)] and 7.36 [H(2,20)] ppm and a triplet at 7.87 [H(3,19)] ppm. The pyrrolic β -CH protons are observed as a doublet at 6.91 [H(8,14)] and 6.46 [H(9,13)] ppm, respectively (Figure 4.8). The pyrrolic NH [H(24)] is observed as a broad singlet at 11.77 ppm, which was further confirmed by $\text{CDCl}_3/\text{D}_2\text{O}$ exchange experiment. The *meso*-phenyl protons are appeared at 7.50 ppm. Overall, the peak positions of **11** are consistent with nonaromatic character.^{32,41} On the other hand, the absence of inner NH signal and slightly deshielded bipyridyl, pyrrolic β -CH protons confirm the metal ion insertion in **11** to form **12**. The bipyridyl protons in **12** are resonated at 8.81 [H(4,18)], 8.33 [H(3,19)] and 8.02 [H(2,20)] ppm, while the pyrrolic β -CH protons are observed at 7.16 [H(8,14)] and 6.87 [H(9,13)] ppm (Figure 4.10). The *meso*-phenyl protons are at 7.58 ppm. In addition, the singlet peak appeared at 1.62 ppm is assigned for the methyl group from the axially coordinated acetate ion, suggests that the Zn^{II} ion is stabilized by *monoanionic* core. All these signals were further confirmed by 2D homonuclear correlation spectroscopy (Figure 4.9 and 4.11).

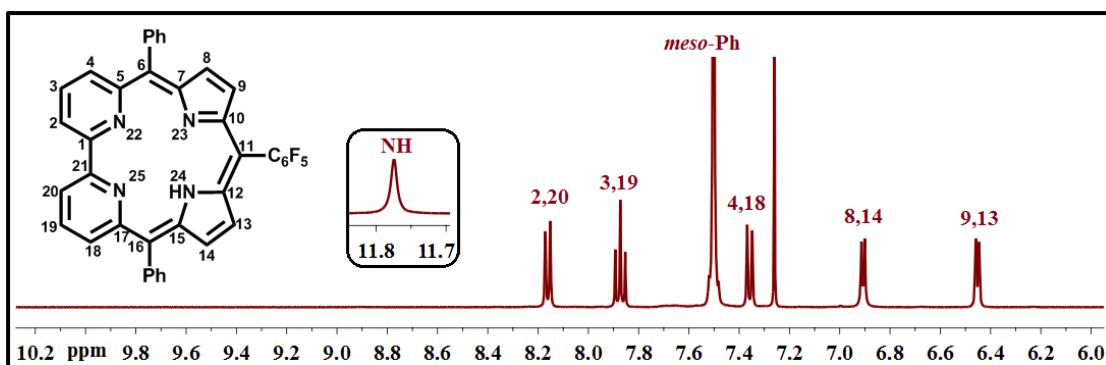


Figure 4.8: $^1\text{H-NMR}$ spectrum of **11** in CDCl_3 .

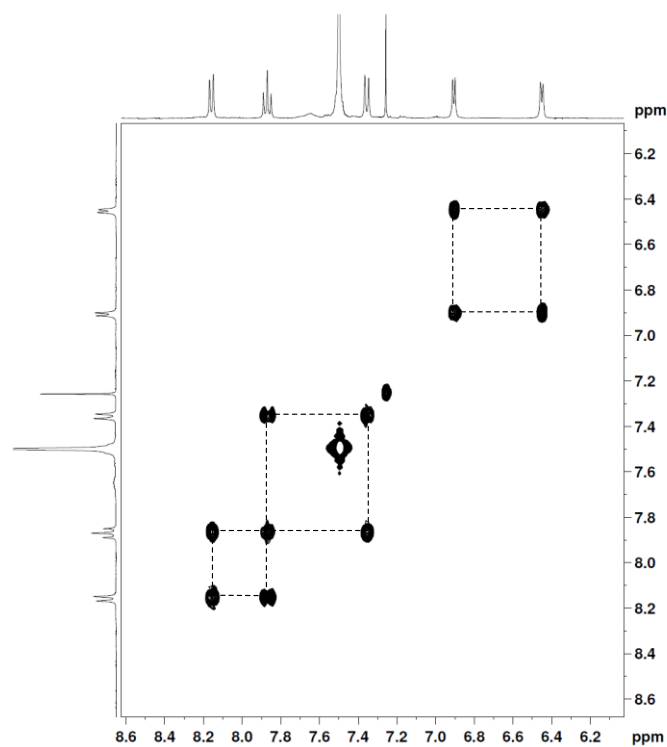


Figure 4.9: $^1\text{H} - ^1\text{H}$ COSY spectrum of **11** in CDCl_3 .

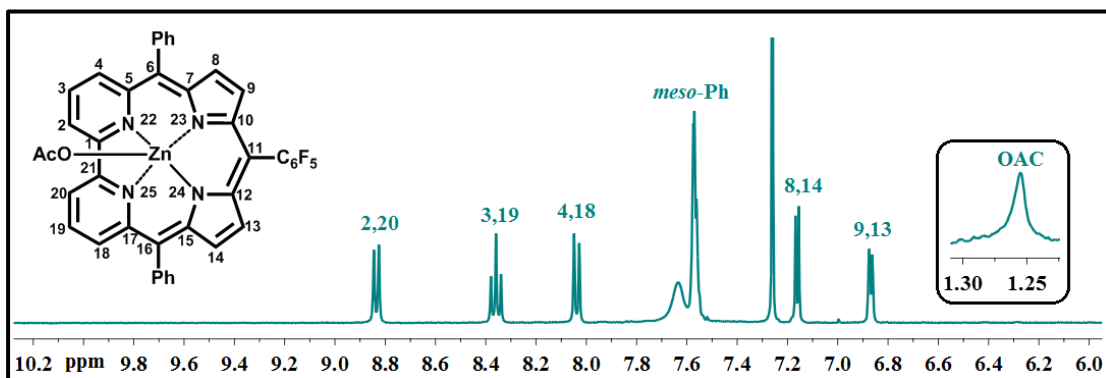


Figure 4.10: $^1\text{H-NMR}$ spectrum of **12** in CDCl_3 .

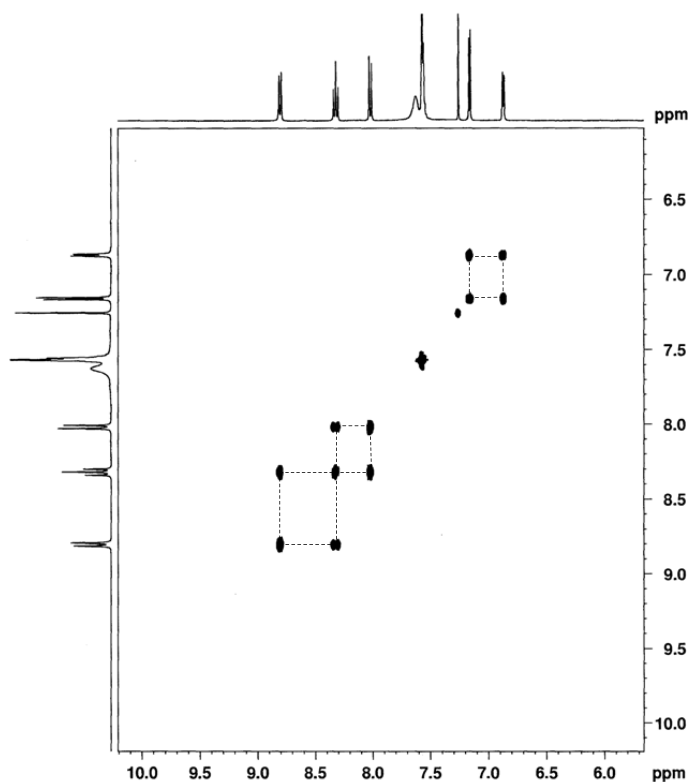


Figure 4.11: ^1H - ^1H COSY spectrum of **12** in CDCl_3 .

4.5.2.3 Single crystal X-ray structure and analysis of **11** and **12**

The structures of **11** and **12** were finally confirmed by single crystal X-ray analysis and shown in Figure 4.12 (Table 2). As predicted from the spectral analysis, the nonaromatic character in **11** is further reflected from the crystal analysis, where (i) the bipyridyl unit and dipyrromethene moieties are connected by $\text{sp}^2\text{-sp}^2$ single bond character with the bond lengths of 1.455 Å (C5-C6) and 1.472 Å (C16-C17); (ii) the $\text{sp}^2\text{-sp}^2$ double bond character (bond lengths are between 1.337 and 1.399 Å) and the average bond angle (119.996°) within the bipyridyl unit⁵² maintains the individual aromatic character and (iii) the $\text{sp}^2\text{-sp}^2$ single and double bond character (bond distances between 1.336 and 1.472 Å) within dipyrromethene moiety proves the effective π -delocalization (Figure 4.12c). The individual aromaticity in the bipyridyl unit and the π -conjugation within the dipyrromethene moiety, thus remain isolated from the overall

macrocyclic aromatization. In addition, the saddling dihedral angles ($\chi_1 - \chi_4$) are between 3.90° and 7.35° (Table 1), which are very less as compared to corrole and its derivatives⁵³ and the pyrrole units are hardly deviated from the mean N4 plane with the maximum deviation of 5.913° , suggests that the macrocycle **11** adopts planar

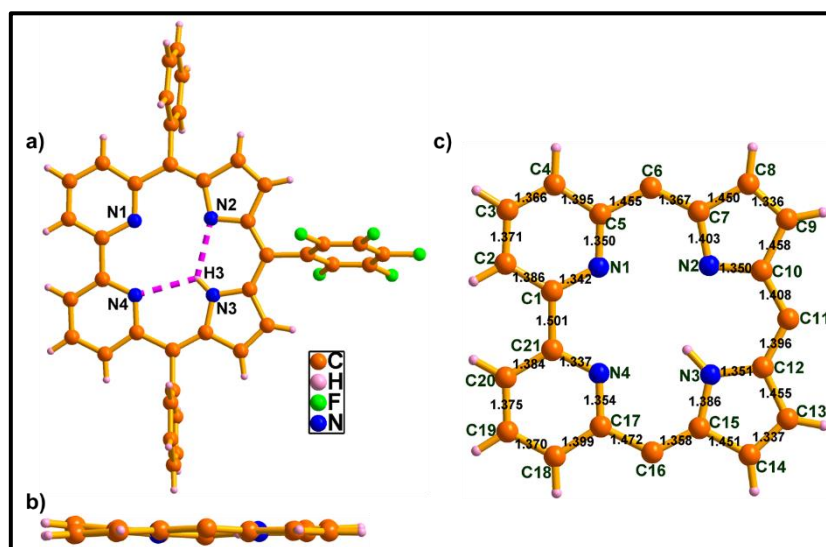


Figure 4.12: Single crystal X-ray structure of **11**. a) Top view and b) side view and c) bond lengths (Å). The *meso*-aryl groups are omitted for clarity in (b) and (c).

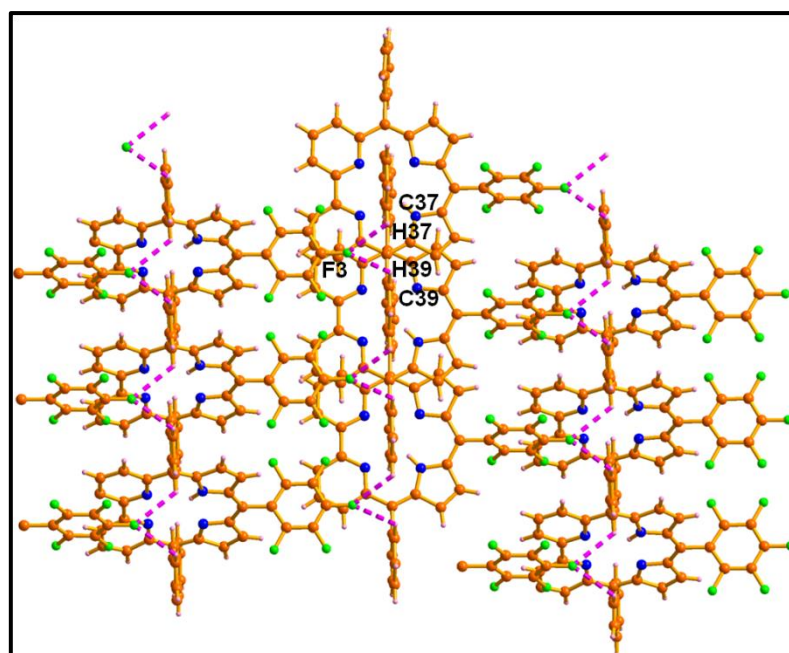


Figure 4.13: 1-D array of **11**.

conformation (Figure 4.12b). The amine hydrogen (N3-H3) in the pyrrolic unit is in intramolecular hydrogen bonding interaction with the neighboring imine nitrogens of pyrrole (N2) as well as pyridine unit (N4) with the bond distances and angles of N3-H3...N2 and N3-H3...N4 are 2.23 Å & 122.31° and 2.34 Å & 118.27° (Figure 4.12a). The presence of fluorine atoms in the pentafluoro unit generates a series of intermolecular hydrogen bonding interactions to form 1-D arrays (Figure 4.13), the bond distances and angles are: C37-H37...F3: 2.64 Å & 113° and C39-H39...F3: 2.71 Å & 123°, respectively.

The metal ion insertion and axial coordination is reflected from the single crystal X-ray structure of **12** (Figure 4.14), where the Zn^{II} ion is 0.54 Å above the mean N4 plane (Figure 4.14b). The geometry around the metal centre is square pyramid with four nitrogens are in equatorial plane and the fifth position is occupied by axially coordinated acetate ion. The bond lengths of Zn-N1 and Zn-N4 are 2.120 and 2.114 Å, which are longer than the Zn-N2 and Zn-N3 with values of 2.016 and 1.997 Å, (Figure 4.14c). The bond distances are comparable with pyriporphyrin [Zn-N_{pyridine}: 2.35 Å and Zn-N_{pyrrole}: 2.05 – 2.11 Å]⁵¹ and Zn^{II} complex of **7** [Zn-N_{pyridine}: 2.16 – 2.17 Å and Zn-N_{pyrrole}: 2.03 – 2.04 Å].⁵⁴ Further, the saddling dihedral angle values ($\chi_1 - \chi_4$) in **12** are between 2.526° and 11.809° (Table 1),⁵⁵ the pyrrole units are slightly tilted from the mean N4 plane with the maximum deviation of 12.468°. The presence of fluorine atoms in the pentafluoro unit generates a series of intermolecular hydrogen bonding interactions. Here one of the *meso*-phenyl-CHs (C23-H23) interacts with the neighbouring molecule fluorine atom (F3) to generate a hexameric structure in the solid state with bond distances and angles are C23-H23...F3: 2.80 Å and 138° (Figure 4.15). Each unit is arranged in alternate fashion, where the distance between the adjacent, alternate and opposite Zn^{II} ions are 13.84 Å, 20.25 Å and 24.53 Å.

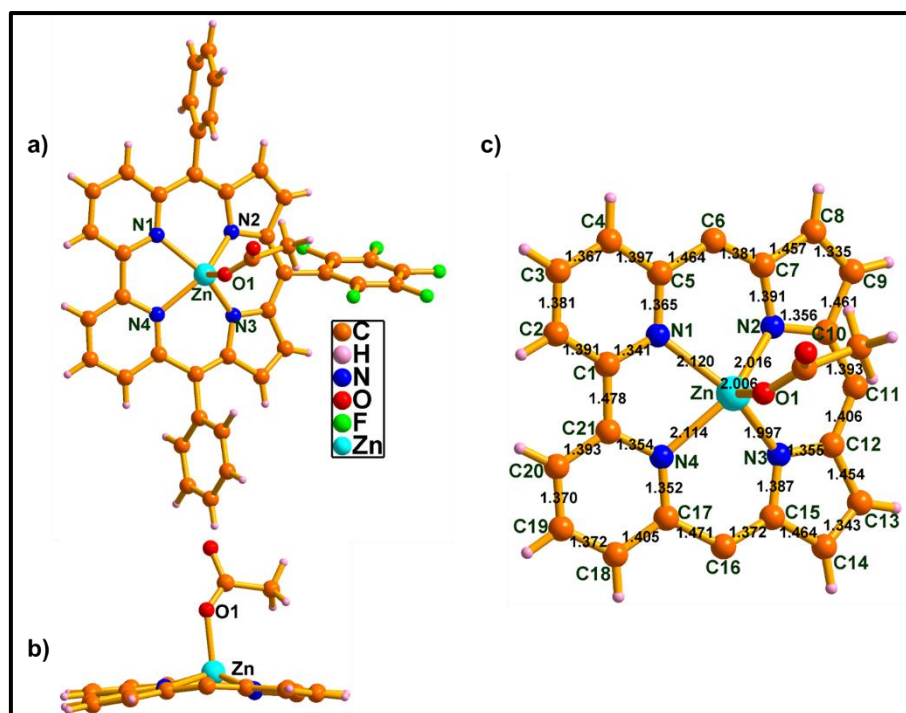
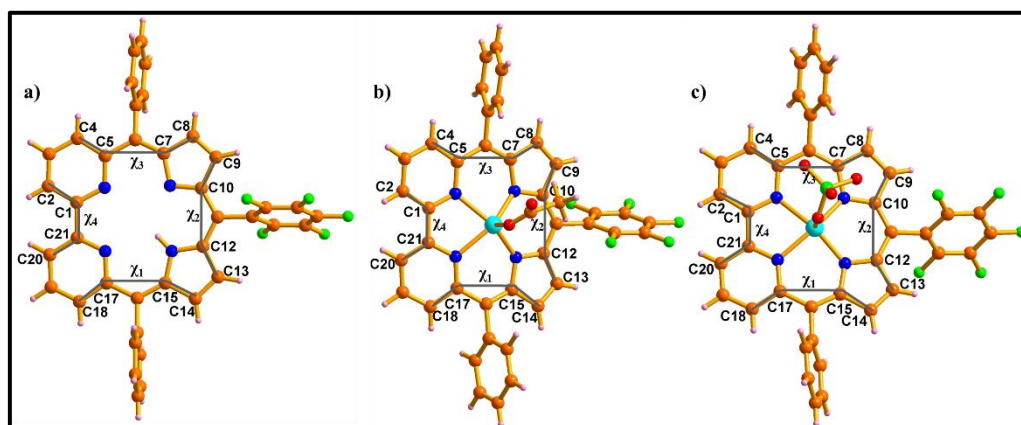


Figure 4.14: Single crystal X-ray structure of **12**. a) Top view, b) side view and c) bond lengths (Å). The *meso*-aryl groups are omitted for clarity in (b) and (c).

Table 4.1: Saddling dihedral angle (χ) value in **11**, **12** and **13** (°)



χ	Saddling dihedral angle	11 (°)	12 (°)	13 (°)
χ_1	C18-C17-C15-C14	3.902	2.526	11.984
χ_2	C13-C12-C10-C9	6.166	11.809	4.364
χ_3	C8-C7-C5-C4	6.366	9.672	0.101
χ_4	C2-C1-C21-C20	7.350	4.725	3.549

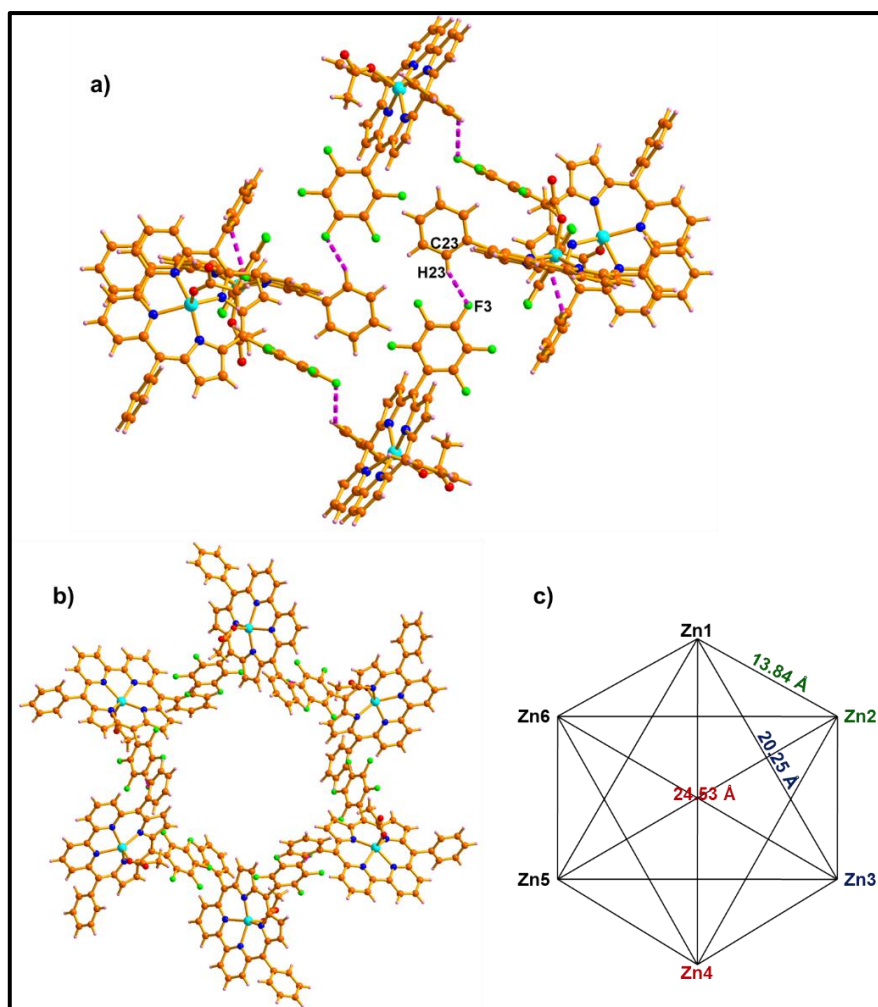


Figure 4.15: Hexameric structure of **12**.

4.5.2.4 UV-Vis and Emission Spectroscopy

The electronic absorption and emission spectrum of both **11** and **12** in CH₃OH is shown in Figure 4.16 along with visible and emission color changes. The absorption spectrum of **11** shows an intense band at 365 nm and the weak Q-type bands between 588 and 628 nm, respectively, with the molar extinction coefficient of 10⁵. The spectral results of **11** are compared with biphenylcorrole,³² pyriporphyrin⁵¹ and corrole⁵⁶ and the results are summarized as follows; (i) the molar absorption coefficient and the spectral pattern are similar to biphenylcorrole and pyriporphyrin, reflects the nonaromatic character in **11**; (ii) the intense band and weak Q-bands in **11** are blue

shifted by 46 and 53 nm, as compared to pyriporphyrin,⁵¹ suggests the reduction in the π -delocalization (dipyrromethene vs tripyrromethene) and (iii) the absence of Soret band and one fold reduction in the molar absorption coefficient of the intense band as compared to corrole,⁵⁶ proves that **11** is not aromatic. Upon Zn^{II} ion insertion (**12**), the color of the solution changes from blue to green. The intense band and weak Q-bands in **11** are red shifted by 8 and 40 to 50 nm and observed at 373 and 628 to 682 nm, respectively, with moderate increase in the ϵ value. The results are further compared with Zn complex of **7**,⁵¹ where the Q-band is 166 nm blue shifted suggests the less π -delocalization in **12** and maintains the nonaromaticity.

The emission spectrum of **11** shows a weaker band at 699 nm with the fluorescence quantum yield (Φ_F) of 0.011. Upon chelation, the emission color changes from light brick red to intense red and the band is red shifted by 10 nm and appears at 709 nm with eight-fold increase in emission intensity and the quantum yield (Φ_F) is 0.089. It is pertinent to point out here that there is no emission intensity observed in

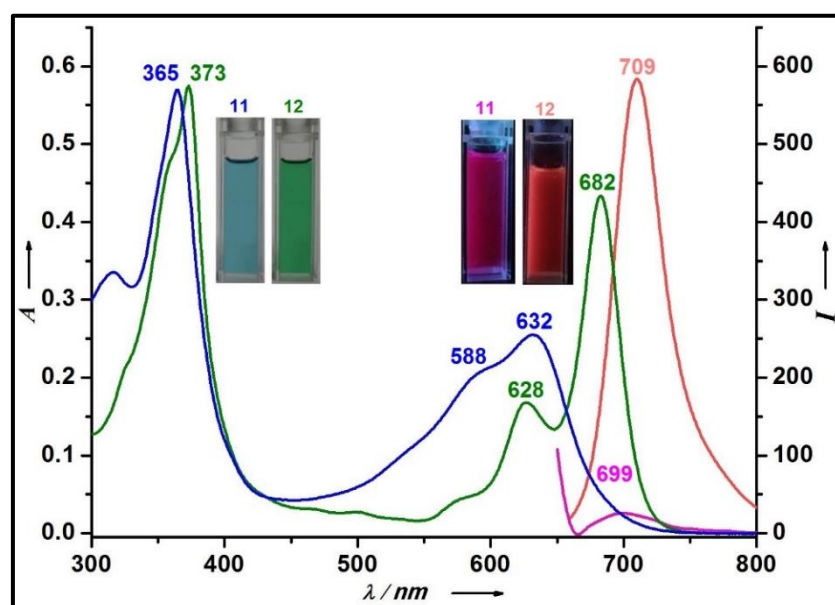


Figure 4.16: The electronic absorption and emission spectrum of **11** and **12** in CH₃OH along with absorption (left) and emission (right) color changes.

the case of Zn^{II} complex of N-substituted corrole derivative^{57,58} and Zn complex of pyriporphyrin.⁵¹ The chelation Induced Emission Enhancement (CIEE) character shown by **11** upon Zn^{II} metalation may find potential application in biological imaging.⁸

4.5.3 Sensing studies

The enhanced emission upon Zn^{II} ion insertion prompted us to perform sensing studies of **11**, in order to find out whether **11** is selective towards Zn^{II} ion or any other metal ions. The preliminary qualitative experiment was performed by using dilute CH₃OH solution of **11** with 10 equiv. of various metal ions such as Ag^I, Ca^{II}, Cd^{II}, Co^{II}, Cr^{III}, Cu^{II}, Fe^{III}, Hg^{II}, Mg^{II}, Mn^{II}, Ni^{II} and Zn^{II} in the form of perchlorate (ClO₄⁻) salts. All the metal ions shows the different absorption spectra as compared to the **11**. However, among the tested metal ions, only Zn^{II} ion exhibited turn-on emission (Figure 4.17c). To have a quantitative picture, various equivalents of Zn^{II} ions are gradually added to the 10 μM CH₃OH solution of **11**. Upon increasing the concentration of Zn^{II} ions, the intensity of the emission band is increased gradually up to 1 equiv (Figure 4.17a). Further, increasing the concentration of Zn^{II} ion, no appreciable change in the emission intensity was observed. The Job's plot shows the change in the emission spectral data suggests the formation of 1:1 binding mode (Figure 4.17b) and the association constant is 5.47 x 10⁴ M⁻¹ from the Benesi-Hildebrand plot. Further, the competitive recognition studies of Zn^{II} ion over other metal ions are tested by studying the changes in emission spectrum of **11**. It is found that **11** selectively shows enhanced emission towards Zn^{II} ions, even in the presence of 100 equiv. of other ions (Figure 4.17d) and the detection limit of **11** for Zn^{II} ion is found to be 1.5 ppm. To test the sensing ability of Zn^{II} in an aqueous solution, the experiments are also conducted in 0.1 M HEPES buffer (pH 7.4) aqueous CH₃OH solution (CH₃OH:H₂O; 4:6 v/v) and exhibits similar trend.

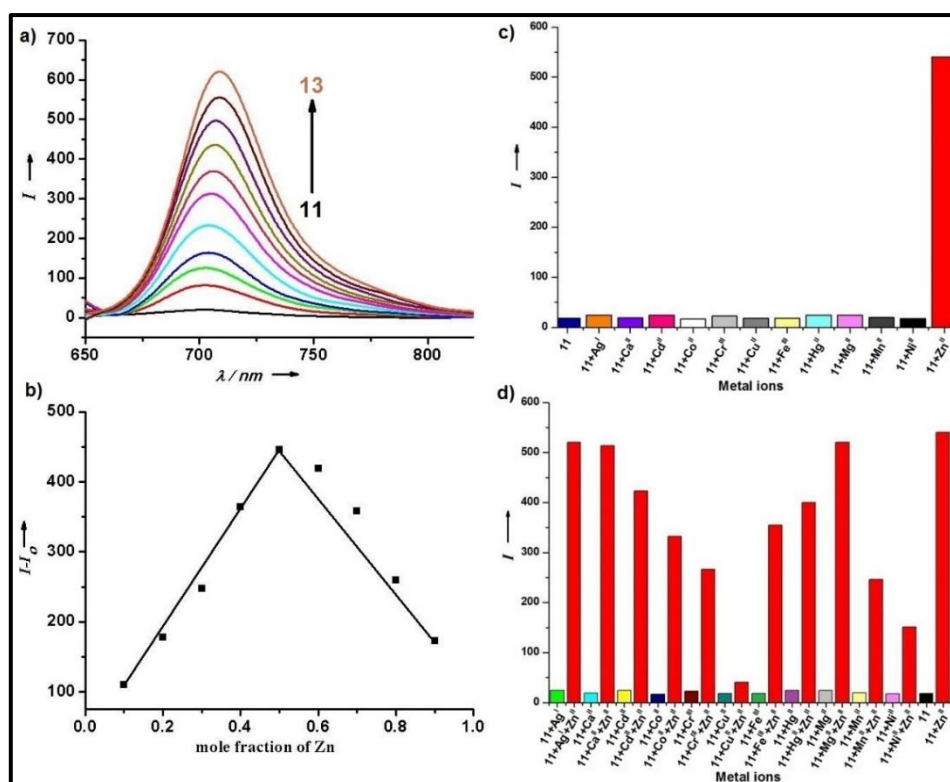


Figure 4.17: Sensing properties of **11**. a) The emission spectral changes upon addition of Zn^{II} in CH_3OH solution; b) The Job's plot for the complexation; c) Metal ion selectivity of **11** in the presence of various metal ions and d) Competitive recognition study of **11** with 10 equiv. of Zn^{II} in presence of 100 equiv. of other metal ions.

The newly formed 1:1 complex **13** was further characterized by mass spectral analysis and shows the molecular ion signal at m/z 703.0888 [$\text{M}-\text{ClO}_4$]. The ^1H NMR analysis proves that the complex retains the nonaromatic character as such. Finally, the complex was unambiguously confirmed by single crystal X-ray analysis, where the geometry around the metal center is square pyramid (Figure 4.18, Table 2). The Zn^{II} ion is 0.35 Å above the mean N4 plane and perchlorate ion is axially coordinated. As observed in **12**, the $\text{Zn}-\text{N}_{\text{pyridine}}$ bond lengths in **13** are 2.11 to 2.12 Å, which are longer than the $\text{Zn}-\text{N}_{\text{pyrrole}}$ bond lengths with the values of 1.98 and 2.02 Å (Figure 4.18c).

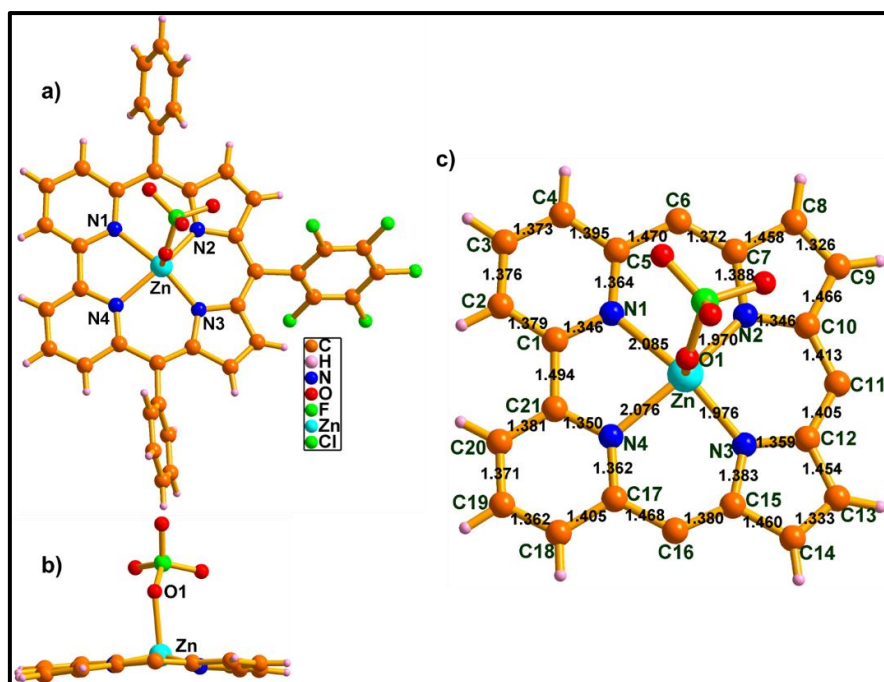


Figure 4.18: Single crystal X-ray structure of 7. a) Top view, b) side view and c) bond lengths in 12 (Å). The *meso*-aryl groups are omitted for clarity in (b) and (c).

4.6 Conclusion

In summary, we have successfully demonstrated the synthesis of 6,11,16-triarylbiopyrrocorrole and its Zn^{II} complex. Their nonaromatic character was reflected by spectral studies and structural analyses. To the best of our knowledge, the *monoanionic* core stabilizes the Zn^{II} ion without altering the internal coordination sphere, which is hitherto unknown in corrole chemistry. The enhanced emission upon metal ion insertion was further exploited for sensing studies, where the ligand was effectively utilized for selective detection of Zn^{II} ion over other metal ions by retaining the nonaromaticity as such.

4.7 Experimental Section

4.7.1 General Information

The reagents and materials for the synthesis were used as obtained from Sigma - Aldrich chemical suppliers. All solvents were purified and dried by standard methods prior to use. The NMR solvents were used as received and the spectra were recorded with Bruker 400 MHz spectrometer with TMS as internal standard. The ESI mass spectra were recorded on Bruker, micro-TOF-QII mass spectrometer. The electronic absorption spectra and steady state fluorescence spectra were recorded on Perkin Elmer–Lambda 750 UV-Visible spectrophotometer and Perkin Elmer LS55 Fluorescence spectrometer respectively. X-ray quality crystals for the compounds were grown by the slow diffusion of *n*-hexane over CH₂Cl₂ solution of the compounds. Single-crystal X-ray diffraction data of **11**, **12** and **13** were collected on a Bruker KAPPA APEX-II, four angle rotation system and Mo-K α radiation (0.71073 Å). Fluorescence quantum yields were determined by using *meso*-tetraphenylporphyrin (TPPH₂) in toluene (Φ_f = 0.11) as a reference. The crystals have been deposited in the Cambridge Crystallographic Data Centre with reference no. **CCDC 985445 (11)**, **985446 (12)**, **1407494 (13)**.

4.7.2 Synthetic procedure and spectral characterization

4.7.2.1 Synthesis of 14: Freshly prepared phenylmagnesiumbromide (13.195 g, 72.5mmol) solution in THF was added under N₂ atmosphere at 0 °C into the solution of **13** (3 g, 14.22 mmol) in 100 ml toluene. The reaction mixture was kept at same temperature for 10 min and then allowed to attain RT. After 4h the reaction was quenched with 1N HCl, extracted with EtOAc, dried over Na₂SO₄ and concentrated by rotary evaporator. The crude compound was purified by column chromatography

using silica gel (silica 100-200 mesh) in 15% EtOAc/*n*-hexane to afford **14** in 75% yield.

¹H NMR (400 MHz, CDCl₃, 298K): δ = 8.55 (dd, J = 7.9, 0.8 Hz, 2H), 8.20 – 8.16 (m, 4H), 8.09 (dd, J = 7.7, 0.8 Hz, 2H), 7.99 (t, J = 7.8 Hz, 2H), 7.65 (t, J = 7.4 Hz, 2H), 7.54 (t, J = 7.6 Hz, 4H).

¹³C NMR (100 MHz, CDCl₃): δ = 193.65, 154.44, 138.43, 136.57, 133.11, 131.43, 128.29, 125.06, 123.79.

m.p: 119-120 °C.

ESI-MS: m/z calculated for C₂₄H₁₆N₂O₂ = 364.1212; found = 365.1271(M+1).

4.7.2.2 Synthesis of 15: NaBH₄ (2.06 g, 54.6 mmol) was added in several portion to the solution of **14** (2 g, 5.5 mmol) in 50 ml (7:3) THF/CH₃OH mixture under N₂ atmosphere at 0 °C. The mixture was allowed to stir at RT for 2 h. Then the reaction mixture was quenched with water and the compound was extracted with CH₂Cl₂, dried over Na₂SO₄ and concentrated by rotary evaporator. Compound was purified by recrystallization in CH₂Cl₂/*n*-hexane to afford white crystalline compound **15** in 90% yield.

¹H NMR (400 MHz, CDCl₃, 298K): δ = 8.40 (d, J = 7.8 Hz, 2H), 7.78 (t, J = 7.8 Hz, 2H), 7.45 – 7.43 (m, 4H), 7.38 – 7.35 (m, 6H), 7.18 (d, J = 7.8 Hz, 2H), 5.84 (s, 2H), 5.52 (s, 2H).

¹³C NMR (100 MHz, CDCl₃): δ = 160.49, 153.61, 143.15, 138.14, 128.82, 128.77, 128.09, 127.34, 121.92, 121.90, 119.97, 75.09, 75.07.

m.p: 126-128°C.

ESI-MS: m/z calculated for C₂₄H₂₀N₂O₂ = 368.1525; found = 369.1543 (M+1).

4.7.2.3 Synthesis of 16: A solution of 6,6'-Bis(phenylhydroxymethyl)2,2'-bipyridine(**15**) (2 g, 5.2 mmol) in dry CH₂Cl₂ (100 ml) was taken in a 250 ml two neck RB flask and kept in an inert atmosphere. To the solution, TEA (3.77 ml, 2.7 mmol) and catalytic amount of DMAP were added and stirred for 10 min. Methanesulfonyl chloride (2.1 ml, 2.7 mmol) in 5 ml dry CH₂Cl₂ was added slowly at 0 °C and allowed to stir for 3 days at same temperature. The completion of the reaction was monitored by TLC and solvent was evaporated by rotary evaporator. The crude reaction mixture was dissolved in pyrrole (20 ml) and stirred at RT for 2 days in dark. The reaction was monitored by TLC and the excess pyrrole was removed in a rotary evaporator. The crude compound was purified through filtration followed by washing with CH₂Cl₂ to afford **16** as grey powder in 40% yield.

¹H NMR (400 MHz, DMSO-d₆, 298K): δ = 10.72 (brs, 2H), 8.24 (d, *J* = 7.8 Hz, 2H), 7.90 (t, *J* = 7.8 Hz, 2H), 7.33 – 7.31 (m, 10H), 7.23 (m, 2H), 6.70 (d, *J* = 1.5 Hz, 2H), 5.98 – 5.96 (m, 2H), 5.79 (s, 2H), 5.66 (s, 2H).

¹³C NMR (100 MHz, DMSO-d₆): δ = 161.88, 154.74, 142.98, 137.84, 132.09, 128.55, 128.18, 126.29, 123.23, 118.41, 117.34, 107.11, 106.85, 52.30.

m.p: 179-181 °C.

ESI-MS: m/z calculated for C₃₂H₂₆N₄ = 466.2157; found = 467.2221 (M+1).

4.7.2.4 Synthesis of 11: To a 300 ml CH₂Cl₂ solution, **16** (400 mg, 0.86 mmol) and pentafluorobenzaldehyde (168 mg, 0.86 mmol) were added under inert atmosphere covered with aluminium foil and stirred for 10 min. Trifluoroacetic acid (0.39 ml, 5.16 mmol) was added and allowed to stir under same condition for 3 h. Then 2,3-dichloro-5,6-dicyano-1,4-benzoquinone (0.585 mg, 2.58 mmol) was added to the reaction mixture and opened to air. The mixture was further allowed stir for 2 h. The crude product was passed through basic alumina column followed by silica gel (silica 100-

200 mesh). The blue band was eluted with 1% CH₃OH/CH₂Cl₂ and identified as **11**. The compound was further recrystallized from CH₂Cl₂/*n*-hexane to afford compound **11** in 12% yield.

¹H NMR (400 MHz, CDCl₃, 298K): δ = 11.77 (brs, 1H), 8.16 (d, *J* = 7.6 Hz, 2H), 7.87 (t, *J* = 7.9 Hz, 2H), 7.52 – 7.48 (m, 10H), 7.36 (d, *J* = 7.9 Hz, 2H), 6.91 (d, *J* = 5.2 Hz, 2H), 6.45 (d, *J* = 5.2 Hz, 2H).

¹³C NMR (100 MHz, CDCl₃): δ = 157.22, 155.00, 140.17, 136.26, 132.34, 128.23, 128.21, 128.03, 127.54, 118.47.

m.p: 300 °C (decomposition).

ESI-MS: *m/z* calculated for (C₃₉H₂₁F₅N₄) = 640.1686; found = 641.1664 (M+1).

UV-Vis (CH₃OH): λ_{\max} (nm) (ϵ [M⁻¹cm⁻¹]) = 365 (49,825), 588 (17,842), 632 (22,208).

4.7.2.5 Synthesis of 12: A solution of Zn(OAc)₂ (57 mg, 0.3 mmol) in 5 ml CH₃OH was added in to the solution of **11** (20 mg, 0.03 mmol) in CH₂Cl₂ (15 ml) under inert atmosphere and allowed to stir for 1.5 h. The completion of the reaction was monitored by TLC and the solvent was evaporated by rotary evaporator. Residue was purified by silica gel (silica 100-200 mesh) in 1% CH₃OH/CH₂Cl₂ and identified as **12**. The compound was further recrystallized from CH₂Cl₂/*n*-hexane to afford green crystalline compound **12** in 90% yield.

¹H NMR (400 MHz, CDCl₃, 298K): δ = 8.81 (d, *J* = 7.8 Hz, 2H), 8.33 (t, *J* = 8.0 Hz, 2H), 8.02 (d, *J* = 8.2 Hz, 2H), 7.58 (dd, *J* = 14.4, 12.9 Hz, 10H), 7.16 (d, *J* = 5.0 Hz, 2H), 6.87 (d, *J* = 5.0 Hz, 2H), 1.62 (s, 3H).

¹³C NMR (100 MHz, CDCl₃): δ = 165.73, 156.76, 154.20, 147.35, 139.72, 138.32, 137.91, 132.57, 130.80, 130.65, 128.45, 128.26, 125.70, 119.43.

m.p: 300 °C (decomposition).

ESI-MS: m/z calculated for $(C_{41}H_{23}F_5N_4O_2Zn) = 762.1033$; without axial ligand $(C_{39}H_{20}F_5N_4Zn) = 703.09$ found = 703.0741.

UV-Vis (CH_2Cl_2): $\lambda_{max}(nm)$ ($\epsilon[M^{-1}cm^{-1}]$) = 373 (50,025), 628 (15,672), 682 (40,281);

^{13}C NMR (400 MHz, $CDCl_3$, 298K): $\delta = 8.84$ (d, $J = 7.8$ Hz, 2H), 8.36 (t, $J = 8.0$ Hz, 2H), 8.04 (d, $J = 8.2$ Hz, 2H), 7.63 – 7.56 (m, 10H), 7.16 (d, $J = 5.0$ Hz, 2H), 6.87 (d, $J = 4.9$ Hz, 2H).

m.p: 300 °C (decomposition).

ESI-MS: m/z calculated for $(C_{39}H_{20}ClF_5N_4O_4Zn) = 802.0385$; without axial ligand $(C_{39}H_{20}F_5N_4Zn) = 703.09$ found = 703.0888.

Table 4.2: Crystal data for **11**, **12** and **13**

Crystal parameters	11	12	13
Formula	C ₃₉ H ₂₁ F ₅ N ₄	C ₄₁ H ₂₃ F ₅ N ₄ O ₂ Zn	C ₃₉ H ₂₀ ClF ₅ N ₄ O ₄ Zn
<i>M</i> /g mol ⁻¹	640.60	764.00	804.41
<i>T</i> /K	100	100	100
Crystal dimensions/mm ³	0.13 x 0.11 x 0.07	0.11 x 0.08 x 0.041	0.18 x 0.12 x 0.08
Crystal system	Monoclinic	Trigonal	Monoclinic
Space group	<i>P2(1)/c</i>	<i>R -3</i>	<i>P2(1)/n</i>
<i>a</i> /Å	18.0791(8)	48.1170(1)	14.8580 (4)
<i>b</i> /Å	6.9173(3)	48.1170(1)	15.0507(4)
<i>c</i> /Å	24.5326(12)	9.5918	15.1244 (4)
α /°	90	90	90
β /°	101.279(3)	90	106.863 (2)
γ /°	90	120	90
<i>V</i> /Å ³	3008.8(2)	19232.1(9)	3236.74(15)
<i>Z</i>	4	18	4
ρ_{calcd} /mg m ⁻³	1.414	1.187	1.651
μ /mm ⁻¹	0.106	0.631	0.923
F(000)	1312	6984	1624
Reflns. collected	29503	87744	61648
Indep.reflns.[<i>R</i> (int)]	5717[0.0683]	9100 [0.0761]	8721 [0.0897]
Max/min transmission	0.9895 and 0.9895	0.660 and 0.745	0.7458 and 0.6549
Data/restraints/parameters	5717 / 0 / 434	9100 / 0 / 479	8721 / 0 / 487
GOF on <i>F</i> ²	0.959	1.090	1.019
Final <i>R</i> indices[<i>I</i> > 2 σ (<i>I</i>)]	<i>R</i> 1 = 0.0538, w <i>R</i> 2 = 0.1281	<i>R</i> 1 = 0.0482, w <i>R</i> 2 = 0.1407	<i>R</i> 1 = 0.0461, w <i>R</i> 2 = 0.1021
<i>R</i> indices (all data)	<i>R</i> 1 = 0.1464, w <i>R</i> 2 = 0.1773	<i>R</i> 1 = 0.0732, w <i>R</i> 2 = 0.1500	<i>R</i> 1 = 0.0878, w <i>R</i> 2 = 0.1174
Largest diff peak and hole [e Å ⁻³]	0.228 and -0.202	0.740 and -0.481	0.561 and -0.474

References

1. Ueno, T.; Nagano, T. *Nat. Methods* **2011**, *8*, 642-645.
2. Nolan, E. M.; Lippard, S. J. *Acc. Chem. Res.* **2008**, *42*, 193-203.
3. Bertini, I. *Biological inorganic chemistry: structure and reactivity*; University Science Books, **2007**.
4. Jiang, P.; Guo, Z. *Coord. Chem. Rev.* **2004**, *248*, 205-229.
5. Cuajungco, M. P.; Lees, G. J. *Neurobiol. Dis.* **1997**, *4*, 137-169.
6. Ding, Y.; Zhu, W.-H.; Xie, Y. *Chem. Rev.* **2016**, DOI: [10.1021/acs.chemrev.6b00021](https://doi.org/10.1021/acs.chemrev.6b00021)
7. Ding, Y.; Tang, Y.; Zhu, W.; Xie, Y. *Chem. Soc. Rev.* **2015**, *44*, 1101-1112.
8. Carter, K. P.; Young, A. M.; Palmer, A. E. *Chem. Rev.* **2014**, *114*, 4564-4601.
9. Ding, Y.; Xie, Y.; Li, X.; Hill, J. P.; Zhang, W.; Zhu, W. *Chem. Commun.* **2011**, *47*, 5431-5433.
10. Tanaka, T.; Osuka, A. *Chem. Soc. Rev.* **2015**, *44*, 943-969.
11. Sessler, J. L.; Lawrence, C. M.; Jayawickramarajah, J. *Chem. Soc. Rev.* **2007**, *36*, 314-325.
12. Kadish, K.; Smith, K.; Guillard, R. *The Porphyrin Handbook, Volume 1: Synthesis and Organic Chemistry*. Academic Press—San Diego, CA and London, UK: **2000**.
13. Sessler, J. L.; Weghorn, S. J. *Expanded, contracted & isomeric porphyrins*; Elsevier, **1997**; Vol. 15.
14. Jasat, A.; Dolphin, D. *Chem. Rev.* **1997**, *97*, 2267-2340.
15. Zhang, X.-a.; Lovejoy, K. S.; Jasanoff, A.; Lippard, S. J. *Proc. Natl. Acad. Sci. USA.* **2007**, *104*, 10780-10785.
16. Lv, Y.; Cao, M.; Li, J.; Wang, J. *Sensors* **2013**, *13*, 3131-3141.

-
17. Hung, C.-H.; Chang, G.-F.; Kumar, A.; Lin, G.-F.; Luo, L.-Y.; Ching, W.-M.; Wei-Guang Diao, E. *Chem. Commun.* **2008**, 978-980.
 18. Ikawa, Y.; Takeda, M.; Suzuki, M.; Osuka, A.; Furuta, H. *Chem. Commun.* **2010**, 46, 5689-5691.
 19. Paollesse, R.; Kadish, K.; Smith, K.; Guillard, R. *Kadish, KM. The porphyrin Handbook Vol. 2: Syntheses of corroles*. Academic Press: New York, **2000**, 201-232.
 20. Erben, C.; Will, S.; Kadish, K. *Kadish, KM. The porphyrin Handbook Vol. 2: Syntheses of corroles*. Academic Press: New York, **2000**, 233-300.
 21. Flamigni, L.; Gryko, D. T. *Chem. Soc. Rev.* **2009**, 38, 1635-1646.
 22. Aviv, I.; Gross, Z. *Chem. Commun.* **2007**, 1987-1999.
 23. Orłowski, R.; Gryko, D.; Gryko, D. T. *Chem. Rev.* **2016**, DOI: 10.1021/acs.chemrev.6b00434.
 24. Buckley, H. L.; Arnold, J. *Dalton Trans.* **2015**, 44, 30-36.
 25. Skonieczny, J.; Latos-Grażyński, L.; Szterenberga, L. *Chem. Eur. J.* **2008**, 14, 4861-4874.
 26. Fujino, K.; Hirata, Y.; Kawabe, Y.; Morimoto, T.; Srinivasan, A.; Toganoh, M.; Miseki, Y.; Kudo, A.; Furuta, H. *Angew. Chem. Int. Ed.* **2011**, 50, 6855-6859.
 27. Toganoh, M.; Kawabe, Y.; Furuta, H. *J. Org. Chem.* **2011**, 76, 7618-7622.
 28. Toganoh, M.; Kawabe, Y.; Uno, H.; Furuta, H. *Angew. Chem. Int. Ed.* **2012**, 51, 8753-8756.
 29. Lee, C. H.; Jo, W. S.; Ga, J. W.; Kim, H. J.; Lee, P. H. *Bull. Korean Chem. Soc.* **2000**, 21, 429-433.
 30. Pawlicki, M.; Latos-Grażyński, L.; Szterenberga, L. *J. Org. Chem.* **2002**, 67, 5644-5653.

-
31. Shetti, V. S.; Prabhu, U. R.; Ravikanth, M. *J. Org. Chem.* **2010**, *75*, 4172-4182.
 32. Adinarayana, B.; Thomas, A. P.; Suresh, C. H.; Srinivasan, A. *Angew. Chem. Int. Ed.* **2015**, *54*, 10478-10482.
 33. Corriu, R. J. P.; Bolin, G.; Moreau, J. J. E.; Vernhet, C. *J. Chem. Soc., Chem. Commun.* **1991**, 211-213.
 34. Bell, T. W.; Cragg, P.; Drew, M. G.; Firestone, A.; Kwok, A.-I.; Liu, J.; Ludwig, R.; Papoulis, A. *Pure Appl. Chem.* **1993**, *65*, 361-366.
 35. Carre, F. H.; Corriu, R. J. P.; Bolin, G.; Moreau, J. J. E.; Vernhet, C. *Organometallics* **1993**, *12*, 2478-2486.
 36. Richter, D. T.; Lash, T. D. *J. Org. Chem.* **2004**, *69*, 8842-8850.
 37. Setsune, J.-i.; Kawama, M.; Nishinaka, T. *Tetrahedron Lett.* **2011**, *52*, 1773-1777.
 38. Setsune, J.-i.; Yamato, K. *Chem. Commun.* **2012**, *48*, 4447-4449.
 39. Zhang, Z.; Lim, J. M.; Ishida, M.; Roznyatovskiy, V. V.; Lynch, V. M.; Gong, H.-Y.; Yang, X.; Kim, D.; Sessler, J. L. *J. Am. Chem. Soc.* **2012**, *134*, 4076-4079.
 40. Zhang, Z.; Cha, W.-Y.; Williams, N. J.; Rush, E. L.; Ishida, M.; Lynch, V. M.; Kim, D.; Sessler, J. L. *J. Am. Chem. Soc.* **2014**, *136*, 7591-7594.
 41. Ishida, M.; Naruta, Y.; Tani, F. *Angew. Chem. Int. Ed.* **2010**, *49*, 91-94.
 42. Arnold, L.; Norouzi-Arasi, H.; Wagner, M.; Enkelmann, V.; Müllen, K. *Chem. Commun.* **2011**, *47*, 970-972.
 43. Quernheim, M.; Liang, H.; Su, Q.; Baumgarten, M.; Koshino, N.; Higashimura, H.; Müllen, K. *Chem. Eur. J.* **2014**, *20*, 14178-14183.
 44. Myśliborski, R.; Latos-Grażyński, L.; Szterenber, L.; Lis, T. *Angew. Chem. Int. Ed.* **2006**, *45*, 3670-3674.
 45. Neya, S.; Suzuki, M.; Matsugae, T.; Hoshino, T. *Inorg. Chem.* **2012**, *51*, 3891-3895.

-
46. Rury, A. S.; Wiley, T. E.; Sension, R. J. *Acc. Chem. Res.* **2015**, *48*, 860-867.
 47. Hong, Y.; Lam, J. W. Y.; Tang, B. Z. *Chem. Soc. Rev.* **2011**, *40*, 5361-5388.
 48. An, B.-K.; Gierschner, J.; Park, S. Y. *Acc. Chem. Res.* **2012**, *45*, 544-554.
 49. Mukkala, V.-M.; Kwiatkowski, M.; Kankare, J.; Takalo, H. *Helv. Chim. Acta* **1993**, *76*, 893-899.
 50. Myśluborski, R.; Latos-Grażyński, L. *Eur. J. Org. Chem.* **2005**, 5039-5048.
 51. Myśluborski, R.; Latos-Grażyński, L.; Szterenber, L. *Eur. J. Org. Chem.* **2006**, 3064-3068.
 52. Merritt, L. L.; Schroeder, E. *Acta Cryst.* **1956**, *9*, 801-804.
 53. Capar, J.; Conradie, J.; Beavers, C. M.; Ghosh, A. *J. Phys. Chem. A* **2015**, *119*, 3452-3457.
 54. Ishida, M.; Lim, J. M.; Lee, B. S.; Tani, F.; Sessler, J. L.; Kim, D.; Naruta, Y. *Chem. Eur. J.* **2012**, *18*, 14329-14341.
 55. Thomas, K. E.; Alemayehu, A. B.; Conradie, J.; Beavers, C. M.; Ghosh, A. *Acc. Chem. Res.* **2012**, *45*, 1203-1214.
 56. Gross, Z.; Galili, N.; Saltsman, I. *Angew. Chem. Int. Ed.* **1999**, *38*, 1427-1429.
 57. Gross, Z.; Galili, N. *Angew. Chem. Int. Ed.* **1999**, *38*, 2366-2369.
 58. Simkhovich, L.; Iyer, P.; Goldberg, I.; Gross, Z. *Chem. Eur. J.* **2002**, *8*, 2595-2601.

CHAPTER 5A

Bipyricorrole: A facile synthesis of *meso*-free corrole homologues

5A.1	Introduction	131
5A.2	Objective of our work	133
5A.3	Results and discussions	134
5A.3.1	Synthesis	134
5A.3.2	Spectral characterisation	135
5A.3.2.1	Mass spectrometric analysis	135
5A.3.2.2	NMR Analysis	135
5A.3.2.3	Single crystal X-ray analysis 6 and 7	136
5A.3.3	Coordination Studies	137
5A.3.3.1	Spectral characterization	138
5A.3.3.1.1	Mass spectrometric analysis	138
5A.3.3.1.2	NMR Analysis	139
5A.3.3.1.3	Single crystal X-ray analysis	140
5A.3.3.1.4	Electronic absorption and Emission spectral analysis	143
5A.4	Possible mechanism	145
5A.5	Conclusion	146
5A.6	Experimental Section	147
5A.6.1	General Information	147
5A.6.2	Synthetic procedure and spectral characterization of 5-9	148
5A.7	References	152

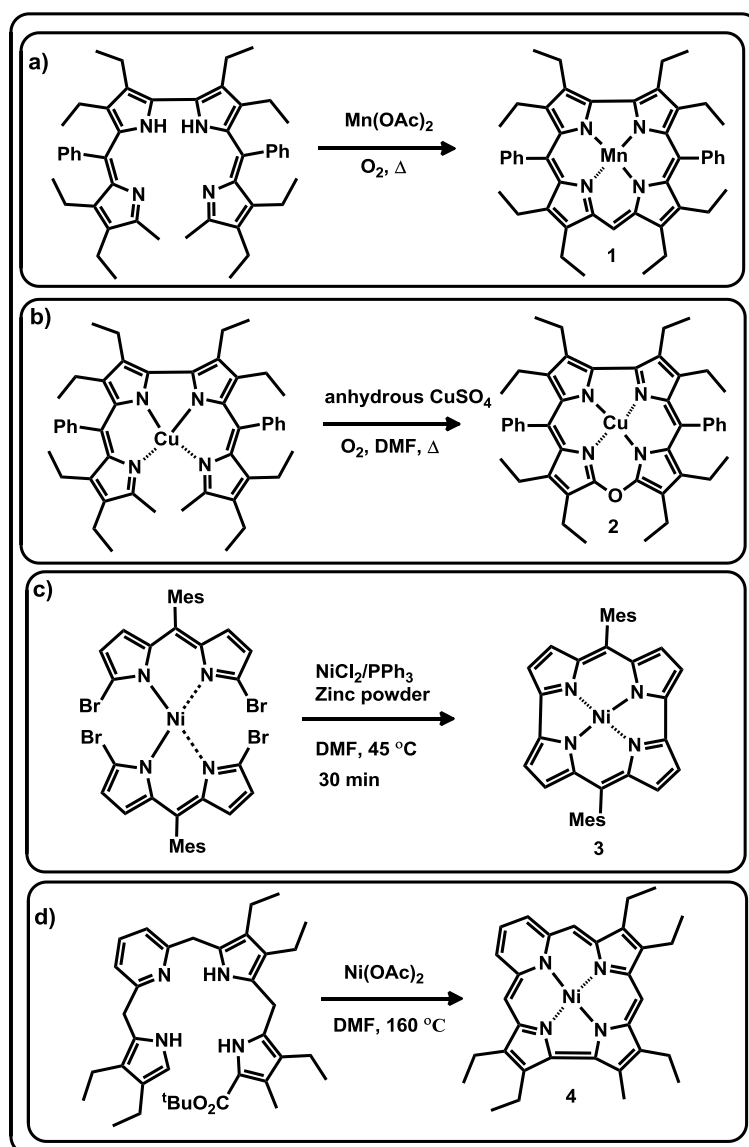
5A.1 Introduction

Corrole is a versatile ligand in the contracted porphyrins and received much attention after introducing the efficient synthesis of *meso*-triarylcorroles by Gross, Paolesse, and Gryko.¹⁻³ The ligand and its high-valent metal complexes are utilized for various applications such as molecular catalysts, sensors, medicines and dye-sensitized solar cells.⁴⁻⁶ Despite these promises; (i) the development of novel synthetic methodologies; (ii) synthesis of corrole analogues and (iii) its reactive studies were far behind from porphyrins. In particular, the synthesis of *meso*-free corrole analogues rather limited, which has been extensively studied in porphyrin chemistry. However, there are few examples, the *meso*-free 5,10-diphenylcorrole;⁷ 5,15-bis(2,6-dichlorophenyl)corrole,⁸ and 5,10- and 5,15-bis(pentafluorophenyl)corrole⁹ ligands were achieved by step-wise strategies, where the acid-catalyzed condensation reaction followed by oxidation were mainly adopted.⁷⁻⁹

On the other hand, the coordination chemistry in corrole and its analogues were mostly achieved from the corresponding free base ligands by treating them with various metal salts. Alternatively, the metal-templated synthetic strategy was recently introduced and received much attention to generate novel contracted porphyrinoids such as corrole, heterocorroles and norcorrole. These are mostly synthesized by Bröring et al and Shinokubo et al.^[8-9]

The manganese(III)corrole (**1**),¹⁰ copper(III)corrole and copper(II)heterocorroles (**2**)¹¹⁻¹² were synthesized by Bröring et al by metal-templated *oxidative* macrocyclization pathway (Scheme 5A.1a and 5.1b). Here the manganese(III)corrole was achieved by treating the 2,2'-bisdipyrins derivative with Mn(OAc)₂ followed by open air oxidation (Scheme 5A.1a). While the

copper(III)corrole and copper(II)hetero-corroles were synthesized by treating the open chain Cu(II)tetrapyrrolic 2,2'-bisdipyrins with anhydrous CuSO_4 in DMF-solution under two different condition; a) in the oxygen free atmosphere copper(III)corrole complex and b) in the presence of oxygen afforded copper(II)oxacorrole complex (Scheme 5A.1b). In addition, the other heterocorroles such as azacorrole, thiacorrole and selenacorrole were synthesized by metal-mediated homo *coupling* of dibrominated dipyrins and their properties were further explored independently by Bröring et al and Shinokubo et al.^{13,14}



Scheme 5A.1: Metal-templated synthetic strategies for contracted porphyrinoids.

Recently, the highly unstable antiaromatic contracted porphyrin, such as norcorrole was stabilized by using a metal-templated strategy. The initial observation for the synthesis of norcorrole has come from Bröring group, where the iron(III) complex of norcorrole was synthesized by oxidative coupling of iron(III)-2,2'-bidipyrrin.¹⁵ However, it was gradually converted into a dimer complex. Later the stable norcorrole was achieved by Shinokubo group by using Ni(0)-mediated intramolecular homo *coupling* strategy, where the Ni(II)-coordinated dibromodipyrrin afforded the corresponding stable antiaromatic Ni(II)-norcorrole (**3**) (Scheme 5A.1c).¹⁶

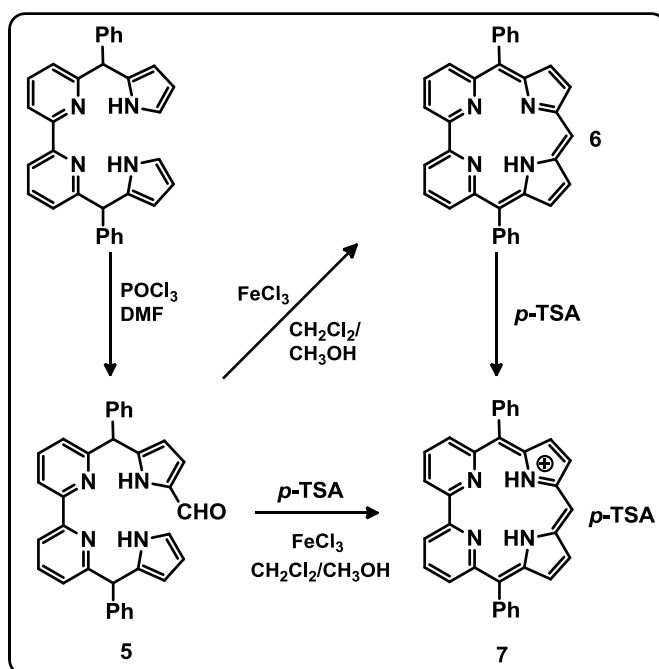
Very recently, the metal-assisted templated reaction was reported by Neya and coworkers for the synthesis of Ni(II)-pyricorrole (**4**), where the Ni(acac)₂ was used as a *coupling* as well as coordinating agent (Scheme 5A.1d).¹⁷

5A.2 Objective of our work

The synthetic methodologies adopted for *meso*-free corroles confined mostly to the β -substituted derivatives, however, the respective β -unsubstituted corrole complexes are scarcely reported. In addition, although Pd^{II}-porphyrins have long been known for their photophysical properties as well as in catalysis, the chemistry of palladium corrole derivatives are not explored so far.¹⁸⁻²⁰ By considering the importance of synthetic methodologies as well as novel complexes, which inspired us to introduce a facile metal-templated *condensation* reaction. Herein, we wish to report an efficient synthetic methodology for the synthesis of *meso*-free corrole homologues. The free base and protonated complexes are achieved by acid-catalysed *condensation* method whereas metal complexes are synthesized by metal-templated *condensation* strategy.

5A.3 Results and discussions

5A.3.1 Synthesis

Scheme 5A.2: Synthesis of **6** and **7**.

The synthesis of free-base *meso*-free bipyricorrole as well as its protonated complex is shown in Scheme-5A.2. The required precursor, formylated bipyridyl dipyrromethane (**5**) was achieved from bipyridyl dipyrromethane²¹ by Vilsmeier-Haack formylation reaction in 65% yield. The final *condensation* reaction of **5** was performed in the presence of FeCl₃ as an acid-catalyst under open air oxidation. After 3 hrs, the crude reaction mixture was purified by column chromatographic separation, where the blue color fraction eluted with CH₂Cl₂ and CH₃OH (99:1) was identified as **6** in 40% yield. Initially, the reaction was performed in the presence of *p*-toluenesulfonic acid (*p*-TSA) followed by oxidation with FeCl₃ afforded the respective macrocycle **7** in the form of its protonated complex with *p*-TSA as a counter anion (Scheme 5A.2).

5A.3.2 Spectral Characterization

5A.3.2.1 Mass spectral analysis

The compound **6** was characterized by ESI mass spectrometric analysis and showed the molecular ion signal at m/z 475.1751 [M+1] (Figure 5A.1). The result was consistent with the exact composition of the macrocycle.

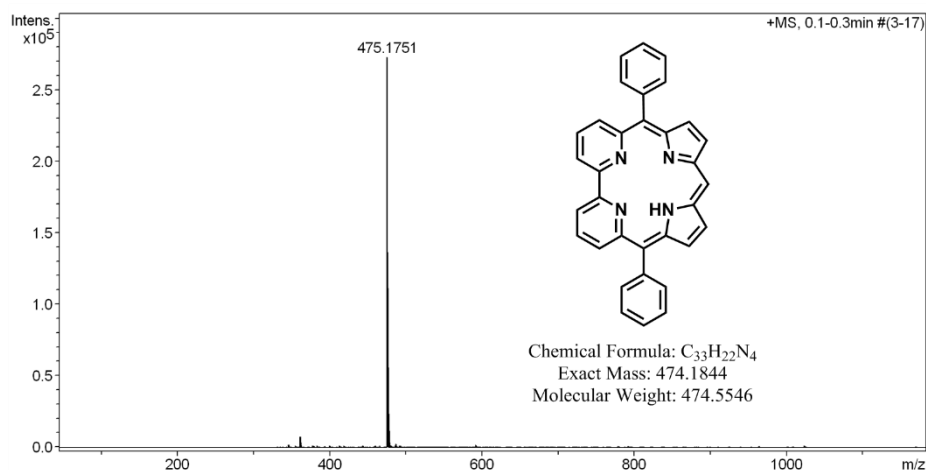


Figure 5A.1: ESI-MS spectrum of **6**.

5A.3.2.2 NMR Analysis

The 1H NMR spectrum of **6** and **7** were recorded in $CDCl_3$ at 298 K (Figure 5A.2). The *meso*-free CH proton is appeared as singlet at 6.21 ppm [H(11)]. The bipyridyl protons in **6** are displayed as two doublets at 8.16 [H(2,20)] and 7.36 [H(4,18)] ppm and a triplet at 7.86 [H(3,19)] ppm. The pyrrolic β -CH protons are resonated as multiplet centered at 6.91 ppm [H(8,14),H(9,13)]. The pyrrolic NH [H(24)] is observed as a broad singlet at 11.47 ppm (Figure 5A.2), which was further confirmed by $CDCl_3/D_2O$ exchange experiment. In the protonated complex **7**, the *meso*-free CH proton is slightly deshielded and appeared at 7.09 ppm. The NH (N3-H3) and protonated NH (N2-H2) is observed as a broad singlet at 10.77 ppm. The aromatic phenyl protons of counter anion (*p*-TSA) is displayed between 7.38 and 7.85 ppm and

the methyl protons are at 2.29 ppm (Figure 5A.2). The bipyridyl and pyrrolic β -CH protons are downfield shifted and appeared between 7.38 to 9.40 ppm. All these signals were further confirmed by 2D homonuclear correlation spectroscopy. Overall, the peak positions of **6** and **7** are consistent with nonaromatic character.²¹

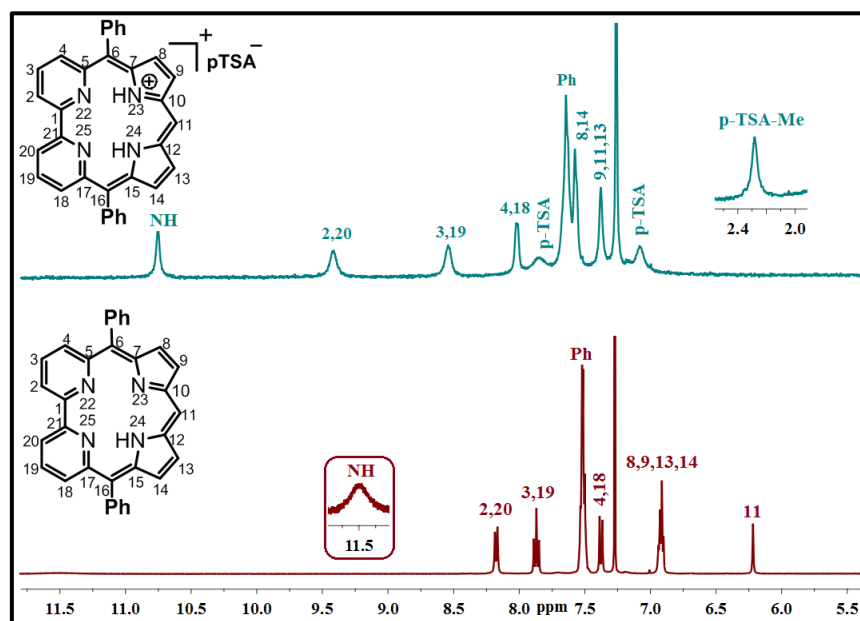


Figure 5A.2: ^1H -NMR spectrum of **6** and **7** in CDCl_3 .

5A.3.2.3 Single crystal X-ray structure and analysis of **6** and **7**

The final confirmation of **6** and **7** has come from the single crystal X-ray analysis (Figure 5A.3, Table 5A.3). In compound **6**, the molecule is located on a crystallographic two-fold axis (Figure 5A.3a). The amino hydrogen atom could not be assigned unequivocally either of N2s, however structure analysis suggests that the hydrogen atom is in 50% probability occupation on each nitrogen atoms. The pyridine rings in the bipyridine unit are deviated by $21.64(13)^\circ$ from the mean plane containing 15 inner core atoms (Figure 5A.3b). Whereas the pyrrole units are less tilted, as compared to bipyridyl units, with the maximum deviation of $11.40(18)^\circ$. In addition, the saddling dihedral angles ($\chi_1 - \chi_4$) are between $5.21(19)^\circ$ and $34.21(92)^\circ$ (Table 5.1A), where the later value is higher as compared to corrole derivatives.^{21,22} On the

other hand, the protonated complex (**7**) is stabilized by intermolecular hydrogen bonding interaction with the anion (bond distance of C9-O3 is 3.129(1) Å, Figure 5A.3c). The NH (N3-H3) as well as the protonated NH (N2-H2) is in intramolecular hydrogen bonding interaction with bipyridyl N (N1 and N4) (bond distance of N1-N2 and N3-N4 is 2.693(1) Å and 2.663(1) Å, Figure 5A.3c). The saddling dihedral angles ($\chi_1 - \chi_4$) of **7** are 0.90(27)° and 19.91(15)° (Table 5.1A), which are lower as compared to **6**, reveals more planar structure.

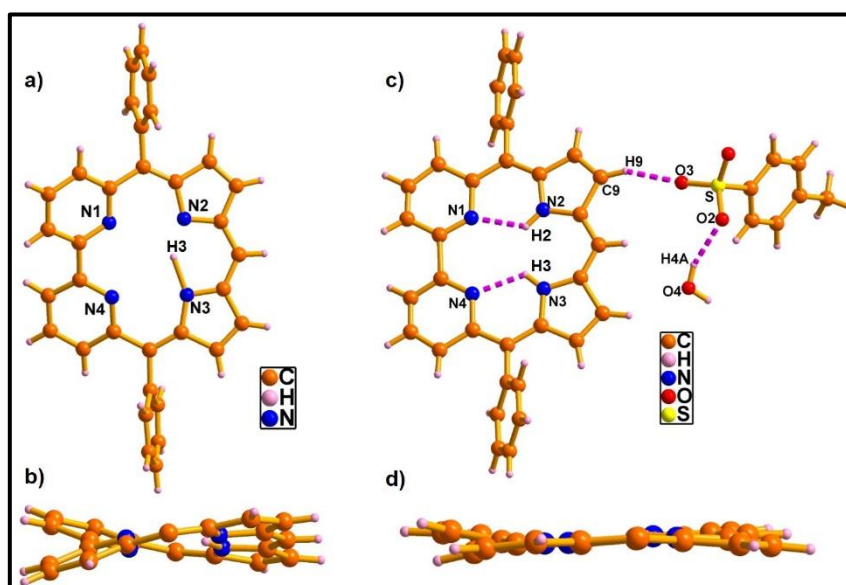
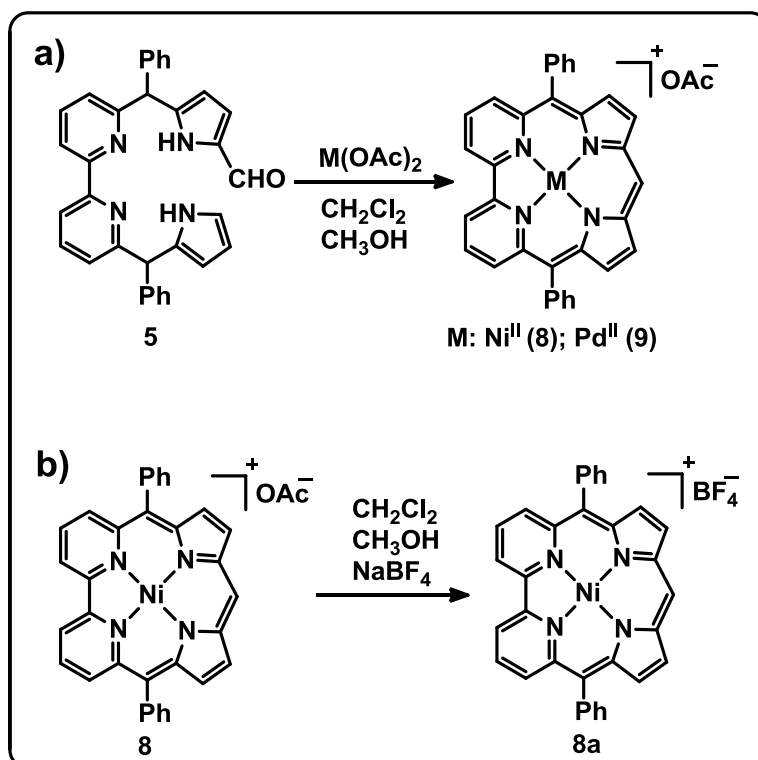


Figure 5A.3: The single crystal X-ray structures of **6** (a & b) and **7** (c & d). The *meso*-aryl groups in (b) & (d) and the counter anion in (d) are omitted for clarity.

5A.3.3 Coordination Studies

As the initial attempts with FeCl₃ was successful for macrocyclic formation, we tried with other metal salts such as Ni^{II} and Pd^{II} in the form of acetate with **5**. Instead of the free ligand (**6**) as observed in the case of FeCl₃, surprisingly, a quantitative formation of respective metal complex was obtained (Scheme 5A.3a). The green color fraction was eluted in the chromatographic separation by CH₂Cl₂ and CH₃OH mixture was identified as **8** and **9** in quantitative yield. Here, the metal salt acts as a metal

template. In order to crystallise the complex **8**, we followed the anion exchange method. The acetate ion in **8** is replaced BF_4 ion upon washing with NaBF_4 to afford the complex **8a** (Scheme 5A.3b). The complexes **8**, **8a** and **9** were characterized by NMR, mass, electronic absorption and emission spectral studies and the structure of **8a** and **9** were confirmed by single crystal X-ray analysis.



Scheme 5A.3: Synthesis of **8**, **8a** and **9**.

5A.3.3.1 Spectral characterization

5A.3.3.1.1 Mass spectrometric analysis

The ESI mass spectrometric analysis of **8** and **9** showed the molecular ion signal at m/z 531.0909 [$\text{M}-\text{BF}_4$] and 579.0691 [$\text{M}-\text{OAc}$] and confirmed the exact composition (Figure 5A.4, 5A.5).

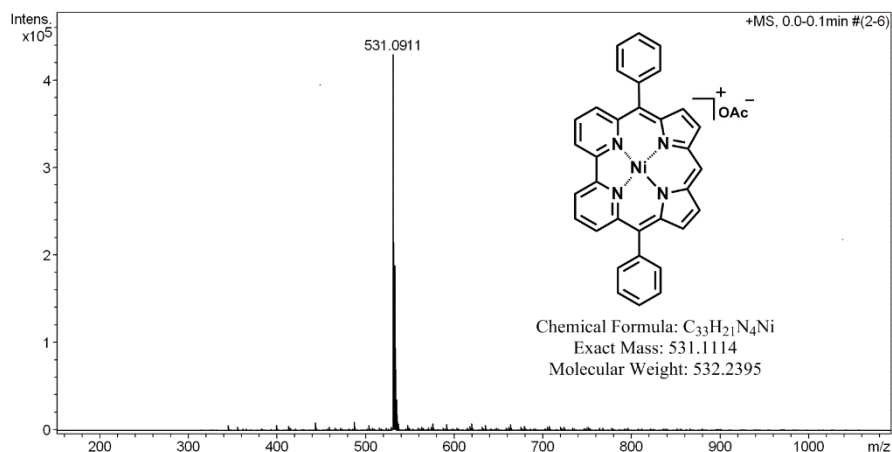


Figure 5A.4: ESI-MS spectrum of **8**.

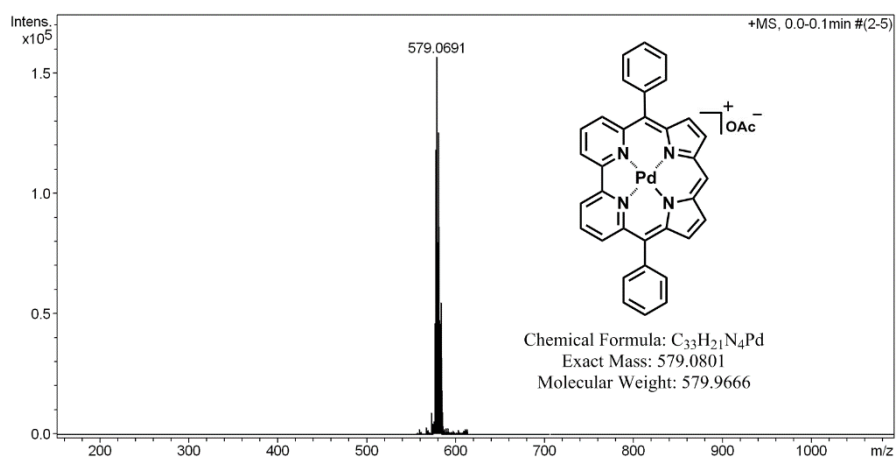


Figure 5A.5: ESI-MS spectrum of **9**.

5A.3.3.1.2 NMR Analysis

The ¹H NMR spectra of **8** and **9** were recorded in CDCl₃ at 298 K (Figure 5A.6). The disappearance of formyl-CH, pyrrolic α-CH and NH signals from **5** and appearance of new *meso*-CH [H(11)] at 7.81 ppm confirm the formation of metal complex **8**. The bipyridyl protons in **8** displayed two doublets at 10.45 [H(2,20)] and 8.52 [H(4,18)] ppm and a triplet at 8.93 [H(3,19)] ppm. The pyrrolic β-CH protons are resonated at 7.82 and 7.61 ppm [H(8,14),H(9,13)]. The acetate methyl protons are observed at 1.25 ppm, respectively. The anion exchange product **8a** showed similar spectral patterns as observed in **8**. The presence of counter anion (BF₄) to stabilize Ni(II) complex is

confirmed by the ^{19}F & ^{11}B NMR. Similar trend was observed in the ^1H NMR spectral analysis of **9**, where the *meso*-CH signal and acetate methyl units are appeared singlet at 7.86 ppm and 1.25 ppm. (Figure 5A.6). Overall, the spectral pattern resembles the typical nonaromatic character.²¹

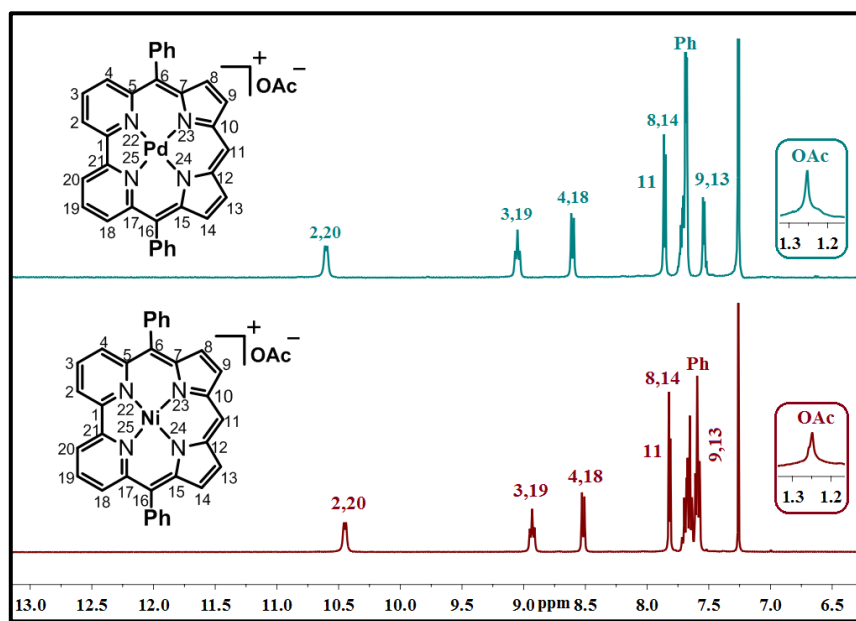


Figure 5.6: ^1H -NMR spectrum of **8** and **9** in CDCl_3 .

5A.3.3.1.3 Single crystal X-ray analysis

The complex **8a** and **9** was further confirmed by single-crystal X-ray analysis (Figure 5A.7, Table 5A.3). In complex **8a**, the BF_4 anion is placed above the mean plane and the distance between the Ni^{II} and BF_4 anion is 4.307(32) Å and act as a counter anion to satisfy the valency of Ni^{II} ion. The geometry around the metal center is square planar (Table 5A.2). The average bond length between the Ni^{II} and N-units is 1.904 Å (Figure 5A.8c, Table 5A.2), which is slightly longer than that of Ni^{II} -corroles (1.846 Å) and Ni^{II} -pyricorroles (1.873 Å) and shorter than that of Ni^{II} -porphyrins (1.958 Å).^{17,22,23} The saddling dihedral angle values are from 0.365 to 3.338 Å, which are less titled as compared to other corrole complexes known in the literature (Table 5A.1).^{22,23}

The crystal analysis reveals that one of the *meso*-phenyl hydrogens [C33- H33] is in intermolecular hydrogen bonding interaction with BF₄ ion (bond distance of C33-F3 is 3.712(4) Å Figure 5A.7b). On the other hand, in complex **9**, the presence of acetate ion satisfies the additional valency of Pd^{II} ion. The methyl unit [C35-H35c] in the acetate ion is in intermolecular hydrogen bonding interaction with the pyridine N1(π) (the bond distance of C35-N1(π) is 3.273(9) Å (Figure 5A.7d). The bond length between the Pd1 and pyridine N1 and N4 units are 1.996 and 1.992 Å, which are moderately longer than the pyrrole N2 and N3 distances, where the respective values are 1.968 and 1.961 Å (Figure 5A.8d, Table 5A.2). These values are slightly shorter than Pd-N [2.009 Å] porphyrin complex.¹⁸ The saddle dihedral angle values are between 0.182(7)° and 12.143(1)° (Table 5A.1). As reflected from the spectral studies, the crystal analysis of **4a** and **5** further confirms the nonaromatic character (Figure 5A.8).²¹

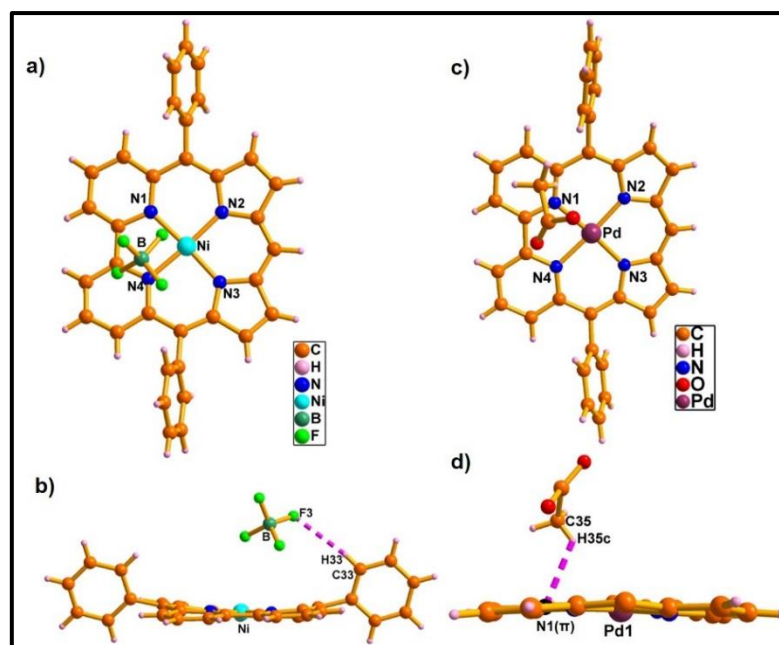
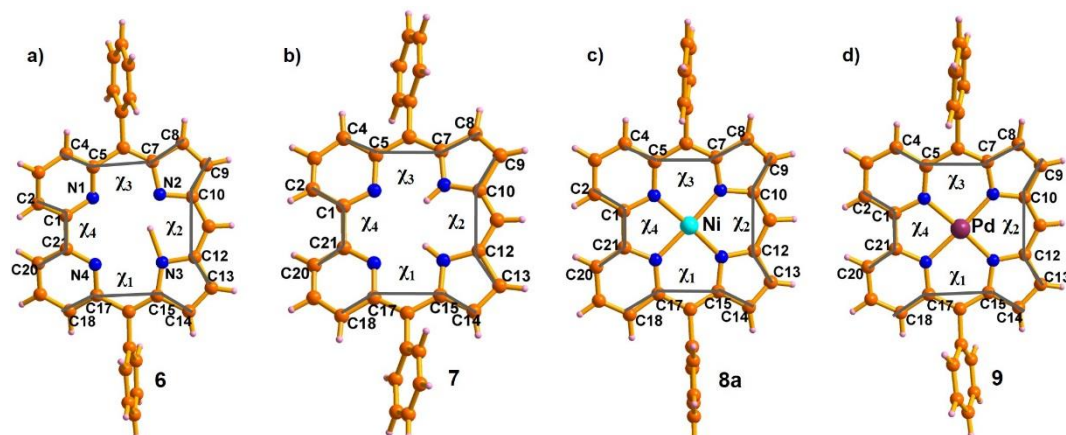


Figure 5A.7: The single crystal X-ray structures of **8a** (a & b) and **9** (c & d). The *meso*-aryl groups in (d) are omitted for clarity.

Table 5A.1: Saddling dihedral angle (χ) value in **6**, **7**, **8a** and **9** ($^\circ$)

χ	Saddling dihedral angle	6 ($^\circ$)	7 ($^\circ$)	8a ($^\circ$)	9 ($^\circ$)
χ_1	C18-C17-C15-C14	20.924(15)	15.542(22)	9.478(8)	7.218(12)
χ_2	C13-C12-C10-C9	5.205(2)	0.900(3)	0.026(9)	2.111(14)
χ_3	C8-C7-C5-C4	20.924(15)	10.454(22)	1.120(8)	12.143(1)
χ_4	C2-C1-C21-C20	34.214(9)	19.910(15)	2.732(5)	0.182(7)

Table 5A.2: Bond angles around the metal ion ($^\circ$) in **8a** and **9**

	8a ($^\circ$)		9 ($^\circ$)
N1-Ni-N2	91.762(10)	N1-Pd-N2	92.590(14)
N2-Ni-N3	91.707(11)	N2-Pd-N3	91.367(15)
N3-Ni-N4	91.927(11)	N3-Pd-N4	92.137(14)
N4-Ni-N1	84.627(10)	N4-Pd-N1	83.906(14)
Average	90.00	Average	90.00

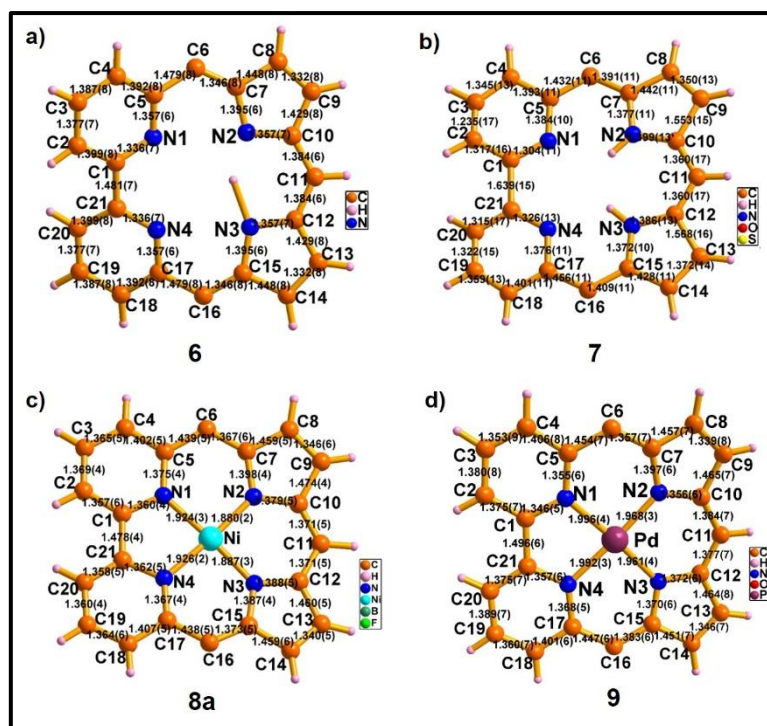


Figure 5A.8: Bond lengths (Å) in **6** (a), **7** (b), **8a** (c) and **9** (d). The anionic ligands in b), c) and d) and *meso*-aryl units in (a-d) are omitted for clarity.

5A.3.3.1.4 Electronic absorption and Emission analyses

The electronic absorption spectra of **6** – **9** were recorded in CH₂Cl₂ (Figure 5A.9 & 5A.10). The absorption spectral analysis of **6** shows the intense band at 364 nm and weak bands at 596, 642 nm. In case of protonated complex **7** intense band is blue shifted, however the weak bands are red shifted observed at 331, 605 and 655 nm respectively (Figure 5A.9). Upon metal ion insertion, the intense band in **8** remains unaltered as that of free base, however the Q-type bands are slightly blue shifted. On the other hand in complex **9**, the split intense band is observed at 360 & 378 nm and the prominent higher wavelength absorption bands appeared at 584 nm and 634 nm with the molar absorption coefficient of these bands are 10⁵ (Figure 5A.10). Overall the spectral pattern resembles the non-aromatic character as observed in bipyricorrole and biphenylcorrole and its complexes. In addition, the free base **6** and palladium complex

9 exhibit emission property (Figure 5A.11). The free base **6** emits at 687 nm with quantum yield (Φ_F) of 0.04 whereas Pd^{II} complex (**9**) shows emission band at 654 nm which is 33 nm blue shifted compared to **6** with the fluorescence quantum yield (Φ_F) of 0.09.

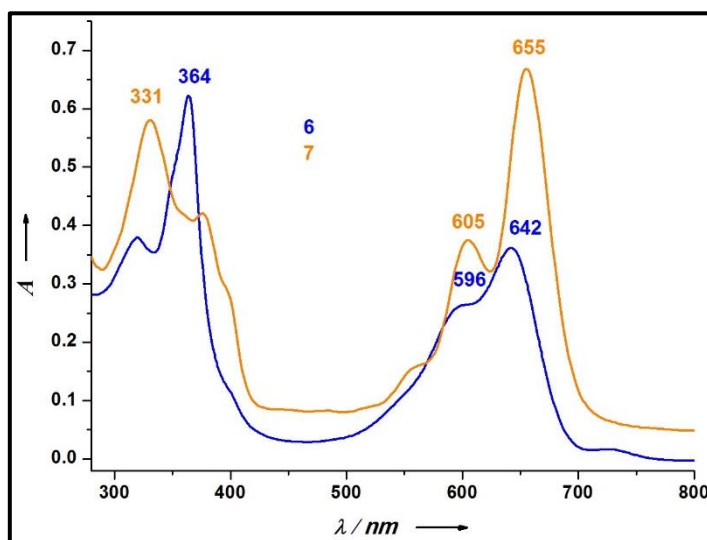


Figure 5A.9: The electronic absorption spectrum of **6** and **7** in CH₂Cl₂.

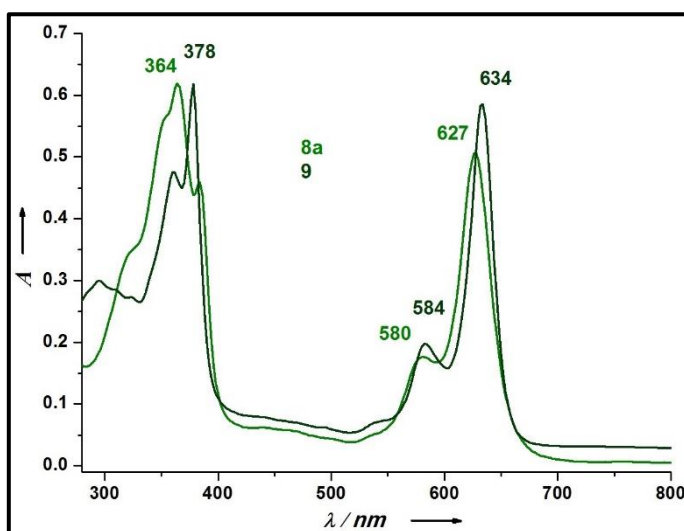


Figure 5A.10: The electronic absorption spectrum of **8a** and **9** in CH₂Cl₂.

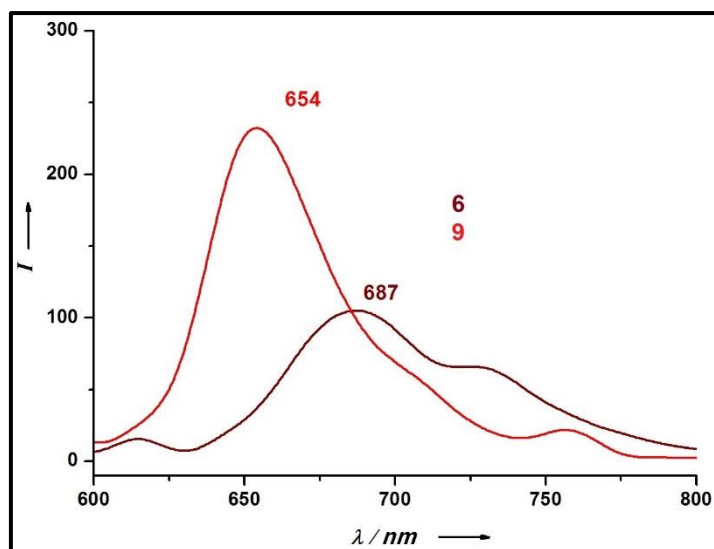
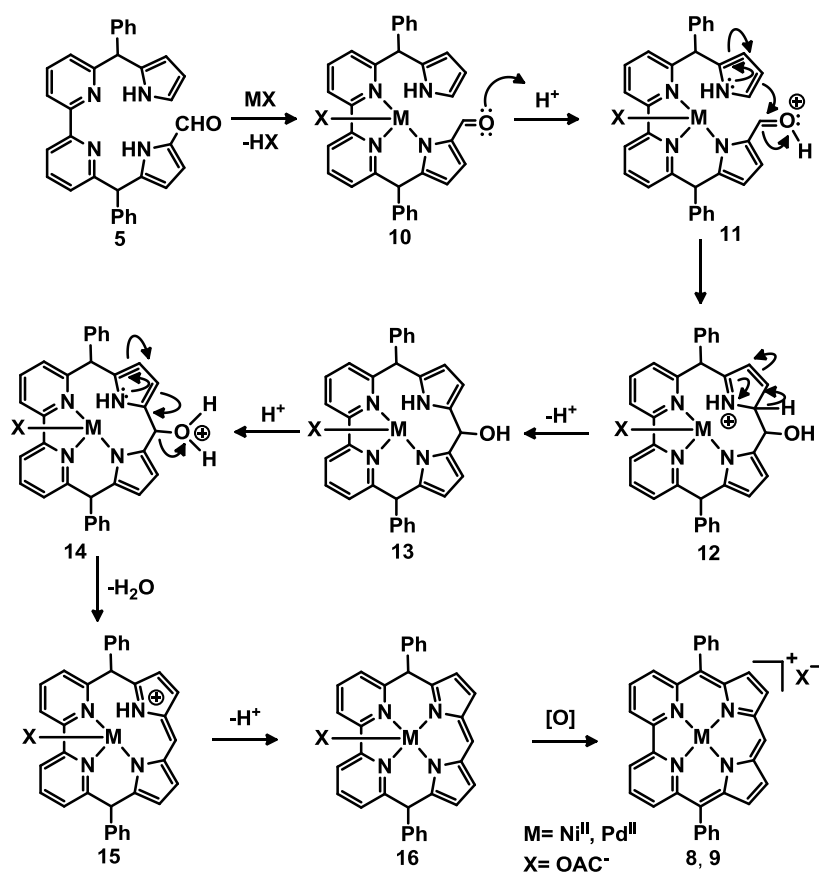


Figure 5A.11: The emission spectrum of **6** and **9** in CH_2Cl_2 .

5A.4 Possible mechanism



Scheme 5A.4: Plausible mechanism for the formation of **8** and **9**.

Based on the formation of complexes (**8** & **9**), a possible mechanism for the metal templated synthesis is shown in Scheme 5A.4. The first step involves coordination of metal to the ligand followed by releasing a molecule of acetic acid. This complexation facilitates the intramolecular electrophilic heteroaromatic substitution reaction of aldehyde (**10**) to afford complex **13** (via **11** & **12**). Further, the complex **13** is readily protonated followed by dehydration yielding the calixphyrin derivative **16** (via **14** & **15**), which on open air oxidation produces the desired complexes **8** and **9**.

5A.5 Conclusion

We have demonstrated new synthetic approach for the synthesis of novel corrole homologues. The presence of FeCl₃ as a Lewis acid and oxidising agent as a result the freebase was obtained, in case of *p*-TSA as an acid the protonated complex was achieved. Whereas the Ni^{II} and Pd^{II} *meso*-free bipyricorrole complexes were synthesized by metal-templated *condensation* reaction, which is an alternative synthetic methodology for i) the routine acid-catalyzed condensation reaction followed by oxidation and metal ion insertion and ii) metal-templated *coupling / oxidative* macrocyclization strategy. The core effectively stabilizes the heavier metal ion within the coordination site, where the additional valency of the metal ion is neutralized by counter anions. To the best of our knowledge, the nonaromatic Pd^{II} *meso*-free corrole homologue complex is characterized by spectral studies and further confirmed by structural analysis, which are hitherto unknown in corrole chemistry. The *meso*-free carbon can be further utilized effectively for the synthesis of covalently linked corrole dimers and hybrid arrays, where some of these results are highlighted as second part of this chapter (Chapter 5B).

5A.6 Experimental Section

5A.6.1 General Information

The reagents and materials for the synthesis were used as obtained from Sigma - Aldrich chemical suppliers. All solvents were purified and dried by standard methods prior to use. The NMR solvents were used as received and the spectra were recorded with Bruker 400 MHz spectrometer with TMS as internal standard. The ESI mass spectra were recorded with Bruker, micro-TOF-QII mass spectrometer. The Electronic absorption spectra and steady state fluorescence spectra were recorded with Perkin Elmer–Lambda 750 UV-Visible spectrophotometer and Perkin Elmer LS55 Fluorescence spectrometer respectively. X-ray quality crystals for the complexes were grown by the slow diffusion of *n*-hexane over CH₂Cl₂ solution of the complexes. Single-crystal X-ray diffraction data of **6**, **7**, **8a** and **9** were collected on a Bruker KAPPA APEX-II, four angle rotation system and Mo-K α radiation (0.71073 Å). The crystals have been deposited in the Cambridge Crystallographic Data Centre for **6**, **7**, **8a** and **9** are **1473609**, **1501403**, **1501404** and **1483381** respectively. Fluorescence quantum yields were determined by using *meso*-tetraphenylporphyrin (TPPH₂) in toluene ($\Phi_f = 0.11$) as a reference.

5A.6.2 Synthesis and spectral characterization

5A.6.2.1 Synthesis of 5: Freshly prepared POCl₃ (0.05 mL, 0.53 mmol), DMF (3 ml) complex solution was added into the solution of bipyridyldipyrromethane (200 mg, 0.41 mmol) in 100 ml ClCH₂CH₂Cl under N₂ atmosphere at 0 °C. The reaction mixture was kept at same temperature for 10 min and then allowed to attain RT. After 8h the reaction was quenched with Na₂CO₃ and extracted with EtOAc, dried over Na₂SO₄ and concentrated by rotary evaporator. The crude compound was purified by column chromatography using silica gel (silica 100-200 mesh) in 25% EtOAc/*n*-hexane to afford **5** in 45% yield.

¹H NMR (400 MHz, CDCl₃, 298K): δ = 10.72 (d, *J* = 12.0 Hz, 1H), 9.45 (d, *J* = 3.3 Hz, 1H), 9.05 (brs, 1H), 8.30 (d, *J* = 8.0 Hz, 1H), 8.24 (d, *J* = 7.9 Hz, 1H), 7.86 (td, *J* = 7.8, 2.2 Hz, 1H), 7.77 (t, *J* = 7.8 Hz, 1H), 7.31 – 7.26 (m, 12H), 6.90 (s, 1H), 6.75 (d, *J* = 1.5 Hz, 1H), 6.17 (dd, *J* = 4.6, 2.6 Hz, 2H), 6.02 (s, 1H), 5.65 (d, *J* = 1.4 Hz, 1H), 5.60 (s, 1H).

¹³C NMR (100 MHz, CDCl₃): δ = 178.86, 161.79, 159.91, 156.27, 156.24, 155.44, 155.41, 142.99, 141.78, 141.38, 138.34, 138.31, 132.62, 132.34, 129.01, 128.71, 128.60, 128.51, 127.40, 126.77, 124.05, 123.78, 121.49, 119.89, 119.85, 119.47, 117.52, 111.03, 108.24, 107.60.

m.p: 119-120 °C.

ESI-MS: *m/z* calculated for C₃₃H₂₆N₄O = 494.2107; found = 495.1731(M+1).

5A.6.2.2 Synthesis of 6: A solution of FeCl₃ (130 mg, 0.80 mmol) in 5 ml CH₃OH was added into the solution of **5** (20 mg, 0.04 mmol) in CH₂Cl₂ (100 ml) under open air atmosphere and allowed to stir for 3 h. The completion of the reaction was monitored by TLC and extracted with CH₂Cl₂, dried over Na₂SO₄ and concentrated by rotary evaporator. Residue was purified by silica gel (silica 100-200 mesh) in 1%

CH₃OH/CH₂Cl₂ and identified as **6**. The compound was further recrystallized from CH₂Cl₂/*n*-hexane to afford blue crystalline compound **6** in 40% yield.

¹H NMR (400 MHz, CDCl₃, 298K): δ = 11.47 (s, 1H), 8.16 (d, *J* = 7.7 Hz, 2H), 7.86 (t, *J* = 7.9 Hz, 2H), 7.52 – 7.48 (m, 10H), 7.36 (d, *J* = 8.0 Hz, 2H), 6.91 (m, 4H), 6.21 (s, 1H).

¹³C NMR (100 MHz, CDCl₃): δ = 157.40, 154.81, 140.46, 135.98, 132.43, 130.37, 128.18, 127.95, 127.20, 117.99, 97.17.

m.p: 300 °C (decomposition).

ESI-MS: *m/z* calculated for C₃₃H₂₂N₄ = 474.1844; found = 475.1751(M+1).

UV-Vis (CH₂Cl₂): λ_{\max} (nm) (ϵ [M⁻¹cm⁻¹]) = 320 (31,293), 364 (50,903), 596 (21,346), 642 (29,557).

Quantum yield (Φ_f) = 0.04.

5A.6.2.3 Synthesis of 7: A solution of *p*-TSA (14 mg, 0.08 mmol) in 5 ml CH₃OH was added into the solution of **5** (20 mg, 0.04 mmol) in CH₂Cl₂ (100 ml) under open air atmosphere and allowed to stir for 15 min. Then FeCl₃ (64 mg, 0.40 mmol) was added in to the reaction crude. The completion of the reaction was monitored by TLC and extracted with CH₂Cl₂, dried over Na₂SO₄ and concentrated by rotary evaporator. Residue was purified by silica gel (silica 100-200 mesh) in 1% CH₃OH/CH₂Cl₂ and identified as **7**. The compound was further recrystallized from CH₂Cl₂/*n*-hexane to afford blue crystalline compound **7** in 60% yield.

¹H NMR (400 MHz, CDCl₃, 298K): δ = 10.77 (s, 2H), 9.40 (s, 2H), 8.54 (s, 2H), 8.02 (s, 2H), 7.85 (s, 2H), 7.64-7.58 (m, 10H), 7.38 (s, 4H), 7.09 (s, 1H), 2.29 (s, 3H).

m.p: 300 °C (decomposition).

UV-Vis (CH₂Cl₂): λ_{\max} (nm) (ϵ [M⁻¹cm⁻¹]) = 331 (45,025), 376 (30,672), 605 (30,281), 655 (50,473).

5A.6.2.4 Synthesis of 8: A solution of Ni(OAc)₂ (70 mg, 0.4 mmol) in 5 ml CH₃OH was added into the solution of **5** (20 mg, 0.04 mmol) in CH₂Cl₂ (100 ml) under open air atmosphere and allowed to stir for 3 h. The completion of the reaction was monitored by TLC. The residue was purified by silica gel (silica 100-200 mesh) in 2% CH₃OH/CH₂Cl₂ and identified as **8**. The complex **8** was further recrystallized from CH₂Cl₂/*n*-hexane to afford green crystalline solid in 90% yield.

¹H NMR (400 MHz, CDCl₃, 298K): δ = 10.45 (d, *J* = 7.0 Hz, 2H), 8.93 (t, *J* = 7.7 Hz, 2H), 8.52 (d, *J* = 8.0 Hz, 2H), 7.82 (d, *J* = 5.0 Hz, 3H), 7.70 – 7.63 (m, 6H), 7.61 – 7.57 (m, 6H), 1.25 (s, 3H).

¹³C NMR (100 MHz, CDCl₃): δ = 157.10, 152.91, 148.39, 146.55, 138.32, 138.23, 137.32, 134.34, 132.48, 131.43, 129.42, 128.58, 125.47, 124.67, 100.65.

m.p: 300 °C (decomposition).

ESI-MS: *m/z* calculated for C₃₃H₂₁N₄Ni (without axial ligand) = 531.1114; found = 531.0909.

UV-Vis (CH₂Cl₂): λ_{max}(nm) (ε[M⁻¹cm⁻¹]) = 364 (45,487), 384 (33,873), 580 (12,518), 627 (36,819).

5A.6.2.5 Synthesis of 8a: In order to crystallize the molecule we followed the anion exchange process. The product was extracted with sodium tetrafluoroborate to exchange the acetate ion with BF₄ ion of the complex **8**. The complex was purified with silica gel (silica 100-200 mesh) in 2% CH₃OH/CH₂Cl₂ and identified as **8a**. The complex **8a** was further recrystallized from CH₂Cl₂/*n*-hexane to afford green crystalline solid.

¹H NMR (400 MHz, CDCl₃, 298K): δ = 9.87 (d, *J* = 7.5 Hz, 2H), 8.88 (t, *J* = 7.8 Hz, 2H), 8.56 (d, *J* = 8.1 Hz, 2H), 7.82 (d, *J* = 4.7 Hz, 3H), 7.71 – 7.61 (m, 12H).

¹⁹F NMR (376 MHz, CDCl₃): δ = -153.73.

^{11}B NMR (128 MHz, CDCl_3): $\delta = -0.66$.

ESI-MS: m/z calculated for $\text{C}_{33}\text{H}_{21}\text{N}_4\text{Ni}$ (without axial ligand) = 531.1114; found = 531.0911.

5A.6.2.6 Synthesis of 9: A solution of $\text{Pd}(\text{OAc})_2$ (45 mg, 0.2 mmol) in 5 ml CH_3OH was added into the solution of **5** (20 mg, 0.04 mmol) in CH_2Cl_2 (100 ml) under open air atmosphere and allowed to stir for 3 h. The completion of the reaction was monitored by TLC. The residue was purified by silica gel (silica 100-200 mesh) in 2% $\text{CH}_3\text{OH}/\text{CH}_2\text{Cl}_2$ and identified as **9**. The complex **9** was further recrystallized from $\text{CH}_2\text{Cl}_2/n$ -hexane to afford green crystalline solid in 90% yield.

^1H NMR (400 MHz, CDCl_3 , 298K): $\delta = 10.60$ (d, $J = 6.5$ Hz, 2H), 9.05 (t, $J = 7.8$ Hz, 2H), 8.60 (d, $J = 8.1$ Hz, 2H), 7.86 (d, $J = 5.3$ Hz, 3H), 7.73 – 7.68 (m, 10H), 7.53 (d, $J = 5.1$ Hz, 2H), 1.25 (s, 3H).

^{13}C NMR (100 MHz, CDCl_3): $\delta = 154.14, 153.90, 148.68, 146.86, 146.33, 144.99, 142.64, 138.47, 138.01, 137.81, 137.36, 134.19, 133.42, 133.01, 132.66, 131.56, 129.46, 128.56, 127.32, 127.20, 115.74, 100.36$.

m.p: 300 °C (decomposition).

ESI-MS: m/z calculated for $\text{C}_{33}\text{H}_{21}\text{N}_4\text{Pd}$ (without axial ligand) = 579.0801; found = 579.0691.

UV-Vis (CH_2Cl_2): $\lambda_{\text{max}}(\text{nm})$ ($\epsilon[\text{M}^{-1}\text{cm}^{-1}]$) = 360 (37,242), 378 (49,128), 584 (15,848) 634 (45,959).

Quantum yield (Φ_f) = 0.09.

Table 5.3: Crystal data for **6**, **7**, **8a** and **9**

Crystal parameters	6	7	8a	9
Formula	C ₃₃ H ₂₂ N ₄	C ₄₀ H ₃₂ N ₄ O ₄ S	C ₃₃ H ₂₁ BF ₄ N ₄ Ni	C ₃₅ H ₂₆ N ₄ O ₃ Pd
<i>M</i> /g mol ⁻¹	474.55	664.75	619.06	657.00
<i>T</i> /K	100	100	100	100
Crystal dimensions/mm ³	0.09 x 0.08 x 0.045	0.1 x 0.08 x 0.045	0.1 x 0.07 x 0.04	0.15 x 0.11 x 0.08
Crystal system	Monoclinic	Orthorhombic	Monoclinic	Monoclinic
Space group	<i>C2/c</i>	<i>P 21 21 2</i>	<i>C2/c</i>	<i>P2(1)/n</i>
<i>a</i> /Å	18.335 (3)	19.4057 (8)	19.271 (5)	8.98110(10)
<i>b</i> /Å	14.464 (3)	25.4381(11)	29.927 (5)	11.11670(10)
<i>c</i> /Å	10.1803 (16)	6.5563(3)	11.004 (5)	27.2624(3)
α /°	90	90	90	90
β /°	121.050 (15)	90	122.153 (5)	99.0560(10)
γ /°	90	90	90	90
<i>V</i> /Å ³	2313.1 (6)	3236.5(2)	5373 (3)	2687.96(5)
<i>Z</i>	4	4	8	4
ρ_{calcd} /mg m ⁻³	1.363	1.364	1.531	1.623
μ /mm ⁻¹	0.082	0.151	0.782	0.737
<i>F</i> (000)	992.0	1392	2528	1336
Reflns. collected	13766	34733	45387	44403
Indep.reflns. [<i>R</i> (int)]	2190 [0.0714]	5939 [0.0801]	7525 [0.1007]	7234 [0.0525]
Max/min transmission	0.745 and 0.661	0.7452 and 0.6479	0.7459 and 0.6357	0.7458 and 0.6887
Data/restraints /parameters	2190 / 0 / 171	5939 / 11 / 428	7525 / 0 / 392	7234 / 27 / 396
GOF on <i>F</i> ²	1.134	1.051	1.027	1.027
Final <i>R</i> indices [<i>I</i> > 2σ(<i>I</i>)]	<i>R</i> 1 = 0.1244, <i>wR</i> 2 = 0.2356	<i>R</i> 1 = 0.0887, <i>wR</i> 2 = 0.2330	<i>R</i> 1 = 0.0532, <i>wR</i> 2 = 0.1100	<i>R</i> 1 = 0.0590, <i>wR</i> 2 = 0.1735
<i>R</i> indices (all data)	<i>R</i> 1 = 0.1519, <i>wR</i> 2 = 0.2471	<i>R</i> 1 = 0.1224, <i>wR</i> 2 = 0.2600	<i>R</i> 1 = 0.1036, <i>wR</i> 2 = 0.1296	<i>R</i> 1 = 0.0768, <i>wR</i> 2 = 0.1880
Largest diff peak and hole [e Å ⁻³]	0.316 and -0.463	1.360 and -0.602	1.190 and -0.881	2.037 and -1.234

5A.7 Reference

- Gross, Z.; Galili, N.; Saltsman, I. *Angew. Chem. Int. Ed.* **1999**, *38*, 1427-1429.
- Paolesse, R.; Mini, S.; Sagone, F.; Boschi, T.; Jaquinod, L.; J. Nurco, D.; M. Smith, K. *Chem. Commun.* **1999**, 1307-1308.
- Gryko, D. T.; Jadach, K. *J. Org. Chem.* **2001**, *66*, 4267-4275.

-
4. Flamigni, L.; Gryko, D. T. *Chem. Soc. Rev.* **2009**, *38*, 1635-1646.
 5. Liu, H.-Y.; Mahmood, M. H. R.; Qiu, S.-X.; Chang, C. K. *Coord. Chem. Rev.* **2013**, *257*, 1306-1333.
 6. Liang, X.; Mack, J.; Zheng, L.-M.; Shen, Z.; Kobayashi, N. *Inorg. Chem.* **2014**, *53*, 2797-2802.
 7. Koszarna, B.; Gryko, D. T. *Chem. Commun.* **2007**, 2994-2996.
 8. Sankar, J.; Rath, H.; Prabhuraja, V.; Gokulnath, S.; Chandrashekar, T. K.; Purohit, C. S.; Verma, S. *Chem. Eur. J.* **2007**, *13*, 105-114.
 9. Ooi, S.; Yoneda, T.; Tanaka, T.; Osuka, A. *Chem. Eur. J.* **2015**, *21*, 7772-7779.
 10. Bröring, M.; Hell, C. *Chem. Commun.* **2001**, 2336-2337.
 11. Bröring, M.; Brégier, F.; Cónsul Tejero, E.; Hell, C.; Holthausen, M. C. *Angew. Chem. Int. Ed.* **2007**, *46*, 445-448.
 12. Sakow, D.; Böker, B.; Brandhorst, K.; Burghaus, O.; Bröring, M. *Angew. Chem. Int. Ed.* **2013**, *52*, 4912-4915.
 13. Horie, M.; Hayashi, Y.; Yamaguchi, S.; Shinokubo, H. *Chem. Eur. J.* **2012**, *18*, 5919-5923.
 14. Kamiya, H.; Kondo, T.; Sakida, T.; Yamaguchi, S.; Shinokubo, H. *Chem. Eur. J.* **2012**, *18*, 16129-16135.
 15. Bröring, M.; Köhler, S.; Kleeberg, C. *Angew. Chem. Int. Ed.* **2008**, *47*, 5658-5660.
 16. Ito, T.; Hayashi, Y.; Shimizu, S.; Shin, J.-Y.; Kobayashi, N.; Shinokubo, H. *Angew. Chem. Int. Ed.* **2012**, *51*, 8542-8545.
 17. Neya, S.; Suzuki, M.; Matsugae, T.; Hoshino, T. *Inorg. Chem.* **2012**, *51*, 3891-3895.
-

-
18. Fleischer, E. B.; Miller, C. K.; Webb, L. E. *J. Am. Chem. Soc.* **1964**, *86*, 2342-2347.
 19. Setsune, J.-i. *J. Porphyrins Phthalocyanines* **2004**, *8*, 93-102.
 20. Grigg, R.; Johnson, A.; Shelton, G. *J. Chem. Soc. C* **1971**, 2287-2294.
 21. Adinarayana, B.; Thomas, A. P.; Yadav, P.; Kumar, A.; Srinivasan, A. *Angew. Chem. Int. Ed.* **2016**, *55*, 969-973.
 22. Thomas, K. E.; Alemayehu, A. B.; Conradie, J.; Beavers, C. M.; Ghosh, A. *Acc. Chem. Res.* **2012**, *45*, 1203-1214.
 23. Will, S.; Lex, J.; Vogel, E.; Schmickler, H.; Gisselbrecht, J.-P.; Hauptmann, C.; Bernard, M.; Gorss, M. *Angew. Chem. Int. Ed.* **1997**, *36*, 357-361.

CHAPTER 5B

Meso-meso linked Corrole Homologues

5B.1	Introduction	157
5B.1.1	Multi-porphyrin arrays through spacer units	157
5B.1.2	Directly linked porphyrin arrays	158
5B.1.3	Corrole arrays	159
5B.2	Objective of our work	162
5B.3	Results and discussions	163
5B.3.1	Syntheses and reactivity studies	163
5B.3.2	Spectral Characterization of	164
5B.3.2.1	NMR Analysis of 20 , 21a and 22a	164
5B.3.2.2	Single crystal X-ray analysis of 20 , 21a and 22a	165
5B.3.2.3	Mass spectrometric analysis	167
5B.3.2.4	NMR Analysis of 23 and 24	167
5B.3.2.5	Single crystal X-ray analysis of 24	168
5B.3.2.6	Electronic absorption and Emission spectral analysis	171
5B.4	Conclusion	172
5B.5	Synthetic procedure and spectral characterization of 20-24	173
5B.6	References	176

5B.1 Introduction

Porphyrins are 18 π conjugated electronic circuits. In the past two decades considerable attention has been focused on extended π -conjugated porphyrinoids due to their potential applications in various fields such as semiconductor devices, molecular electronics, near-infra-red (NIR) dyes, non-linear optical materials (NLO) and photo sensitizers for photodynamic therapy (PDT).¹⁻⁶ There are three important ways to extend the conjugation in porphyrins which includes, i) by increasing more number of heterocyclic units or *meso*-carbon bridges^{7,8}, ii) introducing the fused rings in porphyrin skeleton⁴ and iii) coupling of porphyrin units by covalent linkages.^{5,9-11} Among these porphyrin derivatives, covalently linked porphyrin arrays continue to be unique platform for extension of conjugation and they offer a variety of desirable features such as chemical robustness, high stability, intense electronic absorption and emission bands, fine-tuning, and easy manipulation.^{5,10,11} These arrays are further classified depends on the linkers between the porphyrin units.

5B.1.1 Multi-porphyrin arrays through spacer units

The porphyrin arrays are connected by various spacer units some of the most promising and well-studied spacer units are ethene, ethyne, butadiyne, 1,3- and 1,4-phenylene units (**1**).⁵ In order to achieve these arrays several synthetic strategies have been developed. Earlier, the spacer units are used for synthesizing the linear multi-porphyrin oligomers. Later, the cyclic covalently linked porphyrin arrays are constructed by using mainly the template-directed synthesis and are contributed mostly by Osuka group.^{2,12} The basic idea to construct such kind of conjugated porphyrin arrays is to understand the electronic communication among the constituents and utilizing them as artificial photosynthetic antenna. In addition, these molecules are explored for various applications such as near infrared dyes, molecular wires and

non-linear optical materials.¹⁻⁵

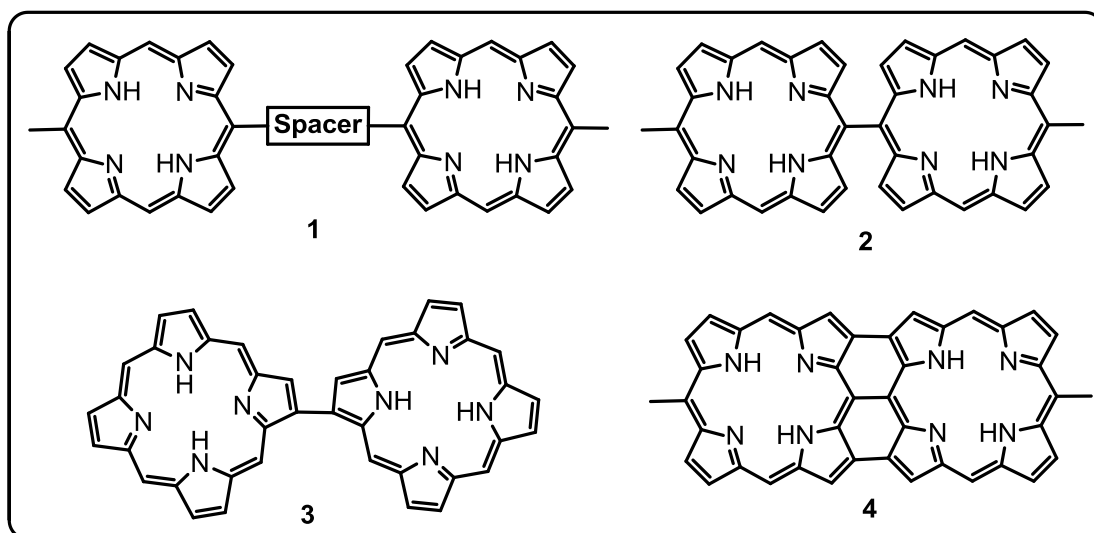


Figure 5B.1: Structures of porphyrin arrays.

5B.1.2 Directly linked porphyrin arrays

Recent progress in the synthesis of porphyrin arrays are mainly focused on the development of directly linked porphyrin arrays (**2**, **3**) (Figure 5B.1).⁹⁻¹¹ The synthesis is often relied on the development of a new oxidative coupling reagents or transition-metal catalysts. Among these, the silver(I)-prompted oxidative coupling reagents has opened up new area of synthetic porphyrin chemistry, where the *meso*-free positions are effectively converted into a variety of directly linked porphyrin arrays with varying electronic interactions and are explored mainly by osuka group.^{5,9-11} The main advantages of these *meso-meso* linked porphyrin arrays (**2**) are found in molecular photonic wires which are capable of transmitting excitation energy over long distance. It can also act as artificial light-harvesting antenna.^{13,14} The properties of these arrays are mainly due to the orthogonal conformation of the array, which tends to minimize the electronic interactions between the neighbouring porphyrins.

Further, osuka and co-workers utilized these single *meso-meso* linked porphyrin arrays by an effective oxidative fusion–dimerization reaction. Initially these reactions were performed with tris(4-bromophenyl)aminium hexachloroantimonate (BAHA). However, later these reactions were modified by using stronger conditions such as a combination of DDQ and Sc(OTf)₃. This method is proved to be quite effective and superior to the former because of the absence of serious halogenation side products. This allows the conversion of *meso-meso*-linked porphyrin arrays to the corresponding *meso-meso*, β - β doubly and triply linked porphyrin arrays.¹⁵⁻¹⁸ These doubly and triply linked porphyrins (**4**) arrays exhibit red shifted electronic absorption band around the far-IR region which are associated with an extensive π -conjugation over the molecules as a consequence of their planar structure. Further, various two dimensional extended porphyrin arrays are also synthesized and explored them in several applications such as multi-charge storage systems, electron-transporting amphiphilic columnar liquid crystals and as nonlinear optical materials. REF

5B.1.3 Corrole arrays

Corrole is one of the unique ligands in the contracted porphyrin series and provided an opportunity to stabilize the high-valent metal complexes. Some of these details were already described in chapter 5A. However, the reactivity studies of corroles are far behind from the porphyrins. In particular, the synthesis of covalently linked corrole arrays are less explored, as compared to porphyrin chemistry. First observation of covalently linked dimer was reported by Zeev Gross and co-workers, where, the respective dimer was achieved by spontaneous reaction of corrole in the presence of Co(OAc)₂ or Cu(OAc)₂.¹⁹⁻²¹ The regioselective synthesis of corrole arrays have been achieved by Osuka group by using oxidative coupling reaction strategy, where 5,10,15-tris(pentafluorophenyl)corrole in the presence of *p*-chloranil afforded β - β linked corrole

dimer and trimer (**5** and **6**) (Figure 5B.2).²² Under similar reaction condition, these dimers further converted into tetramer and hexamer.

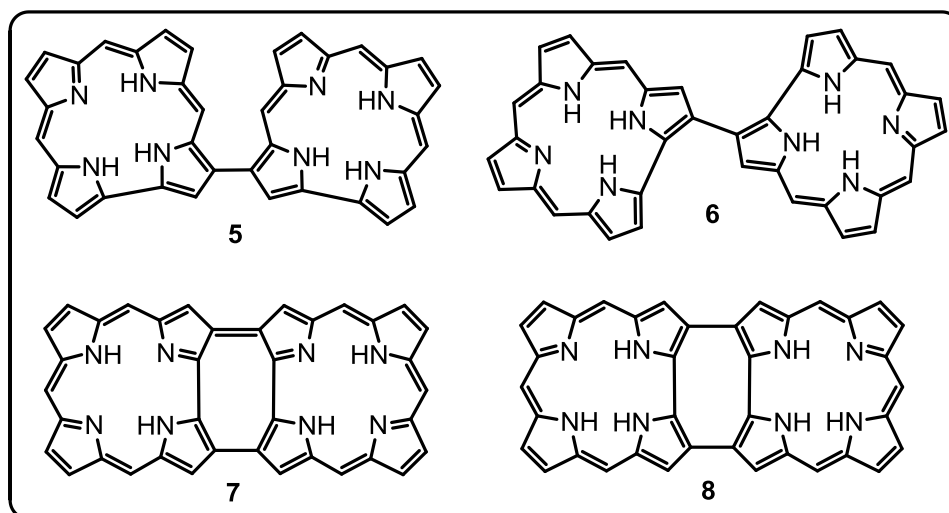
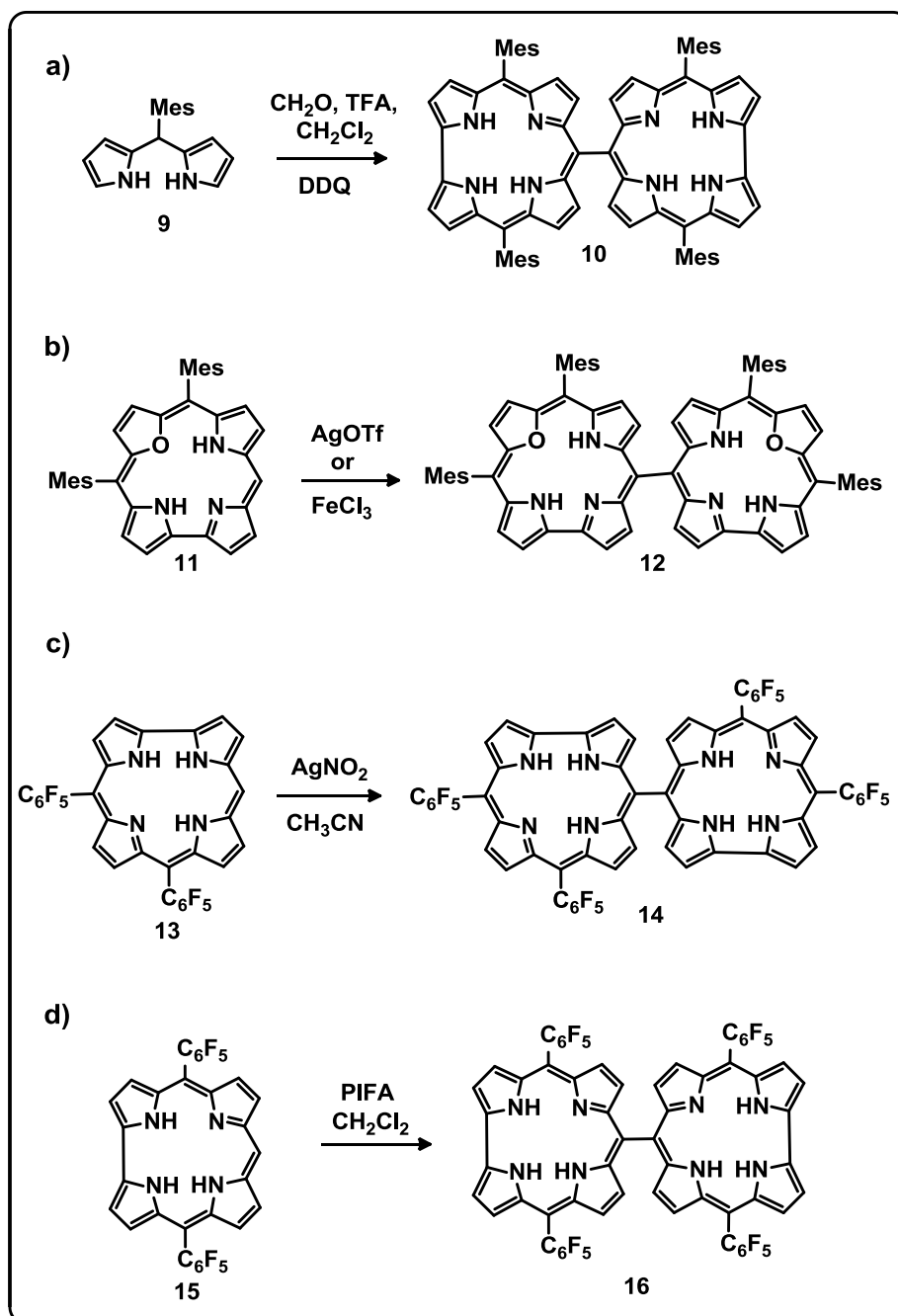


Figure 5B.2: Structures of β - β linked corrole dimer and their fused derivatives.

The first successful synthesis of doubly linked conjugated corrole dimer was reported by osuka and co-workers through Palladium-catalyzed oxidative homocoupling of 2-borylcorrole in the presence of chloroacetone as an oxidant afforded 2,2'-linked corrole dimer. This dimer was further converted into doubly linked (2,2' and 18,18') planar corrole dimer in the presence of DDQ (**7**, **8**) (Figure 5B.2).^{23,24}

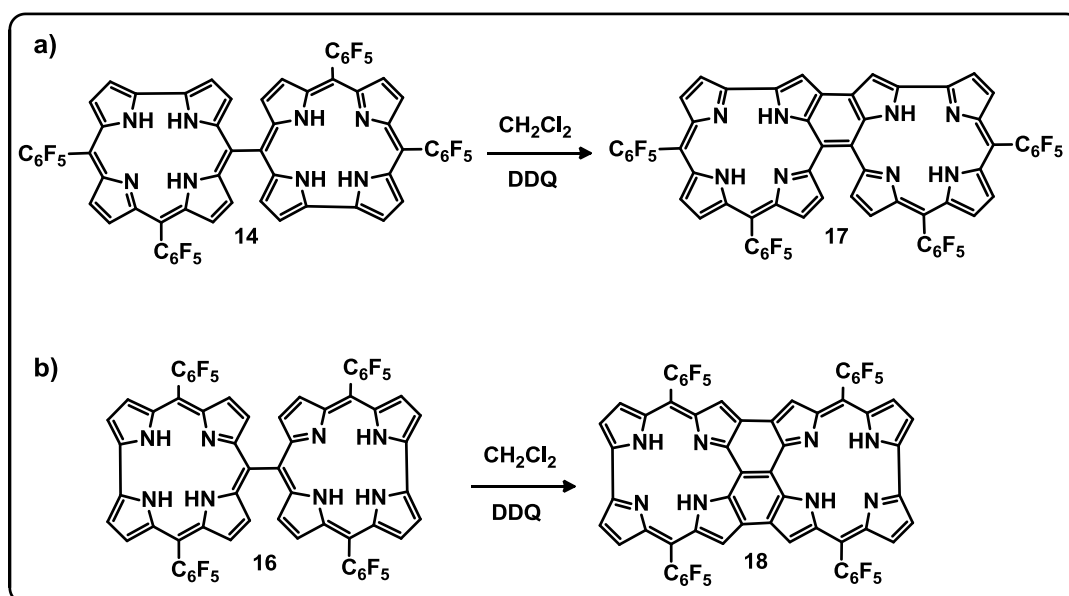
On the other hand, the *meso-meso* linked corrole dimers are achieved by various synthetic methodologies. The first report came from the Gryko and co-workers, where the direct acid-catalyzed condensation of mesityldipyrromethane with formaldehyde afforded the 10,10'-linked corrole dimer (**10**).²⁵ The first core modified 5,5'-linked corrole dimer (**12**) was published by T. K. Chandrashekar and co-workers in 2007 (Scheme 5B.1).²⁷ The 5,10-Dimesityl-22-oxacorrole (**11**) was subjected to oxidative coupling reaction with either silver(I) triflate or iron(III) chloride, resulting in the formation of dimer (**12**). The 5,5'-linked corrole dimer (**14**) was achieved by treating the 5,10 bis(pentafluorophenyl)corrole (**13**) with AgNO_2 , while the reaction of 5,15-bis(pentafluorophenyl)corrole (**15**) in presence of milder reaction conditions by using

[Bis(trifluoroacetoxy)iodo]benzene (PIFA) afforded the 10,10'-linked dimer (**16**) (Scheme 5B.1).²⁶ These dimers were further oxidized with DDQ under dilute condition formed the doubly (**17**) and triply (**18**) linked planar fused corrole dimers (Scheme 5B.2) and explored their properties by Osuka group.^{28,29}



Scheme 5B.1: Syntheses of *meso-meso* linked corrole dimers.

Along with these results, there are few hybrid porphyrin-corrole dimers also reported in recent years. The first *meso-β* directly linked corrole-porphyrin hybrid dimer was reported by Hiroto *et al* through the Palladium catalyzed cross-coupling reaction of *meso*-bromoporphyrin with C2 borylated corrole.³⁰ Later Zheng *et al* synthesized *meso-meso* linked porphyrin-corrole hybrids by simple BF₃.OEt₂-catalyzed condensation of *meso*-formylporphyrin with dipyrromethane followed by DDQ oxidation.³¹ Furthermore, the multi-molecular hybrids such as corrole-porphyrin-corrole, porphyrin-corrole-porphyrin were synthesised recently by Sankar and co-workers and stabilized multi-metals in different oxidation states.^{32,33}



Scheme 5B.2: Synthesis of doubly (**17**) and triply (**18**) linked corrole dimers.

5B.2 Objective of our work

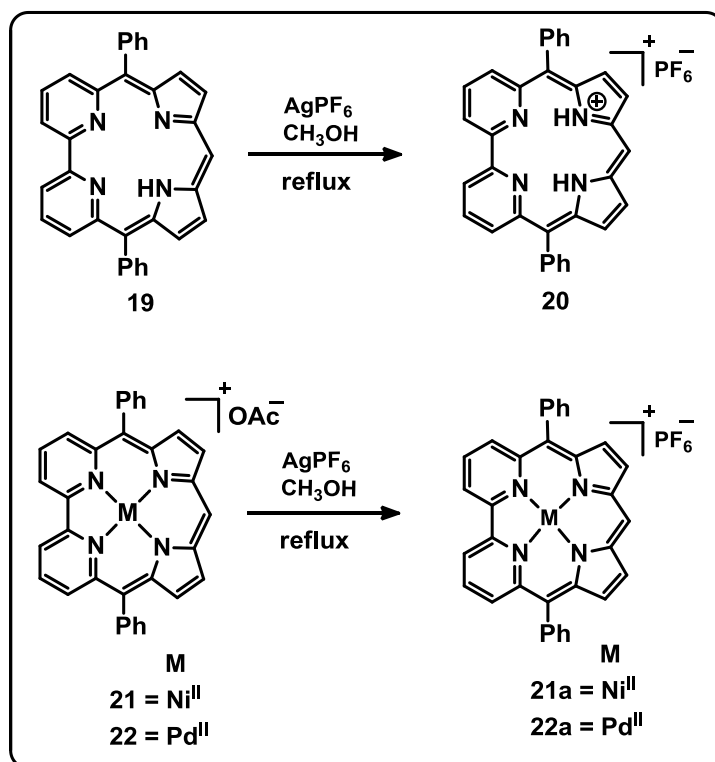
Till date, the covalently linked corrole dimers were achieved in the freebase form and the metal ion insertion were further carried out. Hence, the main objective of this chapter is to explore the reactive studies of *meso*-free corrole homologue complexes. Herein, we wish to report the reactive studies of *meso*-free corrole homologue both in

its freebase and complex form. The reactive CH in the *meso*-free bipyricorrole in its freebase form in the presence of oxidative coupling agents such as AgPF₆ and AgOTf forms the anionic complex. However, in the presence of FeCl₃ no further reaction was observed. On the other hand, the reactive CH in the *meso*-free bipyricorrole complexes by using various oxidative coupling reagents such as AgPF₆, AgOTf and FeCl₃ afforded different complexes. By using Ag^I salts, the anion exchanged products are observed. In the presence FeCl₃, the *meso*-CH is actively participated in oxidative coupling reaction to afford the respective *meso-meso* linked corrole homologue dimer complexes. It is also pertinent to point out that the Pd^{II}-corrole monomer and dimer complex are not known so far. To the best of our knowledge, the nonaromatic Pd^{II} monomer as well as dimer corrole homologue complexes are characterized by spectral studies and further confirmed by structural analyses, which are first time addressed in corrole chemistry.

5B.3 Results and discussions

5B.3.1 Synthesis and reactive studies

The syntheses of *meso*-free corrole homologues in its freebase form (**19**) and its complexes (**21** and **22**) were encouraged us to explore the *meso-meso* covalently linked dimer reaction. The synthesis is depicted in Scheme-5B.3. We adopted similar synthetic methodologies as reported by Osuka and co-workers.²⁶ Initially, the *meso*-free corrole homologues (**19**, **21** and **22**) were treated with various known oxidative coupling agents such as AgPF₆, AgOTf and FeCl₃. The free base corroles, in presence of AgPF₆ and AgOTf, formed protonated anionic complex (**20**). Whereas in case of metal-complexes anion exchanged product was observed. For example, when **19** was treated with AgPF₆, the PF₆ anionic complex of **19** was formed. Whereas, **21** with AgPF₆, the acetate ion was replaced by PF₆ ion and identified as **21a** in quantitative yield.



Scheme 5B.3: Synthesis of anionic (**20**) and anionic exchanged (**21a** and **22a**) corrole homologues complexes.

5B.3.2 Spectral Characterization

5B.3.2.1 NMR Analysis of **20**, **21a** and **22a**

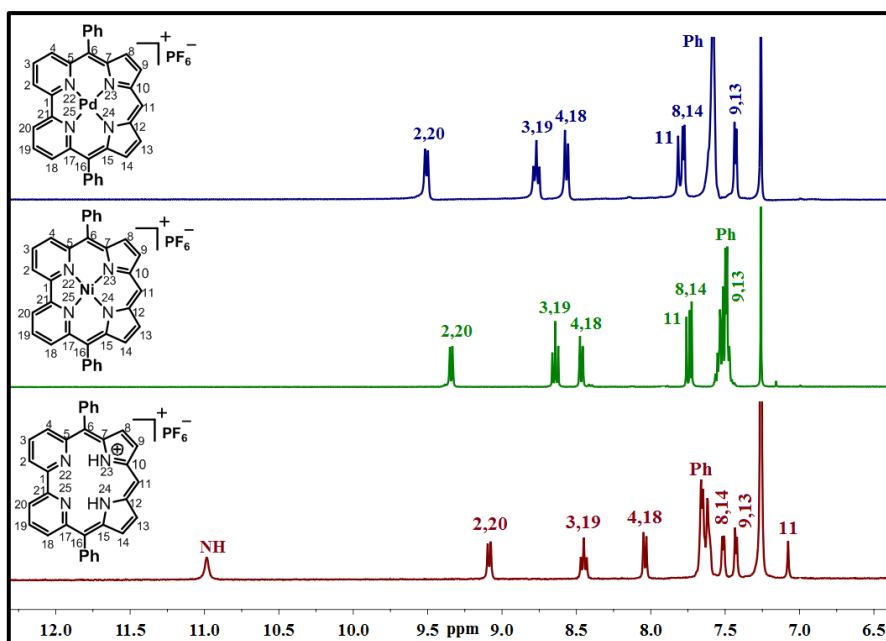


Figure 5B.3: ^1H NMR spectrum of **20**, **21a** and **22a** in CDCl_3 .

The ^1H NMR of newly formed protonated complex as well as anion exchanged products (**20**, **21a** and **22a**) were recorded in CDCl_3 and shown in Figure 5B.3. The ^1H NMR of these molecules show similar spectral pattern as previous molecules which described in the chapter-5A. The protonated complex and the anionic exchanged products of these complexes were further confirmed by the ^{19}F and ^{31}P NMR.

5B.3.2.2 Single crystal X-ray analysis of **20**, **21a** and **22a**

The final confirmation of these molecules has come from the single crystal X-ray analysis which is shown in Figure 5B.4. All the structural features are similar to the earlier reports as discussed in Chapter-5A. As observed earlier, the protonated complex (**20**) shows intramolecular hydrogen bonding interaction between the amine and newly protonated nitrogen with pyridine nitrogen with bond distances and angles of 2.005(5) Å, 129.34(4)° & 1.959(5) Å, 126.68(4)° (N2-H2...N1 & N3-H3...N4). In addition, one of the *meso* phenyl CH is in intermolecular hydrogen bonding interactions with the fluorine atom of the anion with bond distance and angles of C23-H23...F is 2.605(4)

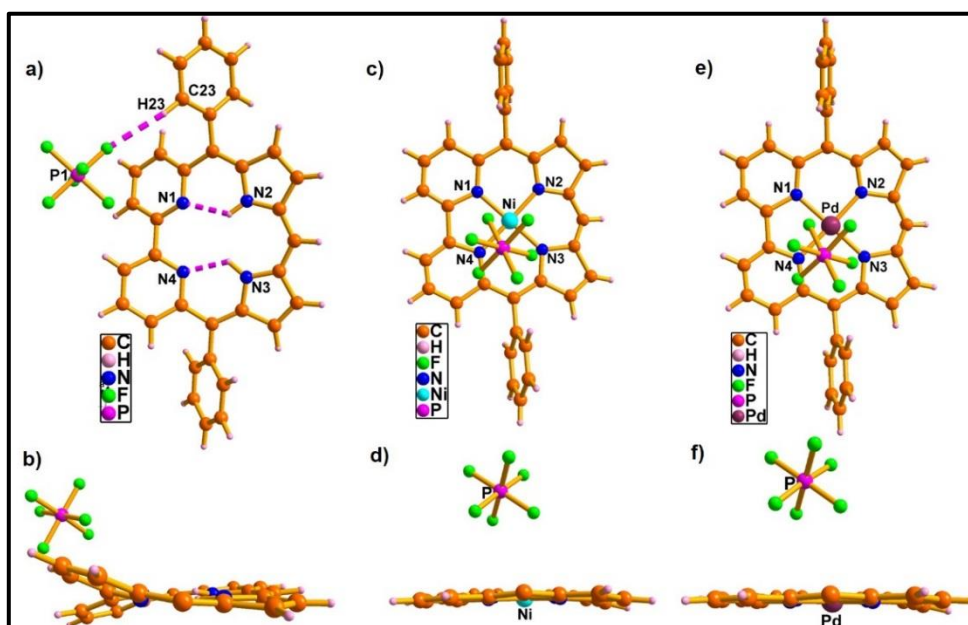
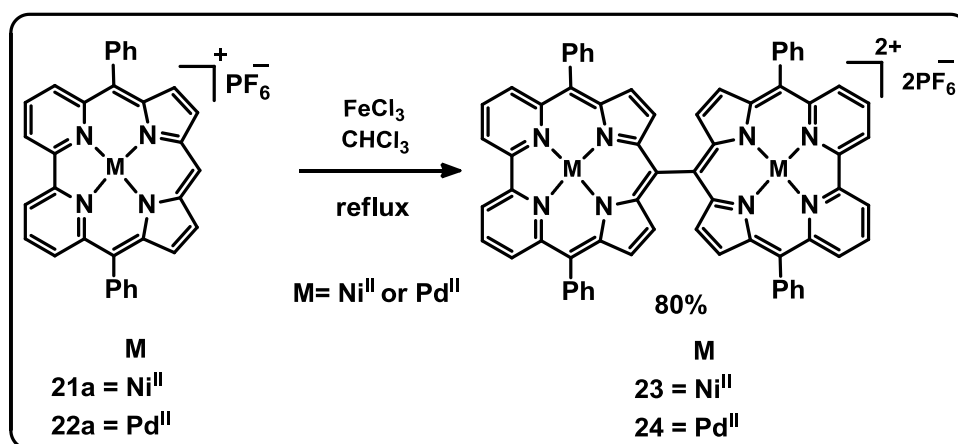


Figure 5B.4: Single crystal X-ray structure of **20** (a & b), **21a** (c & d) and **22a** (e & f).

The *meso*-phenyl groups in **20**, **21a** & **22a** are omitted for clarity in the side view.

Å and $165.45(3)^\circ$. On the other hand, the valencies of the anion exchanged products are satisfied by the newly introduced PF_6^- counter anion (**21a** & **22a**). As observed earlier, the anion is above the mean plane macrocyclic plane. The distance between the Ni & P in **21a** and Pd & P is $4.439(2)$ Å and $4.498(2)$ Å respectively. The geometry around the metal center is square planar. The bond distance and bond angles around the metal ions and saddling dihedral angle values are mentioned in Table (5B.1, 5B.2 & 5B.3). The results are comparable with earlier reports as discussed in the chapter-5A.

The oxidative coupling reaction was further performed with freebase **19** and metal complexes (**21a** & **22a**) in the presence of FeCl_3 . In case of free base (**19**), the reaction was unsuccessful, however to our surprise, when the reaction was performed with metal complex **21a** and **22a** we could achieve the *meso-meso* linked dimer complex **23** and **24** (Scheme 5B.4). During the reaction, the bluish green color solution is gradually changed into green color upon oxidative coupling. The results proved that the complex **21a** and **22a** are highly reactive and the reaction proceeds with regioselectivity as compared to **19**. The crude mixture was purified by column chromatographic separation, where a thick green colour fraction was eluted with CH_2Cl_2 and CH_3OH (97:3) and identified as **23** and **24** in 80% yield.



Scheme 5B.4: Synthesis of **23** and **24**.

5B.3.2.3 Mass spectrometric analysis

The mass spectrometric analysis of **23** and **24** shows the molecular ion signal at 1062.1374 (M-2PF₆) and 1158.0837 (M-2PF₆) respectively and confirms the exact composition of the complex.

5B.3.2.4 NMR Analysis of **23** and **24**

The absence of *meso*-CH signal from the ¹H NMR analysis of **24** clearly suggests the formation of *meso-meso* linked dimer (Figure 5B.5). As compared to **22a**, the bipyridyl protons in **24** are deshielded and resonated at 9.78 [H(2,20)], 8.92 [H(3,19)] and 8.67 [H(4,18)] ppm, whereas the pyrrolic protons are upfield shifted and observed at 7.41 [H(8,14)] and 7.25 [H(9,13)] ppm, respectively. The *meso*-phenyl protons are resonated between 7.74 and 7.63 ppm. Similar trend was observed in the ¹H NMR spectral analysis of **23** (Figure 5B.5). Overall, the spectral pattern resembles the typical nonaromatic character.²¹

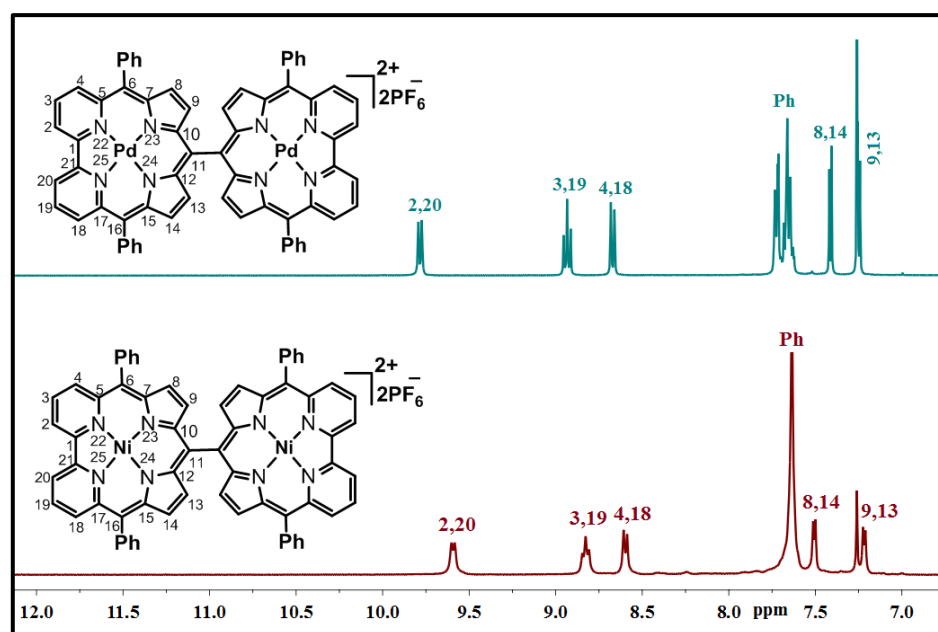


Figure 5B.5: ¹H NMR spectrum of **23** and **24** in CDCl₃.

5B.3.2.5 Single crystal X-ray analysis of **24**

Finally, the structure of **24** was unambiguously confirmed by single crystal X-ray analysis (Figure 5B.6, Table 5B.5). As observed in **22a**, both the Pd^{II} ions are at the center of the cavity with the maximum deviation of 0.0179 Å and the remaining valency of Pd^{II} ions are satisfied by two PF₆ anions. The bond length around the Pd^{II} [Pd1 and Pd2] ions are from 1.939 to 1.989 Å [Pd1 and N1-N4] and 1.962 to 1.977 Å [Pd2 and N5-N8] and the geometry around the metal center is maintained as observed in **22** and **22a** (Table 5B.1). Both the Pd^{II} units are connected by sp²-sp² single bond [C11-C44] character with the bond length of 1.525 Å (Figure 5B.6c). The individual bipyridyl aromatic character and the π -delocalization in the bis-dipyrromethene units combined together to generate the overall nonaromatic character in **24** (Figure 5B.6). The non-

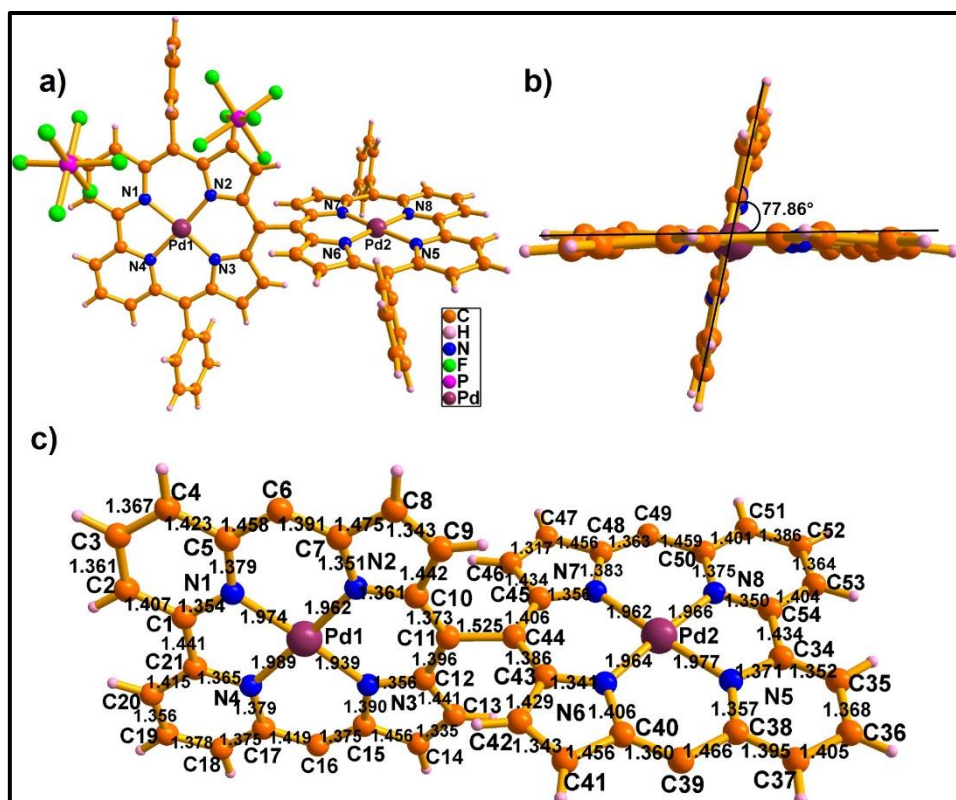


Figure 5B.6: Single crystal X-ray structure of **24**. a) Top view, b) side view and c) bond lengths (Å). The *meso*-aryl groups and counter anions are omitted for clarity in b) and c).

bonded distance between the two Pd^{II} ions are 8.206 Å. Both the Pd^{II} units are perpendicular to each other and the dihedral angle between the two planes is 77.86° (Figure 5B.6b) which are higher than the reported covalently linked corrole dimers²⁶ and the values are comparable with the covalently linked porphyrin dimers.^{10,11} In addition, the saddling dihedral angle values are between 0.323 Å and 12.044 Å, respectively (Table 5B.2). As reflected in **22** and **22a**, the pyrrole and pyridine units are hardly deviated from the plane with maximum deviation of 4.98Å, while the *meso*-phenyl units are deviated between 67.81° and 81.08°, respectively (Table 5B.4).

Table 5B.1: Bond length (Å) and the Bond angle around the metal ion (°) in **22**, **22a** and **24**

	22 (Å)	22a (Å)	24 (Å)		
N1-Pd1	1.996	1.969	1.974	N5-Pd2	1.977
N2-Pd1	1.968	1.964	1.962	N6-Pd2	1.964
N3-Pd1	1.961	1.961	1.939	N7-Pd2	1.962
N4-Pd1	1.992	1.979	1.989	N8-Pd2	1.966

	22 (°)	22a (°)	24 (°)		
N1-Pd-N2	92.590	91.61	93.39	N5-Pd-N6	92.34
N2-Pd-N3	91.367	89.91	92.18	N6-Pd-N7	91.95
N3-Pd-N4	92.137	92.08	91.47	N7-Pd-N8	92.06
N4-Pd-N1	83.906	86.37	83.99	N8-Pd-N5	83.77
Average	90.00	89.99	90.26		90.03

Table 5B.2: Saddling dihedral angle (°) in **22**, **22a** and **24**

	22 (°)	22a (°)	24 (°)		
C4-C5-C7-C8	7.22	3.34	0.32	C37-C38-C40-C41	2.96
C9-C10-C12-C13	2.11	3.26	12.04	C42-C43-C45-C46	2.83
C14-C15-C17-C18	12.14	0.37	6.33	C47-C48-C50-C51	5.56
C20-C21-C1-C2	0.18	1.25	0.78	C53-C54-C34-C34	5.50

Table 5B.3: Selected bond angles in **24** (°)

Bipyridyl (N1 & N4) unit				Bipyridyl (N5 & N8) unit			
N1 unit	Bond angle (°)	N4 unit	Bond angle (°)	N5 unit	Bond angle (°)	N8 unit	Bond angle (°)
C5-N1-C1	120.545	C21-N4-C17	120.395	C38-N5-C34	120.034	C54-N8-C50	118.678
N1-C1-C2	119.930	N4-C17-C18	116.812	N5-C34-C35	120.508	N8-C50-C51	120.832
C1-C2-C3	120.574	C17-C18-C19	124.353	C34-C35-C36	121.847	C50-C51-C52	119.677
C2-C3-C4	119.893	C18-C19-C20	118.159	C35-C36-C37	117.455	C51-C52-C53	119.087
C3-C4-C5	119.996	C19-C20-C21	118.901	C36-C37-C38	120.317	C52-C53-C54	119.995
C4-C5-N1	119.030	C20-C21-N4	121.182	C37-C38-N5	119.554	C53-C54-N8	121.548
Average	119.995	Average	119.967	Average	119.953	Average	119.970

Table 5B.4: Mean plane deviation (containing 25 atoms) of various units in **22**, **22a** and **24**

	22 (°)	22a (°)	24 (°)		
Pyridine (N1)	4.55	4.78	4.98	Pyridine (N5)	4.38
Pyrrole (N2)	5.55	4.54	3.89	Pyrrole (N6)	3.73
Pyrrole (N3)	6.43	5.39	4.82	Pyrrole (N7)	3.98
Pyridine (N4)	4.70	3.22	2.95	Pyridine (N8)	1.29
Phenyl-1 (Ph-1)	75.05	74.09	78.59	Phenyl-3 (Ph-3)	72.69
Phenyl-2 (Ph-2)	66.85	84.85	67.81	Phenyl-4 (Ph-4)	81.08
Pd1...Plane	0.0262	0.0922	0.0179	Pd2...Plane	0.0158

5B.3.2.6 Electronic absorption and Emission spectral analysis

The electronic absorption spectra of **21a** – **24** were recorded in CH_2Cl_2 . The electronic absorption of **21a** and **23** are shown in Figure 5B.7. The monomer **21a** shows the split intense band at 364 nm and 384 nm and prominent Q-type band at 580 nm, 627 nm (Figure 5B.7). The absorption spectrum of respective dimeric complex (**23**) is red shifted as compared to **21a** and the new bands are observed at 401 nm and the Q-type bands are appeared at 600 nm and 639 nm which are red shifted band as compared to monomer **21a**.

The electronic absorption and emission spectral analysis of **22a** and **24** are shown in Figure 5B.8. The intense band at 378 nm and weak Q-like bands between 584 and 634 nm in **22a** are red shifted as compared to **21a**, reflects the heavy atom effect. Upon dimerization the intense band in **24** is 23 nm red shifted as compared to **22a** and observed at 401 nm. Whereas the Q-like bands are at 604 and 643 with molar absorption coefficient of the intense band is 10^5 (Figure 5B.8). The red shift absorption as well as increase in molar absorption coefficient in both the dimer complexes is due to the extension in conjugation between the corrole units.

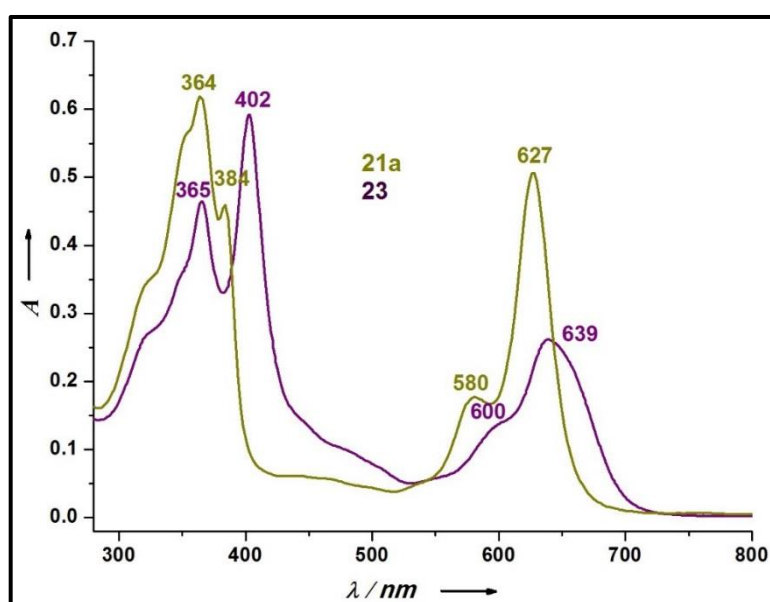


Figure 5B.7: The electronic absorption spectrum of **21a** and **23** in CH_2Cl_2 .

Among the monomer and dimer complexes, palladium complexes (**22a** and **24**) exhibit emission properties. The emission spectrum of **22a** shows an intense emissive band at 652 nm when excited at 426 nm and the fluorescence quantum yield (Φ_F) is found to be 0.09. Whereas the dimer complex **24** shows the red shifted band at 697 nm with moderate decrease in quantum yield and found to be 0.05 (Figure 5B.8).

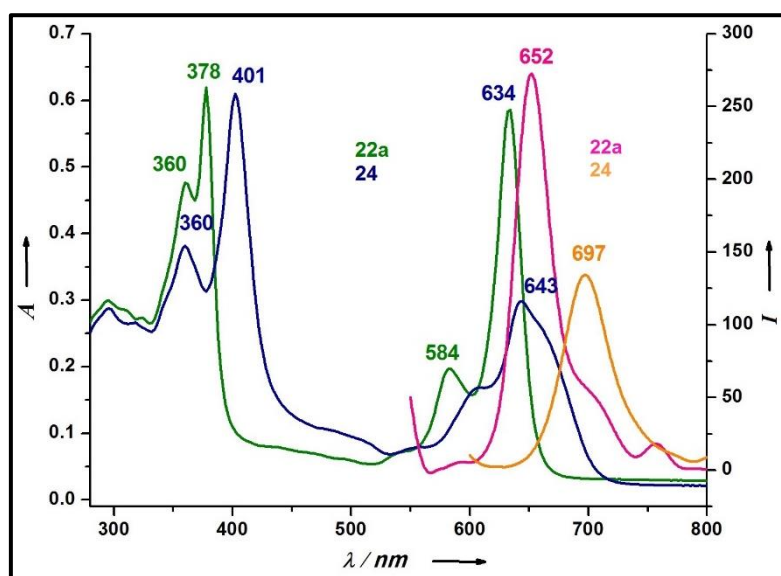


Figure 5B.8: The electronic absorption and emission spectrum of **22a** and **24** in CH_2Cl_2

5B.4 Conclusion

In conclusion, we have demonstrated the reactivity of *meso*-free corrole homologues of free ligand as well as its complexes by using readily available oxidative coupling agents. The Ag^{I} salts afforded protonated complex with free ligand, where as the reaction was not successful by using Fe^{III} ion. In the case of *meso*-free metal complexes, the anion exchanged complexes were obtained by Ag^{I} salts, in contrast, we could achieve the desired *meso-meso* linked dimeric complex by Fe^{III} ion. To the best of our knowledge, the non-aromatic Pd^{II} monomer as well as dimer corrole homologue complexes are characterized by spectral studies and further confirmed by structural analysis, which are hitherto unknown in corrole chemistry.

5B.5 Synthetic procedure and spectral characterization of 20-24

5B.5.1 Synthesis of 20: A solution of AgPF₆ (52 mg, 0.2 mmol) in 5 ml CH₃OH was added into the solution of **19** (20 mg, 0.04 mmol) in CH₂Cl₂ (50 ml) under open air atmosphere and allowed to stir for 3 h and extracted with CH₂Cl₂, dried over Na₂SO₄ and concentrated by rotary evaporator. Residue was purified by silica gel (silica 100-200 mesh) in 1% CH₃OH/CH₂Cl₂ and identified as **20**. The compound was further recrystallized from CH₂Cl₂/*n*-hexane to afford blue crystalline compound **20** in 90% yield.

¹H NMR (400 MHz, CDCl₃, 298K): δ = 10.98 (brs, 2H), 9.09 (d, J = 8.0 Hz, 2H), 8.45 (t, J = 8.1 Hz, 2H), 8.04 (d, J = 7.9 Hz, 2H), 7.66 – 7.52 (m, 10H), 7.51 (d, J = 4.5 Hz, 2H), 7.43 (d, J = 5.1 Hz, 2H), 7.08 (s, 1H).

¹⁹F NMR (376 MHz, CDCl₃): δ = -73.32, -75.21.

³¹P NMR (162 MHz, CDCl₃): δ = -134.92, -139.32, -143.72, -148.12, -152.52.

m.p: 300 °C (decomposition).

5B.5.2 Synthesis of 21a: The complex **21** was dissolved in 5 ml CHCl₃ and added to the solution of AgPF₆ in 5 ml CHCl₃. The mixture was allowed to stir at reflux condition under open air atmosphere for 3 h. The crude reaction mixture was purified by silica gel (silica 100-200 mesh) in 2% CH₃OH/CH₂Cl₂ and identified as **21a**. The complex **21a** was further recrystallized from CH₂Cl₂/*n*-hexane to afford green crystalline solid in 90% yield.

¹H NMR (400 MHz, CDCl₃, 298K): δ = 9.34 (d, J = 8.7 Hz, 2H), 8.64 (t, J = 8.0 Hz, 2H), 8.48 (d, J = 8.2 Hz, 2H), 7.76 (s, 1H), 7.73 (d, J = 5.2 Hz, 2H), 7.55 – 7.47 (m, 12H).

¹⁹F NMR (376 MHz, CDCl₃): δ = -73.04, -74.94.

³¹P NMR (162 MHz, CDCl₃): δ = -135.17, -139.56, -143.95, -148.34, -152.73.

5B.5.3 Synthesis of 22a: The complex **22** was dissolved in 5 ml CHCl₃ and added to the solution of AgPF₆ in 5 ml CHCl₃. The mixture was allowed to stir at reflux condition under open air atmosphere for 3 h. The crude reaction mixture was purified by silica gel (silica 100-200 mesh) in 3% CH₃OH/CH₂Cl₂ and identified as **22a**. The complex **22a** was further recrystallized from CH₂Cl₂/*n*-hexane to afford green crystalline solid in 90% yield.

¹H NMR (400 MHz, CDCl₃, 298K): δ = 9.51 (d, *J* = 7.7 Hz, 2H), 8.77 (t, *J* = 8.0 Hz, 2H), 8.57 (d, *J* = 8.3 Hz, 2H), 7.82 (s, 1H), 7.78 (d, *J* = 5.1 Hz, 2H), 7.58 (m, 10H), 7.43 (d, *J* = 5.1 Hz, 2H).

¹⁹F NMR (376 MHz, CDCl₃): δ = -73.03, -74.92.

³¹P NMR (162 MHz, CDCl₃): δ = -135.11, -139.50, -143.90, -148.29, -152.68.

5B.5.4 Synthesis of 23: The FeCl₃ (135 mg, 0.8475 mmol) was added into the solution of **21a** (20 mg, 0.0169 mmol) in 100 ml CHCl₃ and allowed to stir for 4 h at 55 °C under open air atmosphere. The completion of the reaction was monitored by TLC and extracted with CH₂Cl₂. The organic layer was washed with NaPF₆ aqueous solution to exchange the counter ion of the complex. Residue was purified by silica gel (silica 100-200 mesh) in 2% CH₃OH/CH₂Cl₂ and identified as **23**. The complex was further recrystallized from CH₂Cl₂/*n*-hexane to afford blue crystalline solid **23** in 80% yield.

¹H NMR (400 MHz, CDCl₃, 298K): δ = 9.59 (d, *J* = 7.2 Hz, 4H), 8.83 (t, *J* = 7.6 Hz, 4H), 8.60 (d, *J* = 7.9 Hz, 4H), 7.64 (m, 20H), 7.51 (d, *J* = 5.2 Hz, 4H), 7.22 (d, *J* = 5.3 Hz, 4H).

¹⁹F NMR (376 MHz, CDCl₃): δ = -72.47, -74.36.

³¹P NMR (162 MHz, CDCl₃): δ = -135.05, -139.45, -143.85, -148.25, -152.65.

m.p: 300 °C (decomposition).

ESI-MS: m/z calculated for $C_{66}H_{40}N_8Ni_2$ (without axial ligand) = 1060.2083 and found = 1062.1374 [M+2].

UV-Vis (CH_2Cl_2): $\lambda_{max}(nm)$ ($\epsilon[M^{-1}cm^{-1}]$) = 365 (50,352), 402 (70,742), 600 (15,412), 639 (30,597).

5B.5.5 Synthesis of 24: The $FeCl_3$ (125 mg, 0.7835mmol) was added into the solution of **22a** (20 mg, 0.0157mmol) in 100 ml $CHCl_3$ and allowed to stir for 3 h at 55 °C under open air atmosphere. The completion of the reaction was monitored by TLC and extracted with CH_2Cl_2 , and the organic layer was washed with $NaPF_6$ aqueous solution to exchange the counter ion of the complex. Residue was purified by silica gel (silica 100-200 mesh) in 3% CH_3OH/CH_2Cl_2 and identified as **24**. The complex was further recrystallized from CH_2Cl_2/n -hexane to afford blue crystalline solid **24** in 80% yield.

1H NMR (400 MHz, $CDCl_3$, 298K): δ = 9.78 (d, J = 7.7 Hz, 4H), 8.92 (t, J = 8.1 Hz, 4H), 8.67 (d, J = 8.1 Hz, 4H), 7.74 – 7.72 (m, 8H), 7.71 – 7.63 (m, 12H), 7.41 (d, J = 5.4 Hz, 4H), 7.25 (d, J = 5.5 Hz, 4H).

^{19}F NMR (376 MHz, $CDCl_3$): δ = -73.11, -75.00.

^{31}P NMR (162 MHz, $CDCl_3$): δ = -135.06, -139.46, -143.87, -148.27, -152.67.

m.p: 300 °C (decomposition).

ESI-MS: m/z calculated for $C_{66}H_{40}N_8Pd_2$ (without axial ligand) = 1156.1446 and found = 1158.0837 [M+2].

UV-Vis (CH_2Cl_2): $\lambda_{max}(nm)$ ($\epsilon[M^{-1}cm^{-1}]$) = 360 (45,504), 401 (62,678), 604 (15,041), 643(35,661). Quantum yield (Φ_F)= 0.05.

Table 5B.5: Crystal data for **20**, **21a**, **22a** and **24**

Crystal parameters	20	21a	22a	24
Formula	C ₃₃ H ₂₃ F ₆ N ₄ P	C ₃₃ H ₂₁ N ₄ F ₆ PNi	C ₃₃ H ₂₁ N ₄ F ₆ PPd	C ₆₆ H ₄₀ F ₁₂ N ₈ P ₂ Pd ₂
<i>M</i> /g mol ⁻¹	620.52	677.22	724.91	1447.80
<i>T</i> /K	100	100	100	100
Crystal dimensions/mm ³	0.1 x 0.08 x 0.045	0.1 x 0.07 x 0.04	0.2 x 0.15 x 0.1	0.1 x 0.08 x 0.06
Crystal system	Monoclinic	Orthorhombic	Orthorhombic	Monoclinic
Space group	P2(1)/c	<i>Pcca</i>	<i>Pcca</i>	<i>P2(1)/c</i>
<i>a</i> /Å	9.663 (5)	21.095 (6)	21.095 (15)	15.541 (5)
<i>b</i> /Å	12.879 (5)	9.434 (3)	9.350 (6)	30.436 (5)
<i>c</i> /Å	22.145 (5)	29.833 (9)	30.015 (2)	12.894 (5)
α /°	90	90	90	90.000 (5)
β /°	96.919 (5)	90	90	99.353 (5)
γ /°	90	90	90	90.000 (5)
<i>V</i> /Å ³	2735.9 (19)	5925 (3)	5920.2 (7)	6018 (3)
<i>Z</i>	4	8	8	4
ρ_{calcd} /mg m ⁻³	1.507	1.518	1.627	1.598
μ /mm ⁻¹	0.174	0.778	0.750	0.738
<i>F</i> (000)	1272	2752	2896	2888
Reflns. collected	38757	57462	60449	32568
Indep.reflns. [<i>R</i> (int)]	6770 [0.0629]	5207 [0.1299]	5440 [0.0680]	10945 [0.0986]
Max/min transmission	0.7457 and 0.6662	0.7452 and 0.5420	0.7452 and 0.6388	0.7452 and 0.6660
Data/restraints /parameters	6770 / 0 / 485	5207 / 6 / 406	5440 / 4 / 394	10945 / 0 / 811
GOF on <i>F</i> ²	1.111	1.074	1.073	0.949
Final <i>R</i> indices [<i>I</i> > 2σ(<i>I</i>)]	<i>R</i> 1 = 0.0835, <i>wR</i> 2 = 0.2334	<i>R</i> 1 = 0.0900, <i>wR</i> 2 = 0.2460	<i>R</i> 1 = 0.0690, <i>wR</i> 2 = 0.1865	<i>R</i> 1 = 0.0842, <i>wR</i> 2 = 0.1958
<i>R</i> indices (all data)	<i>R</i> 1 = 0.1071, <i>wR</i> 2 = 0.2565	<i>R</i> 1 = 0.1231, <i>wR</i> 2 = 0.2691	<i>R</i> 1 = 0.1022, <i>wR</i> 2 = 0.2023	<i>R</i> 1 = 0.1753, <i>wR</i> 2 = 0.2274
Largest diff peak and hole [e Å ⁻³]	1.523 and -1.500	1.362 and -0.547	1.175 and -0.583	0.890 and -0.977

The crystals have been deposited in the Cambridge Crystallographic Data Centre for **20**, **21a**, **22a** and **24** are **1052084**, **1473610**, **1473611** and **1473612** respectively.

5B.6 Reference

1. Senge, M. O.; Fazekas, M.; Notaras, E. G. A.; Blau, W. J.; Zawadzka, M.; Locos, O. B.; Ni Mhuircheartaigh, E. M. *Adv. Mater.* **2007**, *19*, 2737-2774.

2. Aratani, N.; Kim, D.; Osuka, A. *Acc. Chem. Res.* **2009**, *42*, 1922-1934.
3. Aratani, N.; Kim, D.; Osuka, A. *Chem.–Asian J.* **2009**, *4*, 1172-1182.
4. Mori, H.; Tanaka, T.; Osuka, A. *J. Mater. Chem. C* **2013**, *1*, 2500-2519.
5. Tanaka, T.; Osuka, A. *Chem. Soc. Rev.* **2015**, *44*, 943-969.
6. Yoon, Z. S.; Yang, J.; Yoo, H.; Cho, S.; Kim, D. *Handbook of Porphyrin Science with Applications to Chemistry, Physics, Materials Science, Engineering Biology and Medicine*, ed. K.M. Kadish, K.M. Smith and R. Guilard, World Scientific Publishers, Singapore **2010**, *1*.
7. Saito, S.; Osuka, A. *Angew. Chem. Int. Ed.* **2011**, *50*, 4342-4373.
8. Tanaka, T.; Osuka, A. *Chem. Rev.* **2016**, DOI: 10.1021/acs.chemrev.6b00371.
9. Osuka, A.; Shimidzu, H. *Angew. Chem. Int. Ed.* **1997**, *36*, 135-137.
10. Aratani, N.; Osuka, A. *Bull. Chem. Soc. Jpn.* **2001**, *74*, 1361-1379.
11. Osuka, A. *The Chem. Rec.* **2015**, *15*, 143-159.
12. Nakamura, Y.; Aratani, N.; Osuka, A. *Chem. Soc. Rev.* **2007**, *36*, 831-845.
13. Holten, D.; Bocian, D. F.; Lindsey, J. S. *Acc. Chem. Res.* **2002**, *35*, 57-69.
14. Kim, D.; Osuka, A. *Acc. Chem. Res.* **2004**, *37*, 735-745.
15. Tsuda, A.; Furuta, H.; Osuka, A. *Angew. Chem. Int. Ed.* **2000**, *39*, 2549-2552.
16. Tsuda, A.; Nakano, A.; Furuta, H.; Yamochi, H.; Osuka, A. *Angew. Chem. Int. Ed.* **2000**, *39*, 558-561.
17. Tsuda, A.; Furuta, H.; Osuka, A. *J. Am. Chem. Soc.* **2001**, *123*, 10304-10321.
18. Cai, H.; Fujimoto, K.; Lim, J. M.; Wang, C.; Huang, W.; Rao, Y.; Zhang, S.; Shi, H.; Yin, B.; Chen, B. *Angew. Chem. Int. Ed.* **2014**, *53*, 11088-11091.
19. Mahammed, A.; Giladi, I.; Goldberg, I.; Gross, Z. *Chem. Eur. J.* **2001**, *7*, 4259-4265.

-
20. Luobeznova, I.; Simkhovich, L.; Goldberg, I.; Gross, Z. *Eur. J. Inorg. Chem.* **2004**, 1724-1732.
 21. Barata, J. F. B.; Silva, A. M. G.; Neves, M. G. P. M. S.; Tomé, A. C.; Silva, A. M. S.; Cavaleiro, J. A. S. *Tetrahedron Lett.* **2006**, *47*, 8171-8174.
 22. Hirabayashi, S.; Omote, M.; Aratani, N.; Osuka, A. *Bull. Chem. Soc. Jpn.* **2012**, *85*, 558-562.
 23. Hiroto, S.; Furukawa, K.; Shinokubo, H.; Osuka, A. *J. Am. Chem. Soc.* **2006**, *128*, 12380-12381.
 24. Cho, S.; Lim, J. M.; Hiroto, S.; Kim, P.; Shinokubo, H.; Osuka, A.; Kim, D. *J. Am. Chem. Soc.* **2009**, *131*, 6412-6420.
 25. Koszarna, B.; Gryko, D. T. *Chem. Commun.* **2007**, 2994-2996.
 26. Ooi, S.; Yoneda, T.; Tanaka, T.; Osuka, A. *Chem. Eur. J.* **2015**, *21*, 7772-7779.
 27. Sankar, J.; Rath, H.; Prabhuraja, V.; Gokulnath, S.; Chandrashekar, T. K.; Purohit, C. S.; Verma, S. *Chem. Eur. J.* **2007**, *13*, 105-114.
 28. Ooi, S.; Tanaka, T.; Park, K. H.; Lee, S.; Kim, D.; Osuka, A. *Angew. Chem. Int. Ed.* **2015**, *54*, 3107-3111.
 29. Ooi, S.; Tanaka, T.; Park, K. H.; Kim, D.; Osuka, A. *Angew. Chem. Int. Ed.* **2016**, *55*, 6535-6539.
 30. Hiroto, S.; Hisaki, I.; Shinokubo, H.; Osuka, A. *Angew. Chem. Int. Ed.* **2005**, *44*, 6763-6766.
 31. Chen, C.; Zhu, Y.-Z.; Fan, Q.-J.; Song, H.-B.; Zheng, J.-Y. *Chem. Lett.* **2013**, *42*, 936-938.
 32. Murugavel, M.; Reddy, R. V. R.; Sankar, J. *RSC Adv.* **2014**, *4*, 13669-13672.
 33. Murugavel, M.; Reddy, R.; Dey, D.; Sankar, J. *Chem. Eur. J.* **2015**, *21*, 14280-14286.
-

CHAPTER 6

Carbahomoporphyrins: Allowed and restricted conjugation in homoporphyrinoids by incorporation of *o*-terphenyl system

6.1	Introduction	181
6.2	Objective of our work	184
6.3	Results and discussions	185
6.3.1	Spectral characterisation	186
6.3.1.1	Mass spectrometric analyses	186
6.3.1.2	NMR Analysis	187
6.3.1.3	Single crystal X-ray structure and analysis of 14	188
6.3.2	Coordination Studies	190
6.3.2.1	NMR Analysis	191
6.3.2.2	Single crystal X-ray structure and analysis of 19a and 20	192
6.3.3	Electronic spectral analysis	193
6.4	Conclusion	195
6.5	Experimental Section	196
6.5.1	General Information	196
6.5.2	Synthetic procedure and spectral characterization of 12- 20	196
6.6	References	201

6.1 Introduction

The expanded porphyrins are versatile ligands and received much attention due to the diverse applications in various fields such as non-linear optical materials, photodynamic therapy (PDT) and magnetic resonance imaging (MRI) contrasting agents.¹⁻⁴ However, among the expanded porphyrins, homoporphyrins are less explored due to their synthetic difficulties as well as stability factors. Homoporphyrins are tetrapyrrolic macrocycles in which four pyrrole rings are connected through five methene bridges. In this class, overall 17 atoms are present in the internal ring pathway, which is a minimum number for the fulfilment of expanded category, hence called as the smallest expanded derivative. These homoporphyrins are further classified based on the type of conjugation involved in macrocycle. There are four types of homoporphyrin derivatives known in the literature where two of them are unconjugated (**A** and **B**) systems and are fully conjugated such as reduced and oxidized 18π and 20π systems (**C** and **D**) (Figure 6.1). Among them, the fully conjugated systems are very less stable in nature. Most of the homoporphyrins are reported between 1967 and 1979 with major contribution by Callot and co-workers.⁵⁻⁷

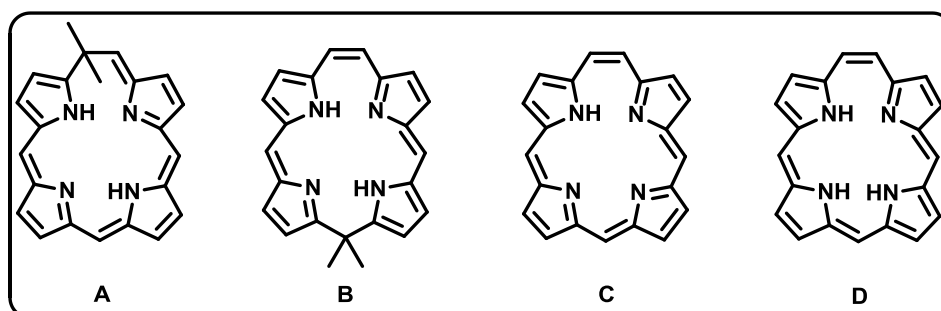
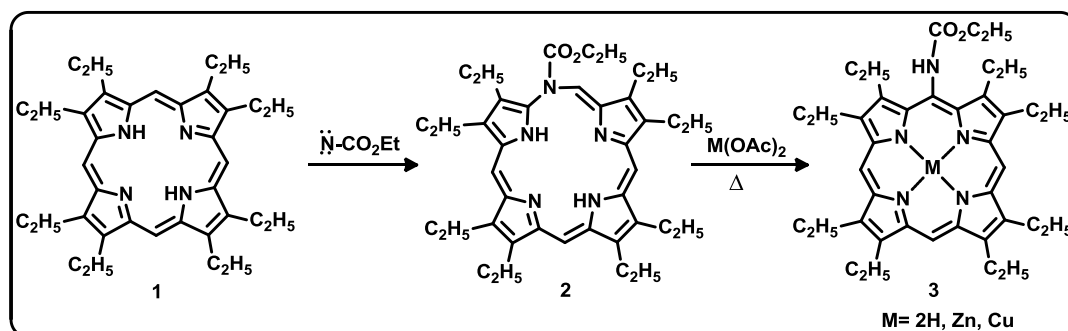


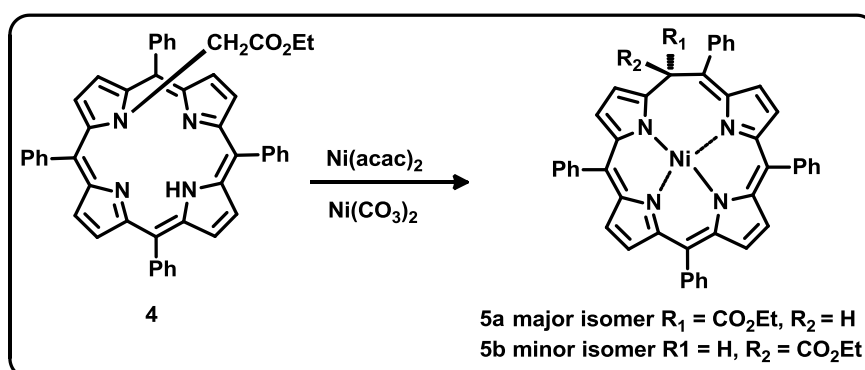
Figure 6.1: Structures of homoporphyrins A-D.

The azahomoporphyrin (**2**) was reported by Grigg *et al.* in 1967 where the “N” was present as an extra atom (17 atom) at the *meso*-position.⁸ The compound (**2**) was

synthesized by treating the free base porphyrin **1** with nitrene and showed the non-aromatic character (Scheme 6.1).⁹ The molecule exhibits Soret like absorption band at 404 nm and two Q-type bands at 610 and 655 nm. The molecule is found to be unstable upon coordination with Zn and Cu salts and produces corresponding metallated porphyrin derivatives (**3**).



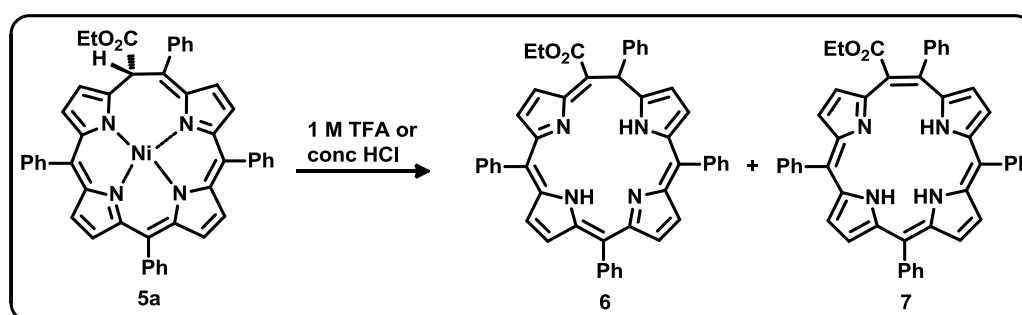
Scheme 6.1: Synthesis of azahomoporphyrin (**2**) and its ring contraction.



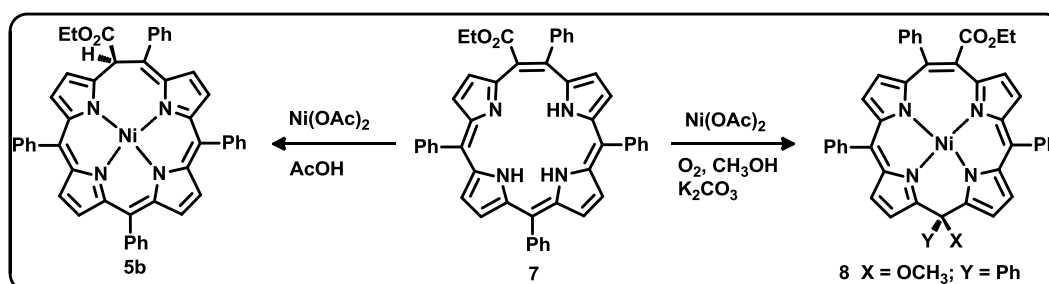
Scheme 6.2: Synthesis of Ni^{II} homoporphyrins.

Later, two isomeric homoporphyrins (**5a** and **5b**) were synthesized by Collot and Tschamber by treating the N-substituted tetraarylporphyrin (**4**) with Ni(acac)₂ and Ni(CO₃)₂ in 1,2-dichloroethane solution (Scheme 6.2).⁵⁻⁷ The electronic absorption spectrum of both the isomers are similar to that of the porphyrin type systems. The highly distorted structure is reflected from crystal analysis and proves non-aromatic character.^{10,11} Demetallation experiments are performed with different acid

concentration. At lower acid concentration, the complex **5a** exist in four different equilibrium forms.¹² However, at strong acid or higher concentration, two different free base homoporphyrin derivatives (**6** and **7**) are obtained.¹³ One of the products (**7**) with three NH in the coordination core is completely conjugated 20π anti-aromatic derivative (Scheme 6.3). Unfortunately the conjugated homoporphyrin (**7**) is reported to be unstable even at 0°C . In order to stabilize the macrocycle, same group has also performed the coordination with various metal salts, however it was unsuccessful and produced the rearranged products (**5b** and **8**) (Scheme 6.4).^{5,13,14,15}



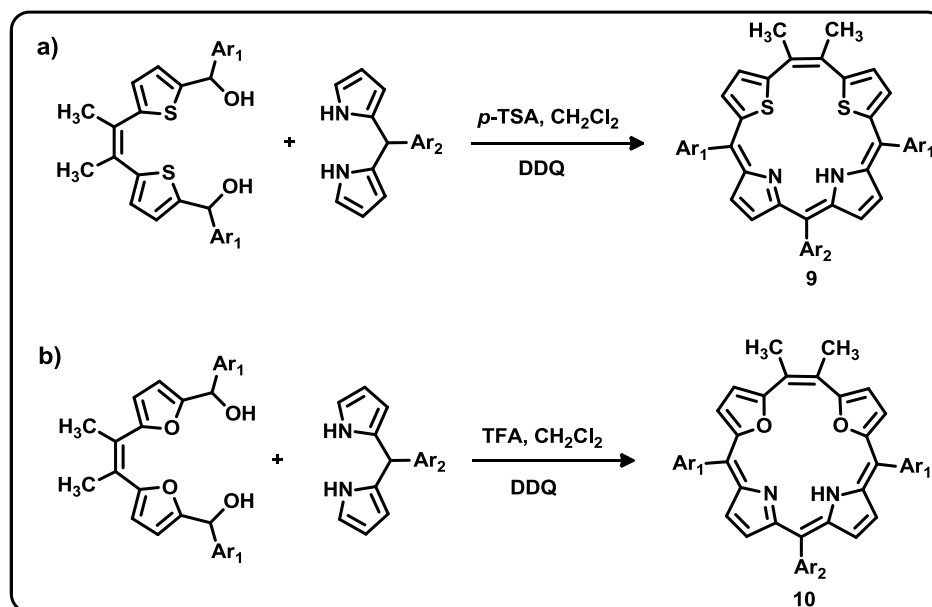
Scheme 6.3: Synthesis of free base homoporphyrins.



Scheme 6.4: Metallation of homoporphyrins.

Recently Ravikanth and co-workers reported the synthesis of stable 20π -core-modified homoporphyrin systems. Both the homoporphyrins such as [20]dithiahomoporphyrin(2.1.1.1) (**9**) and [20]dioxahomoporphyrin(2.1.1.1) (**10**) were synthesized by [2+2] condensation of *meso*-aryldipyrromethanes with dithia or dioxa-

ethanediol derivatives under mild acid-catalyzed conditions (Scheme 6.5). The spectral and structural analyses, proved that the both molecules are significantly distorted and showed non-aromatic character.^{16,17}



Scheme 6.5: Synthesis of core-modified homoporphyrins.

6.2 Objective of our work

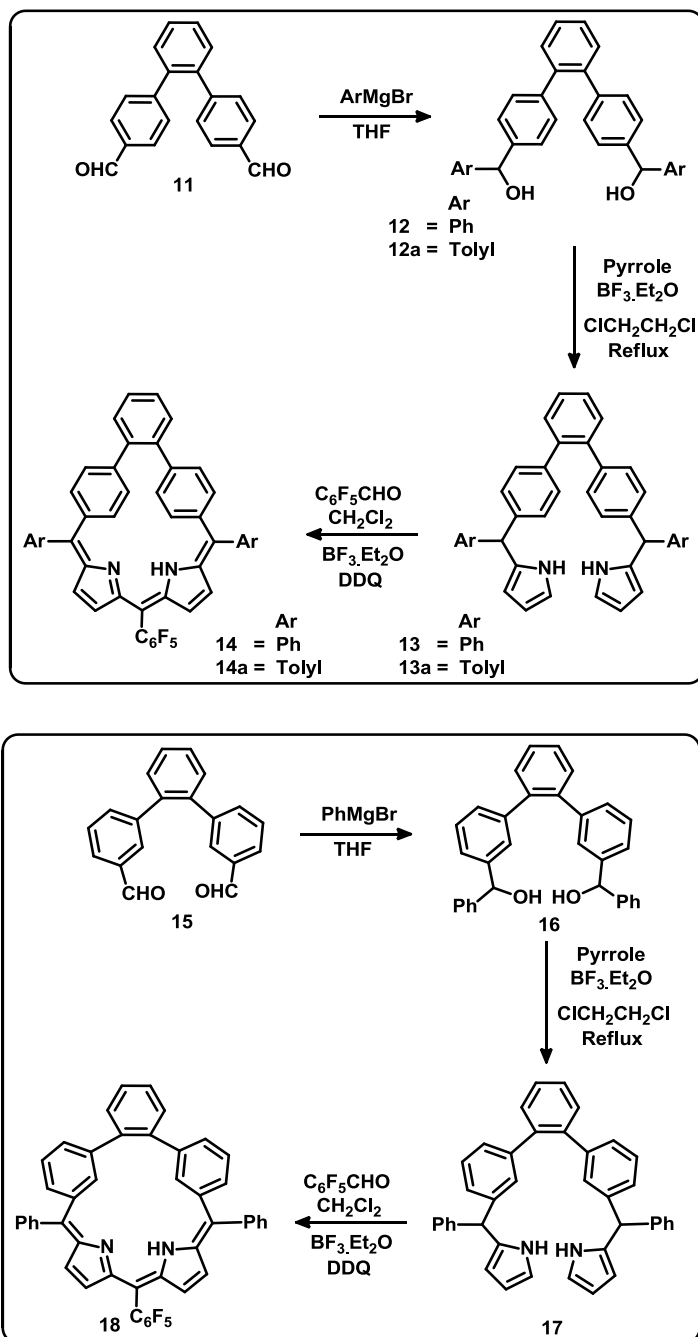
In light of the above discussions, it is clear that a considerable attention has to be paid on the synthesis and stabilization of such unstable homoporphyrins. Even after four decades of the discovery of homoporphyrins, the complete studies of these derivatives are still in its infancy stage. Hence, it is necessary to develop facile synthetic methodologies and novel stable homoporphyrin analogues.

In this chapter, we would like to introduce polycyclic aromatic units as part of the framework for the first time to achieve the stable carbahomoporphyrins. The novel porphyrinoids such as *meso*-aryl di-carba and tetra-carba homoporphyrins are synthesized by introducing the *o*-terphenyl unit into the porphyrin core and are structural isomers to each other. The *o*-terphenyl unit is connected through two different bonding modes: (a) 3,3'' and (b) 4,4''. The presence of *m*-phenyl unit in 3,3''-bonding

mode restricts the overall conjugation and adopts non-aromatic character. The presence of *p*-phenyl unit in 4,4''-bonding mode allows overall conjugation, however the macrocyclic units are highly tilted from the plane and adopts non-aromatic character. Further, the coordination chemistry reveals the insertion of Rh(I) ion in both the macrocycles. The metal ion insertion does not alter the non-aromatic character & maintains as such.

6.3 Results and discussions

Synthesis of target molecules involved three steps which is outlined in scheme 6.6. The aldehyde precursor such as **11** and **15** are achieved by reported procedure.¹⁸ The first step is the conversion of *o*-terphenyl dicarbaldehydes (**11** and **15**) to the corresponding diol derivatives **12**, **12a** and **16** by using freshly prepared phenylmagnesium bromide in THF afforded **12**, **12a** and **16** in 75% yield. The second step is the condensation of diol into respective dipyrromethane by excess pyrrole in presence of BF₃.Et₂O, where the key precursor **13**, **13a** and **17** are obtained in 55% yield. In the final step, the TFA acid-catalyzed condensation reaction of **13**, **13a** and **17** with pentafluorobenzaldehyde followed by oxidation with 2,3-dichloro-5,6-dicyano-*p*-benzoquinone (DDQ) afforded **14**, **14a** and **18** in 12%, 10% and 7% yield respectively.^{19,20} All the macrocycle **14**, **14a** and **18** were characterized by various analytical techniques.



Scheme 6.6: Synthesis of carba-homoporphyrins **14**, **14a** and **18**.

6.3.1 Spectral characterisation

6.3.1.1 Mass spectrometric analysis

The mass spectrometric analysis of **14**, **14a** and **18** is shown in Figure 6.2 and 6.3. The molecular ion signal of **14**, **14a** and **18** is at 715.2159 [M+1], 743.2392 [M+1] and 715.2093 (M+1), respectively and confirms the exact composition (Figure 6.2-6.3).

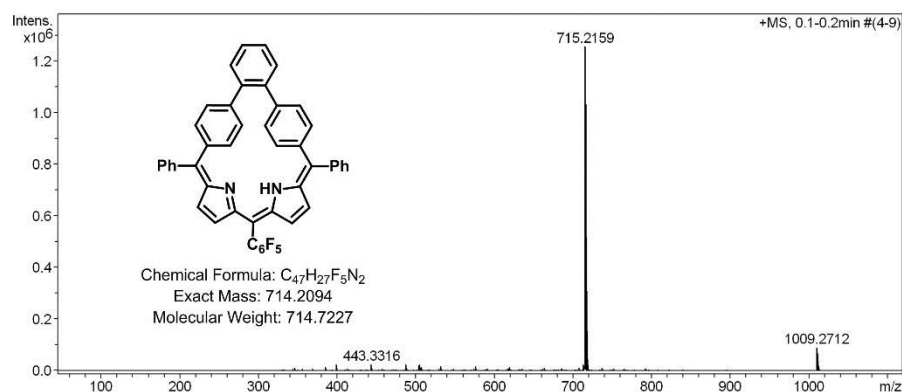


Figure 6.2: ESI-MS spectrum of **14**.

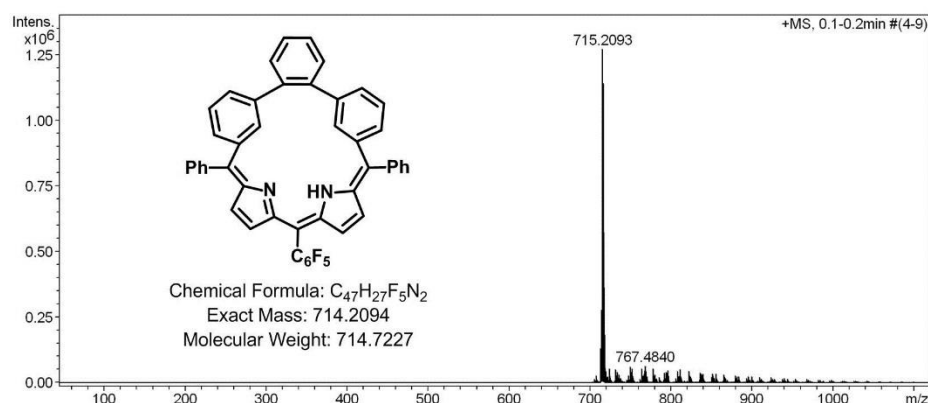


Figure 6.3: ESI-MS spectrum of **18**.

6.3.1.2 NMR Analysis

The 1H NMR spectrum of **14**, and **18** were recorded in $CDCl_3$ at 298 K, and shown in Figure 6.4. In compound **14**, the four inner CH [H2, H3, H2'', H3''] signals from the *p*-phenylene unit are appeared at 7.90 ppm, while the peripheral CH [H5, H6, H5'', H6''] protons are observed at 7.29 ppm. The signals corresponding to *o*-phenylene proton are resonated between 7.44 and 7.36 ppm. The pyrrolic β -CH protons are appeared at 5.93 ppm [H10, 15] and 6.60 ppm [H9, 15], respectively. The similar spectral patterns were observed in case of compound **14a** while the *p*-tolyl methyl protons are resonated at 2.38 ppm. On the other hand, the two inner CH [H2, H2''] signals of *m*-phenylene unit in **18** is resonated at 7.13 ppm, while the remaining peripheral CH signals are appeared between 6.85 and 7.43 ppm. The *o*-phenylene proton signals are observed at 7.28 to

7.60 ppm. The pyrrolic β -CH protons are slightly downfield shifted as compared to **14** and appeared at 6.35 and 6.85 ppm, respectively. The inner NH signal in **14** and **18** is observed as a broad singlet at 11.70 ppm and 12.08 ppm. The signals are conformed by D₂O experiment. The deshielded signals further suggest the intramolecular hydrogen bonding interactions. Overall, the peak positions in **14** and **18** resembles typical non-aromatic characteristics.

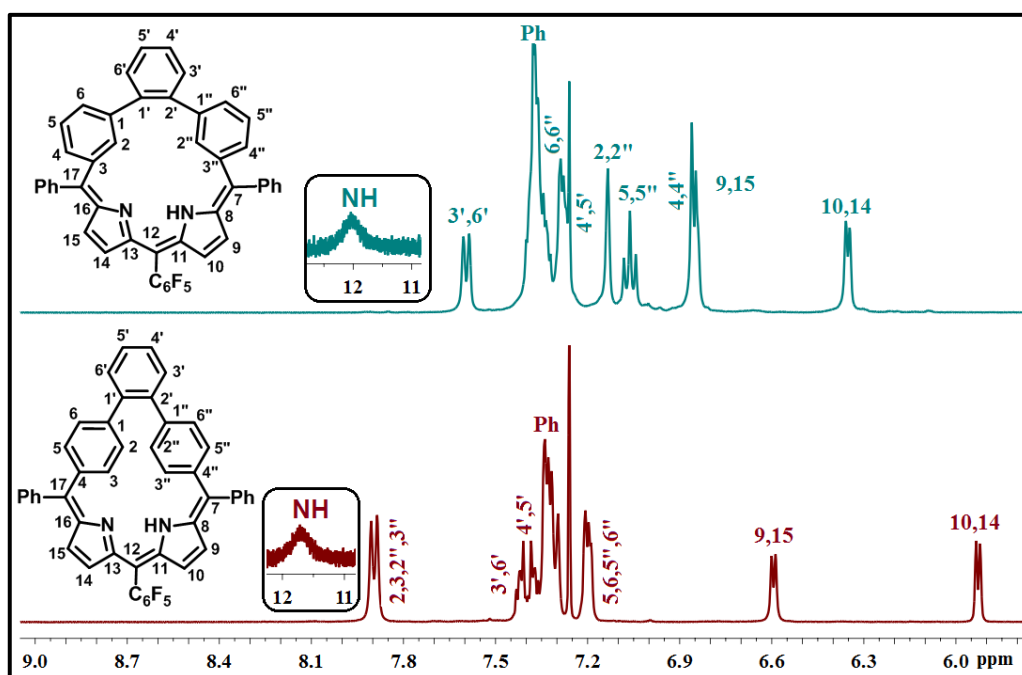


Figure 6.4: ¹H NMR spectrum of **14** and **18** in CDCl₃.

6.3.1.3 Single crystal X-ray structure and analysis of **14**

The structural characterisation of **14** was unambiguously confirmed by single crystal X-ray analysis (Figure 6.5). The compound **14** crystallized in orthorhombic space group *P b c a* (Table 6.1). The down field shift of inner NH signal as observed in ¹H NMR analysis was further reflected from the crystal analysis, where the amine and imine nitrogens of the dipyrromethene units lie within the range (N1-N2 distance 2.907(2) Å) of intramolecular hydrogen-bonding interaction (Figure 6.5). The crystal structure

reveals that the macrocycle is formed by connecting the *o*-terphenyl unit and dipyrromethene with two *meso*-phenyl units, where the *o*-terphenyl is connected by 4,4'' bonding mode. By careful analysis of carbon-carbon bond lengths in the dipyrromethene moiety shows alternative sp^2 - sp^2 single and double bond character (bond distances between 1.339(2) and 1.461(2) Å) within macrocyclic core and proves the effective π -delocalization (Figure 6.10). However, the possible π -electron conjugation reflect from the *o*-terphenyl unit where both the *p*-phenyl units maintain the sp^2 - sp^2 double bond character (bond lengths are between 1.381(2) and 1.402(2) Å) and remain isolated from the overall macrocyclic aromatization. In addition, the *p*-phenyl units are highly deviated from the mean plane containing 19 inner core atoms with the dihedral angle of 50.54(3)° and 47.43(3)°, whereas the pyrrole and *o*-phenyl units are hardly deviated from the plane with the angle of 5.78(3)°, 6.46.89(3)° and 2.29(3)°, respectively. Overall, as observed from the NMR spectral analysis, the non-aromatic character are reflected from the *p*-phenylene units: (a) maintain individual aromatic character and (b) induce non-planarity in the macrocyclic framework. Further, the presence of fluorine atoms in the pentafluorophenyl unit generate self-assembled

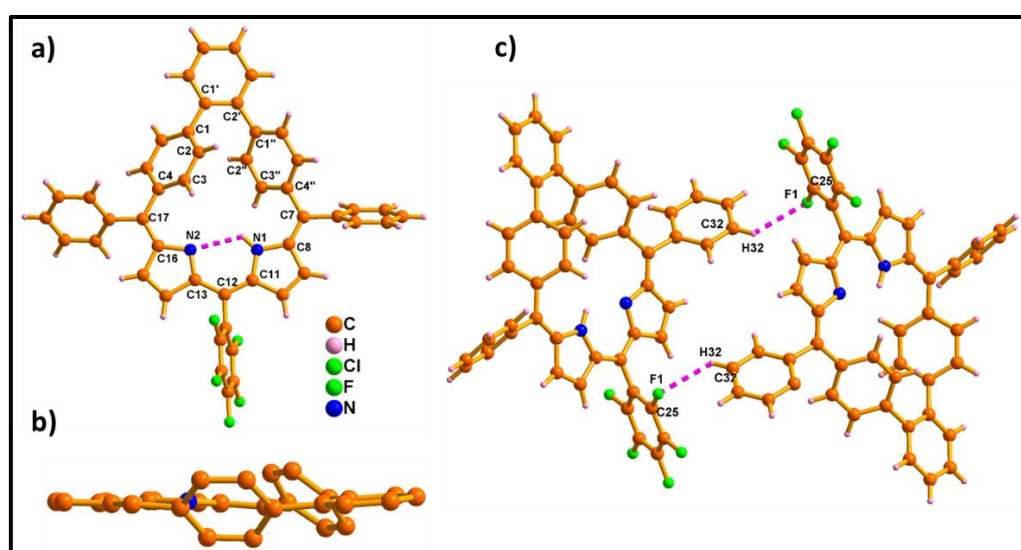
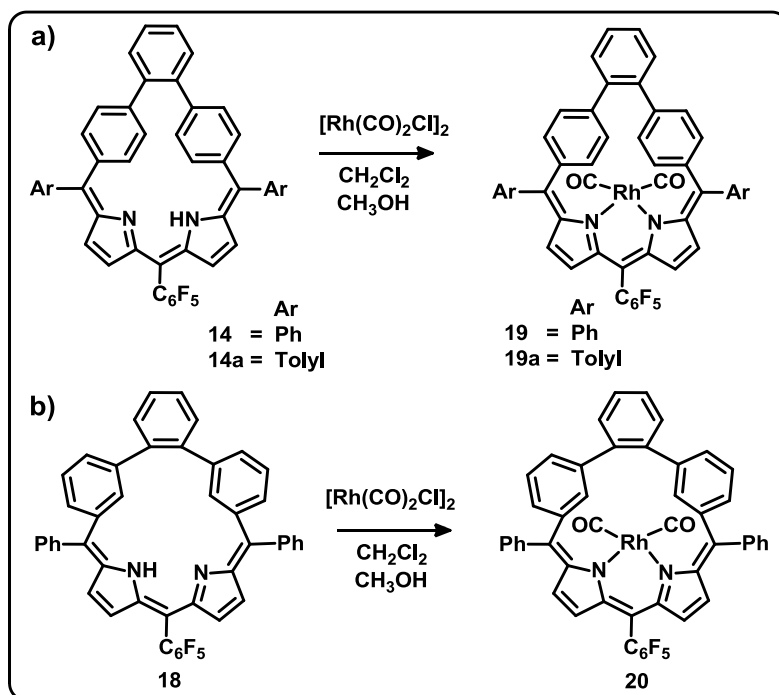


Figure 6.5: Single crystal X-ray structure of **14**. a) Top view; b) side view and c) self-assembled dimer. The *meso*-aryl groups are omitted for clarity in the side view.

dimer by intermolecular hydrogen bonding interactions with the bond distances and angles of C32-H32 ...F1 is 2.616(1) Å and 132.17(1)° (Figure 6.5).

6.3.2 Coordination Studies



Scheme 6.7: Metallation of carba-homoporphyrins.

The coordination chemistry of **14**, **14a** and **18** was performed by using $[\text{Rh}(\text{CO})_2\text{Cl}]_2$ in $\text{CH}_2\text{Cl}_2/\text{CH}_3\text{OH}$ mixture, where the bluish green fraction was eluted by silica gel column and afforded **19**, **19a** and **20** in 40-70% yield (Scheme 6.7). ESI-MS spectrometric analysis of **19**, **19a** and **20** showed the molecular ion signals at 816.1035 $[\text{M}-2\text{CO}]$, 844.1259 $[\text{M}-2\text{CO}]$ and 816.0945 $[\text{M}-2\text{CO}]$ and conformed the exact composition (Figure 6.6-6.7).

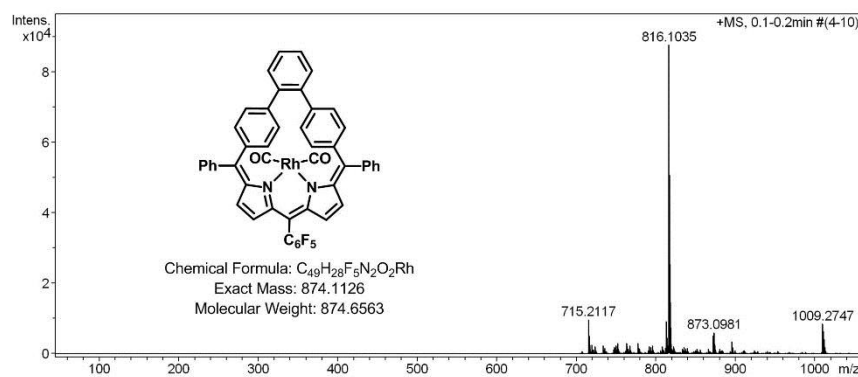


Figure 6.6: ESI-MS spectrum of **19**.

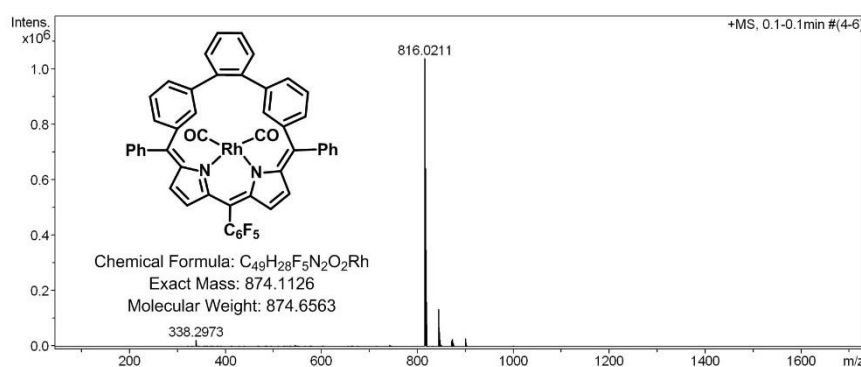


Figure 6.7: ESI-MS spectrum of **20**.

6.3.2.1 NMR Analysis

The insertion of Rh(I) ion in the macrocyclic core was characterised by ^1H -NMR spectrum (Figure 6.8). The absence of inner NH signal and upfield shift of *p*-phenylene four inner CH signals compared to **14** confirms the complex formation **19**. The *o*-phenyl protons are significantly upfield shifted and resonated between 7.07 and 7.28 ppm. However, the pyrrolic β -CH protons are slightly deshielded and appeared at 6.53 and 7.03 ppm. The similar trend was observed in case of **19a**, where the tolyl-CH₃ protons appeared at 2.45 ppm. On the other hand, in complex **20**, in addition to the disappearance of inner NH proton, *m*-phenylene inner-CH signal is significantly upfield shifted as compared to **18** and resonated at 6.51 ppm. The peripheral *m*-phenylene protons are observed from 7.20 to 7.66 ppm. The protons corresponding to *o*-phenyl

and pyrrolic β -CH protons are appeared between 6.51 and 7.29 ppm (Figure 6.8). All these proton signals are assigned by 2D homonuclear correlation spectroscopy. Overall, the spectral features resemble the nonaromatic pattern.^{19,20}

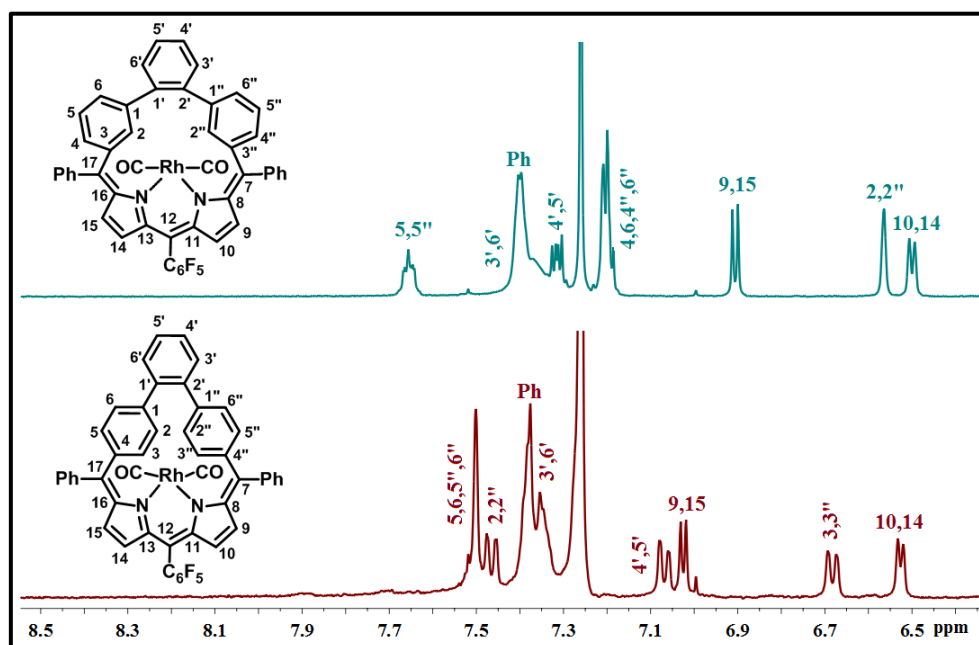


Figure 6.8: ^1H NMR spectrum of **19** and **20** in CDCl_3 .

6.3.2.2 Single crystal X-ray analyses

The final proof of complexes **19a** and **20** has come from the single crystal X-ray analyses (Figure 6.9, Table 6.1). The structural analysis of **19a** reveals that the Rh(I) ion is coordinated with the dipyrromethene unit and two carbonyl groups. The geometry around the metal center is distorted tetrahedral. Upon coordination with Rh(I) ion; i) the dipyrromethene unit is deviated from the mean plane containing 19 inner core atoms, where the pyrrole unit is maximum deviated by $24.85(2)^\circ$ and ii) *p*-phenylene units from *o*-terphenyl system are highly deviated with the dihedral angle of $79.04(1)^\circ$ and $64.99(2)^\circ$ suggests that the macrocycle **19a** adopts non-planar conformation (Figure 6.9). In complex **20** Rh(I) ion follows the similar coordination mode as observed in

complex **19a**. The structural analysis reveals that i) the two pyrrole units are deviated by $31.31(8)^\circ$, $30.82(7)^\circ$; ii) *o*-phenyl unit in *o*-terphenyl system is tilted by $61.85(6)^\circ$ which are higher than the respective angle as in **14** and **19a** and iii) *m*-phenyl unit is maximum deviated by $68.75(7)^\circ$ from the mean plane containig 17 inner core atoms. As observed in **14**, the bond distances in **19a** and **20** (Figure 6.10) proves the interption in the macrocyclic conjugation, thus maintains the non-aromatic charcter.

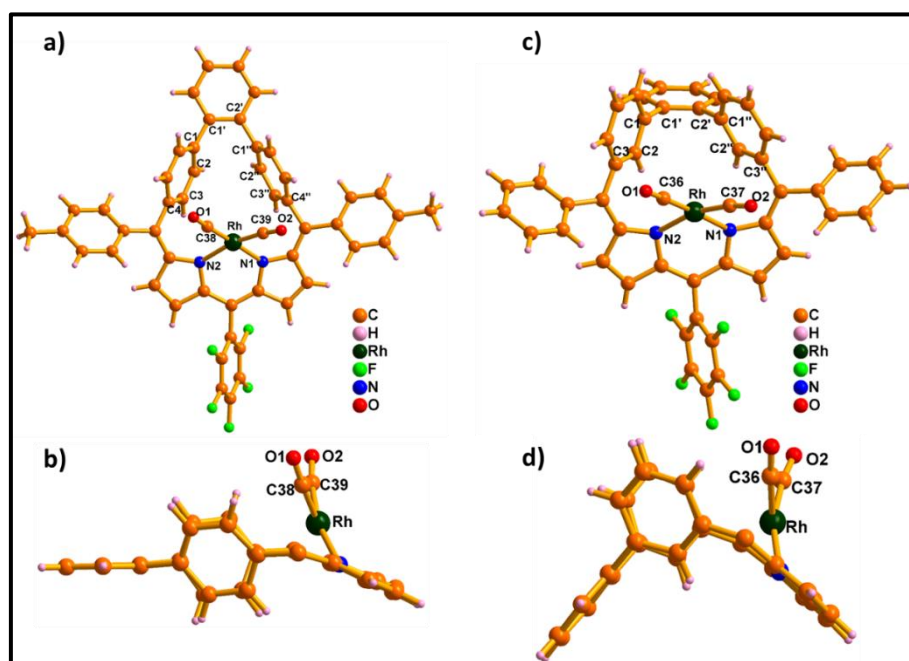


Figure 6.9: Single crystal X-ray structure of **19a** and **20**. a), c) Top view; b), d) side view. The *meso*-aryl groups are omitted for clarity in the side view.

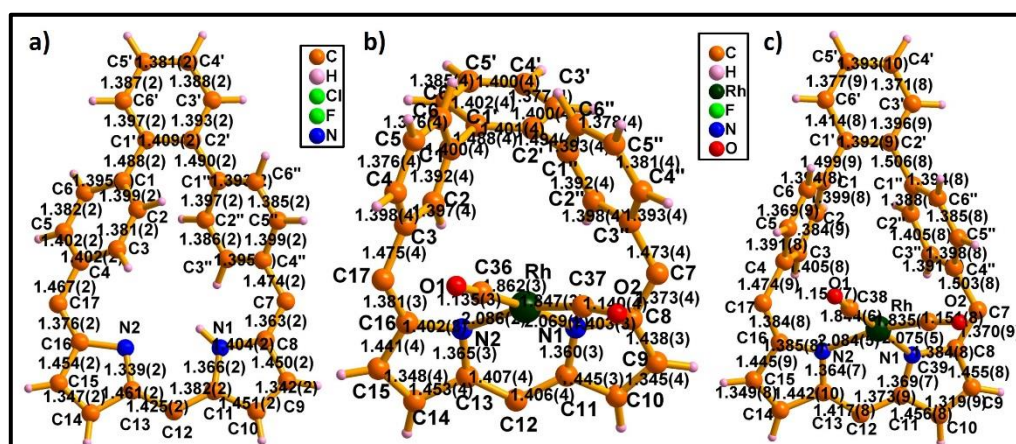


Figure 6.10: Bond distances in **14**, **19a** and **20** (Å).

6.3.3 Electronic spectral analysis

The electronic absorption spectral analyses of compound **14**, **14a**, **18**, **19**, **19a** and **20** were recorded in CH_2Cl_2 solution. As representative examples, **14** & **18** and **19** & **20** were shown in Figure 6.11-6.12. The absorption spectrum of conjugated *para*-isomer **14** shows Soret like strong absorption at 362 nm and a weak Q-type band at 620 nm. Whereas, the *meta*-isomer **18** shows an intense band at 368 nm and a prominent Q-like band at 608 nm. Upon coordination with the Rh(I) ion, the color of the solution changes from blue to green. In case of **19**, the intense band is observed at 388 nm and a prominent band at 716 nm which are red shifted by 8 and 40 to 50 nm as compared to **14**. Whereas, the respective bands in **20** are observed band at 384 nm and 707 nm, respectively. The molar absorption coefficient lower and higher wave length intense bands are in the order of 10^5 in **19** and **20**. Overall, the spectral feature of all the compounds and its Rh(I) complexes are comparable with other non-aromatic molecules such as biphenylcorrole,¹⁹ bipyricorrole²⁰ and core-modified homoporphyrin derivatives,^{16,17} thus confirms the non-aromatic character.

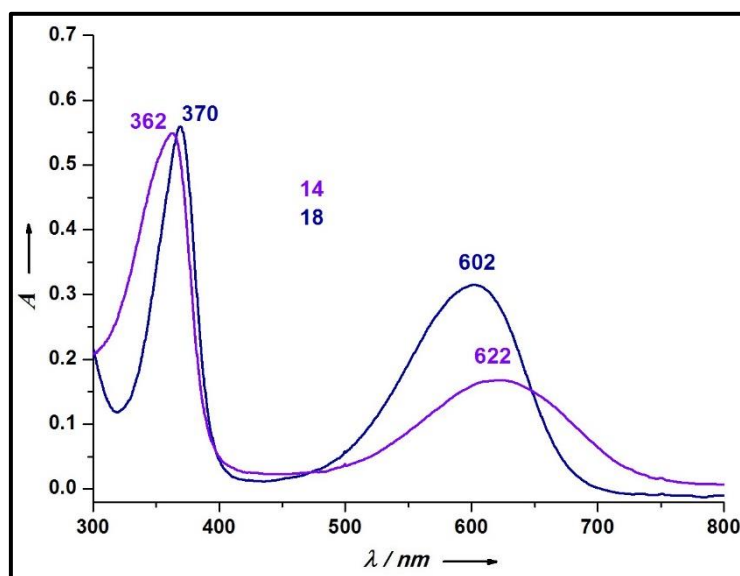


Figure 6.11: Electronic absorption spectrum of **14** and **18** in CH_2Cl_2 .

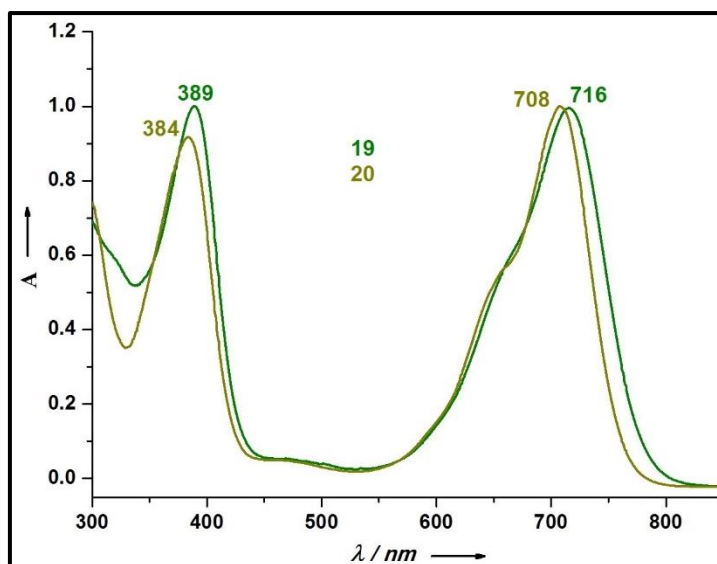


Figure 6.12: Electronic absorption spectrum of **19** and **20** in CH_2Cl_2 (normalized).

6.4 Conclusion

In conclusion, we have demonstrated the synthesis of novel carba-homoporphyrins. The newly formed di-carba and tetra-carba homoporphyrins were achieved by introducing *o*-terphenyl unit in the porphyrin core with two different modes (*p*- and *m*-). Though the para-isomer participates in overall conjugation, however, possesses lower planarity. Whereas the *meta*-isomer maintains individual aromaticity thus both the isomers adopt non-aromatic character. The coordination chemistry of these two isomers was further explored with $[\text{Rh}(\text{CO})_2\text{Cl}]_2$ salt. The dipyrromethene unit is utilized to stabilize the Rh(I) ion. The spectral and structural analysis revealed that the Rh(I) complex retained the non-aromatic character as such. To the best of our knowledge, the carba-homoporphyrins are hitherto unknown in homoporphyrin series and reported for the first time.

6.5 Experimental Section

6.5.1 General Information

The reagents and materials for the synthesis were used as obtained from Sigma Aldrich chemical suppliers. All solvents were purified and dried by standard methods prior to use. The NMR solvents were used as received and the spectra were recorded in Bruker 400 MHz spectrometer with TMS as internal standard. The ESI mass spectra were recorded in Bruker, micro-TOF-QII mass spectrometer. The Electronic absorption spectra were recorded in Perkin Elmer–Lambda 750 UV-Visible spectrophotometer. The X-ray quality crystals for **14**, **19a** and **20** were grown by slow diffusion of *n*-hexane over CH₂Cl₂ solution. Single-crystal X-ray diffraction data of **14**, **19a** and **20** were collected in a Bruker KAPPA APEX-II, four angle rotation system, Mo-K α radiation (0.71073 Å). The crystals have been deposited in the Cambridge Crystallographic Data Centre with reference no. **CCDC 1519961** (**14**), **CCDC 1519963** (**19a**) and **CCDC 1519962** (**20**).

6.5.2 Synthetic procedure and spectral characterization

6.5.2.1 Synthesis of 12: Freshly prepared phenylmagnesiumbromide (9.05 g, 50 mmol) solution in THF (20 ml) was added under N₂ atmosphere at 0 °C into the solution of **11** (2.9 g, 10 mmol) in 100 ml THF and then allowed to stir at RT for 4h. The completion of the reaction was monitored by TLC and the reaction was quenched with 1N HCl. The crude mixture was extracted with EtOAc, dried over Na₂SO₄, and concentrated by rotary evaporator. Compound was purified by column chromatography using silica gel (100-200 mesh) in 20% EtOAc/*n*-hexane to afford **12** in 75% yield.

¹H NMR (400 MHz, CDCl₃, 298K): δ = 7.42 (d, *J* = 4.9 Hz, 4H), 7.37 – 7.27 (m, 10H), 7.20 (d, *J* = 8.2 Hz, 4H), 7.13 (d, *J* = 7.9 Hz, 4H), 5.73 (s, 2H), 2.61 (s, 2H).

¹³C NMR (100 MHz, CD₃OD): δ = 143.91, 142.09, 140.91, 140.39, 130.67, 130.12, 128.62, 127.69, 126.81, 126.31, 76.07.

ESI-MS: *m/z* calculated for C₃₂H₂₆O₂ = 442.1933; found = 465.1787 (M+Na).

6.5.2.2 Synthesis of 12a: ¹H NMR (400 MHz, CDCl₃, 298K): δ = 7.46 (d, *J* = 3.5 Hz, 4H), 7.29 – 7.13 (m, 16H), 5.76 (s, 2H), 2.56 (d, *J* = 2.9 Hz, 2H), 2.40 (s, 6H).

¹³C NMR (100 MHz, CD₃OD): δ = 142.24, 141.05, 140.79, 140.44, 137.35, 130.67, 130.07, 129.30, 127.62, 126.79, 126.23, 75.89, 21.29.

ESI-MS: *m/z* calculated for C₃₄H₃₀O₂ = 470.2246; found = 493.2108 (M+Na).

6.5.2.3 Synthesis of 13: The pyrrole (10 mL) was added into the solution **12** (2 g, 4.5 mmol) in 1,2-dichloroethane (40 mL) which was kept in an inert atmosphere. After 10 min 1.4 mL of BF₃·Et₂O solution was added and the resulting mixture was stirred under reflux for 5 h. The solution was cooled to room temperature and quenched by addition of TEA (2 mL). The compound was extracted with CH₂Cl₂, dried over Na₂SO₄ and concentrated by rotary evaporator. The crude mixture was purified by column chromatography using silica gel (100-200 mesh) in 10% EtOAc/*n*-hexane to afford **13** in 55% yield.

¹H NMR (400 MHz, CDCl₃, 298K): δ = 7.73 (s, 2H), 7.43 – 7.35 (m, 4H), 7.30 – 7.21 (m, 6H), 7.12 (d, *J* = 7.3 Hz, 4H), 7.01 (q, *J* = 8.2 Hz, 8H), 6.66 (s, 2H), 6.13 (dd, *J* = 5.6, 2.8 Hz, 2H), 5.76 (s, 2H), 5.43 (s, 2H).

¹³C NMR (100 MHz, CDCl₃): δ = 143.25, 141.48, 140.62, 140.16, 133.71, 130.45, 130.23, 129.05, 128.70, 128.44, 127.65, 126.87, 117.37, 108.47, 108.09, 50.31.

ESI-MS: *m/z* calculated for C₄₀H₃₂N₂ = 540.2565; found = 579.2248 (M+K).

6.5.2.4 Synthesis of 13a: ¹H NMR (400 MHz, CDCl₃, 298K): δ = 7.75 (s, 2H), 7.49 – 7.40 (m, 4H), 7.13 (d, *J* = 7.6 Hz, 4H), 7.11 – 7.03 (m, 12H), 6.74 – 6.66 (m, 2H), 6.19 (d, *J* = 2.6 Hz, 2H), 5.82 (s, 2H), 5.44 (s, 2H), 2.37 (s, 6H).

^{13}C NMR (100 MHz, CDCl_3): $\delta = 141.70, 140.65, 140.38, 139.97, 136.37, 133.91, 130.43, 130.19, 129.38, 128.92, 128.39, 127.61, 117.25, 108.42, 107.96, 49.90, 21.23$;

ESI-MS: m/z calculated for $\text{C}_{42}\text{H}_{36}\text{N}_2 = 568.2878$; found = 607.2549 (M+K).

6.5.2.5 Synthesis of 14: Compound **13** (200 mg, 0.37 mmol) and pentafluorobenzaldehyde (86 mg, 0.44 mmol) was dissolved in 200 ml CH_2Cl_2 solution and stirred under inert atmosphere covered with aluminium foil. After 10 min TFA (0.08 ml, 1.11 mmol) solution was added and allowed to stir under same condition for 3 h. The 2,3-Dichloro-5,6-dicyano-1,4-benzoquinone (251 mg, 1.11 mmol) was added to the reaction mixture and opened to air. The reaction was further continued for 2 h and the formation of product was monitored by TLC. The crude product was passed through basic alumina column followed by neutral alumina column. The blue band was eluted with 20% $\text{CH}_2\text{Cl}_2/n$ -hexane and identified as **14**. The compound was further recrystallized from $\text{CH}_2\text{Cl}_2/n$ -hexane to afford blue crystalline **14** in 12% yield.

^1H NMR (400 MHz, CD_2Cl_2 , 298K): $\delta = 11.70$ (s, 1H), 7.90 (d, $J = 8.2$ Hz, 4H), 7.44 – 7.36 (m, 4H), 7.35 – 7.29 (m, 10H), 7.20 (dd, $J = 6.5, 3.1$ Hz, 4H), 6.60 (d, $J = 5.2$ Hz, 2H), 5.93 (d, $J = 5.2$ Hz, 2H).

^{13}C NMR (100 MHz, CD_2Cl_2): $\delta = 141.87, 140.58, 138.69, 134.77, 133.62, 131.89, 131.35, 128.35, 127.79$.

ESI-MS: m/z calculated for $\text{C}_{47}\text{H}_{27}\text{F}_5\text{N}_2 = 714.2094$; found = 715.2159 (M+1).

UV-Vis (CH_2Cl_2): $\lambda_{\text{max}}(\text{nm})$ ($\epsilon[\text{M}^{-1}\text{cm}^{-1}]$) = 362 (35,453), 622 (9,965).

6.5.2.6 Synthesis of 14a: **^1H NMR (400 MHz, CD_2Cl_2 , 298K):** $\delta = 11.68$ (s, 1H), 7.90 (d, $J = 7.9$ Hz, 4H), 7.43 – 7.35 (m, 4H), 7.30 (d, $J = 7.9$ Hz, 4H), 7.14 (d, $J = 7.9$ Hz, 4H), 7.08 (d, $J = 8.0$ Hz, 4H), 6.61 (d, $J = 5.1$ Hz, 2H), 5.92 (d, $J = 5.2$ Hz, 2H), 2.38 (s, 6H).

ESI-MS: m/z calculated for $\text{C}_{49}\text{H}_{31}\text{F}_5\text{N}_2 = 742.2407$; found = 743.2392 (M+1).

UV-Vis (CH₂Cl₂): $\lambda_{\max}(\text{nm})$ ($\epsilon[\text{M}^{-1}\text{cm}^{-1}]$) = 368 (34,453), 630 (9,965).

We have followed similar synthetic protocol as mentioned for compound **12**, **13**, **14** for the formation of compound **16**, **17**, **18**.

6.5.2.7 Synthesis of 16: Yield 75%.

¹H NMR (400 MHz, CDCl₃, 298K): δ = 7.43 – 7.34 (m, 4H), 7.26 – 7.08 (m, 16H), 6.95 (d, J = 8.5 Hz, 2H), 5.55 (d, J = 2.3 Hz, 2H), 2.17 (d, J = 7.8 Hz, 2H).

¹³C NMR (100 MHz, CD₃OD): δ = 143.46, 141.74, 140.62, 130.47, 129.22, 128.85, 128.57, 127.79, 127.50, 126.52, 125.27, 76.22.

ESI-MS: m/z calculated for C₃₂H₂₆O₂ = 442.1933; found = 465.1927 (M+Na).

6.5.2.8 Synthesis of 17: Yield 55%.

¹H NMR (400 MHz, CDCl₃, 298K): δ = 7.37 – 7.28 (m, 5H), 7.27 – 7.15 (m, 9H), 7.14 – 7.03 (m, 4H), 6.99 (d, J = 6.7 Hz, 4H), 6.85 (d, J = 11.4 Hz, 2H), 6.51 (d, J = 1.4 Hz, 2H), 6.05 (dd, J = 5.4, 2.6 Hz, 2H), 5.61 (s, 2H), 5.26 (t, J = 4.9 Hz, 2H).

¹³C NMR (100 MHz, CD₃OD): δ = 143.14, 142.75, 142.20, 140.76, 133.39, 130.73, 128.93, 128.77, 128.44, 128.26, 127.73, 127.26, 126.77, 117.49, 108.11, 50.72.

ESI-MS: m/z calculated for C₄₀H₃₂N₂ = 540.2565; found = 579.3568 (M+K).

6.5.2.9 Synthesis of 18: Yield 7%.

¹H NMR (400 MHz, CDCl₃, 298K): δ = 12.08 (s, 1H), 7.60 (d, J = 7.5 Hz, 2H), 7.43 – 7.31 (m, 10H), 7.28 (d, J = 3.6 Hz, 4H), 7.13 (s, 2H), 7.06 (t, J = 7.7 Hz, 2H), 6.85 (d, J = 5.1 Hz, 4H), 6.35 (d, J = 4.9 Hz, 2H).

¹³C NMR (100 MHz, CD₃OD): δ = 160.18, 149.43, 142.43, 141.87, 141.37, 139.76, 135.91, 135.17, 132.73, 131.20, 128.93, 128.44, 128.03, 127.88, 127.20, 126.09.

m.p: 300 °C (decomposition).

ESI-MS: m/z calculated for C₄₇H₂₇F₅N₂ = 714.2094; found = 715.2093 (M+1).

UV-Vis (CH₂Cl₂): $\lambda_{\max}(\text{nm})$ ($\epsilon[\text{M}^{-1}\text{cm}^{-1}]$) = 370 (30,565), 602(16,923).

6.5.2.10 Synthesis of 19: A solution of $[\text{Rh}(\text{CO})_2\text{Cl}]_2$ (54 mg, 0.14 mmol) in 5 ml CH_3OH was added into the solution of **14** (20 mg, 0.028 mmol) in CH_2Cl_2 (20 ml) under inert atmosphere. The reaction was allowed to stir for 4 h and the formation of product was monitored by TLC. The solvent was evaporated by rotary evaporator. The crude metal complex was purified by neutral alumina column. The bluish green band was eluted with 10% $\text{CH}_2\text{Cl}_2/n$ -hexane and identified as **19**. The compound was further recrystallized from $\text{CH}_2\text{Cl}_2/n$ -hexane to afford blue crystalline **19** in 70% yield.

^1H NMR (400 MHz, CD_2Cl_2 , 298K): $\delta = 7.53 - 7.45$ (m, 6H), 7.36 (m, 10H), 7.28 (d, $J = 1.6$ Hz, 2H), 7.07 (dd, $J = 7.9, 1.6$ Hz, 2H), 7.03 (d, $J = 5.0$ Hz, 2H), 6.69 (dd, $J = 7.9, 1.6$ Hz, 2H), 6.53 (d, $J = 4.9$ Hz, 2H).

^{13}C NMR (100 MHz, CD_2Cl_2): $\delta = 186.46, 162.01, 161.68, 143.45, 142.41, 141.71, 141.18, 139.95, 137.62, 132.73, 129.63 - 129.02, 128.36, 127.96, 127.56$.

ESI-MS: m/z calculated for $\text{C}_{49}\text{H}_{26}\text{F}_5\text{N}_2\text{O}_2\text{Rh} = 874.1126$; found = 816.1035 (M-2CO).

UV-Vis (CH_2Cl_2): $\lambda_{\text{max}}(\text{nm})$ ($\epsilon[\text{M}^{-1}\text{cm}^{-1}]$) = 389 (30,214), 716 (32,542).

We have followed similar synthetic protocol as mentioned for compound **19** here we have started **14a** & **18** and got **19a** & **20**.

6.5.2.11 Synthesis of 19a: Yield 70%.

^1H NMR (400 MHz, CD_2Cl_2 , 298K): $\delta = 7.58 - 7.43$ (m, 6H), 7.32 - 7.19 (m, 10H), 7.11 (d, $J = 8.1$ Hz, 4H), 6.67 (d, $J = 7.6$ Hz, 2H), 6.58 (s, 2H), 2.45 (s, 6H).

ESI-MS: m/z calculated for $\text{C}_{51}\text{H}_{30}\text{F}_5\text{N}_2\text{O}_2\text{Rh} = 902.1439$; found = 844.1259 (M-2CO).

UV-Vis (CH_2Cl_2): $\lambda_{\text{max}}(\text{nm})$ ($\epsilon[\text{M}^{-1}\text{cm}^{-1}]$) = 394 (30,578), 723 (32,965).

6.5.2.12 Synthesis of 20: We have followed similar synthetic protocol as mentioned for compound **19** here we have started **18** and got **20** 85% yield.

^1H NMR (400 MHz, CDCl_3 , 298K): $\delta = 7.66$ (s, 2H), 7.47 - 7.29 (m, 12H), 7.20 (t, $J = 4.5$ Hz, 6H), 6.91 (d, $J = 5.0$ Hz, 2H), 6.57 (s, 2H), 6.51 (d, $J = 4.9$ Hz, 2H).

ESI-MS: m/z calculated for $C_{49}H_{26}F_5N_2O_2Rh$ = 874.1126; found = 816.0945 (M-2CO).

UV-Vis (CH_2Cl_2): $\lambda_{max}(nm)$ ($\epsilon[M^{-1}cm^{-1}]$) = 384 (32,453), 708 (33,789).

Table 6.1: Crystal data for **14**, **19a** and **20**

Crystal parameters	14	19a	20
Formula	$C_{48}H_{29}Cl_2F_5N_2$	$C_{53}H_{30}F_5N_2O_4Rh$	$C_{49}H_{26}F_5N_2O_2Rh$
$M/g\ mol^{-1}$	799.63	956.70	872.63
T/K	100	100	100
Crystal dimensions/ mm^3	0.16 x 0.09 x 0.05	0.13 x 0.07 x 0.06	0.11 x 0.08 x 0.06
Crystal system	Orthorhombic	Monoclinic	Monoclinic
Space group	Pbc_a	$P2_1/n$	$P2_1/n$
$a/\text{\AA}$	14.4966(17)	10.305(3)	16.455(2)
$b/\text{\AA}$	20.350(2)	26.878(7)	12.5866(17)
$c/\text{\AA}$	25.307(3)	15.665(4)	18.220(3)
$\alpha/^\circ$	90	90	90
$\beta/^\circ$	90	103.037(17)	98.871(8)
$\gamma/^\circ$	90	90.000	90
$V/\text{\AA}^3$	7465.7(14)	4227(2)	3728.5(9)
Z	8	4	4
$\rho_{calcd}/mg\ m^{-3}$	1.423	1.503	1.555
μ/mm^{-1}	0.238	0.477	0.529
$F(000)$	3280	1936	1760
Reflns. collected	126365	39282	58016
Indep.reflns.[$R(int)$]	10512 [0.0921]	7429 [0.1415]	8931 [0.0753]
Max/min transmission	0.7459 and 0.6813	0.7452 and 0.5721	0.7456 and 0.5914
Data/restraints/parameters	10512 / 0 / 514	7429 / 12 / 586	8931 / 0 / 532
GOF on F^2	1.023	1.018	1.023
Final R indices[$I > 2\sigma(I)$]	$R_1 = 0.0441$, $wR_2 = 0.1026$	$R_1 = 0.0590$, $wR_2 = 0.1458$	$R_1 = 0.0405$, $wR_2 = 0.0904$
R indices (all data)	$R_1 = 0.0653$, $wR_2 = 0.1145$	$R_1 = 0.1096$, $wR_2 = 0.1727$	$R_1 = 0.0615$, $wR_2 = 0.0999$
Largest diff peak and hole [$e\ \text{\AA}^{-3}$]	0.524 and -0.703	1.402 and -1.187	0.645 and -0.796

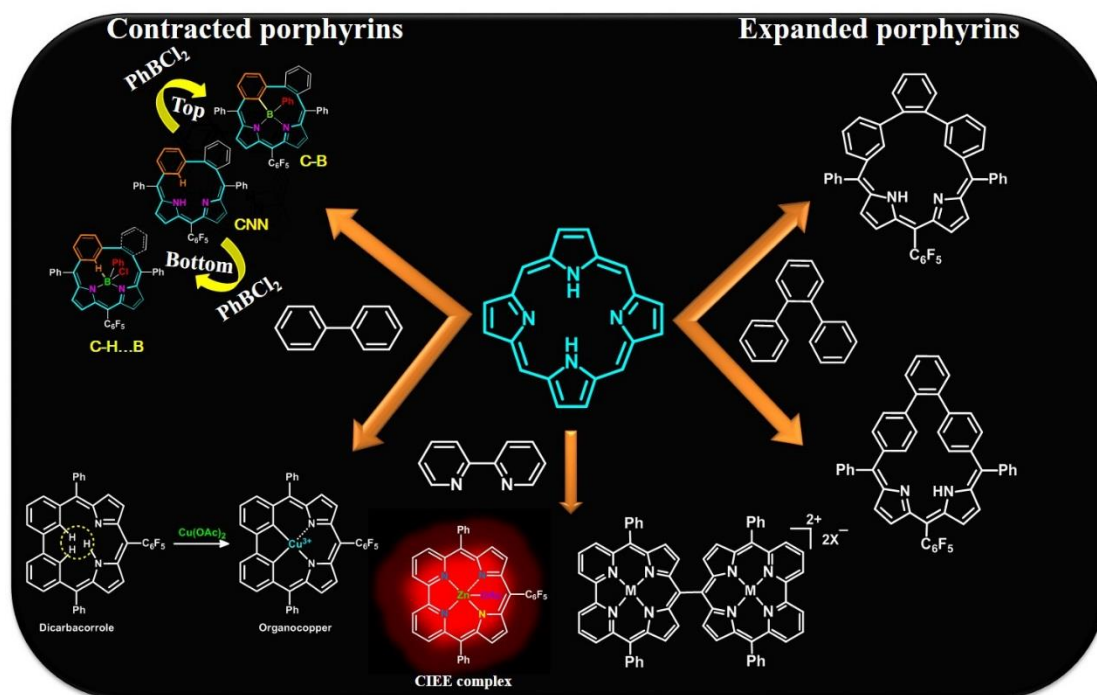
6.6 References

1. Tanaka, T.; Osuka, A. *Chem. Rev.* **2016**, DOI: 10.1021/acs.chemrev.6b00371.
2. Sung, Y. M.; Oh, J.; Cha, W.-Y.; Kim, W.; Lim, J. M.; Yoon, M.-C.; Kim, D. *Chem. Rev.* **2016**, DOI: 10.1021/acs.chemrev.6b00313.

-
3. Ding, Y.; Zhu, W.-H.; Xie, Y. *Chem. Rev.* **2016**, DOI: 10.1021/acs.chemrev.6b00021.
 4. Saito, S.; Osuka, A. *Angew. Chem. Int. Ed.* **2011**, *50*, 4342-4373.
 5. Callot, H. J.; Schaeffer, E. *J. Org. Chem.* **1977**, *42*, 1567-1570.
 6. Callot, H. J.; Tschamber, T. *Tetrahedron Lett.* **1974**, *15*, 3155-3158.
 7. Callot, H. J.; Tschamber, T. *J. Am. Chem. Soc.* **1975**, *97*, 6175-6178.
 8. Grigg, R. *Chem. Commun.* **1967**, 1238-1239.
 9. Grigg, R. *J. Chem. Soc. C* **1971**, 3664-3668.
 10. Chevrier, B.; Weiss, R. *J. Chem. Soc., Chem. Commun.* **1974**, 884-885.
 11. Chevrier, B.; Weiss, R. *J. Am. Chem. Soc.* **1975**, *97*, 1416-1421.
 12. Callot, H. J.; Tschamber, T.; Schaeffer, E. *J. Am. Chem. Soc.* **1975**, *97*, 6178-6180.
 13. Callot, H. J.; Tschamber, T.; Schaeffer, E. *Tetrahedron Lett.* **1975**, *16*, 2919-2922.
 14. Callot, H. J. *Dalton Trans.* **2008**, 6346-6357.
 15. Chevrier, B.; Weiss, R. *Inorg. Chem.* **1976**, *15*, 770-774.
 16. Ganapathi, E.; Lee, W.-Z.; Ravikanth, M. *J. Org. Chem.* **2014**, *79*, 9603-9612.
 17. Ganapathi, E.; Kuilya, S.; Chatterjee, T.; Ravikanth, M. *Eur. J. Org. Chem.* **2016**, 282-290.
 18. Bounos, G.; Ghosh, S.; Lee, A. K.; Plunkett, K. N.; DuBay, K. H.; Bolinger, J. C.; Zhang, R.; Friesner, R. A.; Nuckolls, C.; Reichman, D. R.; Barbara, P. F. *J. Am. Chem. Soc.* **2011**, *133*, 10155-10160.
 19. Adinarayana, B.; Thomas, A. P.; Suresh, C. H.; Srinivasan, A. *Angew. Chem. Int. Ed.* **2015**, *54*, 10478-10482.
 20. Adinarayana, B.; Thomas, A. P.; Yadav, P.; Kumar, A.; Srinivasan, A. *Angew. Chem. Int. Ed.* **2016**, *55*, 969-97.

Conclusion and Future Perspective

Porphyryns are highly conjugated 18π Hückel aromatic tetrapyrrolic organic pigments. They are ubiquitous in the world and referred as the “colours of life”. Because of their application in various fields, the interest has been increased towards the synthesis and studies of novel porphyrin analogues such as contracted, isomeric, expanded and core-modified porphyrins.



In this thesis, we have successfully embedded the bipyridine, biphenyl and terphenyl systems into the porphyrin framework. These molecules are further explored for the following properties; (i) Biphenylcorrole with adj-CCNN core is effectively utilized for stabilizing organocopper(III) complex; (ii) the monoanionic Bipyricorrole binds with Zn^{II} ion and further exploited the metal ion sensing experiments for the

selective detection of Zn^{II} ion; (iii) the smallest contracted porphyrin analogue Carbatriphyrin(3.1.1) – is found suitable to stabilize organoborane and also demonstrated the weak C-H...B interactions; (iv) similarly, the smallest expanded porphyrinoid, carba-homoporphyrins(2.1.1.1) coordinates with Rh(I) ion in the macrocyclic framework; v) finally, serendipitously discovered the metal template synthesis of meso-free bipyricorrole in the absence of any acid-catalysts as well as oxidizing agents and further utilized it for the oxidative coupling reactions. Overall, the synthesis of novel homologues and analogues of contracted and expanded porphyrinoids by introducing the polycyclic aromatic units in the macrocyclic framework are discussed. Also highlights the reactivity, receptor property and coordination chemistry of these macrocycles. These macrocycles pave the way for the various metalion insertion, aromatic properties, catalysis and sensing studies which are in progress in our research group.